Hadronic Properties In Presence Of Magnetic Field

By

Arghya Mukherjee

PHYS05201404010

Saha Institute Of Nuclear Physics, Kolkata

A thesis submitted to

The Board of Studies in Physical Sciences

In partial fulfillment of requirements

For the Degree of

DOCTOR OF PHILOSOPHY

of

HOMI BHABHA NATIONAL INSTITUTE

June, 2020

Homi Bhabha National Institute[1]

Recommendations of the Viva Voce Committee

As members of the Viva Voce Committee, we certify that we have read the dissertation prepared by Arghya Mukherjee entitled "Hadronic Properties In Presence Of Magnetic Field" and recommend that it may be accepted as fulfilling the thesis requirement for the award of Degree of Doctor of Philosophy.

Chairman-	Prof. Sukalyan Chattoapadhyay	Sattirje
Guide/Convener-	Prof. Pradip Kr. Roy	Pradip Kr. Roy
Examiner-	Prof. Subrata Pal	Subrata Pal
Member 1-	Prof. Munshi G. Mustafa	Munshi
Member 2-	Prof. Debasish Das	Debasish Das
Member 3-	Prof. Sourav Sarkar	Sourav Sarkar

Final approval and acceptance of this thesis is contingent upon the candidate's submission of the final copies of the thesis to HBNI.

I hereby certify that I/we have read this thesis prepared under my direction and recommend that it may be accepted as fulfilling the thesis requirement.

Date: 05/08/2020

Place: Saha Instt. of Nuclear Physics, Kolkata

Pradip Kr. Roy

Signature

(Prof. Pradip Kr. Roy)

[1]This page is to be included only for final submission after successful completion of viva voce.

STATEMENT BY AUTHOR

This dissertation has been submitted in partial fulfillment of requirements for an advanced degree at Homi Bhabha National Institute (HBNI) and is deposited in the Library to be made available to borrowers under rules of the HBNI.

Brief quotations from this dissertation are allowable without special permission, provided that accurate acknowledgement of source is made. Requests for permission for extended quotation from or reproduction of this manuscript in whole or in part may be granted by the Competent Authority of HBNI when in his or her judgment the proposed use of the material is in the interests of scholarship. In all other instances, however, permission must be obtained from the author.

Arghya Mukherjee
11/08/2020
Arghya Mukherjee

DECLARATION

I, hereby declare that the investigation presented in the thesis has been carried out by me. The work is original and has not been submitted earlier as a whole or in part for a degree / diploma at this or any other Institution / University.

Arghya Mukherjee
11/08/2020
Arghya Mukherjee

◇ List of publications pertaining to the thesis

1. **"Effect of external magnetic fields on nucleon mass in a hot and dense medium: Inverse magnetic catalysis in the Walecka model"**
   Arghya Mukherjee, Snigdha Ghosh, Mahatsab Mandal, Sourav Sarkar and Pradip Roy.
   Phys. Rev. D **98**, no. 5, 056024 (2018).

2. **"General structure of the neutral ρ meson self-energy and its spectral properties in a hot and dense magnetized medium"**
   Snigdha Ghosh, **Arghya Mukherjee**, Pradip Roy and Sourav Sarkar.
   Phys. Rev. D **99** no. 9, 096004 (2019).

◇ Other publications arising from the thesis

Journal

1. **"Spectral properties of ρ meson in a magnetic field"**
   Snigdha Ghosh,**Arghya Mukherjee**, Mahatsab Mandal, Sourav Sarkar and Pradip Roy.
   Phys. Rev. D **94**, no. 9, 094043 (2016).

2. **"Jet-dilepton conversion from an anisotropic quark-gluon plasma"**
   Arghya Mukherjee, Mahatsab Mandal and Pradip Roy.
   Eur. Phys. J. A **53**, no. 5, 81 (2017)

3. **"Mass modification of hot pions in a magnetized dense medium"**
   Arghya Mukherjee, Snigdha Ghosh, Mahatsab Mandal, Pradip Roy and Sourav Sarkar.
   Phys. Rev. D **96**, no. 1, 016024 (2017).

4. **"Thermal effects on ρ meson properties in an external magnetic field"**
   Snigdha Ghosh, **Arghya Mukherjee**, Mahatsab Mandal, Sourav Sarkar and Pradip Roy.
   Phys. Rev. D **96**, no. 11, 116020 (2017).

5. **"$\rho^0 - \omega$ mixing in the presence of a weak magnetic field"**
   Mahatsab Mandal, **Arghya Mukherjee**, Snigdha Ghosh, Pradip Roy and Sourav Sarkar.
   Eur. Phys. J. A (2018) 54: 99

6. **"Impact of magnetic field on shear viscosity of quark matter in Nambu–Jona-Lasinio model"**
   Sabyasachi Ghosh, Bhaswar Chatterjee, Payal Mohanty, **Arghya Mukherjee**, Hiranmaya Mishra.
   Phys. Rev. D **100** no. 3, 034024 (2019).

Conferences

1. **"Spectral function of ρ at finite temperature in arbitrary external magnetic field"** DAE Symp. Nucl. Phys. **62**, 762 (2017).

Arghya Mukherjee
11/08/2020
Arghya Mukherjee

Dedicated to the feelings of Love and Empathy

ACKNOWLEDGEMENTS

First of all, I express my deepest gratitude and respect to my supervisor *Prof. Pradip Kumar Roy.* Without his guidance and continuous support, this thesis could not have been possible. I am also indebted to *Prof. Sourav Sarkar* for his extremely important advices and learned comments. I am fortunate to be a part of our group with Pradip Sir, Sourav Sir, my junior Nilanjan and my senior Snigdha Da, and my super seniors Mahatsab Da, Subhro Da, Souvik Da and Lusaka Di. I have thoroughly enjoyed the hour long group discussions that along with the tensed decision making sessions also used to include many refreshing anecdotes. Snigdha Da, the flag bearer of our group, possesses magical skills in analytic calculation as well as numerics. Without his help, the obstacles would have been insurmountable. It was Mahatsab Da with whom I first stepped into the domain of research. From teaching me *Mathematica* to helping me in manuscript writing, his sincere guidance helped me to a great extent. I am thankful to Mahatsab da and Subhro Da for sharing their personal experiences with me which enriched me a lot. Apart from my group, the other group I have been strongly correlated with, is Munshi Sir's group. I have been a part of many fruitful discussions with Aritra Da, Aminul Da, Aritra, Ritesh and Bithika. I am grateful to Munshi Sir for helping me every time I approached. I am also thankful to Sabyasachi Da for his important suggestions and academic discussions which helped me in many aspects. I thank Sudip Da, Rajani Da and Souvik Da for standing by me in the time of need. I like to thank my junior Debabrata, Ritesh and Bithika and my batch-mates Anway, Suman, Bhaskar and Bipasha. Their questions, comments and opinions corrected my misconceptions time and again and motivated me the most. I specially like to thank Bipasha who taught me the importance of self-assessment. I would like to thank my beloved sister Upala, my dear juniors Promita, Dipali, Anindita, Tanmay, Arindam and my dearest friends The Great Pracheta and Bithika, the wonderful singers Arannya and Chaitrali Di, and Supriyo the boss for cheering me up in times of my distress. I acknowledge the help and support I got from my juniors Pritam, Wadut and Gaurab. I thank all the 249ers for making this journey an incredible one. Also, special cheers to my batchmates Anway, Suman, and Gaurab for the wonderful time they gifted me. I would like to thank all the members of our SINP library, canteen and CARE facilities for their constant support. Finally, I owe everything to my beloved *parents*, my *sister* and my adorable niece.

Contents

List of Figures

Chapter 5

Summary and Conclusions

The main focus of the thesis has been the modification of hadronic properties in presence of a uniform background magnetic field having magnitude typically of the order of m_π^2. Among the hadrons, specifically nucleons and neutral ρ mesons have been studied in two different contexts. More explicitly, nucleons are considered in the study of vacuum to nuclear matter phase transitions as discussed in chapter 3 whereas the main motivation for studying the spectral properties of ρ^0 (presented in chapter 4) is to investigate the magnetic field effects on the $\rho^0 \to \pi^+\pi^-$ decay in presence of a hot and dense medium.

The study related to nucleons considers Walecka model with mean field approximation in presence of weak external background magnetic field. The most important feature of the study is the incorporation of the anomalous magnetic moment of nucleons which brings in non-trivial correction terms in the nucleon propagators. As a result, unlike the case with vanishing magnetic moment, it is observed that the critical temperature decreases with the external magnetic field. Thus, it can be inferred that in presence of external magnetic field, the anomalous magnetic moment of the nucleons plays a crucial role in characterizing the nature of vacuum to nuclear matter transition at finite temperature and density. It should be mentioned here that Haber et.al [146] had speculated that the incorporation of AMM could counteract the effect of magnetic catalysis [153]. Our study not only supports the speculation but also concludes that the effect is significant enough to alter the qualitative behavior of the nucleon effective mass even in weak magnetic field regime. However, it should be noted here that the weak field approximation actually restricts the regime of validity of the present study. The maximum value of the external magnetic field used in the present study is taken to be 0.04 GeV^2 and it has been argued to be considered as ‘weak’ only up to density 1.8 ρ_0 where the assumption of ‘weakness’ is fixed by the condition that the chosen external field has to remain less than 50% of the effective mass. One should also notice that in case of

Walecka model, MC or IMC can only be seen indirectly. Similar studies in extended linear sigma model might be interesting as in that case the possibility of (approximate) chiral symmetry restoration is incorporated within the model framework. However, we should also mention that in case of zero magnetic moment, only the quantitative difference in the behavior of the effective mass is found to be attributed to the presence of the chiral partners [146] whereas the qualitative behavior, which has been the main interest throughout our work, seems to show model independence. Before applying the present results to obtain the characteristics of compact stars such as mass radius relationship or the equation of state, beta equilibrium and charge neutrality conditions have to be properly incorporated which can be an important extension of the present study.

The main observation in the study of neutral ρ meson is that at certain critical value of magnetic field, the decay width for $\rho^0 \to \pi^+\pi^-$ channel vanishes. The magnitude of the critical magnetic field depends on the temperature (T) and baryon chemical potential (μ_B) and is different for the two decay modes. Though the corresponding variation of the critical field with T and μ_B shows increasing trend for large baryonic chemical potential, there exists a maximum value of μ_B below which the temperature dependence gets reversed.

In Ref. [168], charged rho meson condensation has been studied at finite temperature and density. For charged rho mesons, the critical field for which the vector meson mass vanishes is observed to lie in the range of 0.2-0.6 GeV^2 at zero density with temperature in the range 0.2-0.5 GeV. However, in case of ρ^0, the absence of the trivial Landau shift in the energy eigenvalue results in much slower decrease in the effective mass. As a consequence, unrealistically high magnetic field values are required to observe neutral rho condensation in presence of temperature and medium (see Fig.4.14). In this scenario, the suppression in the $\rho^0 \to \pi^+\pi^-$ channel can serve as an important alternative. However, one has to remember that the magnetic modification of rho meson properties studied in this work deals with effective hadronic interactions. Thus, the observable modification can only occur if the initial burst of magnetic field survives up to hadronization retaining an appreciable field strength. However, the recent report [201] suggests no detectable suppression in the branching ratio of $\rho^0 \to \pi^+\pi^-$ channel implying that the magnetic field effects in the neutral ρ decay is negligible in HIC experiments. On the other hand, the present study can be relevant in situations present inside magnetars.

Summary

In this thesis, the hadronic spectral properties are studied in presence of two non-trivial backgrounds: one is the presence of background medium which is assumed to be in thermal equilibrium and another is the presence of uniform magnetic field having magnitude typically of the order of m_π^2. The main focus of the thesis is to analyze the modification of effective mass of hadrons, specifically nucleons and neutral ρ mesons in presence of finite temperature and magnetic field. Nucleons are considered in the study of vacuum to nuclear matter phase transitions whereas the spectral properties of ρ^0 is studied to investigate the magnetic field effects on the $\rho^0 \to \pi^+\pi^-$ decay in presence of a hot and dense medium. The temperature/density and the magnetic field intensity considered in these theoretical works possess significant relevance in the studies of strongly interacting matter created in the ultra-relativistic heavy ion collison experiments at RHIC and LHC as well as in the studies of magnetars.

The study related to nucleons considers Walecka model with mean field approximation in presence of weak external background magnetic field. The most important feature of the study is the incorporation of the anomalous magnetic moment of nucleons. For this purpose, the weak field expansion of the fermion propagator including the anomalous magnetic moment, is derived for the first time up to second order in external magnetic field. It is observed that the anomalous magnetic moment brings in non-trivial correction terms in the nucleon propagators. Implementing the derived propagator in the one loop self energy, it is found that, unlike the case with vanishing magnetic moment, the critical temperature of vacuum to nuclear matter phase transition decreases with the external magnetic field. Though in this case, it occurs in an entirely different system, the decreasing nature of the critical temperature is similar to the inverse magnetic catalysis of the chiral/de-confinement phase transition observed in LQCD studies. The study establishes that it is the incorporation of the anomalous magnetic moments of the nucleons that changes the qualitative nature of the phase transition. On the other hand, in the study of neutral ρ meson, the complete Landau quantized propagators are used to obtain the one loop self energy. For this purpose, the effective $\rho\pi\pi$ and ρNN interactions are considered. Two main aspects of the study is the introduction of an improved regularization procedure which is used to extract eB-dependent vacuum part of the self energy and the step by step formulation of the general Lorentz structure for the in-medium vector boson polarization tensor. The procedures are quite general and can be implemented in similar studies with other gauge bosons such as photons and gluons. The main observation in this study is that, at certain critical value of the background magnetic field, the decay width for $\rho^0 \to \pi^+\pi^-$ channel vanishes. The magnitude of the critical magnetic field depends on the temperature (T) and baryon chemical potential (μ_B) and is observed to be different for the two decay modes. Though the corresponding variation of the critical field with T and μ_B shows increasing trend for large baryonic chemical potential, there exists a maximum value of μ_B below which the temperature dependence gets reversed suggesting a possibility of observing suppression in the $\rho^0 \to \pi^+\pi^-$ decay channel.

Chapter 1

Introduction

1.1 Heavy-Ion Collisions

In the framework of the standard model (SM) of particle physics, the strong interaction between the quarks and gluons is described by quantum chromodynamics(QCD) which is a non-abelian gauge field theory based on color $SU(3)$ gauge symmetry. One of the most remarkable properties of QCD is the *color confinement* for which the detection of any isolated quark or gluon is forbidden. Instead of isolated manifestation, the colorful quarks bind together to form colorless hadrons which we observe in nature. However, QCD predicts that at high temperature and(or) density, the hadronic matter undergoes a phase transition. As a consequence, a new state of matter is created where the hadrons, loosing individual identities, dissolve into their constituents. The existence of such a deconfined state has been conjectured in the mid-seventies [1, 2] just two years after the fascinating discovery of *asymptotic freedom* [3, 4] that predicts the weakening of the inter-quark forces at short distances. In high temperature studies of QCD, it is found that unlike the vacuum fluctuations of gluon fields that provide anti-screening, thermal fluctuations lead to *debye screening* of the inter-quark potential which is familiar in case of the classical electromagnetic plasma systems. This novel state of matter with quarks and gluons as degrees of freedom is known as *quark-gluon plasma*(QGP)[5].

The deconfined QGP state of matter is expected to be present in the early universe during the first few microseconds after the big bang and may also exist in the cores of compact stars [6] where highest possible densities of nature can be found. Understanding such strongly interacting matter at extreme conditions is important for several reasons. For example, the commonly accepted scenario of the evolution of the universe suggests that, since its creation, the universe has gone through a series of first or second order phase transitions which are associated with the spontaneous symmetry breaking of the non-abelian gauge fields [7]. In the standard model of particle physics we have two such transitions, one is the electroweak symmetry breaking at temperatures of a few hundred GeV and other is the transition from quark matter(QM) to hadronic matter that occurs at temperatures of the order of hundred MeV. Apart from this confinement-deconfinement phase transition, spontaneous chiral symmetry breaking occurs also at the same temperature scale and is related to the dynamical generation of constituent quark mass. As the chiral symmetry is an exact symmetry of QCD lagrangian only for massless quarks, at higher temperatures, the restoration of chiral symmetry is only approximate. While the mass generation of elementary particles is explained by the Higgs mechanism, studies of such QCD phase transition gives insights into the mechanism of mass generation of hadrons. As the initial condition for nucleosynthesis is the hadronic phase, the nature of the QCD phase transition possesses significant importance in our current understanding of the evolution of the universe.

Ultra-relativistic heavy-ion collision experiments make it possible to create and study such extreme state of matter. Historically, the quest for producing QGP under laboratory conditions has started in the late 1980s at the European Center for Nuclear Research known by its French abbreviation CERN (Geneva, Switzerland) and Brookhaven National Laboratory (BNL) [8, 9]. In the year 2000, CERN announced circumstantial evidence for the creation of a new state of matter in Pb + Pb collisions [10]. However, the real discovery of QGP took place in 2005, when first five years of measurements of Au + Au collisions at the Relativistic Heavy Ion Collider (RHIC) at BNL is announced [11–14]. The deconfined matter produced is found to be the strongly coupled quark-gluon plasma (sQGP), which, having unexpectedly small viscosity to entropy density ratio, lies among “the most perfect fluids” known in nature. Since 2010, a new era of precision measurements in understanding QCD at high temperatures has started with LHC providing Pb–Pb collisions at the energies more than an order of magnitude larger than RHIC, thereby allowing us to explore to temperatures well beyond what needed for the creation of QGP. A huge collection of measurements starting from the the first run of LHC, from 2009 to 2013, with pp collisions at $\sqrt{s}$ from 0.9 to 8 TeV, p-Pb collisions at $\sqrt{s_{NN}} = 5.02$ TeV, and Pb-Pb collisions at $\sqrt{s_{NN}} = 2.76$ TeV to the second run with pp collisions at $\sqrt{s} = 13$ TeV and Pb–Pb collisions at $\sqrt{s_{NN}} = 5.02$ TeV have substantially enriched our knowledge. A comprehensive view of the current understanding of the results as well as future perspectives can be found in Refs. [15–24] and in the vast collection of references therein.

1.2 Phases of QCD

One of the major goals of ultra-relativistic heavy-ion collisions is to unravel the structure of the entire phase diagram of the strongly interacting matter. Though QCD allows the application of perturbative methods at extremely high temperatures (T) and/or baryonic chemical potential (μ_B), the underlying mechanism related to phase transions at intermediate values of T and μ_B belongs to the non-perturbative regime. As a consequence, familiar perturbative methods fail to describe a large sector of the QCD phase diagram. One of the possible ways to study QCD in non-perturbative regime is to take recourse to the functional approaches using Dyson-Schwinger Equation(DSE) and Bethe-Salpeter Equation (BSE) [25, 26]. In general, the functional approaches require a truncation procedure so that the infinite system of equations can be restricted to a level which can be handled numerically. Another possible first principle approach is to implement numerical QCD simulations on four dimensional discretized space-time lattice, known as lattice quantum chromodynamics(LQCD) [27, 28].

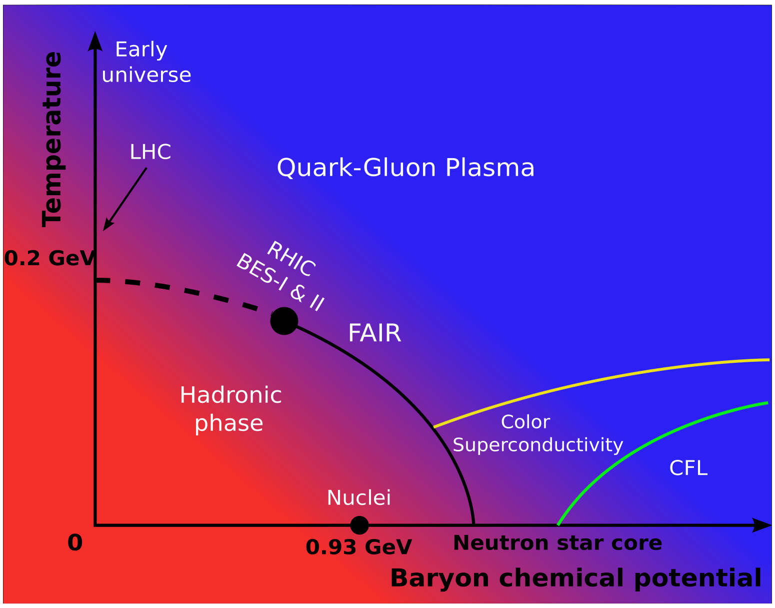

Figure 1.1: Schematic phase structure of different phases of the strongly interacting matter.

Over the years, lattice QCD has emerged as the most successful non-perturbative framework to study QCD in the strong coupling regime. Precise lattice results for hadronic masses and decay widths, having excellent agreement with experimental values [29] justify its applicability in the study of the strongly interacting matter under extreme conditions. However, there exist few shortcomings in the LQCD framework. Perhaps, the most important of those is the well known *sign problem* for which the LQCD methods can not be applied in case of finite baryonic chemical potential. So far, though several procedures have been developed to circumvent this problem, the issue remains an active area of research [30]. The most widely used procedure is the Taylor series expansion method with which probing the low chemical potential region becomes possible. On the other hand, effective models provide a reliable alternative framework to investigate the whole QCD phase structure. In general, whenever a natural separation of energy scale is possible for the phenomenon under investigation, the effective description becomes useful. Time and again, different effective model descriptions are proposed and confronted with lattice results of thermodynamic observables like pressure, trace anomaly, entropy density, sound velocity, fluctuations and correlation of conserved charges and so on. Indeed, effective descriptions like the Hadron Resonance Gas (HRG) model [31–37], Polyakov loop extended version of Nambu–Jona-Lasinio (PNJL) [38–41] model as well as Polyakov loop extended Quark-Meson (PQM) model [42–44] have achieved considerable success in explaining the lattice data as well as giving insights into the finite baryon density region of the phase diagram schematically shown in Fig. 1.1.

At zero baryonic chemical potential, LQCD simulations with physical quark masses suggest that the transition from ordinary hadronic matter to the QGP is an analytic transition, known as crossover [45–47]. As a consequence, the order parameteres for the phase transions are only approximate. The approximate order parameter for the deconfinement phase transition is the renormalized Polyakov loop whereas renormalized quark condensate plays the similar role for the chiral phase transition. In case of crossover transitions, as there is no characteristic singular behavior, a unique critical temperature can not be defined. However, pseudocritical temperature can be defined from the location of inflexion points or peak positions of thermodynamic observables. It is observed that different observables correspond to different pseudocritical transition temperatures [45, 48, 49]. In recent studies with 2+1 flavour QCD incorporating physical quark masses, a span of temperature from 147 to 157 MeV is obtained from different chiral observables [50]. On the other extreme of the phase diagram that is with low temperatures and high values of baryonic chemical potential, color superconducting (CSC) and color flavor locked (CFL) phases [51–53] may appear which play important role in the studies of equation of state of comapct stars. Different approaches at finite μ_B suggests that the phase transition from hadronic to CSC matter is a first order phase transition (shown as black solid line in Fig. 1.1) and remains to be so between hadronic and QGP phase up to the *critical end point* (CEP) where the phase transition changes its nature and becomes a crossover. One of the major objectives of the Beam Energy Scan

(BES-I and II) programme at RHIC is the experimental discovery of QCD critical point [54, 55]. Other experimental endeavours like the Facility of Anti-proton and Ion Research (FAIR) at GSI and the Nucotron-based Ion Collider Facility (NICA) at JINR will further enrich our understanding of the colder and denser regimes of the phase diagram. Ref. [56] provides the theoretical overview of our current understanding of the QCD phase structure whereas recent progresses in experimental side as well as future opportunities in relativistic heavy-ion physics are reviewed in Ref. [57].

1.3 Extreme states of matter in presence of background magnetic field

Different external parameters can influence the characteristics of the QCD phase diagram. One such parameter is the external magnetic field which has gained significant research interests in recent years. There exists compelling experimental evidences for the existence of large scale magnetization in galaxies, clusters and super-clusters indicating the existence of primordial seed fields in the early universe. The origin of such primordial magnetic fields [58, 59] is still an active area of research [60–62]. Imprints of cosmological magnetic fields on the temperature and the polarization anisotropies of the cosmic microwave background radiation (CMBR) can provide useful insights in the generation of the cosmological magnetic fields [63–66]. Furthermore, the strong magnetic fields might have played a significant role in several important phenomena in the early universe [67].

Strong magnetic fields also possess astrophysical consequences. The effect of external magnetic fields in the dense phases of the strongly interacting matter [68–75] is extremely important in the studies of compact stars [76–79] as they are also the sources of the strongest magnetic fields observed in nature. While the surface magnetic field of radio pulsars is of the order of 10^{13}–10^{14} G [80], in the inner core of *magnetars* [81–83], magnetic field strength may reach up to 10^{20} G depending upon the core constituents [84]. In presence of such strong uniform magnetic field, the longitudinal and transverse pressure with respect to the magnetic field direction are no longer degenerate and the equation of state becomes anisotropic. As, it is the equation of state that determines the global properties of neutron stars [85, 86], studies of magnetic field modification should play a crucial role in the analysis and interpretation of astrophysical observations related to the neutron stars.

A terrestrial source of extremely strong magnetic field is the non-central heavy-ion collision experiments where magnitude of the produced magnetic field can be of the order of 10^{18}–10^{19} G in RHIC and even larger at LHC [87–91]. The magnitude and time evolution of the produced field depends on various parameters like the collision energy, impact parameter, the conductivity of the medium and so on [92–94]. So far, magnetic influences on various observables have been studied [95–99]. However, complete understanding of the consequences of the strong magnetic field on the evolution of QGP requires relativistic magneto-hydrodynamic framework which is still under active investigation [100–102]. Apart from the magnetic field, electric fields of similar magnitudes can also be generated in HIC due to the event-by-event fluctuations [90, 91]. Electric fields can also be generated in case of asymmetric collisions as discussed in Refs. [103–105].

On one hand, electromagnetic fields of extreme intensities are generated in HIC experiments, on the other hand, the extreme temperatures achieved in heavy ion collisions provide very large sphaleron transition rate which can generate P and CP-odd domains in QGP [87]. The electromagnetic fields in presence of such P and CP-odd domains can give rise to various anomalous transport phenomena such as *chiral magnetic effect*(CME) [106], *chiral separation effect*(CSE) [107, 108], *chiral electric separation effect*(CESE) [109, 110], *chiral magnetic wave*(CMW) [111], *chiral vortical effect*(CVE) [112] and so on which have attracted significant amount of contemporary research interests. Review of theoretical understanding as well as experimental searches of different anomalous transports can be found in Refs. [113–117].

As already mentioned, the background magnetic fields can have remarkable influences on the QCD phase diagram. At vanishing chemical potential, modification due to the presence of magnetic background can be obtained from first principle using lattice QCD simulations [118, 119] which shows monotonic increase in critical temperature with the increasing magnetic field. The effects of external magnetic field on the chiral phase transition has been studied using different effective models in recent years [120–133]. As discussed earlier, effective theories are employed to describe the low energy behavior of the strong interaction. In such a theory, the condensate is described as the non-zero expectation value of the sigma field which is basically a composite operator of two quark fields. Now, if the condensate is already present without any background field, the effect of its enhancement in presence of the external magnetic field is described as *magnetic catalysis* (MC). Effective field theoretic models in general contain a few parameters which can be fixed from experimental inputs. Although most of the model calculations are in support of MC, some lattice results had shown inverse magnetic catalysis (IMC) where critical temperature follows the opposite trend [134–137]. It was pointed out in [138] that IMC is attributed to the dominance of the sea contribution over the valence contribution of the quark condensate. The sea effect has not been incorporated even in the Polyakov loop extended versions of Nambu–Jona-Lasinio (PNJL) model and Quark-Meson(PQM) model which might be a possible reason for the disagreement. To investigate the apparent contradiction, a significant amount of work has been done in quest of proper modifications of the effective models, most of which are focused on the magnetic field dependence of the coupling constants or other magnetic field dependent parameters in the model. A comprehensive list of literature in this line can be found in the review article [139].

1.4 Work Outline

This thesis essentially concerns with the thermo-magnetic modification of hadronic properties. More specifically, only the nucleons and neutral ρ mesons are considered. The modifications arising from the background medium as well as external magnetic fields are incorporated through one loop self energy with modified propagators. The derivation of the thermal propagators are common in the literature. Some excellent monographs with detailed descriptions of thermal field theory methods are collected in Refs. [140–144] which can be considered for this purpose. However, at each chapter, the expressions of the real time propagators to be used, are explicitly mentioned for completeness. Since the seminal work by *Julian Schwinger* "On gauge invariance and vacuum polarization" [145], bosonic and fermionic propagators in presence of magnetic fields have been extensively used in the literature. It is well known that in presence of uniform background magnetic fields, the translational invariance of the propagators is lost. The Momentum space representation of the translationally invariant part now becomes a sum over infinite number of Landau levels. In chapter 2, the detailed derivation of fermion propagator in presence of background magnetic field is discussed. Though, bosonic propagators are also used in the study of ρ^0, only the fermion propagator is considered in detail as the method of obtaining the bosonic propagator remains essentially similar. Rather, the bosonic case is comparatively less involved than the fermionic case where the presence of the anti-commutating Dirac matrices brings in additional complicacies. However, it should be mentioned that the derivation of the fermionic propagator presented here is not new and in principle, only serves the purpose of completeness.

In chapter 3, we discuss the effect of external magnetic field on nucleon mass at finite temperature and density. In the context of nuclear physics, the MC effect was first discussed by Haber et al in Ref. [146]. There, the effect of background magnetic field on the transition between vacuum to nuclear matter at zero temperature was studied using the Walecka model [147] as well as the extended linear sigma model. The study includes the B-dependent Dirac sea contribution of the free energy density which was ignored previously (see for example [148–156]) in the case of magnetized nuclear matter. Following the renormalization procedure similar to the case of magnetized quark matter, the cut-off dependence of the B-dependent sea contribution is absorbed into a renormalized magnetic field and a renormalized electric charge. The onset of the vacuum to nuclear matter phase transition is determined by equating the corresponding free energies. From the qualitative agreement between the two models, it is evident that with the proper incorporation of the magnetic catalysis effect, the creation of the nuclear matter becomes energetically more expensive in presence of the background magnetic field. However, there exist an important qualitative difference between the two models. As the analysis suggests, only in case of the Walecka model, there exists a region where the critical chemical potential for the vacuum to nuclear matter transition is lower than the same in the absence of the background field. This feature has surprising similarities with the *inverse magnetic catalysis*(IMC) shown in NJL and holographic Sakai-Sugimoto model [157]. It is interesting to see whether similar feature exists also in a more generalized scenario. Now, as the anomalous magnetic moment (AMM) of the nucleons has not been taken into account in the analysis, an obvious generalization will be to incorporate it in the study of vacuum to nuclear matter phase transition under external magnetic field at non-zero temperature. A recent study [158] incorporating the magnetic field dependent vacuum in presence of finite temperature and density, however, shows that the AMM of charged fermions makes no significant contribution to the equation of state at any external field value. Thus, among others, it will be interesting to see whether MC persists in the presence of anomalous magnetic moment.

In our work [159], we restrict ourselves only in the "weak" field regime of the external magnetic field and use the Walecka model to describe the nucleon-nucleon interaction. In this model, the interaction between the nucleons are described by the exchange of scalar (σ) and vector(ω) mesons. More realistic extension of the Walecka model where the self-interactions of the meson fields are also considered, is ignored here for the sake of simplicity as they hardly contribute to the qualitative nature of the results presented in here. Now, to obtain the effective mass of the nucleons, instead of minimizing the free energy density with respect to the condensate [146], we calculate the effective nucleon propagator by summing up the scalar and vector tadpole diagrams self-consistently. In that case, the effective mass of the nucleon appears as a pole of the effective nucleon propagator. In case of weak magnetic field, the nucleon propagator can be expressed as a series in powers of qB and κB where q and κ represent the charge and the anomalous magnetic moment of the nucleons. It should be mentioned here that in the calculation of the tadpole diagrams using the interacting propagator, we employ mean field approximation. It is essentially equivalent to solving the meson field equations with the replacement of the meson field operators by their expectation values. In other words, under this approximation, the meson field operators are rendered into classical fields assumed to be uniform in space and time and the fluctuation around this background is neglected.

Spectral properties of neutral ρ meson is discussed in chapter 4. Such studies of effective mass and dispersion relations of ρ meson are important in the context of magnetic field induced vacuum superconductivity [160–167]. Using NJL model in presence of magnetic background, Liu. et.al. have shown that the charged rho condensation in vacuum occurs at critical magnetic field $eB_c \sim 0.2\text{GeV}^2$ [166]. Generalization of the study to finite temperature and density shows that the condensation survives even in presence of finite temperature and density [168]. At vanishing chemical potential, the corresponding critical magnetic field is observed to lie in the range 0.2 -0.6 GeV^2 for temperatures in between 0.2-0.5 GeV. However, the neutral ρ meson in vacuum, having no trivial Landau shifts in the energy eigenvalue, shows a slow decrease in the effective mass [169] in weak magnetic field region. Thus, if neutral rho condensation is possible, extremely large magnetic field values will be required to observe the condensation. It should be mentioned here that it has been shown using NJL model that the effective mass of ρ^0 meson in fact increases at higher values of magnetic fields showing no possibility of condensation [166]. In this scenario, $\rho^0 \to \pi^+\pi^-$ decay may serve as an important probe to observe the influence of the magnetic field. As argued in Ref. [160], even if point like ρ^0 meson is considered without any influence by magnetic field, there exists a critical value of the external magnetic field for which the ρ^0 to $\pi^+\pi^-$ decay stops due to the trivial enhancement of the charged pion mass. Later the magnetic modification arising from the loop corrections are taken into account at weak [169, 170] as well as at strong field limits [171] at zero temperature. An immediate generalization of the previous works will be to incorporate the medium effects of the ρ^0 meson which may reflect in the modification of the decay rate and the required critical magnetic field. It should be noted here that apart from being important in the study of dense hadronic matter at extreme conditions usually expected to be present within compact stars, the incorporation of the medium effects is also essential for the proper estimation of pion production in non-central heavy ion collisions.

In our work [172] we focus on the temperature and density modifications of neutral

ρ meson properties in presence of a static homogeneous magnetic background. The one loop self energy of ρ meson is calculated for the effective $\rho\pi\pi$ and ρNN interaction with magnetically modified pion and nucleon propagators corresponding to general field strength. After decomposing the self energy in terms of the form factors, the decay width for $\rho^0 \to \pi^+\pi^-$ channel is obtained. It should be mentioned here that the spectral properties of rho meson in presence of finite temperature and magnetic field have been studied in our earlier work [173]. However, unlike the previous case, dimensional regularization technique is used here to extract the ultraviolet divergence as pole singularities of gamma and Hurwitz zeta functions[174]. Also, instead of considering only the spin averaged thermal self energy contribution, the general Lorentz structure has been addressed in detail. Apart from the technical differences, the density dependence arising from the charged nucleon loop serves as the most important extension of the previous study. Its importance can be understood as follows. It is well known that the general expression of decay width is related to the imaginary part of the self energy. Now, as far as the $\rho^0 \to \pi^+\pi^-$ decay is concerned, the invariant mass regime of interest does not allow the nucleon loop to directly contribute to the imaginary part as the unitary cut threshold of NN loop begins at much higher value. However, it should be noted that in the rest frame of the decaying particle, the decay width depends on its effective mass. The contribution from the nucleon loop incorporates significant modification in the effective mass of ρ^0 which in turn influences the decay. As we shall see, the critical field required to stabilize the neutral ρ against the $\pi^+\pi^-$ decay has a non-trivial dependence on the baryonic chemical potential. Finally, in chapter 5, the thesis concludes with a brief summary of the presented work.

Chapter 2

Fermion Propagator in presence of magnetic field

Fermion propagator in presence of external electro-magnetic field is obtained in the seminal work *"On gauge invariance and vacuum polarization"* [145] by *Julian Schwinger* in 1951. The propagator in that case is represented as an integral over proper time variable. However, the integral can be manipulated in such a way that the propagator becomes an infinite sum over Landau levels which is familiar in the conventional non-relativistic quantum mechanics of electron gas in external magnetic field. The infinite sum can be reorganized to be expressed as a power series of external field strength also known as *weak field expansion* [175]. There exists different approaches to obtain the fermion propagator in presence of external magnetic fields. Among them, *Ritus eigenfunction method* is another widely used approach [176–181]. Here, unlike the mentioned approaches, we will follow mainly Ref. [182]. In this approach, the sum over Landau levels arises simply from the completeness relation of the wave-functions which are basically the solutions of the Dirac equation in presence of constant external magnetic field. It is needless to say, the Schwinger proper time integral representation can be deduced from *Ritus method* [179] as well as from our approach [182] with simple manipulations.

2.1 Derivation of the Green's function

As already mentioned, our aim is to obtain the propagator using *Green's function* approach. Specifically, we want to solve the Dirac equation in presence of a constant external magnetic field with a delta source i.e

$$(i\not{D} - m)S(x, x') = i\delta^4(x - x')$$

$$(i\partial\!\!\!/ - eA\!\!\!/ - m)S(x,x') = i\delta^4(x-x') \tag{2.1}$$

where we have used the definition

$$D\!\!\!\!/ \;=\; \partial\!\!\!/ + ieA\!\!\!/ \tag{2.2}$$

More explicitely, with $A^0 = 0$, we have

$$\Big[i\gamma^0\frac{\partial}{\partial t} - \big(-i\gamma^1\frac{\partial}{\partial x^1} - e\gamma^1 A^1 - i\gamma^2\frac{\partial}{\partial x^2} - e\gamma^2 A^2\big) \\ - (-i\gamma^3\frac{\partial}{\partial x^3} - e\gamma^3 A^3) - m\Big]S(x,x') = i\delta^4(x-x') \tag{2.3}$$

where the convention used is given by

$$\begin{aligned} x^\mu &\equiv (x^0, x^1, x^2, x^3) \equiv (t, x, y, z) \\ x_\mu &\equiv (x_0, x_1, x_2, x_3) \equiv (x^0, -x^1, -x^2, -x^3) \\ p^2 &\equiv p^y \equiv -p_2 \end{aligned} \tag{2.4}$$

and now choosing the gauge as $\mathbf{A} \equiv (0, Bx^1, 0)$ and with the definitions

$$\Pi^i_\perp = -i\frac{\partial}{\partial x^i} - eA^i \tag{2.5}$$

$$\boldsymbol{\Pi}_\perp \cdot \boldsymbol{\gamma}_\perp = \Pi^1\gamma^1 + \Pi^2\gamma^2 \tag{2.6}$$

we find

$$\Big[i\gamma^0\partial_t - \boldsymbol{\Pi}_\perp \cdot \boldsymbol{\gamma}_\perp - \gamma^3\Pi^3 - m\Big]S(x,x') \;=\; i\delta^4(x-x')\;. \tag{2.7}$$

We can Fourier transform the delta function in terms of plane waves in time and x^3 variables as they do not contain any position or time dependence except in the form of derivatives. Thus putting

$$\delta^4(x-x') = \int \frac{d\omega}{2\pi}\frac{dp^3}{2\pi} e^{-i\omega(t-t')} e^{ip^3(x^3-x^{3'})}\delta^2(\boldsymbol{r}_\perp - \boldsymbol{r}'_\perp) \tag{2.8}$$

$$S(x,x') = \int \frac{d\omega}{2\pi}\frac{dp^3}{2\pi} e^{-i\omega(t-t')} e^{ip^3(x^3-x^{3'})} S(\omega, p^3; \boldsymbol{r}_\perp, \boldsymbol{r}'_\perp) \tag{2.9}$$

we obtain

$$S(\omega, p^3; \boldsymbol{r}_\perp, \boldsymbol{r}'_\perp) = i\Big[\gamma^0\omega - (\boldsymbol{\Pi}_\perp \cdot \boldsymbol{\gamma}_\perp) - \gamma^3 p^3 - m\Big]^{-1} \delta^2(\boldsymbol{r}_\perp - \boldsymbol{r}'_\perp) \; . \tag{2.10}$$

We can simplify the above expression as

$$\begin{aligned} S(\omega, p^3; \boldsymbol{r}_\perp, \boldsymbol{r}'_\perp) &= i\frac{\gamma^0\omega - (\boldsymbol{\Pi}_\perp \cdot \boldsymbol{\gamma}_\perp) - \gamma^3 p^3 + m}{\big[\gamma^0\omega - (\boldsymbol{\Pi}_\perp \cdot \boldsymbol{\gamma}_\perp) - \gamma^3 p^3 + m\big]\big[\gamma^0\omega - (\boldsymbol{\Pi}_\perp \cdot \boldsymbol{\gamma}_\perp) - \gamma^3 p^3 - m\big]}\delta^2(\boldsymbol{r}_\perp - \boldsymbol{r}'_\perp) \\ &= i\frac{\gamma^0\omega - (\boldsymbol{\Pi}_\perp \cdot \boldsymbol{\gamma}_\perp) - \gamma^3 p^3 + m}{\omega^2 - p^{3^2} - m^2 + (\boldsymbol{\Pi}_\perp \cdot \boldsymbol{\gamma}_\perp)^2}\delta^2(\boldsymbol{r}_\perp - \boldsymbol{r}'_\perp) \end{aligned} \tag{2.11}$$

where after multiplication, all the cross terms vanish from the denominator because of the anti-commutation relation among of gamma matrices. Now, we need to express the δ function in terms of the completeness relation of the wave function obtained by solving the *Dirac equation* in presence of magnetic field. We only need here the spatio-temporal part of the wave-function and not the entire spinor and its two dimensional portion is given by

$$\psi_{kp_2}(\boldsymbol{r}_\perp) = \frac{1}{\sqrt{2\pi\ell}}\frac{1}{\sqrt{2^k k!\sqrt{\pi}}}H_k\Big(\frac{x^1}{\ell} + p_2\ell\Big)e^{-\frac{1}{2\ell^2}(x^1 + p_2\ell^2)^2}e^{-is_\perp x^2 p_2} \tag{2.12}$$

where $\ell = \frac{1}{\sqrt{|eB|}}$ and $s_\perp = sgn(eB)$. One may notice that the form of the wave-function can be defined with a minus sign in the argument of the *Hermite* polynomial and in that case using $H_k(-x) = (-1)^k H_k(x)$ we should have an overall factor $(-1)^k$ multiplied with our definition of ψ_{kp_2}. But this will not matter in the analysis as we are always going to start from the completeness relation where two ψ_{kp_2} s are multiplied and that makes overall factor $(-1)^{2k} = 1$. Now, using this wave-function we can write the Dirac delta function as

$$\delta^2(\boldsymbol{r}_\perp - \boldsymbol{r}'_\perp) = \int_{-\infty}^{\infty} dp_2 \sum_{k=0}^{k=\infty} \psi_{kp_2}(\boldsymbol{r}_\perp)\psi^*_{kp_2}(\boldsymbol{r}'_\perp) \; . \tag{2.13}$$

Another relation we need is

$$\begin{aligned} (\boldsymbol{\Pi}_\perp \cdot \boldsymbol{\gamma}_\perp)^2 &= (\Pi^1\gamma^1 + \Pi^2\gamma^2)(\Pi^1\gamma^1 + \Pi^2\gamma^2) \\ &= -\Pi^{1^2} - \Pi^{2^2} + \Pi^1\gamma^1\Pi^2\gamma^2 + \Pi^2\gamma^2\Pi^1\gamma^1 \\ &= -\boldsymbol{\Pi}_\perp^2 + [\Pi^1, \Pi^2]\gamma^1\gamma^2 \\ &= -\boldsymbol{\Pi}_\perp^2 + ieB\gamma^1\gamma^2 \end{aligned} \tag{2.14}$$

We need this relation as we are going to use the fact that the ψ_{kp_2} is the eigenfunction of the operator $\mathbf{\Pi}_\perp^2$ with eigenvalue $\frac{2k+1}{\ell^2}$. Now as the operator can be simply replaced with its eigenvalue when operating on its eigenbasis, we have the following simplification

$$\begin{aligned} S(\omega, p^3; \boldsymbol{r}_\perp, \boldsymbol{r}'_\perp) &= i\int_{-\infty}^{\infty} dp_2 \sum_{k=0}^{k=\infty} \frac{\gamma^0\omega - \gamma^3 p^3 + m}{\omega^2 - p^{3^2} - m^2 - (2k+1)|eB| + ieB\gamma^1\gamma^2} \psi_{kp_2}(\boldsymbol{r}_\perp)\psi^*_{kp_2}(\boldsymbol{r}'_\perp) \\ &- i\int_{-\infty}^{\infty} dp_2 \sum_{k=0}^{k=\infty} \frac{\mathbf{\Pi}_\perp \cdot \boldsymbol{\gamma}_\perp}{\omega^2 - p^{3^2} - m^2 - (2k+1)|eB| + ieB\gamma^1\gamma^2} \psi_{kp_2}(\boldsymbol{r}_\perp)\psi^*_{kp_2}(\boldsymbol{r}'_\perp) \\ &= E1(\omega, p^3; \boldsymbol{r}_\perp, \boldsymbol{r}'_\perp) - E2(\omega, p^3; \boldsymbol{r}_\perp, \boldsymbol{r}'_\perp) \; . \end{aligned} \tag{2.15}$$

Before evaluating the individual Expressions we need a few more relations regarding the operator $\mathbf{\Pi}_\perp \cdot \boldsymbol{\gamma}_\perp$ and also we have not shown the eigenvalue of $\mathbf{\Pi}_\perp^2$. But again to obtain them, first we should verify the completeness relation used. These are discussed in Appendix A. Using the relations the first term can be simplified as

$$\begin{aligned} E1(\omega, p^3; \boldsymbol{r}_\perp, \boldsymbol{r}'_\perp) &= i\frac{e^{i\Phi(\boldsymbol{r}_\perp,\boldsymbol{r}'_\perp)}}{2\pi\ell^2} e^{-\frac{\zeta}{2}} \sum_{k=0}^{k=\infty} \frac{\gamma^0\omega - \gamma^3 p^3 + m}{\omega^2 - p^{3^2} - m^2 - (2k+1)|eB| + ieB\gamma^1\gamma^2} \mathrm{L}_k(\zeta) \\ &= i\frac{e^{i\Phi(\boldsymbol{r}_\perp,\boldsymbol{r}'_\perp)}}{2\pi\ell^2} e^{-\frac{\zeta}{2}} \sum_{k=0}^{k=\infty} \frac{\gamma^0\omega - \gamma^3 p^3 + m}{\omega^2 - p^{3^2} - m^2 - (2k+1)|eB| + s_\perp s|eB|} \mathrm{L}_k(\zeta) \end{aligned} \tag{2.16}$$

where

$$\Phi(\boldsymbol{r}_\perp, \boldsymbol{r}'_\perp) = s_\perp \frac{(x^1 + x^{1'})(x^2 - x^{2'})}{2\ell^2} \tag{2.17}$$

$$\zeta = \frac{(x^1 - x^{1'})^2 + (x^2 - x^{2'})^2}{2\ell^2} = \frac{(\boldsymbol{r}_\perp - \boldsymbol{r}'_\perp)^2}{2\ell^2} \; . \tag{2.18}$$

Now, we can not specify here the spin direction and charge as we have considered only the two dimensional wave function not the Dirac spinors. The wave function is in fact a part of them i.e $U_\pm$ spinor or $V_\pm$ spinor with $\pm$ denoting the spin directions. As $i\gamma^1\gamma^2 = \Sigma^{12}$, in that case, s takes into account the spin directions.

Let us take $s_\perp = +1$. In that case :

- $s = +1$:

$$\omega^2 - p^{3^2} - m^2 - (2k+1)|eB| + |eB| = \omega^2 - p^{3^2} - m^2 - 2k|eB| \tag{2.19}$$

So $k = n$ in this case. We can replace then $\mathrm{L}_k(\zeta) \equiv \mathrm{L}_n(\zeta)$.

- $s = -1$:

$$\omega^2 - p^{3^2} - m^2 - (2k+1)|eB| - |eB| \quad = \quad \omega^2 - p^{3^2} - m^2 - 2(k+1)|eB| \quad (2.20)$$

So $k+1 = n$ in this case. We can replace then $\mathrm{L}_k(\zeta) \equiv \mathrm{L}_{n-1}(\zeta)$.

Thus to write it in a compact notation we can use $\mathrm{L}_k(\zeta) \equiv \mathrm{L}_n(\zeta)\mathcal{P}_+ + \mathrm{L}_{n-1}(\zeta)\mathcal{P}_-$. This notation is valid also in case of $s_\perp = -1$ as in that case the $\mathcal{P}_+$ behaves as $\mathcal{P}_-$. Finally we have

$$E1(\omega, p^3; \boldsymbol{r}_\perp, \boldsymbol{r}'_\perp) = i\frac{e^{i\Phi(\boldsymbol{r}_\perp,\boldsymbol{r}'_\perp)}}{2\pi\ell^2} e^{-\frac{\zeta}{2}} \sum_{n=0}^{n=\infty} \frac{\gamma^0\omega - \gamma^3 p^3 + m}{\omega^2 - p^{3^2} - m^2 - 2n|eB|} \Big[\mathrm{L}_n(\zeta)\mathcal{P}_+ + \mathrm{L}_{n-1}(\zeta)\mathcal{P}_-\Big] . \tag{2.21}$$

In case of the second part we obtain

$$\begin{aligned} E2(\omega, p^3; \boldsymbol{r}_\perp, \boldsymbol{r}'_\perp) = i\frac{e^{i\Phi(\boldsymbol{r}_\perp,\boldsymbol{r}'_\perp)}}{2\pi\ell^2} e^{-\frac{\zeta}{2}} &\sum_{k=0}^{k=\infty} \frac{1}{\omega^2 - p^{3^2} - m^2 - (2k+1)|eB| + ieB\gamma^1\gamma^2} \frac{i\gamma^1}{\ell} \\ &\times \Big[2y\mathrm{L}^1_k(\zeta)\mathcal{P}_- - 2z\mathrm{L}^1_{k-1}(\zeta)\mathcal{P}_+\Big] . \end{aligned} \tag{2.22}$$

Now, if we take $s_\perp = +1$ then for $s = +1$ we know from the consideration of the denominator that if one wants to replace the sum to sum over n instead of k then she/he has to put $k = n$ and if $s = -1$ then $k = n - 1$. However, from the numerator, we have the factor $\frac{i\gamma^1}{\ell}\Big[2y\mathrm{L}^1_k(\zeta)\mathcal{P}_- - 2z\mathrm{L}^1_{k-1}(\zeta)\mathcal{P}_+\Big]$. The consideration of this factor suggests that in both of the cases we can represent the numerator as $\frac{i}{\ell^2}\boldsymbol{\gamma}_\perp \cdot (\boldsymbol{r}_\perp - \boldsymbol{r}'_\perp)\mathrm{L}^1_{n-1}(\zeta)$. Similarly, same expression can be shown to be valid even for $s_\perp = -1$ case(as in that case the $\mathcal{P}_\pm$ operators interchange among each other). Thus the final expression in terms of sum over n for this part is given by

$$\begin{aligned} E2(\omega, p^3; \boldsymbol{r}_\perp, \boldsymbol{r}'_\perp) &= i\frac{e^{i\Phi(\boldsymbol{r}_\perp,\boldsymbol{r}'_\perp)}}{2\pi\ell^2} e^{-\frac{\zeta}{2}} \sum_{n=0}^{n=\infty} \frac{1}{\omega^2 - p^{3^2} - m^2 - 2n|eB|} \\ &\times \Big[\frac{i}{\ell^2}\boldsymbol{\gamma}_\perp \cdot (\boldsymbol{r}_\perp - \boldsymbol{r}'_\perp)\mathrm{L}^1_{n-1}(\zeta)\Big] . \end{aligned} \tag{2.23}$$

Combining with the expression from (2.21) we get

$$\begin{aligned} S(\omega, p^3; \boldsymbol{r}_\perp, \boldsymbol{r}'_\perp) &= i\frac{e^{i\Phi(\boldsymbol{r}_\perp,\boldsymbol{r}'_\perp)}}{2\pi\ell^2} e^{-\frac{\zeta}{2}} \sum_{n=0}^{n=\infty} \frac{1}{\omega^2 - p^{3^2} - m^2 - 2n|eB|} \\ &\times \Big[\big(\gamma^0\omega - \gamma^3 p^3 + m\big)\big(\mathrm{L}_n(\zeta)\mathcal{P}_+ + \mathrm{L}_{n-1}(\zeta)\mathcal{P}_-\big) \end{aligned}$$

$$- \frac{i}{\ell^2}\boldsymbol{\gamma}_\perp \cdot (\boldsymbol{r}_\perp - \boldsymbol{r}'_\perp)\mathrm{L}^1_{n-1}(\zeta)\Big] \,. \tag{2.24}$$

It should be noted that the final form of the propagator possess a translationally non-invariant phase factor $\Phi(\boldsymbol{r}_\perp, \boldsymbol{r}'_\perp)$. Apart from this multiplicative phase, the rest of the expression is translationally invariant i.e it depends on $\boldsymbol{r}_\perp$ and $\boldsymbol{r}'_\perp$ only in the combination $\boldsymbol{r}_\perp - \boldsymbol{r}'_\perp$. Whether one needs to consider this non-trivial phase factor depends on the particular loop integral involving the propagator(s). A discussion on this can be found in Ref. [175]. It should be mentioned here, in all the applications presented in the thesis, the translationally non-invariant phase factor will not play any roll and only the momentum space representation of the translationally invariant part will be used.

2.2 Fourier transformation of the trnaslationally invariant part

To obtain the momentum space representation we need to Fourier transform the translationally invariant part of the mixed representation of the fermion propagator i.e Eq. (2.25). Let us put $\boldsymbol{r}'_\perp = 0$ and denote the conjugate momentum variable for x^1 and x^2 as p^1 and p^2 respectively. Thus we have to Fourier transform

$$\begin{aligned} \tilde{S}(\omega, p^3; \boldsymbol{r}_\perp) &= i\frac{e^{-\frac{\zeta}{2}}}{2\pi\ell^2}\sum_{n=0}^{n=\infty}\frac{1}{\omega^2 - p^{3^2} - m^2 - 2n|eB|} \\ &\times \Big[\big(\gamma^0\omega - \gamma^3 p^3 + m\big)\big(\mathrm{L}_n(\zeta)\mathcal{P}_+ + \mathrm{L}_{n-1}(\zeta)\mathcal{P}_-\big) \\ &- \frac{i}{\ell^2}\boldsymbol{\gamma}_\perp \cdot (\boldsymbol{r}_\perp - \boldsymbol{r}'_\perp)\mathrm{L}^1_{n-1}(\zeta)\Big] \end{aligned} \tag{2.25}$$

where $\zeta = \frac{\boldsymbol{r}_\perp^2}{2\ell^2}$. In this regard we require two different kinds of integrals. One of them is given by

$$\begin{aligned} I_n &= \int dx^2 \int dx^1 e^{-ip^1x^1} e^{-ip^2x^2} e^{-\frac{(x^1)^2}{4\ell^2}} e^{-\frac{(x^2)^2}{4\ell^2}} \mathrm{L}_n(\zeta) \\ &= e^{-p_\perp^2\ell^2} \int dx^1 \int dx^2 e^{-\frac{1}{4\ell^2}(x^1+2ip^1\ell^2)^2} e^{-\frac{1}{4\ell^2}(x^2+2ip^2\ell^2)^2} \mathrm{L}_n\Big[\frac{(x^1)^2+(x^2)^2}{2\ell^2}\Big] \,. \end{aligned} \tag{2.26}$$

At this point one can perform a variable transformation of the form :

$$x^1 = 2\ell r\cos\theta, \quad x^2 = 2\ell r\sin\theta, \quad dx^1dx^2 = 4\ell^2 r dr d\theta \,. \tag{2.27}$$

Note that here r is a dimensionless quantity. With the variable transformation, we now have

$$I_n = e^{-p_\perp^2\ell^2} 4\ell^2 \int_0^\infty r dr e^{-(r^2-\ell^2 p_\perp^2)} \mathrm{L}_n(2r^2) \int_0^{2\pi} d\theta e^{-2i\ell r(p^1\cos\theta + p^2\sin\theta)} \tag{2.28}$$

Using the result

$$\int_0^{2\pi} d\theta e^{-ia(b\cos\theta + c\sin\theta)} = 2\pi J_0\big(a\sqrt{b^2+c^2}\big) \tag{2.29}$$

the integral becomes

$$I_n = 8\pi\ell^2 \int_0^\infty r dr e^{-(r^2-\ell^2 p_\perp^2)} \mathrm{L}_n(2r^2) J_0\big(2\ell p_\perp r\big) \ . \tag{2.30}$$

To compute the r integral one can use [183]

$$\int_0^\infty dx \ x e^{-\frac{1}{2}\alpha x^2} \mathrm{L}_n\Big[\frac{1}{2}\beta x^2\Big] J_0(xy) = \frac{(\alpha-\beta)^n}{\alpha^{n+1}} e^{-\frac{y^2}{2\alpha}} \mathrm{L}_n\Big[\frac{\beta y^2}{2\alpha(\beta-\alpha)}\Big], \quad y>0, \ \mathrm{Re}\ \alpha > 0 \ . \tag{2.31}$$

In our case with $\alpha = 2$, $\beta = 4$ and $y = 2\ell p_\perp$ we obtain

$$I_n = 4\pi\ell^2(-1)^n e^{-\ell^2 p_\perp^2} \mathrm{L}_n\big[2\ell^2 p_\perp^2\big] \ . \tag{2.32}$$

Apart from this we need another integral to obtain the fourier transform of $(\boldsymbol{r}_\perp.\boldsymbol{\gamma}_\perp)\mathrm{L}_{n-1}^1(\zeta)$. The procedure remains exactly similar. However, in that case, the θ and r integral requires different identities as listed below [183]:

$$\begin{aligned}
\int_0^{2\pi} d\theta \cos\theta \ e^{-2ir\ell(p^1\cos\theta+p^2\sin\theta)} &= \frac{2\pi}{i} J_1\big(2\ell r p_\perp\big)\frac{p^1}{p_\perp} \\
\int_0^{2\pi} d\theta \sin\theta \ e^{-2ir\ell(p^1\cos\theta+p^2\sin\theta)} &= \frac{2\pi}{i} J_1\big(2\ell r p_\perp\big)\frac{p^2}{p_\perp} \\
\int_0^\infty dx x^{\nu+1} e^{-\beta x^2} \mathrm{L}_n^\nu\big[\alpha x^2\big] J_\nu(xy) &= 2^{-\nu-1}\beta^{-\nu-n-1}(\beta-\alpha)^n y^\nu e^{-\frac{y^2}{4\beta}} \mathrm{L}_n^\nu\Big[\frac{\alpha y^2}{4\beta(\alpha-\beta)}\Big] \ .
\end{aligned} \tag{2.33}$$

Thus, after performing the r integrals one obtains the momentum space representation of the translationally invariant part given by

$$\tilde{S}(\omega, p^3; \mathbf{p}_\perp) = 2ie^{-p_\perp^2\ell^2} \sum_{n=0}^\infty \frac{(-1)^n \mathcal{D}_n(\omega, p^3; \mathbf{p}_\perp)}{\omega^2 - p^{3^2} - m^2 - 2n|eB|} \tag{2.34}$$

with $\mathcal{D}_n(\omega, p^3; \mathbf{p}_\perp) = (\gamma^0\omega - \gamma^3 p^3 + m)\Big[L_n\big[2\ell^2 p_\perp^2\big]\mathcal{P}_+ - L_{n-1}\big[2\ell^2 p_\perp^2\big]\mathcal{P}_-\Big] + 2(\boldsymbol{\gamma}_\perp\cdot\mathbf{p}_\perp)\mathrm{L}_{n-1}^1\big[2\ell^2 p_\perp^2\big]$.

Chapter 3

Effect of external magnetic field on nucleon mass

In this chapter, vacuum to nuclear matter phase transition has been studied in presence of constant external background magnetic field under the mean field approximation of Walecka model. The anomalous nucleon magnetic moment has been taken into account using the modified "weak" field expansion of the fermion propagator having non-trivial correction terms for charged as well as for the neutral particles. The effect of nucleon magnetic moment is found to favour the magnetic catalysis effect at zero temperature and zero baryon density. However, the critical temperature, at which the effective nucleon mass suffers a sudden decrease corresponding to the vacuum to nuclear medium phase transition, is observed to decrease with the external magnetic field which can be identified as the inverse magnetic catalysis in Walecka model.

The chapter is organized as follows: The essential steps to obtain the weak field expanded propagators of the charged and neutral fermion with non-zero magnetic moment is described in Sec. 3.1. The suitable form of the corresponding thermal propagators are also discussed which are used to obtain the effective mass of the nucleons in case of Walecka model described in Sec. 3.2. Sec. 3.3 contains the numerical results and discussions. Finally a summary is added in Sec. 3.4. Some of the relevant calculational details are provided in the Appendix.

3.1 Fermion propagator with anomalous magnetic moment

The Dirac equation with anomalous magnetic moment (κ) in the momentum space representation is given by [184, 185]

$$\left[\not{p} - \frac{i}{2}qF^{\mu\nu}\gamma_\mu\frac{\partial}{\partial p^\nu} - m_f - \frac{1}{2}\kappa\sigma\cdot F\right]S_B(p) = 1. \tag{3.1}$$

The strategy to obtain the power expansion is to write

$$S_B = S_0 + S_1. \tag{3.2}$$

where S_0 represents the vacuum propagator and S_1 represents its linear order correction in presence of external magnetic field. Now, let us define the operator

$$\hat{O} = \left[\frac{i}{2}qF^{\mu\nu}\gamma_\mu\frac{\partial}{\partial p^\nu} + \frac{1}{2}\kappa\sigma\cdot F\right] \tag{3.3}$$

Using the perturbative expansion in the Dirac equation and neglecting the higher order $\hat{O}S_1$ term one obtains

$$S_1 = S_0\hat{O}S_0. \tag{3.4}$$

Thus the linear order correction to the weak expansion of the propagator is nothing but an operator of non-commutative gamma matrices and differentials sandwiched between the familiar vacuum propagators. Following the similar strategy one can extend the series to higher order terms in powers of B. As we shall see that in our case, the leading order contribution of the external magnetic field occurs due to the quadratic correction of the weak field propagator and not due to the simpler linear order one, we must extend the perturbative series as

$$S_B = S_0 + S_1 + S_2 \tag{3.5}$$

for which one obtains

$$S_2 = S_0\hat{O}S_1 \tag{3.6}$$

where $S_1 = S_0 \hat{O} S_0$ is given by (see [184, 185])

$$
\begin{aligned}
S_1 &= \frac{1}{(p^2 - m_f^2 + i\epsilon)^2} \\
&\times \Big[qB\gamma_5 \big[(p\cdot b)\not{u} - (p\cdot u)\not{b} + m_f \not{u}\not{b}\big] + \kappa B \big[(\not{p} + m_f)\gamma_5 \not{u}\not{b}(\not{p} + m_f)\big]\Big]
\end{aligned} \tag{3.7}
$$

with $u^\mu \equiv (1,0,0,0)$ and $b^\mu \equiv (0,0,0,1)$ in the fluid rest frame. It is straightforward to derive the expression of S_2 (see Appendix B for details). After plugging the correction terms we finally obtain the weak field expansion of the fermion propagator given by

$$
\begin{aligned}
S_B(p,m) &= \frac{-(\not{p}+m)}{p^2 - m^2 + i\epsilon} + (qB)\frac{i\gamma^1\gamma^2\left(\not{p}_\parallel + m\right)}{\left(p^2 - m^2 + i\epsilon\right)^2} + (\kappa B)\frac{(\not{p}+m)\, i\gamma^1\gamma^2\,(\not{p}+m)}{\left(p^2 - m^2 + i\epsilon\right)^2} \\
&+ (qB)^2 \frac{-2\left\{p_\perp^2\left(\not{p}_\parallel + m\right) - \not{p}_\perp\left(p_\parallel^2 - m^2\right)\right\}}{\left(p^2 - m^2 + i\epsilon\right)^4} + (qB)(\kappa B)\frac{-4\not{p}_\parallel\left(\not{p}_\parallel + m\right) + p^2 - m^2}{\left(p^2 - m^2 + i\epsilon\right)^3} \\
&+ (\kappa B)^2 \frac{-(\not{p}+m)\left(\not{p}_\parallel - \not{p}_\perp + m\right)(\not{p}+m)}{\left(p^2 - m^2 + i\epsilon\right)^3} + \mathcal{O}\left(B^3\right) .
\end{aligned} \tag{3.8}
$$

In order to express $S_B(p,m)$ in a more compact form, we use the procedure given in Ref. [186] and write

$$
\left(\frac{-1}{p^2 - m^2 + i\epsilon}\right)^n = \hat{A}_{n-1}\Delta_F(p, m_1)\Big|_{m_1 = m} \tag{3.9}
$$

where,

$$
\Delta_F(p,m) = \left(\frac{-1}{p^2 - m^2 + i\epsilon}\right) \tag{3.10}
$$

and

$$
\hat{A}_n = \frac{(-1)^n}{n!}\frac{\partial^n}{\partial\left(m_1^2\right)^n} . \tag{3.11}
$$

Using Eqs. (3.9)-(3.11), we can rewrite Eq. (3.8) as

$$
S_B(p,m) = \hat{F}(p,m,m_1)\,\Delta_F(p,m_1)\Big|_{m_1=m} \tag{3.12}
$$

where,

$$
\hat{F}(p,m,m_1) = (\not{p}+m) + (qB)\, i\gamma^1\gamma^2\left(\not{p}_\parallel + m\right)\hat{A}_1 + (\kappa B)(\not{p}+m)\, i\gamma^1\gamma^2\,(\not{p}+m)\,\hat{A}_1
$$

$$
\begin{aligned}
&-2\,(qB)^2\left\{p_\perp^2\left(\not{p}_\parallel+m\right)-\not{p}_\perp\left(p_\parallel^2-m^2\right)\right\}\hat{A}_3\\
&+(qB)\,(\kappa B)\left\{4\not{p}_\parallel\left(\not{p}_\parallel+m\right)-p^2+m^2\right\}\hat{A}_2\\
&+(\kappa B)^2\,(\not{p}+m)\left(\not{p}_\parallel-\not{p}_\perp+m\right)(\not{p}+m)\,\hat{A}_2+\mathcal{O}\left(B^3\right)\ .
\end{aligned}
\tag{3.13}
$$

The 11-component of the thermal propagator in this case can be written as [187],

$$
S_{11}\,(p,m)=S_B\,(p)-\eta\,(p\cdot u)\left[S_B\,(p)-\gamma^0 S_B^\dagger\,(p)\,\gamma^0\right]
\tag{3.14}
$$

where,

$$
\eta\,(p\cdot u)=\Theta\,(p\cdot u)\,f_+\,(p\cdot u)+\Theta\,(-p\cdot u)\,f_-\,(-p\cdot u)
\tag{3.15}
$$

with

$$
f_\pm\,(p\cdot u)=\left[\exp\left(\frac{p\cdot u\mp\mu}{T}\right)+1\right]^{-1}\ .
\tag{3.16}
$$

Substituting Eq. (3.12) into Eq. (3.14) and using the fact that $\gamma^0\hat{F}^\dagger\,(p,m,m_1)\,\gamma^0=\hat{F}\,(p,m,m_1)$, we get

$$
S_{11}\,(p,m)=\hat{F}\,(p,m,m_1)\left[\,\Delta_F\,(p,m_1)-2\pi i\eta\,(p\cdot u)\,\delta\left(p^2-m_1^2\right)\right]\Big|_{m_1=m}
\tag{3.17}
$$

3.2 Effective mass of nucleon in Walecka model

The propagation of nucleons in hot and dense nuclear matter is well described using Quantum Hadrodynamics (QHD) details of which can be found in Ref. [188, 189]. We briefly summarize the main the formalism of QHD at *zero magnetic field*. We start with the real time thermal propagator matrix of the nucleon [140, 141],

$$
\boldsymbol{S}_0\,(p,m_N)=(\not{p}+m_N)\,\boldsymbol{V}\begin{bmatrix}\Delta_F\,(p,m_N) & 0\\ 0 & -\Delta_F^*\,(p,m_N)\end{bmatrix}\boldsymbol{V}
\tag{3.18}
$$

where the diagonalizing matrix $\boldsymbol{V}$ is given by,

$$
\boldsymbol{V}=\begin{bmatrix}N_2 & -N_1e^{\beta\mu/2}\\ N_1e^{-\beta\mu/2} & N_2\end{bmatrix}
\tag{3.19}
$$

with

$$
\begin{aligned}
N_1(p\cdot u) &= \sqrt{f_+(p\cdot u)}\Theta(p\cdot u)+\sqrt{f_-(-p\cdot u)}\Theta(-p\cdot u)\\
N_2(p\cdot u) &= \sqrt{1-f_+(p\cdot u)}\Theta(p\cdot u)+\sqrt{1-f_-(-p\cdot u)}\Theta(-p\cdot u)\ .
\end{aligned}
$$

In Walecka model, the nucleons interact with the scalar meson σ and vector meson ω. The interaction Lagrangian is

$$\mathscr{L}_{QHD} = g_{\sigma NN}\bar{\Psi}\Psi\sigma - g_{\omega NN}\bar{\Psi}\gamma^\mu\Psi\omega_\mu\ , \tag{3.20}$$

where $\Psi = \begin{bmatrix} p \\ n \end{bmatrix}$ is the nucleon isospin doublet and the value of the coupling constants are given by $g_{\sigma NN} = 9.57$ and $g_{\omega NN} = 11.67$ [188]. The complete nucleon propagator matrix $\boldsymbol{S'}(p, m_N)$ in presence of these interactions is obtained from the Dyson-Schwinger equation given by,

$$\boldsymbol{S'} = \boldsymbol{S}_0 - \boldsymbol{S}_0\boldsymbol{\Sigma}\boldsymbol{S'} \tag{3.21}$$

where, $\boldsymbol{\Sigma}$ is the one-loop thermal self energy matrix of the nucleon. It can be shown that [141], the complete propagator and the self energy matrices are diagonalized by $\boldsymbol{V}$ and $\boldsymbol{V}^{-1}$ respectively. This in turn diagonalizes the Dyson-Schwinger equation and Eq. (3.21) becomes an algebraic equation (in thermal space),

$$\overline{S'} = \overline{S}_0 - \overline{S}_0\overline{\Sigma}\ \overline{S'}\ . \tag{3.22}$$

It is to be noted that, each term in the above equation is 4×4 matrix in Dirac space. Here $\overline{S}_0(p, m_N) = -(\not{p} + m_N)\Delta_F(p, m_N)$ and $\overline{\Sigma}$ is the 11-component of the matrix $\boldsymbol{V}^{-1}\boldsymbol{\Sigma}\boldsymbol{V}^{-1}$ and is called the thermal self energy function. In Walecka model the Dirac structure of $\overline{\Sigma}$ comes out to be,

$$\overline{\Sigma} = (\Sigma_s \mathbb{1} + \Sigma_v^\mu\gamma_\mu) = (\Sigma_s\mathbb{1} + \not{\Sigma}_v)\ . \tag{3.23}$$

Using Eq. (3.23), we can solve Eq. (3.22) and obtain

$$\overline{S'}(p, m_N) = (\not{P} + m_N^*)\,\Delta_F(P, m_N^*) \tag{3.24}$$

where

$$P = (p - \Sigma_v) \quad \text{and} \quad m_N^* = (m + \Sigma_s) \ . \tag{3.25}$$

We can finally write down the complete propagator matrix

$$\boldsymbol{S'}(p, m_N) = \left(\not{P} + m_N^*\right) \boldsymbol{V} \begin{bmatrix} \Delta_F(P, m_N^*) & 0 \\ 0 & -\Delta_F^*(P, m_N^*) \end{bmatrix} \boldsymbol{V} \ , \tag{3.26}$$

whose 11-component is,

$$S'_{11}(p, m_N) = S_F(P, m_N^*) - \eta(P \cdot u)\left[S_F(P, m_N^*) - \gamma^0 S_F^\dagger(P, m_N^*)\gamma^0\right] \ . \tag{3.27}$$

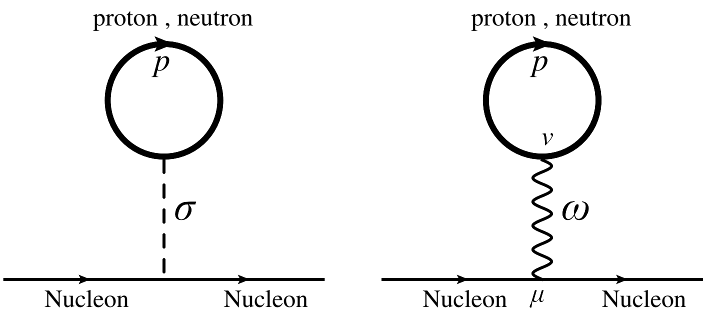

Figure 3.1: Feynman diagrams for the one-loop self energy of nucleon in Walecka model. Bold line indicates the complete/dressed propagator

Let us now calculate, the nucleon self energy function $\bar{\Sigma}$ using the interaction Lagrangian given in Eq. (3.20) and consider only the tadpole Feynman diagrams as shown in Fig. 3.1. It is to be noted that, the loop particles are dressed i.e. the propagator for the loop particles is $\boldsymbol{S'}(p, m_N)$ as given in Eq. (3.26). Applying Feynman rule to Fig. 3.1 we obtain the 11-component of the thermal self energy as,

$$\begin{aligned} \Sigma_{11} \ = \ & -\left(\frac{g_{\sigma NN}^2}{m_\sigma^2}\right) i \int \frac{d^4p}{(2\pi)^4} \mathrm{Tr}\left[S'^{(\mathrm{p})}_{11}(p, m_N) + S'^{(\mathrm{n})}_{11}(p, m_N)\right] \\ & + \gamma_\mu \left(\frac{g_{\omega NN}^2}{m_\omega^2}\right) i \int \frac{d^4p}{(2\pi)^4} \mathrm{Tr}\left[\gamma^\mu S'^{(\mathrm{p})}_{11}(p, m_N) + \gamma^\mu S'^{(\mathrm{n})}_{11}(p, m_N)\right] \end{aligned} \tag{3.28}$$

where (p) and (n) in the superscript corresponds to proton and neutron respectively. It is easy to show that $\mathrm{Re}\Sigma_{11} = \mathrm{Re}\overline{\Sigma}$. So we get from Eq. (3.23),

$$\mathrm{Re}\Sigma_s \ = \ -\left(\frac{g_{\sigma NN}^2}{m_\sigma^2}\right) \mathrm{Re}\, i \int \frac{d^4p}{(2\pi)^4} \mathrm{Tr}\left[S'^{(\mathrm{p})}_{11}(p, m_N) + S'^{(\mathrm{n})}_{11}(p, m_N)\right] \tag{3.29}$$

$$\mathrm{Re}\Sigma_v^\mu = \left(\frac{g_{\omega NN}^2}{m_\omega^2}\right) \mathrm{Re}\ i \int \frac{d^4p}{(2\pi)^4} \mathrm{Tr}\left[\gamma^\mu S_{11}^{\prime\,(\mathrm{p})}(p, m_N) + \gamma^\mu S_{11}^{\prime\,(\mathrm{n})}(p, m_N)\right] . \tag{3.30}$$

Substituting $S'_{11}(p, m_N)$ from Eq. (4.19) into Eqs. (3.29) and (3.30) and performing the dp^0 integral, we get

$$\mathrm{Re}\Sigma_s(m_N^*) = \mathrm{Re}\Sigma_s^{(\text{pure vacuum})} - \left(\frac{4g_{\sigma NN}^2 m_N^*}{m_\sigma^2}\right) \int \frac{d^3p}{(2\pi)^3} \left(\frac{1}{\Omega_p}\right) \left[N_+^p + N_-^p\right] \tag{3.31}$$

$$\mathrm{Re}\Sigma_v^\mu(m_N^*) = \left(\frac{4g_{\omega NN}^2}{m_\omega^2}\right) \int \frac{d^3p}{(2\pi)^3} \left[N_+^p - N_-^p\right] \delta_0^\mu \tag{3.32}$$

where, $\Omega_p = \sqrt{\vec{p}^2 + (m_N^*)^2}$ and

$$N_\pm^p = \left[\exp\left(\frac{\Omega_p \mp \mu}{T}\right) + 1\right]^{-1} . \tag{3.33}$$

In Eq. (3.31), $\mathrm{Re}\Sigma_s^{(\text{pure vacuum})}$ is given by

$$\mathrm{Re}\Sigma_s^{(\text{pure vacuum})} = \left(\frac{8m_N^* g_{\sigma NN}^2}{m_\sigma^2}\right) \mathrm{Re}\ i \int \frac{d^4p}{(2\pi)^4} \left[\frac{1}{p^2 - (m_N^*)^2 + i\epsilon}\right] . \tag{3.34}$$

We will neglect the contribution of vacuum self energy term $\mathrm{Re}\Sigma_s^{(\text{pure vacuum})}$ in Eq. (3.31) following the Mean Field Theory (MFT) [188] approach.

The effective mass of the nucleon (m_N^*) can be calculated from the pole of the complete nucleon propagator which essentially means solving the self consistent equation,

$$m_N^* = m_N + \mathrm{Re}\Sigma_s(m_N^*) . \tag{3.35}$$

Let us now turn on the *external magnetic field*. Since we are only interested in the effective mass of nucleon, let us calculate the scalar self energy $\mathrm{Re}\Sigma_s(m_N^*)$. In this case, the proton and neutron propagators in Eq. (3.29) have to be replaced as $S'_{11}(p, m_N) \to S_{11}(P, m_N^*)$ where $S_{11}(p, m)$ is defined in Eq. (3.17). This implies,

$$\begin{aligned} S_{11}^{\prime\,(\mathrm{p,n})}(p, m_N) = {} & \hat{F}^{(\mathrm{p,n})}(P, m_N^*, m_1) \\ & \times \left[\Delta_F(P, m_1) - 2\pi i\eta (P\cdot u)\, \delta\left(P^2 - m_1^2\right)\right]\Big|_{m_1 = m_N^*} \end{aligned} \tag{3.36}$$

where $\hat{F}^{(\mathrm{p})}(p, m, m_1)$ and $\hat{F}^{(\mathrm{n})}(p, m, m_1)$ are obtained from Eq. (3.13) by replacing q and κ with the corresponding values of proton and neutron respectively i.e. for proton $q \to |e|, \kappa \to \kappa_{\mathrm{p}}$ and for neutron $q \to 0, \kappa \to \kappa_{\mathrm{n}}$. Here $|e|$ is the absolute electronic charge and the anomalous magnetic moments of proton and neutron are given by $\kappa_{\rm p} = g_{\rm p}\left(\frac{|e|}{2m_N}\right)$ and $\kappa_{\rm n} = g_{\rm n}\left(\frac{|e|}{2m_N}\right)$ respectively with $g_{\rm p} = 1.79, g_{\rm n} = -1.91$. Substituting Eq. (3.36) into Eq. (3.29), and shifting the momentum $p \to (p + \Sigma_V)$, we get

$$\mathrm{Re}\Sigma_s = \Sigma_s^{(\mathrm{vacuum})} + \Sigma_s^{(\mathrm{medium})} \tag{3.37}$$

with,

$$\Sigma_s^{(\mathrm{vacuum})} = -\left(\frac{g_{\sigma NN}^2}{m_\sigma^2}\right)\mathrm{Re}\, i\int\frac{d^4p}{(2\pi)^4}\hat{T}\left(p, m_N^*, m_1\right)\ \Delta_F\left(p, m_1\right)\Big|_{m_1=m_N^*} \tag{3.38}$$

$$\Sigma_s^{(\mathrm{medium})} = -\left(\frac{g_{\sigma NN}^2}{m_\sigma^2}\right)\int\frac{d^4p}{(2\pi)^4}\hat{T}\left(p, m_N^*, m_1\right)\ 2\pi\eta\left(p\cdot u\right)\delta\left(p^2 - m_1^2\right)\Big|_{m_1=m_N^*}. \tag{3.39}$$

In the above equations,

$$\begin{aligned}
&\hat{T}\left(p, m_N^*, m_1\right) = \mathsf{Tr}\left[\hat{F}^{(\mathrm{p})}\left(p, m_N^*, m_1\right) + \hat{F}^{(\mathrm{n})}\left(p, m_N^*, m_1\right)\right] \\
&= 8m_N^* - 8m_N^*\left(eB\right)^2 p_\perp^2\hat{A}_3 + 4m_N^*\left\{\left(\kappa_{\rm p}B\right)^2 + \left(\kappa_{\rm n}B\right)^2\right\}\left\{\left(m_N^*\right)^2 + p^2 - 2p_\perp^2 + 2p_\parallel^2\right\}\hat{A}_2 \\
&+\ 4\left(|e|\,B\right)\left(\kappa_{\rm p}B\right)\left\{\left(m_N^*\right)^2 - p^2 + 4p_\parallel^2\right\}\hat{A}_2
\end{aligned} \tag{3.40}$$

The detailed calculation of $\Sigma_s^{(\mathrm{vacuum})}$ and $\Sigma_s^{(\mathrm{medium})}$ are provided in Appendices C.1 and C.2. The expression for $\Sigma_s^{(\mathrm{vacuum})}$ can be read off Eq. (C.11) as

$$\begin{aligned}
\Sigma_s^{(\mathrm{vacuum})} = \left(\frac{g_{\sigma NN}^2}{4\pi^2 m_\sigma^2}\right)&\left[\frac{\left(eB\right)^2}{3m_N^*} + \left\{\left(\kappa_{\rm p}B\right)^2 m_N^* + \left(\kappa_{\rm n}B\right)^2 m_N^* + \left(|e|\,B\right)\left(\kappa_{\rm p}B\right)\right\}\right. \\
&\left.\times\left\{\frac{1}{2} + 2\ln\left(\frac{m_N^*}{m_N}\right)\right\}\right] .
\end{aligned} \tag{3.41}$$

The calculation of $\Sigma_s^{(\mathrm{medium})}$ is performed for two different cases separately, namely (1) the zero temperature case and (2) the finite temperature case. For *zero temperature*, we have from Eq. (C.23)

$$\begin{aligned}
\Sigma_s^{(\mathrm{medium})} = -\left(\frac{2g_{\sigma NN}^2}{\pi^2 m_\sigma^2}\right)&\left[m_N^* I_2\left(\mu_{\rm B}, m_N^*\right) + \frac{1}{3}\left(eB\right)^2 m_N^* C_1\left(\mu_{\rm B}, m_N^*\right)\right. \\
+2\left\{m_N^*\left(\kappa_{\rm p}B\right)^2 + m_N^*\left(\kappa_{\rm n}B\right)^2 + \left(|e|\,B\right)\left(\kappa_{\rm p}B\right)\right\}&\left.\left\{m_N^{*2}C_1\left(\mu_{\rm B}, m_N^*\right) + \frac{1}{3}C_2\left(\mu_{\rm B}, m_N^*\right)\right\}\right] .
\end{aligned} \tag{3.42}$$

Whereas For *finite temperature*, we have from (C.27),

$$\Sigma_s^{(\text{medium})} = -\left(\frac{2g_{\sigma NN}^2}{\pi^2 m_\sigma^2}\right)\int_0^\infty |\vec{p}|^2\, d\,|\vec{p}| \left[m_N^*\left(\tilde{C}_1^{+p}+\tilde{C}_1^{-p}\right)+\frac{2}{3}m_N^*\,(eB)^2\,|\vec{p}|^2\left(\tilde{C}_3^{+p}+\tilde{C}_3^{-p}\right)\right.$$
$$\left. +2\left(m_N^{*2}+\frac{2}{3}|\vec{p}|^2\right)\left\{m_N^*\,(\kappa_{\text{p}}B)^2+m_N^*\,(\kappa_{\text{n}}B)^2+(|e|\,B)\,(\kappa_{\text{p}}B)\right\}\left(\tilde{C}_2^{+p}+\tilde{C}_2^{-p}\right)\right] \tag{3.43}$$

The definition of the functions I_2, C_1, C_2, $\tilde{C}_1^{\pm}$, $\tilde{C}_2^{\pm}$ and $\tilde{C}_3^{\pm}$ can be found in Appendix C.2.

3.3 Numerical Results

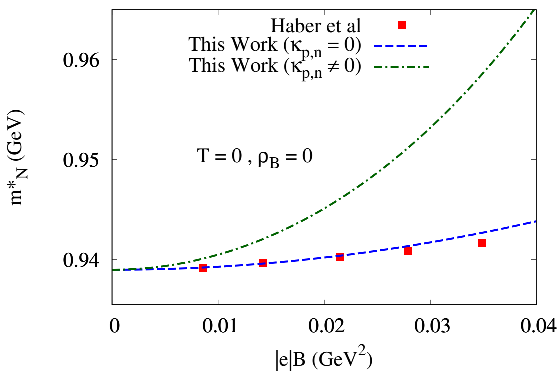

Figure 3.2: Variation of m_N^* with $|e|\,B$ at *zero temperature and zero density*. Results with and without the anomalous magnetic moment of nucleons are compared with results from Ref. [146].

We begin this section by obtaining the effective nucleon mass with external magnetic field at *zero temperature and zero density*. In this case the contribution from $\Sigma_s^{(\text{medium})} = 0$. Thus we need to solve the transcendental equation,

$$m_N^* = m_N + \Sigma_s^{(\text{vacuum})}\left(m_N^*\right) \tag{3.44}$$

where, $\Sigma_s^{(\text{vacuum})}\left(m_N^*\right)$ is given in Eq. (3.41). At first we neglect the effect of anomalous magnetic moment of nucleons so that the above equation simplifies to

$$m_N^* = m_N + \frac{g_{\sigma NN}^2\,(eB)^2}{12\pi^2 m_\sigma^2 m_N^*} \tag{3.45}$$

which can be solved analytically to obtain

$$m_N^* = \frac{1}{2}\left[m_N + \sqrt{m_N^2 + \frac{g_{\sigma NN}^2\,(eB)^2}{3\pi^2 m_\sigma^2}}\,\right]. \tag{3.46}$$

As can be seen from the above equation, the effective nucleon mass increases monotonically with the increase of eB. This enhancement is shown in Fig. 3.2 where it is also compared with the result from Ref. [146]. Though the current approach to obtain the effective nucleon mass differs from Ref. [146], there exists a noticeable quantitative agreement between the two results in the weak magnetic field regime. Now we include the anomalous magnetic moments of nucleons and solve Eq. (3.44) numerically. It is found that the incorporation of nucleon magnetic moment further increases the effective mass and this effect remains significant even in case of weak magnetic fields as shown in Fig. 3.2. In other words, the nucleon magnetic moment favors the magnetic catalysis effect at zero temperature and zero baryon density.

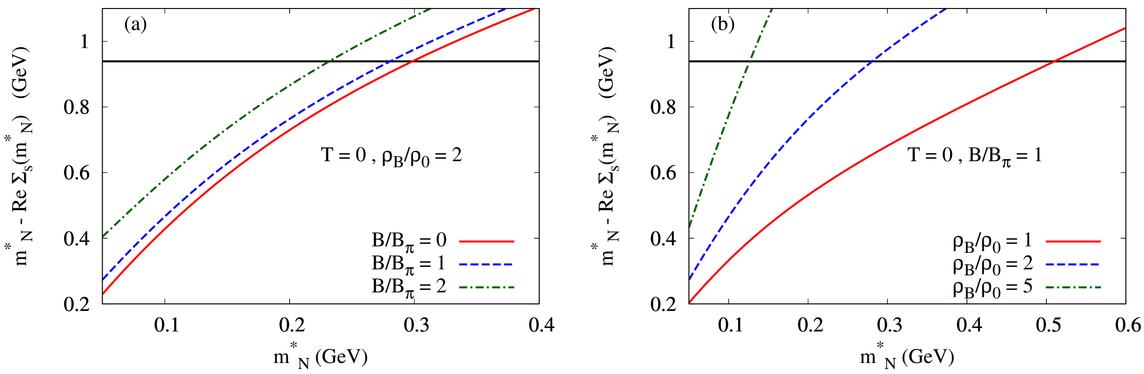

Figure 3.3: Variation of $m_N^* - \mathrm{Re}\Sigma_s\left(m_N^*\right)$ with m_N^* at *zero temperature* for (a) three different values of magnetic field ($B = 0, B_\pi, 2B_\pi$) at baryon density $\rho_{\rm B} = 2\rho_0$ (b) three different values of baryon density ($\rho_B = \rho_0, 2\rho_0, 5\rho_0$) at magnetic field ($B = B_\pi$). Here $|e|B_\pi = m_\pi^2 = 0.0196$ GeV^2 and $\rho_0 = 0.16$ fm^{-3}. The horizontal black solid line corresponds to $m_N^* = m_N = 939$ MeV.

Let us now proceed to the study of nucleon effective mass in presence of external magnetic field at *at finite baryon density* and *zero temperature*. As can be seen from Eqs. (3.41)-(3.42), the scalar self energy Σ_s is functions of magnetic field B and baryon chemical potential $\mu_{\rm B}$ of the medium. It is customary to use total baryon density $\rho_{\rm B}$ instead of $\mu_{\rm B}$ where

$$\rho_{\rm B} = 4\int \frac{d^3p}{(2\pi)^3}\Theta\left(\mu_{\rm B} - \sqrt{|\vec{p}|^2 + m_N^{*2}}\right) = \left(\frac{2}{3\pi^2}\right)\left[\mu_{\rm B}^2 - m_N^{*2}\right]^{3/2} . \tag{3.47}$$

Inverting the above equation, we get the baryon chemical potential in terms of the baryon density as

$$\mu_{\rm B} = \sqrt{\left(\frac{3\pi^2}{2}\rho_{\rm B}\right)^{2/3} + m_N^{*2}} . \tag{3.48}$$

We have expressed the strength of the magnetic field B with respect to the pion mass scale

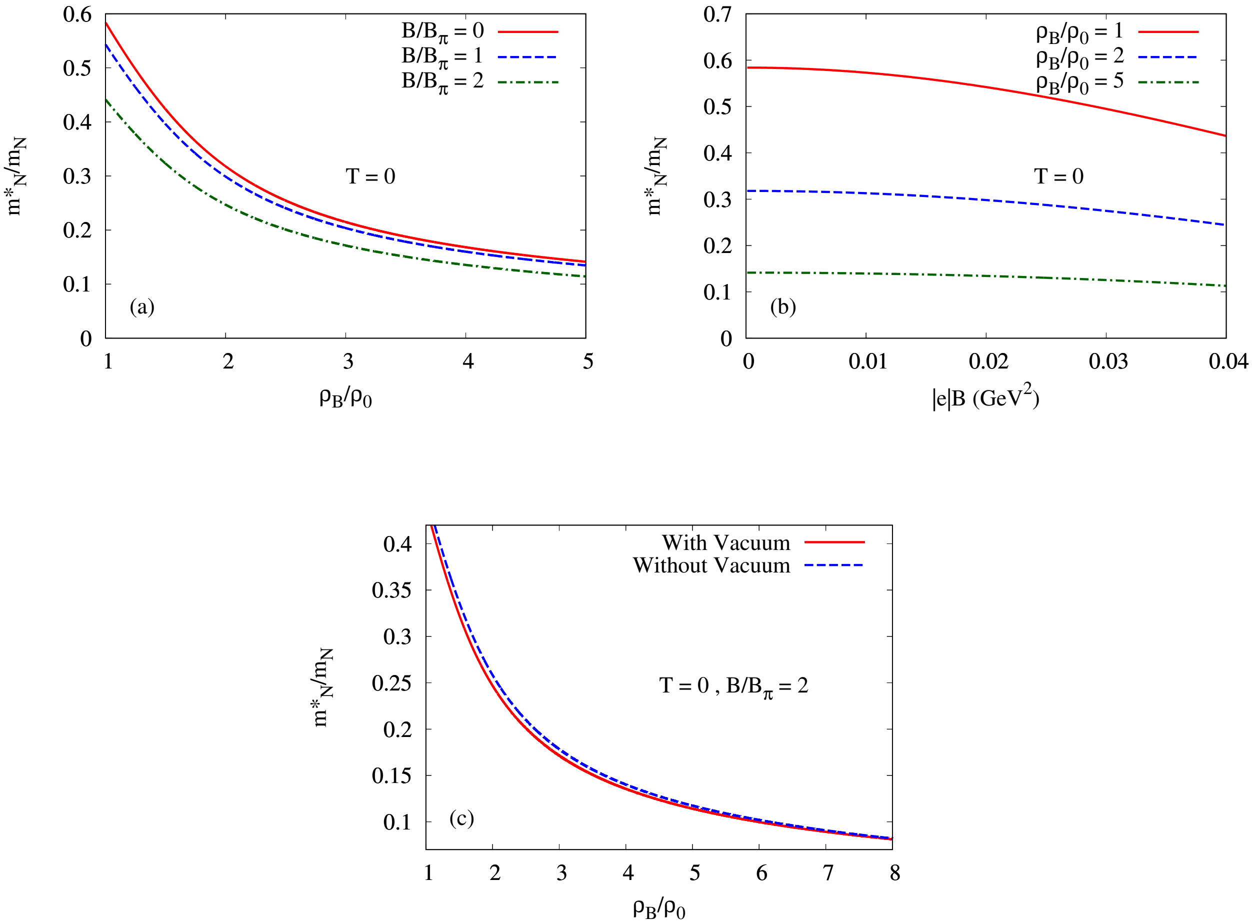

Figure 3.4: Variation of effective mass of nucleon at *zero temperature* (a) with baryon density for three different values of magnetic field ($B = 0, B_\pi, 2B_\pi$). The horizontal axis starts at $\rho_B = 0.1\rho_0$. (b) with magnetic field for three different values of baryon density ($\rho_B = \rho_0, 2\rho_0, 5\rho_0$). Here $|e|B_\pi = m_\pi^2 = 0.0196$ GeV^2 and $\rho_0 = 0.16$ fm^{-3}. (c) At $B = 2B_\pi$, the variation of the effective nucleon mass with baryon density is compared with the case where the vacuum contribution is ignored.

(B_π) defined as

$$|e|\, B_\pi = m_\pi^2 = 0.0196 \text{ GeV}^2. \tag{3.49}$$

Similarly the total baryon density ρ_B is expressed with respect to the normal nuclear matter density $\rho_0 = 0.16$ fm^{-3}.

Since we will be solving the transcendental Eq. (3.35), we first plot $m_N^* - \text{Re}\Sigma_s\,(m_N^*)$ as a function of m_N^* in Fig. 3.3. Fig. 3.3-(a) depicts the variation of this quantity at three different values of magnetic field ($B/B_\pi = 0$, 1 and 2) with baryon density $\rho_B = 2\rho_0$ whereas Fig. 3.3-(b) shows its variation at three different values of total baryon density ($\rho_B/\rho_0 = 1$, 2 and 3) with magnetic field $B = B_\pi$. The intersections of this graphs with the horizontal line corresponding to $m_N^* = m_N = 939$ MeV represent the solutions of Eq. (3.35). We notice

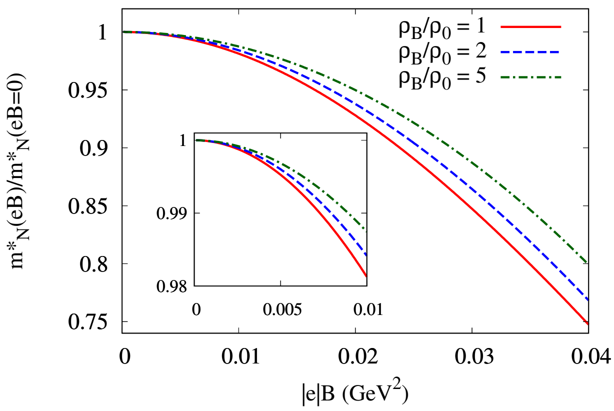

Figure 3.5: At T=0, the ratio of effective mass m^* at non-zero eB and at zero eB is plotted as a function of eB for three different values of baryon density ($\rho_B = \rho_0, 2\rho_0, 5\rho_0$). The inset plot shows the low eB region upto $eB = 0.01$ GeV^2 relevant for neutron star/magnetar case. Here $\rho_0 = 0.16$ fm^{-3}.

from these figures that $\text{Re}\Sigma\,(m_N^*)$ is always less than zero and it monotonically decreases as we increase m_N^*. Also for a particular value of m_N^*, $\text{Re}\Sigma\,(m_N^*)$ decreases with the increase of B and ρ_B. In Fig. 3.4-(a), the variation of the effective nucleon mass with baryon density has been shown at three different values of magnetic field ($B = 0, B_\pi, 2B_\pi$). As can be seen from the figure, m_N^*/m_N decreases with the increase of $\rho_{\rm B}$ and becomes less than 0.5 at $\rho_{\rm B} = 2\rho_0$. It can be checked that the contribution from the first term within the square brackets in Eq. (3.42) plays the dominant role in determining the $\rho_{\rm B}$ as well as the eB dependences of the effective mass whereas the net contribution from all the other terms in $\Sigma_s^{(\rm medium)}$ and $\Sigma_s^{(\rm vacuum)}$ (see Eq. (3.41)) remains sub-leading throughout. Also, it is clear from Fig. 3.4-(a) that, with the increase of $|e|B$, the effective mass decreases and the effect of the external magnetic field is more at a lower $\rho_{\rm B}$ region. At very high $\rho_{\rm B}(\gtrsim 5\rho_0)$ it is expected that the effect of $|e|\,B$ on nucleon effective mass becomes negligible. However, the conclusions based on the weak field approximation will not be reliable for arbitrary large or small densities as will be discussed later.

In Fig. 3.4-(b), the variation of m_N^*/m_N with $|e|\,B$ is shown at three different values of baryon density ($\rho_B = \rho_0, 2\rho_0, 5\rho_0$). We find a small decrease in effective nucleon mass with $|e|B$. In order to observe the effect of the vacuum self energy correction to the effective mass of nucleon, we have compared the density variations of m_N^* with and without the vacuum contribution as shown in Fig. 3.4(c). Here the external magnetic field is kept fixed at $B = 2B_\pi$. It has been noticed that the effect of vacuum correction is subleading with respect to the medium contribution at non-zero baryon density and the correction to m_N^* due to vacuum self energy remains less than 6%. It is also interesting to observe the relative importance of the external magnetic field on the effective nucleon mass as shown in Fig. 3.5 where the ratio $m_N^*(eB)/m_N^*(eB = 0)$ is plotted as a function of eB at three different baryon densities($\rho_B = \rho_0, 2\rho_0, 5\rho_0$). It can be noticed that m_N^* decreases by about 25% at a magnetic field $eB \sim 0.04$ GeV^2. The inset plot shows the lower eB region upto $eB = 0.01$ GeV^2 which corresponds to the typical values of magnetic field expected inside a neutron star/magnetar. At the maximum value $eB = 0.01$ GeV^2, the effective mass of nucleon is found to be lowered by less than 2%.

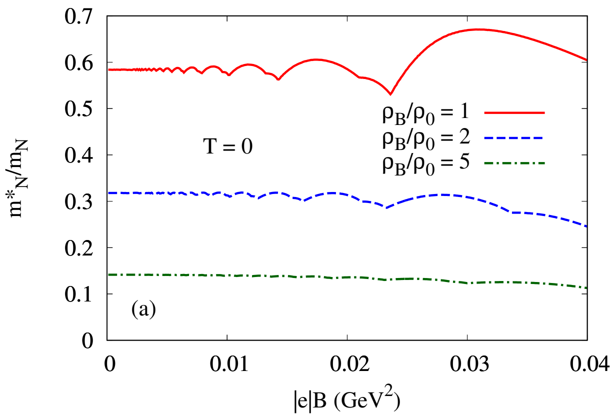

Figure 3.6: Variation of effective mass of nucleon at *zero temperature* (a) with baryon density for three different values of magnetic field ($B = 0, B_\pi, 2B_\pi$). The horizontal axis starts at $\rho_B = 0.1\rho_0$. (b) with magnetic field for three different values of baryon density ($\rho_B = \rho_0, 2\rho_0, 5\rho_0$). Here $|e|B_\pi = m_\pi^2 = 0.0196$ GeV^2 and $\rho_0 = 0.16$ fm^{-3}.

Until now we have considered that under weak field approximation, the modifications from the non-vanishing anomalous magnetic moment arise only through the effective mass. Moreover, it is assumed that the modification in the expression of proton density as a summation over Landau levels can also be ignored for weak external fields. The motivation behind this approximation lies in the fact that with smaller values of external field, the Landau levels become more and more closely spaced giving rise to a continuum at $eB \to 0$. In that case, the summations that appeared due to the Landau quantization, can be replaced by the corresponding momentum integrals giving rise to exactly similar expression for proton and neutron density in isospin symmetric matter. As a result, the expression of baryon density as given in Eq. (3.47) remains to be valid even in presence of eB as long as the external fields are sufficiently weak to make the summation to integral conversion plausible. It is advantageous to use this approximate expression to obtain the effective mass of the nucleons as, in this case, $\mu_{\rm B}$ can be analytically expressed in terms of $\rho_{\rm B}$ providing useful simplifications in the numerics. However, to check the validity of the approximations, it is reasonable to incorporate this magnetic modifications in the expression for the net baryon density which now becomes [190, 191]

$$\rho_{\rm B} = \sum_{s\in\{\pm1\}}\int\frac{d^3p}{(2\pi)^3}\Theta\left\{\mu_{\rm B}-\sqrt{p_z^2+\left(\sqrt{m_N^{*2}-p_\perp^2}-s\kappa_{\rm n}B\right)^2}\right\}$$
$$+\frac{eB}{(2\pi)^2}\sum_{s\in\{\pm1\}}\sum_{n=0}^{\infty}(1-\delta_0^n\delta_{-1}^s)\int_{-\infty}^{\infty}dp_z\Theta\left\{\mu_{\rm B}-\sqrt{p_z^2+\left(\sqrt{m_N^{*2}+2n|e|B}-s\kappa_{\rm p}B\right)^2}\right\}. \tag{3.50}$$

Performing the momentum integral in the above equation, we obtain

$$\begin{aligned}\rho_{\rm B} &= \sum_{s\in\{\pm1\}}\frac{1}{12\pi^2}\left[3\pi\mu_{\rm B}^2 s\kappa_{\rm n}B+2\sqrt{\mu_{\rm B}^2-(m_N^*-s\kappa_{\rm n}B)^2}\left\{2\mu_{\rm B}^2-2m_N^{*2}+m_N^* s\kappa_{\rm n}B+(s\kappa_{\rm n}B)^2\right\}\right.\\ &\left.+6\mu_{\rm B}^2 s\kappa_{\rm n}B\tan^{-1}\left\{\frac{s\kappa_{\rm n}B-m_N^*}{\sqrt{\mu_{\rm B}^2-(m_N^*-s\kappa_{\rm n}B)^2}}\right\}\right]\\ &+\frac{eB}{2\pi^2}\sum_{s\in\{\pm1\}}\sum_{n=0}^{n_{\rm max}}(1-\delta_0^n\delta_{-1}^s)\sqrt{\mu_{\rm B}^2-\left(\sqrt{m_N^{*2}+2n|e|B}-s\kappa_{\rm p}B\right)^2}\end{aligned} \tag{3.51}$$

where, $n_{\rm max}=\left[\frac{(\mu_{\rm B}+s\kappa_{\rm p}B)^2-m_N^{*2}}{2|e|B}\right]$ in which $[x]$ = greatest integer less than or equal to x. The above equation can not be inverted analytically in order to express μ_B as a function of ρ_B which was possible for $eB=0$ case (see Eq. (3.48)). Thus we invert the equation numerically to obtain $\mu_B=\mu_B(\rho_B,eB)$. Using the above modified ρ_B, we have re-plotted the effective mass variation with the external field for the same set of densities $\rho_B=\rho_0, 2\rho_0$ and $5\rho_0$ as shown in Fig. 3.6. The oscillating behavior is consistent with Ref. [146]. Comparison with Fig. 3.4(b) suggests that the usual baryon density expression provides the average qualitative behavior reasonably well even in presence of external magnetic field as long as the background field strength is small and the agreement is more pronounced in higher density regime. However, going to arbitrary large densities is restricted by the assumption of weak field expansion of the propagator which demands the external eB to be much smaller than m_N^{*2}. Now, apart from the external magnetic field, this effective mass depends on density as well and more importantly, the dependence is of decreasing nature. Thus, even if one starts with a constant eB much lower than m_N^{*2}, the decreasing trend of m_N^* with density invalidates this basic weak field assumption at some higher $\rho_{\rm B}$ value for which m_N^{*2} becomes comparable with the constant eB used. To estimate this density value, we fix the maximum possible value of eB to be considered as a fraction times m_N^{*2} where the fraction is chosen to be 0.5 and 0.1. The corresponding variation with respect to $\rho_{\rm B}$ are shown in Fig. 3.6(b) where the case $eB = m_N^{*2}$ is also plotted for comparison. Each of these curves in fact serves the purpose of a boundary and for a given value of ρ_{B}, only those eB values are allowed which lie below it. The horizontal lines denote the constant magnetic field values used in this work. It is clear from the figure that, once we have chosen the maximum eB curve(say $eB = 0.5m_N^{*2}$ curve), its intersection with each horizontal lines provides the maximum density (i.e around $3\rho_0$ for $B = B_\pi$ and around $1.8\rho_0$ for $B = 2B_\pi$) up to which the eB value corresponding to that line can be considered as 'weak'.

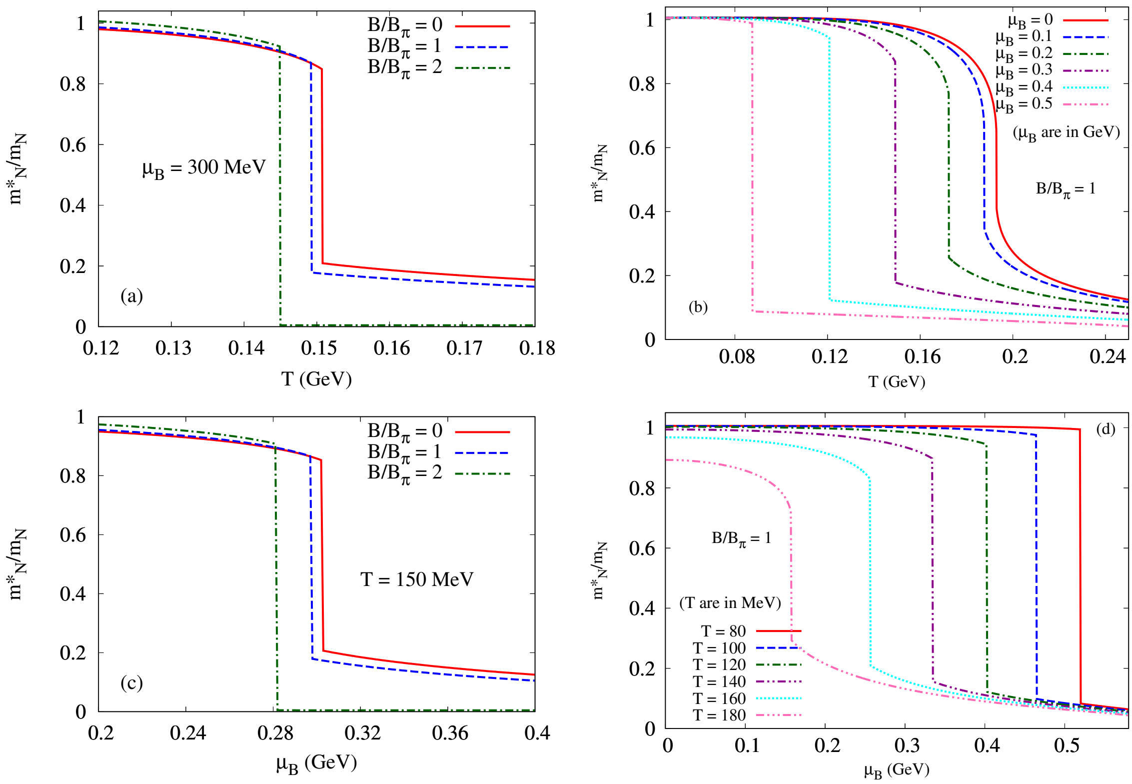

Figure 3.7: Variation of effective mass of nucleon with temperature (a) at μ_{B}=300 MeV for three different values B $(0, B_\pi$ and $2B_\pi)$ (b) at $B = B_\pi$ for six different values μ_{B} (0, 100, 200, 300, 400 and 500 MeV). Variation of effective mass of nucleon with baryon chemical potential (c) at T=150 MeV for three different values of magnetic field $(B = 0, B_\pi, 2B_\pi)$ (d) at $B = B_\pi$ for six different value of T = 80, 100, 120, 140, 160 and 180 MeV. Here $|e|B_\pi = m_\pi^2 = 0.0196$ GeV^2.

We now turn on the *temperature* and study the variation of m_N^*/m_N with temperature and baryon chemical potential in Fig. 3.7. Fig. 3.7-(a) depicts the variation of m_N^*/m_N with T at at μ_{B}=300 MeV and at three different values B $(0, B_\pi$ and $2B_\pi)$ whereas Fig. 3.7-(b) shows its variation at $B = B_\pi$ and at six different values μ_{B} (0, 100, 200, 300, 400 and 500 MeV). As can be seen from the figure, that the effective nucleon mass suffers a sudden decrease at a particular temperature corresponding to the vacuum to nuclear medium phase transition [146, 188]. We call this transition temperature as T_C which we calculate

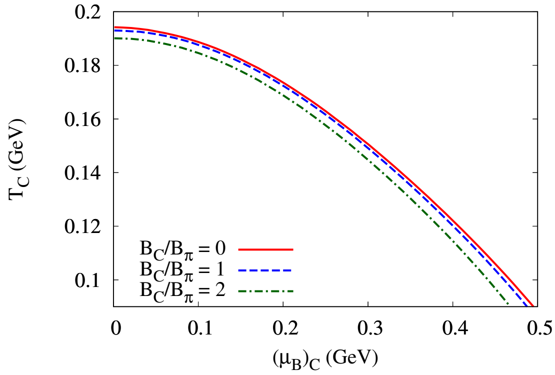

Figure 3.8: Phase diagram for vacuum to nuclear medium phase transition in Walecka model for three different values of B $(0, B_\pi$ and $2B_\pi)$.

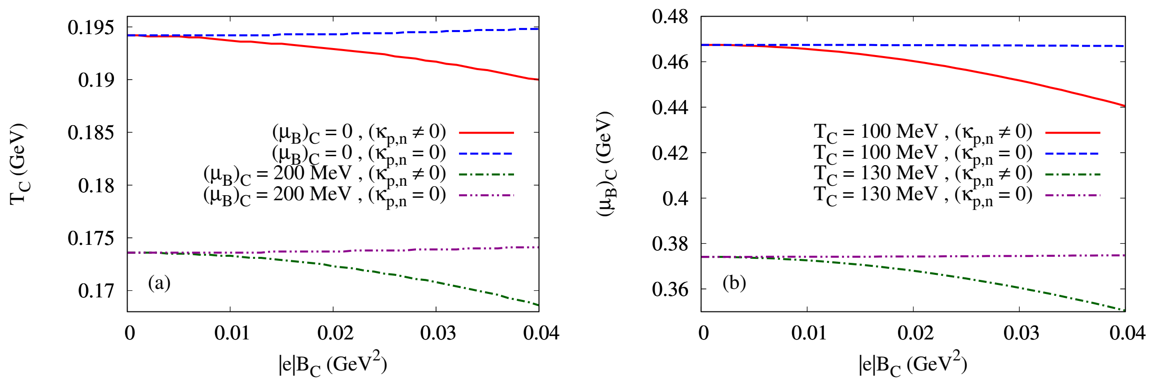

Figure 3.9: (a) Variation of transition temperature with magnetic field at two different values of μ_B (0 and 200 MeV). (b) Variation of transition baryon chemical potential with magnetic field at two different values of T (100 and 130 MeV). Cases with and without the ANM of nucleons are shown separately.

numerically from the slope of of these plots. As can be seen from Fig. 3.7-(a), T_C decreases with the increase of B, which may be identified as IMC in Walecka model. In Fig. 3.7-(b), we observe that T_C decreases with the increase of μ_B. The corresponding variation of m_N^*/m_N with μ_B is shown in Fig. 3.7-(b) and (c). Analogous to the upper panels, we see the phase transition at a particular μ_B and we call this transition chemical potential as $(\mu_\text{B})_C$. As can be seen in the graphs, $(\mu_\text{B})_C$ decreases with the increase in B and T.

The behavior of T_C and $(\mu_\text{B})_C$ at different B can be seen in Fig. 3.8, where, we have presented the phase diagram for the vacuum to nuclear medium phase transition at three different values of B $(0, B_\pi$ and $2B_\pi)$. With the increase in $(\mu_\text{B})_C$, T_C decreases and vice-versa. Also, with the increase in B, the phase boundary in this $T - \mu_\text{B}$ plane moves towards lower values of T and μ_B showing IMC.

We conclude this section by presenting the variation of T_C and $(\mu_\text{B})_C$ with external magnetic field in Fig. 3.9. Fig. 3.9-(a) shows the variation of T_C with $|e|B$ at two different values of $\mu_{\rm B}$ (0 and 200 MeV) whereas Fig. 3.9-(b) shows the corresponding variation at at two different values of T (100 and 130 MeV). As already discussed, both the T_C and $(\mu_{\rm B})_C$ decreases with the increase in B characterizing the IMC effect. However, once the anomalous magnetic moment is ignored, T_C as well as $(\mu_{\rm B})_C$ can be observed to slowly increase with the external magnetic field showing MC as expected [146].

3.4 Summary

In this chapter we have used the Walecka model to study the vacuum to nuclear matter phase transition in presence of a weak and constant background magnetic field within mean field approximation. In case of weak magnetic field, the nucleon propagators are derived as a series in powers of qB and κB where q and κ represents the charge and the anomalous magnetic moment of the nucleons. The effective mass of the nucleon (m_N^*) is obtained from the pole of the nucleon propagator self-consistently. At zero temperature and zero density, the incorporation of anomalous magnetic moment is shown to favour the effective mass enhancement with the external magnetic field. The functional dependence of m_N^* on the background field is extended to the case of non-zero nuclear density and further extended to the finite temperature regime. It is observed that in the case of vanishing temperature within dense nuclear medium, the effective mass decreases with the background magnetic field and this trend is shown to survive in case of non-zero temperature as well. Moreover, there exists a particular temperature (denoted by T_C in the text) for which the effective nucleon mass suffers a sudden decrease corresponding to the vacuum to nuclear medium phase transition. It has been shown that this critical temperature decreases with the increase of B which can be identified as inverse magnetic catalysis in Walecka model whereas the opposite behavior is obtained in case of vanishing magnetic moment [159].

Chapter 4

Spectral properties of neutral ρ meson

In this chapter the one loop self energy of the neutral rho meson is obtained for the effective $\rho\pi\pi$ and ρNN interaction at finite temperature and density in presence of a constant background magnetic field of arbitrary strength. The eB-dependent vacuum part of the self energy is extracted by means of dimensional regularization where the ultraviolet divergences corresponding to the pure vacuum self energy manifest as the pole singularities of gamma as well as Hurwitz zeta functions. This improved regularization procedure consistently reproduces the expected results in the vanishing magnetic field limit and can be used quite generally in other self energy calculations dealing with arbitrary magnetic field strength. In presence of the external magnetic field, the general Lorentz structure for the in-medium vector boson self energy is derived which can also be implemented in case of the gauge bosons such as photons and gluons. It is shown that with vanishing perpendicular momentum of the external particle, essentially two form factors are sufficient to describe the self energy completely. Consequently, two distinct modes are observed in the study of the effective mass, dispersion relations and the spectral function of ρ^0 where one of the modes possesses two fold degeneracy.

The chapter is organised as follows: In Sec. 4.1 the vacuum self energy of ρ is discussed followed by evaluation of the in-medium ρ self-energy at zero magnetic field in Sec. 4.2. Next in Sec. 4.3, the in-medium self energy at non-zero external magnetic field is presented. Sec. 4.4 is devoted to the discussion of the general Lorentz structure of the in-medium self energy function in presence of a constant background magnetic field. After addressing the Lorentz structure of the interacting ρ propagator in Sec.4.5, the analytic structure of the self energy is discussed in Sec. 4.6. Sec. 4.7 contains the numerical results. Finally a summary is added in Sec. 4.8. Some of the relevant calculational details are provided in the Appendix.

4.1 ρ^0 Self Energy in the Vacuum

The effective Lagrangian for $\rho\pi\pi$ and ρNN interaction is [192]

$$\mathscr{L}_{\rm int} = -g_{\rho\pi\pi}\partial_\mu\vec{\rho}_\nu\cdot(\partial^\mu\vec{\pi}\times\partial^\nu\vec{\pi}) - g_{\rho NN}\bar{\Psi}\left[\gamma^\mu - \frac{\kappa_\rho}{2m_N}\sigma^{\mu\nu}\partial_\nu\right]\vec{\tau}\cdot\vec{\rho}_\mu\Psi \tag{4.1}$$

where, $\Psi = \begin{bmatrix} p \\ n \end{bmatrix}$ is the nucleon isospin doublet, $\sigma^{\mu\nu} = \frac{i}{2}[\gamma^\mu,\gamma^\nu]$ and the components of $\vec{\tau}$ correspond to the Pauli isospin matrices. It is understood that, the derivative within the square bracket in the above equation acts only on the ρ field. The value of the coupling constants are given by $g_{\rho\pi\pi} = 20.72$ GeV^{-2}, $g_{\rho NN} = 3.25$ and $\kappa_\rho = 6.1$ with $m_N = 939$ MeV as the mass of the nucleons. The metric tensor in this work is taken as $g^{\mu\nu} = diag(1,-1,-1,-1)$. Using Eq. (4.1), the one-loop vacuum self energy of ρ^0 is obtained

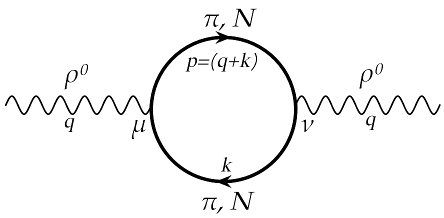

Figure 4.1: Feynman diagram for the one-loop self energy of neutral ρ meson.

as

$$\Pi^{\mu\nu}_{\text{pure-vac}} = (\Pi^{\mu\nu}_\pi)_{\text{pure-vac}} + (\Pi^{\mu\nu}_{\rm N})_{\text{pure-vac}} \tag{4.2}$$

where, $(\Pi^{\mu\nu}_\pi)_{\text{pure-vac}}$ and $(\Pi^{\mu\nu}_{\rm N})_{\text{pure-vac}}$ are respectively the contributions from the $\pi\pi$-loop and NN-loop which are given by

$$(\Pi^{\mu\nu}_\pi)_{\text{pure-vac}}(q) = i\int\frac{d^4k}{(2\pi)^4}\mathcal{N}^{\mu\nu}_\pi(q,k)\Delta_F(k,m_\pi)\Delta_F(p=q+k,m_\pi) \tag{4.3}$$

$$(\Pi^{\mu\nu}_{\rm N})_{\text{pure-vac}}(q) = -i\int\frac{d^4k}{(2\pi)^4}\text{Tr}\Big[\Gamma^\nu(q)S_{\rm p}(p=q+k,m_N)\Gamma^\mu(-q)S_{\rm p}(k,m_N) + \Gamma^\nu(q)S_{\rm n}(p=q+k,m_N)\Gamma^\mu(-q)S_{\rm n}(k,m_N)\Big] \tag{4.4}$$

where,

$$\Delta_F(k,m_\pi) = \frac{-1}{k^2-m_\pi^2+i\epsilon} \tag{4.5}$$

is the vacuum Feynman propagator for the charged pion. $S_{\rm p}$ and $S_{\rm n}$ are respectively the vacuum Feynman propagators for proton and neutron and are given by

$$S_{\rm p}(k,m_N) = S_{\rm n}(k,m_N) = (\not{k}+m_N)\Delta_F(k,m_N). \tag{4.6}$$

The second rank tensor $\mathcal{N}_\pi^{\mu\nu}(q,k)$ and the vector $\Gamma^\mu(q)$ in Eqs. (4.3) and (4.4) contain the factors coming from the interaction vertices:

$$\begin{aligned} \mathcal{N}_\pi^{\mu\nu}(q,k) &= g_{\rho\pi\pi}^2\left[q^4k^\mu k^\nu + (q\cdot k)^2q^\mu q^\nu - q^2(q\cdot k)(q^\mu k^\nu + q^\nu k^\mu)\right] & (4.7)\\ \Gamma^\mu(q) &= g_{\rho NN}\left[\gamma^\mu - i\frac{\kappa_\rho}{2m_N}\sigma^{\mu\nu}q_\nu\right] . & (4.8)\end{aligned}$$

The evaluations of the momentum integrals in Eqs. (4.3) and (4.4) are briefly sketched in Appendix D.2 and the final results can be read off from Eqs. (D.17) and (D.18)

$$\left(\Pi_\pi^{\mu\nu}\right)_{\text{pure-vac}}(q) = (q^2g^{\mu\nu} - q^\mu q^\nu)\left(\frac{-g_{\rho\pi\pi}^2q^2}{32\pi^2}\right)\int_0^1 dx\Delta_\pi\left[\frac{1}{\varepsilon} - \gamma_{\rm E} + 1 - \ln\left(\frac{\Delta_\pi}{4\pi\Lambda_\pi}\right)\right]\Bigg|_{\varepsilon\to 0} \tag{4.9}$$

$$\begin{aligned}\left(\Pi_{\rm N}^{\mu\nu}\right)_{\text{pure-vac}}(q) = (q^2g^{\mu\nu} - q^\mu q^\nu)&\left(\frac{g_{\rho NN}^2}{2\pi^2}\right)\int_0^1 dx\left[\left\{2x(1-x) + \kappa_\rho + \frac{\kappa_\rho^2}{2} - \frac{\kappa_\rho^2}{4m_N^2}\Delta_{\rm N}\right\}\right.\\ &\left.\times\left\{\frac{1}{\varepsilon} - \gamma_{\rm E} - \ln\left(\frac{\Delta_{\rm N}}{4\pi\Lambda_{\rm N}}\right)\right\} - \frac{\kappa_\rho^2}{4m_N^2}\Delta_{\rm N}\right]\Bigg|_{\varepsilon\to 0}\end{aligned} \tag{4.10}$$

where Δ_π and $\Delta_{\rm N}$ are defined in Eqs. (D.13) and (D.14). As can be seen from the above equations, the vacuum self energy is divergent and scale dependent which renormalizes the bare ρ^0 mass to its physical mass after adding proper vacuum counter terms in the Lagrangian. The particular Lorentz structure in the above equations renders the self energy transverse to the ρ^0 momentum i.e. $q_\mu\Pi^{\mu\nu}_{\text{pure-vac}} = 0$.

4.2 ρ^0 Self Energy in the Medium

In order to calculate the ρ^0 self energy at finite temperature and density, we employ the real time formalism of finite temperature field theory where all the two point correlation functions such as the propagator and the self energy become 2×2 matrices in the thermal space [140, 141]. However, they can be put in a diagonal form where the diagonal elements can be obtained from any one component (say the 11-component) of the said 2×2 matrix.

The 11-components of real time thermal pion and nucleon propagators are

$$
\begin{aligned}
D^{11}(k) &= \Delta_F(k,m_\pi) + \eta(k\cdot u)\left[\Delta_F(k,m_\pi) - \Delta_F^*(k,m_\pi)\right] \qquad (4.11)\\
S^{11}_{\rm p,n}(k) &= S_{\rm p,n}(k,m_N) - \tilde{\eta}(k\cdot u)\left[S_{\rm p,n}(k,m_N) - \gamma^0 S^\dagger_{\rm p,n}(k,m_N)\gamma^0\right] \qquad (4.12)
\end{aligned}
$$

where $\eta(x) = \Theta(x)f(x) + \Theta(-x)f(-x)$ and $\tilde{\eta}(x) = \Theta(x)f^+(x) + \Theta(-x)f^-(-x)$ in which $f(x)$ and $f^\pm(x)$ are respectively the Bose-Einstein and Fermi-Dirac distribution functions corresponding to pions and nucleons:

$$
f(x) = \left[e^{x/T} - 1\right]^{-1} \quad , \quad f^\pm(x) = \left[e^{(x\mp\mu_B)/T} + 1\right]^{-1} . \qquad (4.13)
$$

Here, $\Theta(x)$ is the unit step function, u^μ is the medium four-velocity; T and μ_B are respectively the temperature and baryon chemical potential of the medium. In the local rest frame (LRF) of the medium, $u^\mu_{\rm LRF} \equiv (1,\vec{0})$.

For the evaluation of the 11-component of the thermal self energy matrix, the vacuum pion and nucleon propagators in Eqs. (4.3) and (4.4) are replaced by the respective 11-components of the thermal propagators given in Eqs. (4.11) and (4.12) as [141]

$$
\begin{aligned}
\left(\Pi^{\mu\nu}_\pi\right)_{11}(q) &= i\int\frac{d^4k}{(2\pi)^4}\mathcal{N}^{\mu\nu}_\pi(q,k)D^{11}(k,m_\pi)D^{11}(p=q+k,m_\pi) \qquad (4.14)\\
\left(\Pi^{\mu\nu}_{\rm N}\right)_{11}(q) &= -i\int\frac{d^4k}{(2\pi)^4}\mathsf{Tr}\Big[\Gamma^\nu(q)S^{11}_{\rm p}(k,m_N)\Gamma^\mu(-q)S^{11}_{\rm p}(p=q+k,m_N)\\
&\quad +\Gamma^\nu(q)S^{11}_{\rm n}(k,m_N)\Gamma^\mu(-q)S^{11}_{\rm n}(p=q+k,m_N)\Big] . \qquad (4.15)
\end{aligned}
$$

The thermal self energy function of ρ^0 denoted as ${\rm Re}\overline{\Pi}^{\mu\nu}(q^0,\vec{q}) = {\rm Re}\overline{\Pi}^{\mu\nu}_\pi(q^0,\vec{q}) + {\rm Re}\overline{\Pi}^{\mu\nu}_{\rm N}(q^0,\vec{q})$ is related to the above quantities by the relations [141]

$$
\begin{aligned}
{\rm Re}\overline{\Pi}^{\mu\nu}_{\pi,N}(q^0,\vec{q}) &= \left({\rm Re}\Pi^{\mu\nu}_{\pi,N}\right)_{11}(q^0,\vec{q}) \qquad (4.16)\\
{\rm Im}\overline{\Pi}^{\mu\nu}_{\pi,N}(q^0,\vec{q}) &= {\rm sign}\left(q^0\right)\tanh\left(\frac{q^0}{2T}\right)\left({\rm Im}\Pi^{\mu\nu}_{\pi,N}\right)_{11}(q^0,\vec{q}) \qquad (4.17)
\end{aligned}
$$

where, ${\rm sign}\,(x) = \Theta(x) - \Theta(-x)$. After rewriting Eqs. (4.11) and (4.12) as

$$
\begin{aligned}
D^{11}(k) &= \Delta_F(k,m_\pi) + 2\pi i\eta(k\cdot u)\delta\left(k^2 - m_\pi^2\right) \qquad (4.18)\\
S^{11}_{\rm p,n}(k) &= (\not{k} + m_N)\left[\Delta_F(k,m_N) - 2\pi i\tilde{\eta}(k\cdot u)\delta\left(k^2 - m_N^2\right)\right] \qquad (4.19)
\end{aligned}
$$

and substituting into Eqs. (4.14) and (4.15) the dk^0 integration can be performed using the

Dirac delta functions. Following Eqs. (4.16) and (4.17) one can obtain the the real parts as,

$$\begin{aligned}
\mathrm{Re}\overline{\Pi}^{\mu\nu}_{\pi}(q^0,\vec{q}) &= \mathrm{Re}\left(\Pi^{\mu\nu}_{\pi}\right)_{\text{pure-vac}}(q) \\
&+ \int\frac{d^3k}{(2\pi)^3}\mathcal{P}\left[\frac{f(\omega_k)}{2\omega_k}\left\{\frac{\mathcal{N}^{\mu\nu}_{\pi}(k^0=-\omega_k)}{(q^0-\omega_k)^2-(\omega_p)^2}+\frac{\mathcal{N}^{\mu\nu}_{\pi}(k^0=\omega_k)}{(q^0+\omega_k)^2-(\omega_p)^2}\right\}\right. \\
&\left.+\frac{f(\omega_p)}{2\omega_p}\left\{\frac{\mathcal{N}^{\mu\nu}_{\pi}(k^0=-q^0-\omega_p)}{(q^0+\omega_p)^2-(\omega_k)^2}+\frac{\mathcal{N}^{\mu\nu}_{\pi}(k^0=-q^0+\omega_p)}{(q^0-\omega_p)^2-(\omega_k)^2}\right\}\right] \qquad (4.20)
\end{aligned}$$

$$\begin{aligned}
\mathrm{Re}\overline{\Pi}^{\mu\nu}_{\mathrm{N}}(q^0,\vec{q}) &= \mathrm{Re}\left(\Pi^{\mu\nu}_{\mathrm{N}}\right)_{\text{pure-vac}}(q) \\
&- \int\frac{d^3k}{(2\pi)^3}\mathcal{P}\left[\frac{1}{2\Omega_k}\left\{\frac{f^-(\Omega_k)\mathcal{N}^{\mu\nu}_{\mathrm{N}}(k^0=-\Omega_k)}{(q^0-\Omega_k)^2-(\Omega_p)^2}+\frac{f^+(\Omega_k)\mathcal{N}^{\mu\nu}_{\mathrm{N}}(k^0=\Omega_k)}{(q^0+\Omega_k)^2-(\Omega_p)^2}\right\}\right. \\
&\left.+\frac{1}{2\Omega_p}\left\{\frac{f^-(\Omega_p)\mathcal{N}^{\mu\nu}_{\mathrm{N}}(k^0=-q^0-\Omega_p)}{(q^0+\Omega_p)^2-(\Omega_k)^2}+\frac{f^+(\Omega_p)\mathcal{N}^{\mu\nu}_{\mathrm{N}}(k^0=-q^0+\Omega_p)}{(q^0-\Omega_p)^2-(\Omega_k)^2}\right\}\right]. \qquad (4.21)
\end{aligned}$$

The imaginary parts are given by,

$$\begin{aligned}
\mathrm{Im}\overline{\Pi}^{\mu\nu}_{\pi}(q^0,\vec{q}) &= -\mathrm{sign}\left(q^0\right)\tanh\left(\frac{\beta q^0}{2}\right)\pi\int\frac{d^3k}{(2\pi)^3}\frac{1}{4\omega_k\omega_p} \\
&\times\left[\{1+f(\omega_k)+f(\omega_p)+2f(\omega_k)f(\omega_p)\}\mathcal{N}^{\mu\nu}_{\pi}(k^0=-\omega_k)\delta(q^0-\omega_k-\omega_p)\right. \\
&+\{1+f(\omega_k)+f(\omega_p)+2f(\omega_k)f(\omega_p)\}\mathcal{N}^{\mu\nu}_{\pi}(k^0=\omega_k)\delta(q^0+\omega_k+\omega_p) \\
&+\{f(\omega_k)+f(\omega_p)+2f(\omega_k)f(\omega_p)\}\mathcal{N}^{\mu\nu}_{\pi}(k^0=-\omega_k)\delta(q^0-\omega_k+\omega_p) \\
&\left.+\{f(\omega_k)+f(\omega_p)+2f(\omega_k)f(\omega_p)\}\mathcal{N}^{\mu\nu}_{\pi}(k^0=\omega_k)\delta(q^0+\omega_k-\omega_p)\right] \qquad (4.22)
\end{aligned}$$

$$\begin{aligned}
\mathrm{Im}\overline{\Pi}^{\mu\nu}_{\mathrm{N}}(q^0,\vec{q}) &= -\mathrm{sign}\left(q^0\right)\tanh\left(\frac{\beta q^0}{2}\right)\pi\int\frac{d^3k}{(2\pi)^3}\frac{1}{4\Omega_k\Omega_p} \\
&\times\left[\left\{1-f^-(\Omega_k)-f^+(\Omega_p)+2f^-(\Omega_k)f^+(\Omega_p)\right\}\mathcal{N}^{\mu\nu}_{\mathrm{N}}(k^0=-\Omega_k)\delta(q^0-\Omega_k-\Omega_p)\right. \\
&+\left\{1-f^+(\Omega_k)-f^-(\Omega_p)+2f^+(\Omega_k)f^-(\Omega_p)\right\}\mathcal{N}^{\mu\nu}_{\mathrm{N}}(k^0=\Omega_k)\delta(q^0+\Omega_k+\Omega_p) \\
&+\left\{-f^-(\Omega_k)-f^-(\Omega_p)+2f^-(\Omega_k)f^-(\Omega_p)\right\}\mathcal{N}^{\mu\nu}_{\mathrm{N}}(k^0=-\omega_k)\delta(q^0-\Omega_k+\Omega_p) \\
&\left.+\left\{-f^+(\Omega_k)-f^+(\Omega_p)+2f^+(\Omega_k)f^+(\Omega_p)\right\}\mathcal{N}^{\mu\nu}_{\mathrm{N}}(k^0=\Omega_k)\delta(q^0+\Omega_k-\Omega_p)\right] \qquad (4.23)
\end{aligned}$$

where, $\mathcal{P}$ denotes the *Cauchy Principal Value* integration, $\omega_k=\sqrt{m_\pi^2+\vec{k}^2}$, $\Omega_k=\sqrt{m_N^2+\vec{k}^2}$ and $\mathcal{N}_{\mathrm{N}}(q,k)$ is defined in Eq. (D.10).

4.3 ρ^0 Self Energy in the Magnetized Medium

In presence of the external magnetic field $\vec{B} = B\hat{z}$, the propagations of the charged pion and proton are modified. One of the possible ways to incorporate the effect of external magnetic field is the Schwinger proper time formalism in which the 11-components of charged pion and proton propagators respectively become [145, 193]

$$D_B^{11}(k) = \Delta_B(k,m_\pi) + \eta(k\cdot u)\left[\Delta_B(k,m_\pi) - \Delta_B^*(k,m_\pi)\right] \quad \text{and} \tag{4.24}$$

$$S_B^{11}(k) = S_B(k,m_N) - \tilde{\eta}(k\cdot u)\left[S_B(k,m_N) - \gamma^0 S_B^\dagger(k,m_N)\gamma^0\right] \tag{4.25}$$

where, $\Delta_B(k,m_\pi)$ and $S_B(k,m_N)$ denote the momentum space vacuum (zero temperature) Schwinger proper time propagators for charged pion and proton respectively [145]:

$$\Delta_B(k) = i\int_0^\infty ds \exp\left[is\left\{k_\parallel^2 + \frac{\tan(eBs)}{eBs}k_\perp^2 - m_N^2\right\}\right] \tag{4.26}$$

$$S_B(k) = i\int_0^\infty ds \exp\left[is\left\{k_\parallel^2 + \frac{\tan(eBs)}{eBs}k_\perp^2 - m_N^2\right\}\right] \times\left[\left(\not{k}_\parallel + m_N\right)\left\{1-\gamma^1\gamma^2\tan(eBs)\right\} + \not{k}_\perp \sec^2(eBs)\right]. \tag{4.27}$$

In the above equations, $e = |e|$ is the charge of the proton; the four-vector k is decomposed into $k = (k_\parallel + k_\perp)$ where $k_\parallel^\mu = g_\parallel^{\mu\nu}k_\nu$ and $k_\perp^\mu = g_\perp^{\mu\nu}k_\nu$ corresponding to the decomposition of the metric tensor $g^{\mu\nu} = (g_\parallel^{\mu\nu} + g_\perp^{\mu\nu})$ with $g_\parallel^{\mu\nu} = \text{diag}(1,0,0,-1)$ and $g_\perp^{\mu\nu} = \text{diag}(0,-1,-1,0)$. The above decomposition can be done in a Lorentz covariant way by introducing another four-vector

$$b^\mu = \frac{1}{B}G^{\mu\nu}u_\nu \tag{4.28}$$

where $G^{\mu\nu} = \frac{1}{2}\epsilon^{\mu\nu\alpha\beta}F_{\alpha\beta}$ is the dual of the electromagnetic field tensor $F^{\mu\nu}$. In the local rest frame of the medium, $b^\mu_{\text{LRF}} \equiv (0,0,0,1)$, which is the direction of the external magnetic field. Using b^μ, we can write

$$g_\parallel^{\mu\nu} = (u^\mu u^\nu - b^\mu b^\nu) \quad \text{and} \quad g_\perp^{\mu\nu} = (g^{\mu\nu} - u^\mu u^\nu + b^\mu b^\nu). \tag{4.29}$$

It is important to note that, the coordinate space Schwinger propagator contains a gauge dependent translationally non-invariant phase factor. However, for the one-loop graphs containing equally charged particle in the loop, the phase factor gets canceled and the momentum space propagator is sufficient for the calculation of the self energy. The proper time integral in Eqs. (4.26) and (4.27) can be performed in order to express the propagators as a sum over discrete Landau levels as

$$\Delta_B(k) = -\sum_{l=0}^{\infty} \frac{2(-1)^l e^{-\alpha_k} L_l(2\alpha_k)}{k_\parallel^2 - m_\pi^2 - (2l+1)eB + i\epsilon} \tag{4.30}$$

$$S_B(k) = -\sum_{l=0}^{\infty} \left[\frac{(-1)^l e^{-\alpha_k} \mathcal{D}_l(k)}{k_\parallel^2 - m_N^2 - 2leB + i\epsilon}\right] \tag{4.31}$$

where,

$$\mathcal{D}_l(k) = \left(\not{k}_\parallel + m_N\right)\left[\left(1 + i\gamma^1\gamma^2\right) L_l(2\alpha_k) - \left(1 - i\gamma^1\gamma^2\right) L_{l-1}(2\alpha_k)\right] - 4\not{k}_\perp L_{l-1}^1(2\alpha_k) \tag{4.32}$$

with $\alpha_k = -k_\perp^2/eB$. Here, $L_l^a(z)$ denotes the generalized Laguerre polynomial with $L_{-1}^a(z) = 0$ and $L_l(z) = L_l^0(z)$. We now rewrite Eqs. (4.24) and (4.25) using Eqs. (4.30) and (4.31) as

$$D_B^{11}(k) = \sum_{l=0}^{\infty} 2(-1)^l e^{-\alpha_k} L_l(2\alpha_k)\left[\frac{-1}{k_\parallel^2 - m_l^2 + i\epsilon} + 2\pi i\eta(k\cdot u)\delta\left(k_\parallel^2 - m_l^2\right)\right] \tag{4.33}$$

$$S_B^{11}(k) = \sum_{l=0}^{\infty} (-1)^l e^{-\alpha_k} \mathcal{D}_l(k)\left[\frac{-1}{k_\parallel^2 - M_l^2 + i\epsilon} - 2\pi i\tilde{\eta}(k\cdot u)\delta\left(k_\parallel^2 - M_l^2\right)\right] \tag{4.34}$$

where we have defined the Landau level dependent "dimensionally reduced effective masses" (as a consequence of dimensional reduction) of pion and proton as

$$m_l = \sqrt{m_\pi^2 + (2l+1)eB} \quad \text{and} \quad M_l = \sqrt{m_N^2 + 2leB}\ . \tag{4.35}$$

We now replace the 11-component of the charged pion and proton propagators in Eqs. (4.14) and (4.15) as $D^{11} \to D_B^{11}, S_{\rm p}^{11} \to S_B^{11}$ i.e by the respective magnetized ones given in Eqs. (4.33) and (4.34) and then perform the dk^0 integrations (using the Dirac delta functions). Following Eqs. (4.16) and (4.17) we get the thermal self energy functions under external magnetic field which we will denote by a *double bar* to distinguish them from the thermal self energy functions in the absence of magnetic field. Their explicit expressions are given by

$$\begin{aligned}
&\mathrm{Re}\overline{\overline{\Pi}}_\pi^{\mu\nu}(q^0,\vec{q}) = \mathrm{Re}\left(\Pi_\pi^{\mu\nu}\right)_{\rm vac}(q,eB) \\
&+\sum_{l=0}^{\infty}\sum_{n=0}^{\infty}\int\frac{d^3k}{(2\pi)^3}\mathcal{P}\left[\frac{f(\omega_k^l)}{2\omega_k^l}\left\{\frac{\mathcal{N}_{\pi,nl}^{\mu\nu}(k^0=-\omega_k^l)}{(q^0-\omega_k^l)^2-(\omega_p^n)^2}+\frac{\mathcal{N}_{\pi,nl}^{\mu\nu}(k^0=\omega_k^l)}{(q^0+\omega_k^l)^2-(\omega_p^n)^2}\right\}\right. \\
&\left.+\frac{f(\omega_p^n)}{2\omega_p^n}\left\{\frac{\mathcal{N}_{\pi,nl}^{\mu\nu}(k^0=-q^0-\omega_p^n)}{(q^0+\omega_p^n)^2-(\omega_k^l)^2}+\frac{\mathcal{N}_{\pi,nl}^{\mu\nu}(k^0=-q^0+\omega_p^n)}{(q^0-\omega_p^n)^2-(\omega_k^l)^2}\right\}\right]
\end{aligned} \tag{4.36}$$

$$
\begin{aligned}
{\rm Re}\overline{\overline{\Pi}}^{\mu\nu}_{\rm N}(q^0,\vec{q}) &= \frac{1}{2}{\rm Re}\overline{\Pi}^{\mu\nu}_{\rm N}(q^0,\vec{q}) + {\rm Re}\left(\Pi^{\mu\nu}_{\rm p}\right)_{\rm vac}(q,eB) \\
&- \sum_{l=0}^{\infty}\sum_{n=0}^{\infty}\int\frac{d^3k}{(2\pi)^3}\mathcal{P}\left[\frac{1}{2\Omega^l_k}\left\{\frac{f^-(\Omega^l_k)\mathcal{N}^{\mu\nu}_{{\rm p},nl}(k^0=-\Omega^l_k)}{(q^0-\Omega^l_k)^2-(\Omega^n_p)^2}+\frac{f^+(\Omega^l_k)\mathcal{N}^{\mu\nu}_{{\rm p},nl}(k^0=\Omega^l_k)}{(q^0+\Omega^l_k)^2-(\Omega^n_p)^2}\right\}\right. \\
&\left.+\frac{1}{2\Omega^n_p}\left\{\frac{f^-(\Omega^n_p)\mathcal{N}^{\mu\nu}_{{\rm p},nl}(k^0=-q^0-\Omega^n_p)}{(q^0+\Omega^n_p)^2-(\Omega^l_k)^2}+\frac{f^+(\Omega^n_p)\mathcal{N}^{\mu\nu}_{{\rm p},nl}(k^0=-q^0+\Omega^n_p)}{(q^0-\Omega^n_p)^2-(\Omega^l_k)^2}\right\}\right] \qquad (4.37)
\end{aligned}
$$

$$
\begin{aligned}
{\rm Im}\overline{\overline{\Pi}}^{\mu\nu}_{\pi}(q^0,\vec{q}) &= -{\rm sign}\left(q^0\right)\tanh\left(\frac{\beta q^0}{2}\right)\pi\sum_{l=0}^{\infty}\sum_{n=0}^{\infty}\int\frac{d^3k}{(2\pi)^3}\frac{1}{4\omega^l_k\omega^n_p} \\
&\times\left[\left\{1+f(\omega^l_k)+f(\omega^n_p)+2f(\omega^l_k)f(\omega^n_p)\right\}\right. \\
&\times\left\{\mathcal{N}^{\mu\nu}_{\pi,nl}(k^0=-\omega^l_k)\delta(q^0-\omega^l_k-\omega^n_p)+\mathcal{N}^{\mu\nu}_{\pi,nl}(k^0=\omega^l_k)\delta(q^0+\omega^l_k+\omega^n_p)\right\} \\
&+\left\{f(\omega^l_k)+f(\omega^n_p)+2f(\omega^l_k)f(\omega^n_p)\right\} \\
&\times\left.\left\{\mathcal{N}^{\mu\nu}_{\pi,nl}(k^0=-\omega^l_k)\delta(q^0-\omega^l_k+\omega^n_p)+\mathcal{N}^{\mu\nu}_{\pi,nl}(k^0=\omega^l_k)\delta(q^0+\omega^l_k-\omega^n_p)\right\}\right] \qquad (4.38)
\end{aligned}
$$

$$
\begin{aligned}
{\rm Im}\overline{\overline{\Pi}}^{\mu\nu}_{\rm N}(q^0,\vec{q}) &= \frac{1}{2}{\rm Im}\overline{\Pi}^{\mu\nu}_{\rm N}(q^0,\vec{q}) - {\rm sign}\left(q^0\right)\tanh\left(\frac{\beta q^0}{2}\right)\pi\sum_{l=0}^{\infty}\sum_{n=0}^{\infty}\int\frac{d^3k}{(2\pi)^3}\frac{1}{4\Omega^l_k\Omega^n_p} \\
&\times\left[\left\{1-f^-(\Omega^l_k)-f^+(\Omega^n_p)+2f^-(\Omega^l_k)f^+(\Omega^n_p)\right\}\mathcal{N}^{\mu\nu}_{{\rm p},nl}(k^0=-\Omega^l_k)\delta(q^0-\Omega^l_k-\Omega^n_p)\right. \\
&+\left\{1-f^+(\Omega^l_k)-f^-(\Omega^n_p)+2f^+(\Omega^l_k)f^-(\Omega^n_p)\right\}\mathcal{N}^{\mu\nu}_{{\rm p},nl}(k^0=\Omega^l_k)\delta(q^0+\Omega^l_k+\Omega^n_p) \\
&+\left\{-f^-(\Omega^l_k)-f^-(\Omega^n_p)+2f^-(\Omega^l_k)f^-(\Omega^n_p)\right\}\mathcal{N}^{\mu\nu}_{{\rm p},nl}(k^0=-\omega^l_k)\delta(q^0-\Omega^l_k+\Omega^n_p) \\
&+\left.\left\{-f^+(\Omega^l_k)-f^+(\Omega^n_p)+2f^+(\Omega^l_k)f^+(\Omega^n_p)\right\}\mathcal{N}^{\mu\nu}_{{\rm p},nl}(k^0=\Omega^l_k)\delta(q^0+\Omega^l_k-\Omega^n_p)\right] \quad (4.39)
\end{aligned}
$$

where,

$$
\begin{aligned}
\mathcal{N}^{\mu\nu}_{\pi,nl}(q,k) &= 4(-1)^{n+l}e^{-\alpha_k-\alpha_p}L_l(2\alpha_k)L_n(2\alpha_p)\mathcal{N}^{\mu\nu}_{\pi}(q,k) && (4.40)\\
\mathcal{N}^{\mu\nu}_{{\rm p},nl}(q,k) &= -g^2_{\rho NN}(-1)^{n+l}e^{-\alpha_k-\alpha_p}\,\mathsf{Tr}\left[\Gamma^\nu(q)\mathcal{D}_n(q+k)\Gamma^\mu(-q)\mathcal{D}_l(k)\right] && (4.41)\\
\omega^l_k &= \sqrt{k_z^2+m_l^2}=\sqrt{k_z^2+m_\pi^2+(2l+1)eB} && (4.42)\\
\Omega^l_k &= \sqrt{k_z^2+M_l^2}=\sqrt{k_z^2+m_N^2+2leB}\,. && (4.43)
\end{aligned}
$$

The first terms on the RHS of Eqs. (4.37) and (4.39) are the contributions from the neutron-neutron loop which are not affected by the external magnetic field. The last terms on the RHS of Eqs. (4.36) and (4.37) are the contributions from $\pi\pi$ and proton-proton loop which depend on the external magnetic field but independent of temperature. Their explicit forms are given by

$$\mathrm{Re}\,(\Pi_\pi^{\mu\nu})_{\text{vac}}(q,eB) = \mathrm{Re}\sum_{l=0}^{\infty}\sum_{n=0}^{\infty} i\int\frac{d^4k}{(2\pi)^4}\mathcal{N}_{\pi,nl}^{\mu\nu}\Delta_F(k_\parallel,m_l)\Delta_F(q_\parallel+k_\parallel,m_n) \tag{4.44}$$

$$\mathrm{Re}\left(\Pi_{\text{p}}^{\mu\nu}\right)_{\text{vac}}(q,eB) = \mathrm{Re}\sum_{l=0}^{\infty}\sum_{n=0}^{\infty} i\int\frac{d^4k}{(2\pi)^4}\mathcal{N}_{\text{p},nl}^{\mu\nu}\Delta_F(k_\parallel,M_l)\Delta_F(q_\parallel+k_\parallel,M_n)\;. \tag{4.45}$$

It is important to note that, the above quantities respectively contain the divergent pure vacuum contributions $(\Pi_\pi^{\mu\nu})_{\text{pure-vac}}(q)$ and $\frac{1}{2}(\Pi_{\text{N}}^{\mu\nu})_{\text{pure-vac}}(q)$ in a nontrivial way (as the above equations seem to appear non-perturbative in eB). In contrast, for the case of weak magnetic field expansion of the Schwinger propagator, the pure vacuum contribution to the self energy trivially decouples from the magnetic field dependent terms. Since we are working with the full propagator including all the Landau levels, we have to properly regularize the above expressions in order to extract the pure vacuum contributions from these quantities. We use dimensional regularization in which the ultraviolet divergence appear as the pole of Gamma and Hurwitz zeta function the details of which are provided in the Appendices D.3 and D.4. Here, we take the transverse momentum of ρ^0 to be zero i.e. $q_\perp = 0$ which makes substantial simplifications of the analytic calculations. The final result can be read off from Eqs. (D.26) and (D.35) as

$$(\Pi_\pi^{\mu\nu})_{\text{vac}}(q_\parallel,eB) = (\Pi_\pi^{\mu\nu})_{\text{pure-vac}}(q_\parallel) + (\Pi_\pi^{\mu\nu})_{\text{eB-vac}}(q_\parallel,eB) \tag{4.46}$$

$$\left(\Pi_{\text{p}}^{\mu\nu}\right)_{\text{vac}}(q_\parallel,eB) = \frac{1}{2}(\Pi_{\text{N}}^{\mu\nu})_{\text{pure-vac}}(q_\parallel) + \left(\Pi_{\text{p}}^{\mu\nu}\right)_{\text{eB-vac}}(q_\parallel,eB) \tag{4.47}$$

where, the scale dependent divergent pure-vacuum parts are completely decoupled as the first term on the RHS of the above equation; the scale independent and finite "eB-dependent vacuum contribution" to the real part of the self energy functions are

$$\begin{aligned}(\Pi_\pi^{\mu\nu})_{\text{eB-vac}}(q_\parallel,eB) = \frac{-g_{\rho\pi\pi}^2 q_\parallel^2}{32\pi^2}\int_0^1 dx\Bigg[&\left\{\ln\left(\frac{\Delta_\pi(q_\perp=0)}{2eB}\right)-1\right\}\Delta_\pi(q_\perp=0)(q_\parallel^2 g^{\mu\nu}-q_\parallel^\mu q_\parallel^\nu)\\ &-(q_\parallel^2 g_\parallel^{\mu\nu}-q_\parallel^\mu q_\parallel^\nu)2eB\left\{\ln\Gamma\left(z_\pi+\frac{1}{2}\right)-\ln\sqrt{2\pi}\right\}\\ &+q_\parallel^2 g_\perp^{\mu\nu}\Bigg\{\Delta_\pi(q_\perp=0)+\frac{eB}{2}\\ &-\frac{1}{2}\Delta_\pi(q_\perp=0)\left\{\psi\left(z_\pi+\frac{1}{2}\right)+\psi\left(z_\pi+x+\frac{1}{2}\right)\right\}\Bigg\}\Bigg]\end{aligned} \tag{4.48}$$

$$\left(\Pi_{\text{p}}^{\mu\nu}\right)_{\text{eB-vac}}(q_\parallel,eB) = \frac{g_{\rho NN}^2}{4\pi^2}$$

$$\times \int_0^1 dx \Bigg[\ln\left(\frac{\Delta_N(q_\perp=0)}{2eB}\right) \left\{ 2x(1-x) + \kappa_\rho + \frac{\kappa_\rho^2}{2} - \frac{\kappa_\rho^2}{4m_N^2}\Delta_N(q_\perp=0) \right\} (q_\parallel^2 g^{\mu\nu} - q_\parallel^\mu q_\parallel^\nu)$$
$$- 2x(1-x)\left(\psi(z_N) + \frac{1}{2z_N}\right)(q_\parallel^2 g_\parallel^{\mu\nu} - q_\parallel^\mu q_\parallel^\nu) + 2eB g_\perp^{\mu\nu} \left\{ \left(z_N - \frac{m_N^2}{eB}\right)\psi(z_N+x) + z_N \right.$$
$$\left. + \ln\Gamma(z+x) - \ln\sqrt{2\pi} \right\} - \kappa_\rho \left\{ (q_\parallel^2 g_\parallel^{\mu\nu} - q_\parallel^\mu q_\parallel^\nu)\left(\psi(z_N) + \frac{1}{2z_N}\right) + q_\parallel^2 g_\perp^{\mu\nu}\psi(z+x) \right\}$$
$$+ \frac{\kappa_\rho^2}{4m_N^2} 2eB \Bigg[(q_\parallel^2 g_\parallel^{\mu\nu} - q_\parallel^\mu q_\parallel^\nu) \left\{ -\frac{m_N^2}{eB}\left(\psi(z_N) + \frac{1}{2z_N}\right) + \frac{1}{2}\ln(z_N) + \ln\Gamma(z_N) - \ln\sqrt{2\pi} \right\}$$
$$- q_\parallel^2 g_\perp^{\mu\nu} \left\{ \left(\frac{m_N^2}{eB} - z_N\right)\psi(z_N+x) + \Delta_N(q_\perp=0) \right\} + \frac{\kappa_\rho^2}{4m_N^2}(q_\parallel^2 g^{\mu\nu} - q_\parallel^\mu q_\parallel^\nu)\Delta_N(q_\perp=0) \Bigg]. \tag{4.49}$$

Eqs. (4.46) and (4.47) imply that the vacuum counter terms are sufficient to renormalize the theory and thus the external magnetic field does not create additional divergences. For $q_\perp = 0$, the $d^2k_\perp$ integrals in Eqs. (4.36)-(4.39) can be analytically performed (see Appendix D.5) and the real parts become

$$\mathrm{Re}\overline{\overline{\Pi}}_\pi^{\mu\nu}(q^0, q_z) = \mathrm{Re}\,(\Pi_\pi^{\mu\nu})_{\text{pure-vac}}(q_\parallel) + \mathrm{Re}\,(\Pi_\pi^{\mu\nu})_{\text{eB-vac}}(q_\parallel, eB)$$
$$+ \sum_{n=0}^{\infty} \sum_{l=(n-1)}^{(n+1)} \int_{-\infty}^{\infty} \frac{dk_z}{2\pi} \mathcal{P} \left[\frac{f(\omega_k^l)}{2\omega_k^l} \left\{ \frac{\tilde{\mathcal{N}}_{\pi,nl}^{\mu\nu}(k^0 = -\omega_k^l)}{(q^0 - \omega_k^l)^2 - (\omega_p^n)^2} + \frac{\tilde{\mathcal{N}}_{\pi,nl}^{\mu\nu}(k^0 = \omega_k^l)}{(q^0 + \omega_k^l)^2 - (\omega_p^n)^2} \right\} \right.$$
$$\left. + \frac{f(\omega_p^n)}{2\omega_p^n} \left\{ \frac{\tilde{\mathcal{N}}_{\pi,nl}^{\mu\nu}(k^0 = -q^0 - \omega_p^n)}{(q^0 + \omega_p^n)^2 - (\omega_k^l)^2} + \frac{\tilde{\mathcal{N}}_{\pi,nl}^{\mu\nu}(k^0 = -q^0 + \omega_p^n)}{(q^0 - \omega_p^n)^2 - (\omega_k^l)^2} \right\} \right] \tag{4.50}$$

$$\mathrm{Re}\overline{\overline{\Pi}}_{\mathrm{N}}^{\mu\nu}(q^0, q_z) = \mathrm{Re}\overline{\Pi}_{\mathrm{N}}^{\mu\nu}(q^0, q_z) + \mathrm{Re}\left(\Pi_{\mathrm{p}}^{\mu\nu}\right)_{\text{eB-vac}}(q_\parallel, eB)$$
$$- \sum_{n=0}^{\infty} \sum_{l=(n-1)}^{(n+1)} \int_{-\infty}^{\infty} \frac{dk_z}{2\pi} \mathcal{P} \left[\frac{1}{2\Omega_k^l} \left\{ \frac{f^-(\Omega_k^l)\tilde{\mathcal{N}}_{\mathrm{p},nl}^{\mu\nu}(k^0 = -\Omega_k^l)}{(q^0 - \Omega_k^l)^2 - (\Omega_p^n)^2} + \frac{f^+(\Omega_k^l)\tilde{\mathcal{N}}_{\mathrm{p},nl}^{\mu\nu}(k^0 = \Omega_k^l)}{(q^0 + \Omega_k^l)^2 - (\Omega_p^n)^2} \right\} \right.$$
$$\left. + \frac{1}{2\Omega_p^n} \left\{ \frac{f^-(\Omega_p^n)\tilde{\mathcal{N}}_{\mathrm{p},nl}^{\mu\nu}(k^0 = -q^0 - \Omega_p^n)}{(q^0 + \Omega_p^n)^2 - (\Omega_k^l)^2} + \frac{f^+(\Omega_p^n)\tilde{\mathcal{N}}_{\mathrm{p},nl}^{\mu\nu}(k^0 = -q^0 + \Omega_p^n)}{(q^0 - \Omega_p^n)^2 - (\Omega_k^l)^2} \right\} \right] \tag{4.51}$$

whereas the imaginary parts are given by

$$\mathrm{Im}\overline{\overline{\Pi}}_\pi^{\mu\nu}(q^0, q_z) = -\mathrm{sign}\left(q^0\right)\tanh\left(\frac{\beta q^0}{2}\right)\pi \sum_{n=0}^{\infty} \sum_{l=(n-1)}^{(n+1)} \int_{-\infty}^{\infty} \frac{dk_z}{2\pi} \frac{1}{4\omega_k^l \omega_p^n}$$
$$\times \left[\left\{ 1 + f(\omega_k^l) + f(\omega_p^n) + 2f(\omega_k^l)f(\omega_p^n) \right\} \right.$$
$$\times \left\{ \tilde{\mathcal{N}}_{\pi,nl}^{\mu\nu}(k^0 = -\omega_k^l)\delta(q^0 - \omega_k^l - \omega_p^n) + \tilde{\mathcal{N}}_{\pi,nl}^{\mu\nu}(k^0 = \omega_k^l)\delta(q^0 + \omega_k^l + \omega_p^n) \right\}$$
$$+ \left\{ f(\omega_k^l) + f(\omega_p^n) + 2f(\omega_k^l)f(\omega_p^n) \right\}$$

$$\times \left\{ \tilde{\mathcal{N}}^{\mu\nu}_{\pi,nl}(k^0 = -\omega^l_k)\delta(q^0 - \omega^l_k + \omega^n_p) + \tilde{\mathcal{N}}^{\mu\nu}_{\pi,nl}(k^0 = \omega^l_k)\delta(q^0 + \omega^l_k - \omega^n_p) \right\} \Bigg] \tag{4.52}$$

$$\mathrm{Im}\overline{\overline{\Pi}}^{\mu\nu}_{\rm N}(q^0,q_z) = \frac{1}{2}\mathrm{Im}\overline{\Pi}^{\mu\nu}_{\rm N}(q^0,q_z) - \mathrm{sign}\left(q^0\right)\tanh\left(\frac{\beta q^0}{2}\right)\pi\sum_{n=0}^{\infty}\sum_{l=(n-1)}^{(n+1)}\int_{-\infty}^{\infty}\frac{dk_z}{2\pi}\frac{1}{4\Omega^l_k\Omega^n_p}$$

$$\times \Bigg[\left\{ 1 - f^-(\Omega^l_k) - f^+(\Omega^n_p) + 2f^-(\Omega^l_k)f^+(\Omega^n_p) \right\} \tilde{\mathcal{N}}^{\mu\nu}_{\mathrm{p},nl}(k^0 = -\Omega^l_k)\delta(q^0 - \Omega^l_k - \Omega^n_p)$$

$$+ \left\{ 1 - f^+(\Omega^l_k) - f^-(\Omega^n_p) + 2f^+(\Omega^l_k)f^-(\Omega^n_p) \right\} \tilde{\mathcal{N}}^{\mu\nu}_{\mathrm{p},nl}(k^0 = \Omega^l_k)\delta(q^0 + \Omega^l_k + \Omega^n_p)$$

$$+ \left\{ - f^-(\Omega^l_k) - f^-(\Omega^n_p) + 2f^-(\Omega^l_k)f^-(\Omega^n_p) \right\} \tilde{\mathcal{N}}^{\mu\nu}_{\mathrm{p},nl}(k^0 = -\Omega^l_k)\delta(q^0 - \Omega^l_k + \Omega^n_p)$$

$$+ \left\{ - f^+(\Omega^l_k) - f^+(\Omega^n_p) + 2f^+(\Omega^l_k)f^+(\Omega^n_p) \right\} \tilde{\mathcal{N}}^{\mu\nu}_{\mathrm{p},nl}(k^0 = \Omega^l_k)\delta(q^0 + \Omega^l_k - \Omega^n_p) \Bigg] \tag{4.53}$$

where, $\tilde{\mathcal{N}}^{\mu\nu}_{\pi,nl}(q_\parallel, k_\parallel)$ and $\tilde{\mathcal{N}}^{\mu\nu}_{\mathrm{p},nl}(q_\parallel, k_\parallel)$ can be read off from Eq. (D.41) and (D.44). The presence of Kronecker delta functions in the expressions of $\tilde{\mathcal{N}}^{\mu\nu}_{\pi,nl}(q_\parallel, k_\parallel)$ and $\tilde{\mathcal{N}}^{\mu\nu}_{\mathrm{p},nl}(q_\parallel, k_\parallel)$ has eliminated one of the double sums or in other words, the sum over index l now runs from $(n-1)$ to $(n+1)$.

4.4 Lorentz Structure of the vector boson self energy in magnetized medium

In this section, we will derive the tensorial decomposition of the massive vector boson self energy. We note that, the self energy $\Pi^{\mu\nu}(q)$ being a second rank tensor, has sixteen components which will mix among themselves with the change of frame. It is useful to use linearly independent basis tensors (constructed with the available vectors and tensors) to express $\Pi^{\mu\nu}(q)$ so that the form factors (corresponding to each basis) remain Lorentz invariant. This will also enable one to solve the Dyson-Schwinger equation in order to obtain the complete interacting vector boson propagator. In order to proceed, we first note that the vector boson self energy satisfies the following constrain

$$\Pi^{\mu\nu}(q) = \Pi^{\nu\mu}(q) \quad \text{and} \quad q_\mu\Pi^{\mu\nu}(q) = 0 \ . \tag{4.54}$$

Let us first consider the pure vacuum case i.e. for zero temperature and zero external magnetic field. In this case, the only available vector is the momentum q^μ along with the metric tensor $g^{\mu\nu}$ so that $\Pi^{\mu\nu}(q)$ is a linear combination of $q^\mu q^\nu$ and $g^{\mu\nu}$ i.e $\Pi^{\mu\nu}(q) = (\alpha_1 g^{\mu\nu} + \alpha_2 q^\mu q^\nu)$. Imposing the constrains of Eq. (4.54), we get $\alpha_1 + \alpha_2 q^2 = 0$ which makes the only possible Lorentz structure of the self energy as

$$\Pi^{\mu\nu} = \alpha_1 \left(g^{\mu\nu} - \frac{q^\mu q^\nu}{q^2} \right) \tag{4.55}$$

where the Lorentz invariant form factor $\alpha_1 = \alpha_1(q^2) = \frac{1}{3}\Pi^\mu_{\ \mu}$. Note that, with q^μ and $g^{\mu\nu}$, the only possible Lorentz scalar that can be formed by contracting with $\Pi^{\mu\nu}(q)$ is the quantity $g_{\mu\nu}\Pi^{\mu\nu} = \Pi^\mu_{\ \mu}$ implying the existence of only one form factor.

We now consider the case with finite temperature but zero magnetic field. In this case we have an additional four vector u^μ (medium four-velocity) along with q^μ and $g^{\mu\nu}$. This makes $\Pi^{\mu\nu}$ to be a linear combination of $g^{\mu\nu}$, $q^\mu q^\nu$, $u^\mu u^\nu$, $q^\mu u^\nu$ and $q^\nu u^\mu$ i.e.

$$\Pi^{\mu\nu}(q) = (\alpha_1 g^{\mu\nu} + \alpha_2 q^\mu q^\nu + \alpha_3 u^\mu u^\nu + \alpha_4 q^\mu u^\nu + \alpha_5 q^\nu q^\mu) \tag{4.56}$$

However, imposing the constrains in Eq. (4.54), we find the following relationship among the coefficients

$$\alpha_5 = \alpha_4 \tag{4.57}$$

$$\alpha_1 + \alpha_2 q^2 + \alpha_4 (q \cdot u) = 0 \tag{4.58}$$

$$\alpha_3 (q \cdot u) + \alpha_4 q^2 = 0 \tag{4.59}$$

which makes only two of the coefficients independent. Choosing α_1 and α_2 as independent, we get,

$$\begin{aligned}\Pi^{\mu\nu}(q) = {} & \alpha_1 \left[g^{\mu\nu} + \frac{q^2}{(q \cdot u)} u^\mu u^\nu - \frac{1}{(q \cdot u)} (q^\mu u^\nu + q^\nu u^\mu) \right] \\ & + \alpha_2 \left[q^\mu q^\nu + \frac{q^4}{(q \cdot u)^2} u^\mu u^\nu - \frac{q^2}{(q \cdot u)} (q^\mu u^\nu + q^\nu u^\mu) \right] .\end{aligned} \tag{4.60}$$

where the Lorentz invariant form factors $\alpha_1 = \alpha_1(q^2, q \cdot u)$ and $\alpha_2 = \alpha_2(q^2, q \cdot u)$ can be obtained by contracting both side of the above equations with $g_{\mu\nu}$ and $u_\mu u_\nu$ so that the form factors will become functions of the Lorentz scalars $g_{\mu\nu}\Pi^{\mu\nu} = \Pi^\mu_{\ \mu}$ and $u_\mu u_\nu \Pi^{\mu\nu}$. Note that, with q^μ, u^μ and $g^{\mu\nu}$, only two possible Lorentz scalars that can be formed by contracting with $\Pi^{\mu\nu}(q)$ are the quantities $\Pi^\mu_{\ \mu}$ and $u_\mu u_\nu \Pi^{\mu\nu}$ implying the existence of only two form factors. Unlike the pure vacuum case given in Eq. (4.55), here the decomposition of $\Pi^{\mu\nu}$ in Eq. (4.60) is not unique. As already mentioned, it is useful to construct linearly independent (and mutually orthogonal) basis tensors (note that the basis tensors within square brackets in Eq. (4.60) are not mutually orthogonal). One such choice of orthogonal tensor basis could be

$$P_1^{\mu\nu} = \left(g^{\mu\nu} - \frac{q^\mu q^\nu}{q^2} - \frac{\tilde{u}^\mu \tilde{u}^\nu}{\tilde{u}^2}\right) \quad \text{and} \quad P_2^{\mu\nu} = \left(\frac{\tilde{u}^\mu \tilde{u}^\nu}{\tilde{u}^2}\right) \tag{4.61}$$

where

$$\tilde{u}^\mu = u^\mu - \frac{(q\cdot u)}{q^2} q^\mu , \tag{4.62}$$

which is constructed from u^μ by subtracting out its projection along q^μ. It is easy to check that $P_1^{\mu\nu}$ and $P_2^{\mu\nu}$ satisfy all the properties of projection tensors i.e.

$$g_{\alpha\beta} P_i^{\mu\alpha} P_j^{\beta\nu} = \delta_{ij} P_i^{\mu\nu} \quad \text{and} \quad g_{\alpha\beta} g_{\mu\nu} P_i^{\mu\alpha} P_j^{\beta\nu} = \delta_{ij} \ . \tag{4.63}$$

Therefore, $\Pi^{\mu\nu}$ can be written as

$$\Pi^{\mu\nu}(q) = \Pi_1(q^2, q\cdot u) P_1^{\mu\nu} + \Pi_2(q^2, q\cdot u) P_2^{\mu\nu} \tag{4.64}$$

where the form factors are

$$\Pi_1(q^2, q\cdot u) = \left(\Pi^\mu{}_\mu - \frac{1}{\tilde{u}^2} u_\mu u_\nu \Pi^{\mu\nu}\right) \quad \text{and} \quad \Pi_2(q^2, q\cdot u) = \left(\frac{1}{\tilde{u}^2} u_\mu u_\nu \Pi^{\mu\nu}\right) \ . \tag{4.65}$$

Care should be taken when considering the special case like $\vec{q} = \vec{0}$ [141]. To see this, let us consider $q^i = |\vec{q}| n^i$ so that the spatial components of the projectors at $\vec{q} = \vec{0}$ become (in the LRF)

$$P_1^{ij} = g^{ij} + n^i n^j \quad \text{and} \quad P_2^{ij} = -n^i n^j \ . \tag{4.66}$$

This implies that the spatial components of self energy at vanishing three momentum

$$\Pi^{ij}(q^0, \vec{q} = \vec{0}) = \Pi_1 g^{ij} + n^i n^j \left(\Pi_1 - \Pi_2\right) \tag{4.67}$$

depend on the direction of $\vec{q}$ even at $|\vec{q}| = 0$. This ambiguity is eliminated by setting additional constraint on the form factors as $\Pi_1(q^0, \vec{q} = \vec{0}) = \Pi_2(q^0, \vec{q} = \vec{0})$.

Following the same strategy, we now construct suitable orthogonal tensor basis for the vector bososn self energy at finite temperature under external magnetic field. In this case we have an additional four vector b^μ (corresponding to the magnetic field direction) along with q^μ, u^μ and $g^{\mu\nu}$. This makes the symmetric $\Pi^{\mu\nu}$ to be a linear combination of seven tensors as

$$\begin{aligned}\Pi^{\mu\nu}(q) &= \alpha_1 g^{\mu\nu} + \alpha_2 q^\mu q^\nu + \alpha_3 u^\mu u^\nu + \alpha_4 b^\mu b^\nu \\ &\quad + \alpha_5(q^\mu u^\nu + q^\nu u^\mu) + \alpha_6(q^\mu b^\nu + q^\nu b^\mu) + \alpha_7(u^\mu b^\nu + u^\nu b^\mu)\end{aligned} \tag{4.68}$$

However, imposing the constrains in Eq. (4.54), we find the following relationship among the coefficients

$$\alpha_1 + \alpha_2 q^2 + \alpha_5(q\cdot u) + \alpha_6(q\cdot b) = 0 \tag{4.69}$$

$$\alpha_3 + \alpha_5 q^2 + \alpha_7(q\cdot b) = 0 \tag{4.70}$$

$$\alpha_4(q\cdot b) + \alpha_6 q^2 + \alpha_7(q\cdot u) = 0 \tag{4.71}$$

which makes only (7-3=4) four of the coefficients independent. The Lorentz invariant form factors $\alpha_i = \alpha_i(q^2, q\cdot u, q\cdot b)$ with $i = 1, 2, ..., 7$ can be obtained by contracting both side of the above equations separately with $g_{\mu\nu}$, $u_\mu u_\nu$, $b_\mu b_\nu$ and $u_\mu b_\nu$ so that the form factors will become functions of the Lorentz scalars $\Pi^\mu{}_\mu$, $u_\mu u_\nu \Pi^{\mu\nu}$, $b_\mu b_\nu \Pi^{\mu\nu}$ and $u_\mu b_\nu \Pi^{\mu\nu}$. Note that, with q^μ, u^μ, b^μ and $g^{\mu\nu}$, only four possible Lorentz scalars that can be formed by contracting with $\Pi^{\mu\nu}(q)$ are the quantities $\Pi^\mu{}_\mu$, $u_\mu u_\nu \Pi^{\mu\nu}$, $b_\mu b_\nu \Pi^{\mu\nu}$ and $u_\mu b_\nu \Pi^{\mu\nu}$ implying the existence of only four form factors. Like the finite temperature case, here the the decomposition of $\Pi^{\mu\nu}$ is also not unique. One convenient choice of tensor basis could be

$$P_1^{\mu\nu} = \left(g^{\mu\nu} - \frac{q^\mu q^\nu}{q^2} - \frac{\tilde{u}^\mu \tilde{u}^\nu}{\tilde{u}^2} - \frac{\tilde{b}^\mu \tilde{b}^\nu}{\tilde{b}^2}\right) \tag{4.72}$$

$$P_2^{\mu\nu} = \left(\frac{\tilde{u}^\mu \tilde{u}^\nu}{\tilde{u}^2}\right) \tag{4.73}$$

$$P_3^{\mu\nu} = \left(\frac{\tilde{b}^\mu \tilde{b}^\nu}{\tilde{b}^2}\right) \tag{4.74}$$

$$Q^{\mu\nu} = \frac{1}{\sqrt{\tilde{u}^2 \tilde{b}^2}}\left(\tilde{u}^\mu \tilde{b}^\nu + \tilde{u}^\nu \tilde{b}^\mu\right) \tag{4.75}$$

where $\tilde{u}^\mu$ is defined in Eq. (4.62) and $\tilde{b}^\mu$ is defined as

$$\tilde{b}^\mu = b^\mu - \frac{(q\cdot b)}{q^2} q^\mu - \frac{b\cdot\tilde{u}}{\tilde{u}^2}\tilde{u}^\mu \ . \tag{4.76}$$

The basis tensors in Eqs. (4.72)-(4.75) satisfy the following relations:

$$g_{\alpha\beta}g_{\mu\nu}P_i^{\mu\alpha}P_j^{\beta\nu} = \delta_{ij} \tag{4.77}$$
$$g_{\alpha\beta}g_{\mu\nu}P_i^{\mu\alpha}Q^{\beta\nu} = 0 \tag{4.78}$$
$$g_{\alpha\beta}g_{\mu\nu}Q^{\mu\alpha}Q^{\beta\nu} = 2 \tag{4.79}$$
$$g_{\alpha\beta}P_i^{\mu\alpha}P_j^{\beta\nu} = \delta_{ij}P_i^{\mu\nu} \tag{4.80}$$
$$g_{\alpha\beta}Q^{\mu\alpha}Q^{\beta\nu} = P_2^{\mu\nu} + P_3^{\mu\nu} \tag{4.81}$$
$$g_{\alpha\beta}P_1^{\mu\alpha}Q^{\beta\nu} = g_{\alpha\beta}Q^{\mu\alpha}P_1^{\beta\nu} = 0 \tag{4.82}$$
$$g_{\alpha\beta}P_2^{\mu\alpha}Q^{\beta\nu} = g_{\alpha\beta}Q^{\mu\alpha}P_3^{\beta\nu} = \frac{\tilde{u}^\mu\tilde{b}^\nu}{\sqrt{\tilde{u}^2\tilde{b}^2}} \tag{4.83}$$
$$g_{\alpha\beta}P_3^{\mu\alpha}Q^{\beta\nu} = g_{\alpha\beta}Q^{\mu\alpha}P_2^{\beta\nu} = \frac{\tilde{u}^\nu\tilde{b}^\mu}{\sqrt{\tilde{u}^2\tilde{b}^2}} \tag{4.84}$$

Using the basis given in Eqs. (4.72)-(4.75), the self energy at finite temperature under external magnetic can be written as

$$\Pi^{\mu\nu}(q) = \Pi_\alpha P_1^{\mu\nu} + \Pi_\beta P_2^{\mu\nu} + \Pi_\gamma P_3^{\mu\nu} + \Pi_\delta Q^{\mu\nu} \tag{4.85}$$

where the form factors are obtained as

$$\Pi_\beta = \frac{1}{\tilde{u}^2}u_\mu u_\nu \Pi^{\mu\nu} \tag{4.86}$$
$$\Pi_\gamma = \frac{1}{\tilde{b}^2}\left[b_\mu b_\nu \Pi^{\mu\nu} + \frac{(b\cdot\tilde{u})^2}{\tilde{u}^4}u_\mu u_\nu \Pi^{\mu\nu} - 2\frac{(b\cdot\tilde{u})}{\tilde{u}^2}u_\mu b_\nu \Pi^{\mu\nu}\right] \tag{4.87}$$
$$\Pi_\delta = \frac{1}{\sqrt{\tilde{u}^2\tilde{b}^2}}\left[u_\mu b_\nu \Pi^{\mu\nu} - \frac{(b\cdot\tilde{u})}{\tilde{u}^2}u_\mu u_\nu \Pi^{\mu\nu}\right] \tag{4.88}$$
$$\Pi_\alpha = \left(\Pi^\mu{}_\mu - \Pi_\beta - \Pi_\gamma\right) \tag{4.89}$$

Analogous to the case of only finite temperature, care should be taken while considering the special case $q_\perp = 0$. To see this, let us consider $q_\perp^i = |\vec{q}_\perp|n^i$ with $i = 1, 2$ so that the following components of self energy at vanishing $q_\perp$ become (in the LRF)

$$\Pi_{ij}(q^0, q_\perp = 0, q_z) = \Pi_\alpha g_{ij} + n_i n_j\left(\Pi_\alpha - \Pi_\gamma\right) \tag{4.90}$$
$$\Pi_{i3}(q^0, q_\perp = 0, q_z) = \frac{q^0}{\sqrt{q_\parallel^2}}n_i\Pi_\delta \tag{4.91}$$

which depend on the direction of $\vec{q}_\perp$ even at $q_\perp = 0$. This ambiguity is eliminated by setting additional constraints on the form factors as

$$\Pi_\alpha(q^0, q_\perp = 0, q_z) = \Pi_\gamma(q^0, q_\perp = 0, q_z) \text{ and } \Pi_\delta(q^0, q_\perp = 0, q_z) = 0 \ . \tag{4.92}$$

4.5 The Interacting ρ meson Propagator and its Lorentz Structure

Let us first consider the zero temperature and zero magnetic field case for which the complete interacting ρ propagator $D^{\mu\nu}$ is obtained by solving the Dyson-Schwinger equation

$$D^{\mu\nu} = \Delta^{\mu\nu} - \Delta^{\mu\alpha}\Pi_{\alpha\beta}D^{\beta\nu} \tag{4.93}$$

where

$$\Delta^{\mu\nu} = \left(-g^{\mu\nu} + \frac{q^\mu q^\nu}{m_\rho^2}\right)\Delta_F(q, m_\rho) \tag{4.94}$$

is the free vacuum Feynman propagator and $\Pi^{\mu\nu}$ is the one-loop self energy of ρ meson which has the Lorentz structure given in Eq. (4.55) as

$$\Pi^{\mu\nu} = \left(g^{\mu\nu} - \frac{q^\mu q^\nu}{q^2}\right)\Pi \tag{4.95}$$

with the form factor $\Pi = \frac{1}{3}\Pi^\mu_{\ \mu}$. In order to solve Eq. (4.93), we rewrite it as

$$\left(D^{\mu\nu}\right)^{-1} = \left(\Delta^{\mu\nu}\right)^{-1} + \Pi^{\mu\nu} \tag{4.96}$$

where $\left(\Delta^{\mu\nu}\right)^{-1} = (q^2 - m_\rho^2)g^{\mu\nu} - q^\mu q^\nu$ which satisfies $\Delta^{\mu\alpha}\left(\Delta_{\alpha\nu}\right)^{-1} = g^\mu_{\ \nu}$. Substituting $\Pi^{\mu\nu}$ from Eq. (4.95) in the above equation, we get the inverse of the complete propagator which can be inverted using the relation $D^{\mu\alpha}\left(D_{\alpha\nu}\right)^{-1} = g^\mu_{\ \nu}$ to obtain the complete propagator as

$$D^{\mu\nu}(q) = \left(-g^{\mu\nu} + \frac{q^\mu q^\nu}{q^2}\right)\left(\frac{-1}{q^2 - m_\rho^2 + \Pi}\right) - \frac{q^\mu q^\nu}{q^2 m_\rho^2} \tag{4.97}$$

We now consider the case of finite temperature and zero magnetic field. As already mentioned in Sec. 4.2, in RTF of finite temperature field theory all the two point correlation functions become 2×2 matrices in thermal space. In this case the Dyson-Schwinger equation also becomes a matrix equation [141]

$$\mathbf{D}^{\mu\nu} = \mathbf{\Delta}^{\mu\nu} - \mathbf{\Delta}^{\mu\alpha}\mathbf{\Pi}_{\alpha\beta}\mathbf{D}^{\beta\nu} \ . \tag{4.98}$$

Each term of the above equation can be diagonalized in terms of the respective analytic functions (denoted by a bar) so that the above equation becomes an algebric one

$$\overline{D}^{\mu\nu} = \overline{\Delta}^{\mu\nu} - \overline{\Delta}^{\mu\alpha}\overline{\Pi}_{\alpha\beta}\overline{D}^{\beta\nu} \tag{4.99}$$

where $\overline{\Delta}^{\mu\nu} = \Delta^{\mu\nu}$. The above equation can be rewritten as

$$\left(\overline{D}^{\mu\nu}\right)^{-1} = \left(\overline{\Delta}^{\mu\nu}\right)^{-1} + \overline{\Pi}^{\mu\nu} \ . \tag{4.100}$$

In this case, the Lorentz structure of the thermal self energy function is given in Eq. (4.64) as

$$\overline{\Pi}^{\mu\nu}(q) = \Pi_1(q^2, q\cdot u)P_1^{\mu\nu} + \Pi_2(q^2, q\cdot u)P_2^{\mu\nu} \tag{4.101}$$

where the projection tensors and form factors are respectively defined in Eqs. (4.61) and (4.65). Substituting the above equation in Eq. (4.100), we get the inverse of the complete propagator. In order to obtain the complete propagator, we write

$$\overline{D}^{\mu\nu} = A_1 P_1^{\mu\nu} + A_2 P_2^{\mu\nu} + \xi q^\mu q^\nu \tag{4.102}$$

and use the relation $\overline{D}^{\mu\alpha}\left(\overline{D}_{\alpha\nu}\right)^{-1} = g^\mu_{\ \nu}$ to extract A_1, A_2 and ξ. The final form of the complete interacting thermal propagator is obtained as

$$\overline{D}^{\mu\nu} = \frac{P_1^{\mu\nu}}{q^2 - m_\rho^2 + \Pi_1} + \frac{P_2^{\mu\nu}}{q^2 - m_\rho^2 + \Pi_2} - \frac{q^\mu q^\nu}{q^2 m_\rho^2} \tag{4.103}$$

Finally we consider the case with both finite temperature and external magnetic field. In this case we need to solve the Dyson-Schwinger equation

$$\left(\overline{\overline{D}}^{\mu\nu}\right)^{-1} = \left(\overline{\Delta}^{\mu\nu}\right)^{-1} + \overline{\overline{\Pi}}^{\mu\nu} \ . \tag{4.104}$$

where a double bar is used to denote thermal self energy function and complete propagator under external magnetic field as discussed in Sec. 4.3. In this case, the Lorentz structure of the thermal self energy function is given in Eq. (4.85) as

$$\overline{\overline{\Pi}}^{\mu\nu}(q) = \Pi_\alpha P_1^{\mu\nu} + \Pi_\beta P_2^{\mu\nu} + \Pi_\gamma P_3^{\mu\nu} + \Pi_\delta Q^{\mu\nu} \tag{4.105}$$

where the basis tensors and form factors are given in Eqs. (4.72)-(4.75) and (4.86)-(4.89). Substituting the above equation in Eq. (4.104), we get the inverse of the complete propagator. In order to obtain the complete propagator, we write

$$\overline{\overline{D}}^{\mu\nu} = A_\alpha P_1^{\mu\nu} + A_\beta P_2^{\mu\nu} + A_\gamma P_3^{\mu\nu} + A_\delta Q^{\mu\nu} + \xi q^\mu q^\nu \tag{4.106}$$

and use the relation $\overline{\overline{D}}^{\mu\alpha}\left(\overline{\overline{D}}_{\alpha\nu}\right)^{-1} = g^\mu_{\ \nu}$ to extract the coefficients as

$$A_\alpha = \frac{1}{q^2 - m_\rho^2 + \Pi_\alpha} \tag{4.107}$$

$$A_\beta = \frac{q^2 - m_\rho^2 + \Pi_\gamma}{\left(q^2 - m_\rho^2 + \Pi_\gamma\right)\left(q^2 - m_\rho^2 + \Pi_\beta\right) - \Pi_\delta^2} \tag{4.108}$$

$$A_\gamma = \frac{q^2 - m_\rho^2 + \Pi_\beta}{\left(q^2 - m_\rho^2 + \Pi_\beta\right)\left(q^2 - m_\rho^2 + \Pi_\gamma\right) - \Pi_\delta^2} \tag{4.109}$$

$$A_\delta = \frac{-\Pi_\delta}{\left(q^2 - m_\rho^2 + \Pi_\beta\right)\left(q^2 - m_\rho^2 + \Pi_\gamma\right) - \Pi_\delta^2} \tag{4.110}$$

$$\xi = \frac{-1}{q^2 m_\rho^2} \ . \tag{4.111}$$

4.6 Analytic Structure of the Self Energy

In this work, we have considered the transverse momentum of the rho meson to be zero i.e. $q_\perp = 0$. As shown in Eq. (4.92), for the special case $q_\perp = 0$, the additional constraints to be imposed on the form factors are

$$\Pi_\alpha(q^0, q_\perp = 0, q_z) = \Pi_\gamma(q^0, q_\perp = 0, q_z) \ \text{ and } \ \Pi_\delta(q^0, q_\perp = 0, q_z) = 0 \ . \tag{4.112}$$

Using the above constraints, we get from Eqs. (4.86)-(4.89)

$$\Pi_\alpha = \Pi_\gamma = \frac{1}{2}\left(\overline{\overline{\Pi}}^\mu_{\ \mu} - \frac{1}{\tilde{u}^2}u_\mu u_\nu \overline{\overline{\Pi}}^{\mu\nu}\right) \tag{4.113}$$

$$\Pi_\beta = \frac{1}{\tilde{u}^2}u_\mu u_\nu \overline{\overline{\Pi}}^{\mu\nu} \tag{4.114}$$

$$\Pi_\delta = 0 \tag{4.115}$$

which imply that we need to calculate only the two quantities quantities $\overline{\overline{\Pi}}^{\mu}_{\ \mu}$ and $u_\mu u_\nu \overline{\overline{\Pi}}^{\mu\nu} = \overline{\overline{\Pi}}^{00}$. These are obtained from Eqs. (4.50)-(4.53) by contracting them with $g_{\mu\nu}$ and $u_\mu u_\nu$. This essentially means replacing $\mathcal{N}^{\mu\nu}$ for all the loops with $\mathcal{N}^{\mu}_{\ \mu}$ or $\mathcal{N}^{00}$, an explicit list for which has been provided in Appendix D.6.

Let us now discuss the analytic structure of the self energy functions. We first consider the zero magnetic field case. The imaginary part of the self energy function for $\pi\pi$ and NN loops as given in Eqs. (4.22) and (4.23) each contains four Dirac delta functions. These delta functions represent energy-momentum conservation and they are non vanishing in certain kinematic domain. They are termed as the Unitary-I, Unitary-II, Landau-II and Landau-I cuts as they appear in those equations. The kinematic regions for the Unitary-I and Unitary-II cuts are given by [141] $\sqrt{\vec{q}^2 + 4m_L^2} < q^0 < \infty$ and $-\infty < q^0 < -\sqrt{\vec{q}^2 + 4m_L^2}$ whereas the same for the two Landau cuts are $|q^0| < |\vec{q}|$ where m_L is the mass of the loop particle i.e. $m_L = m_\pi$ or m_N. These cuts correspond to different physical processes such as decay or scattering. For example, Unitary cuts correspond to the decay of ρ^0 into a $\pi^+\pi^-$ or $N\bar{N}$ pair and the Landau cuts correspond to the scattering of a ρ^0 with a pion or nucleon producing the same in the final state along with their time reversed processes. If we restrict ourselves to the physical timelike kinematic regions defined in terms of $q^0 > 0$ and $q^2 > 0$, then only the Unitary-I cut contributes. It is important to note that, a non-trivial Landau cut appears in the physical timelike region only if the loop particles have different masses and lie in the kinematic domain $|\vec{q}| < q^0 < \sqrt{\vec{q}^2 + \Delta m^2}$ where Δm is the mass difference of the loop particles.

Let us now consider the case of both finite temperature and non zero external magnetic field. In this case the imaginary parts of the self energy as given in Eqs. (4.52) and (4.53) also contain four Dirac delta functions corresponding to the Unitary and Landau cuts. It is important to note that the arguments of the delta functions contain only the longitudinal dynamics (because of dimensional reduction) which implies that the analytic structure of the self energy functions will only depend on the longitudinal momentum of ρ. On the other hand, the transverse dynamics has appeared as Landau level dependent "dimensionally reduced effective mass" to the loop particles as given in Eq. (4.35). Therefore, even if the loop particles have the same masses, a non-trivial Landau cut may appear in the physical timelike kinematic domain if the two loop particles reside in different Landau levels. Physically, this means that ρ^0 can get absorbed in a scattering with a pion or a proton in a lower Landau level producing another pion or proton in a higher Landau level as the final state. A detailed discussions on the analytic structure in presence of external magnetic field can be found in

Refs. [173, 194]. The Unitary-I and Unitary-II terms for the $\pi\pi$ loop are non-vanishing in the kinematic domains $\sqrt{q_z^2+4(m_\pi^2+eB)} < q^0 < \infty$ and $-\infty < q^0 < -\sqrt{q_z^2+4(m_\pi^2+eB)}$ whereas the kinematic domain for both the Landau cuts is

$$|q^0| < \sqrt{q_z^2+(\sqrt{m_\pi^2+eB}-\sqrt{m_\pi^2+3eB})^2}\ . \tag{4.116}$$

The corresponding kinematic domains for the NN loop are $\sqrt{q_z^2+4m_N^2} < q^0 < \infty$ and $-\infty < q^0 < -\sqrt{q_z^2+4m_N^2}$ for the Unitary-I and Unitary-II cuts respectively and

$$|q^0| < \sqrt{q_z^2+(m_N-\sqrt{m_N^2+2eB})^2} \tag{4.117}$$

for the Landau cuts. Note that, the threshold of the Landau cuts appears when the "dimensionally reduced effective mass" difference between the loop particles is the maximum. As can be seen from Eqs. (4.52) and (4.53), for a particular value of the index n, the sum over the index l runs only for three values $(n-1)$, n and $(n+1)$ which implies that, the Landau level difference between the loop particles can be at most one. Thus the maximum difference in their "dimensionally reduced effective mass" appears when one of them is at the lowest Landau level and the other one is at the first Landau level which in turn defines the Landau cut threshold in Eqs. (4.116) and (4.117).

We now simplify the expressions of the imaginary parts given in Eqs. (4.22), (4.23), (4.52) and (4.53) by evaluating one of the integrals using the Dirac delta functions. For the imaginary parts at zero magnetic field, we evaluate the $d(\cos\theta)$ integrals and get (after imposing the kinematic restrictions discussed above),

$$\begin{aligned}
\mathrm{Im}\overline{\Pi}^{\mu\nu}_{\pi,\mathrm{N}}(q^0,\vec{q}) = &-\mathrm{sign}\left(q^0\right)\tanh\left(\frac{q^0}{2T}\right)\frac{1}{16\pi|\vec{q}|} \\
&\times\left[\int_{\omega_-}^{\omega_+} d\left(\omega_k,\Omega_k\right)\left(U_1^{\pi,\mathrm{N}}\right)^{\mu\nu}(\cos\theta=\cos\theta_0^{\pi,\mathrm{N}})\Theta\left(q^0-\sqrt{\vec{q}^2+4m^2_{\pi,\mathrm{N}}}\right)\right. \\
&+\int_{-\omega_+}^{-\omega_-} d\omega_k\left(U_2^{\pi,\mathrm{N}}\right)^{\mu\nu}(\cos\theta=\cos\theta_0'^{\pi,\mathrm{N}})\Theta\left(-q^0-\sqrt{\vec{q}^2+4m^2_{\pi,\mathrm{N}}}\right) \\
&+\int_{-\omega_+}^{\infty} d\omega_k\left(L_1^{\pi,\mathrm{N}}\right)^{\mu\nu}(\cos\theta=\cos\theta_0'^{\pi,\mathrm{N}})\Theta\left(-|q^0|+|\vec{q}|\right) \\
&\left.+\int_{\omega_-}^{\infty} d\omega_k\left(L_2^{\pi,\mathrm{N}}\right)^{\mu\nu}(\cos\theta=\cos\theta_0^{\pi,\mathrm{N}})\Theta\left(-|q^0|+|\vec{q}|\right)\right]
\end{aligned} \tag{4.118}$$

where,

$$\omega_\pm = \begin{cases} \frac{1}{2q^2}\left[q^0q^2 \pm |\vec{q}|\lambda^{1/2}\left(q^2, m_\pi^2, m_\pi^2\right)\right] & \text{for } \pi\pi \text{ loop} \\ \frac{1}{2q^2}\left[q^0q^2 \pm |\vec{q}|\lambda^{1/2}\left(q^2, m_N^2, m_N^2\right)\right] & \text{for NN loop} \end{cases} \tag{4.119}$$

$$(U_1^\pi)^{\mu\nu} = \{1 + f(\omega_k) + f(\omega_p) + 2f(\omega_k)f(\omega_p)\}\, N_\pi^{\mu\nu}(k^0 = -\omega_k) \tag{4.120}$$

$$(U_2^\pi)^{\mu\nu} = \{1 + f(\omega_k) + f(\omega_p) + 2f(\omega_k)f(\omega_p)\}\, N_\pi^{\mu\nu}(k^0 = \omega_k) \tag{4.121}$$

$$(L_1^\pi)^{\mu\nu} = \{f(\omega_k) + f(\omega_p) + 2f(\omega_k)f(\omega_p)\}\, N_\pi^{\mu\nu}(k^0 = \omega_k) \tag{4.122}$$

$$(L_2^\pi)^{\mu\nu} = \{f(\omega_k) + f(\omega_p) + 2f(\omega_k)f(\omega_p)\}\, N_\pi^{\mu\nu}(k^0 = -\omega_k) \tag{4.123}$$

$$\left(U_1^{\rm N}\right)^{\mu\nu} = \left\{1 - f^-(\Omega_k) - f^+(\Omega_p) + 2f^-(\Omega_k)f^+(\Omega_p)\right\} N_{\rm N}^{\mu\nu}(k^0 = -\Omega_k) \tag{4.124}$$

$$\left(U_2^{\rm N}\right)^{\mu\nu} = \left\{1 - f^+(\Omega_k) - f^-(\Omega_p) + 2f^+(\Omega_k)f^-(\Omega_p)\right\} N_{\rm N}^{\mu\nu}(k^0 = \Omega_k) \tag{4.125}$$

$$\left(L_1^{\rm N}\right)^{\mu\nu} = \left\{-f^+(\Omega_k) - f^+(\Omega_p) + 2f^+(\Omega_k)f^+(\Omega_p)\right\} N_{\rm N}^{\mu\nu}(k^0 = \Omega_k) \tag{4.126}$$

$$\left(L_2^{\rm N}\right)^{\mu\nu} = \left\{-f^-(\Omega_k) - f^-(\Omega_p) + 2f^-(\Omega_k)f^-(\Omega_p)\right\} N_{\rm N}^{\mu\nu}(k^0 = -\Omega_k) \tag{4.127}$$

$$\cos\theta_0^\pi = \left(\frac{-2q^0\omega_k + q^2}{2|\vec{q}||\vec{k}|}\right) \tag{4.128}$$

$$\cos\theta_0'^\pi = \left(\frac{2q^0\omega_k + q^2}{2|\vec{q}||\vec{k}|}\right) \tag{4.129}$$

$$\cos\theta_0^{\rm N} = \left(\frac{-2q^0\Omega_k + q^2}{2|\vec{q}||\vec{k}|}\right) \tag{4.130}$$

$$\cos\theta_0'^{\rm N} = \left(\frac{2q^0\Omega_k + q^2}{2|\vec{q}||\vec{k}|}\right) \tag{4.131}$$

with $\lambda(x,y,z) = x^2 + y^2 + z^2 - 2xy - 2yz - 2zx$ being the Källén function.

For the imaginary parts at finite magnetic field, we evaluate the dk_z integrals in Eqs. (4.52) and (4.53) using the Dirac delta functions. The imaginary part due to $\pi\pi$ loop simplifies to

$$\begin{aligned} \mathrm{Im}\overline{\overline{\Pi}}_\pi^{\mu\nu}(q^0, q_z) = &-\mathrm{sign}\left(q^0\right)\tanh\left(\frac{q^0}{2T}\right)\sum_{n=0}^{\infty}\sum_{l=(n-1)}^{(n+1)}\frac{1}{4\lambda^{1/2}(q_\parallel^2, m_l^2, m_n^2)} \\ &\times\sum_{\tilde{k}_z\in\tilde{k}_z^\pm}\left[\left(\tilde{U}_{1,nl}^\pi\right)^{\mu\nu}(k_z = \tilde{k}_z)\Theta\left(q^0 - \sqrt{q_z^2 + (m_l+m_n)^2}\right)\right. \\ &+\left(\tilde{U}_{2,nl}^\pi\right)^{\mu\nu}(k_z = \tilde{k}_z)\Theta\left(-q^0 - \sqrt{q_z^2 + (m_l+m_n)^2}\right) \end{aligned}$$

$$+\left(\tilde{L}^{\pi}_{1,nl}\right)^{\mu\nu}(k_z=\tilde{k}_z)\Theta\left(q^0-\min\left(q_z,E_{\pm}\right)\right)\Theta\left(-q^0+\max\left(q_z,E_{\pm}\right)\right)$$
$$+\left(\tilde{L}^{\pi}_{2,nl}\right)^{\mu\nu}(k_z=\tilde{k}_z)\Theta\left(-q^0-\min\left(q_z,E_{\pm}\right)\right)\Theta\left(q^0+\max\left(q_z,E_{\pm}\right)\right)\Big] \tag{4.132}$$

where,

$$\left(\tilde{U}^{\pi}_{1,nl}\right)^{\mu\nu}=\left\{1+f(\tilde{\omega}^l_k)+f(\tilde{\omega}^n_p)+2f(\tilde{\omega}^l_k)f(\tilde{\omega}^n_p)\right\}\tilde{N}^{\mu\nu}_{\pi,nl}(k^0=-\tilde{\omega}^l_k) \tag{4.133}$$
$$\left(\tilde{U}^{\pi}_{1,nl}\right)^{\mu\nu}=\left\{1+f(\tilde{\omega}^l_k)+f(\tilde{\omega}^n_p)+2f(\tilde{\omega}^l_k)f(\tilde{\omega}^n_p)\right\}\tilde{N}^{\mu\nu}_{\pi,nl}(k^0=\tilde{\omega}^l_k) \tag{4.134}$$
$$\left(\tilde{L}^{\pi}_{1,nl}\right)^{\mu\nu}=\left\{f(\tilde{\omega}^l_k)+f(\tilde{\omega}^n_p)+2f(\tilde{\omega}^l_k)f(\tilde{\omega}^n_p)\right\}\tilde{N}^{\mu\nu}_{\pi,nl}(k^0=\tilde{\omega}^l_k) \tag{4.135}$$
$$\left(\tilde{L}^{\pi}_{1,nl}\right)^{\mu\nu}=\left\{f(\tilde{\omega}^l_k)+f(\tilde{\omega}^n_p)+2f(\tilde{\omega}^l_k)f(\tilde{\omega}^n_p)\right\}\tilde{N}^{\mu\nu}_{\pi,nl}(k^0=-\tilde{\omega}^l_k) \tag{4.136}$$

with, $\tilde{k}^{\pm}_z=\frac{1}{2q^2_\parallel}\left[-yq_z\pm|q^0|\lambda^{1/2}\left(q^2_\parallel,m^2_l,m^2_n\right)\right]$, $y=(q^2_\parallel+m^2_l-m^2_n)$, $\tilde{\omega}^l_k=\sqrt{\tilde{k}^2_z+m^2_l}$, and $E_{\pm}=\frac{m_l-m_n}{|m_l\pm m_n|}\sqrt{q^2_z+(m_l\pm m_n)^2}$.

The corresponding expression of the imaginary part due to NN loop reads

$$\mathrm{Im}\overline{\overline{\Pi}}^{\mu\nu}_{\mathrm{N}}(q^0,q_z)=\frac{1}{2}\mathrm{Im}\overline{\Pi}^{\mu\nu}_{\mathrm{N}}(q^0,q_z)-\mathrm{sign}\left(q^0\right)\tanh\left(\frac{q^0}{2T}\right)\sum_{n=0}^{\infty}\sum_{l=(n-1)}^{(n+1)}\frac{1}{4\lambda^{1/2}(q^2_\parallel,M^2_l,M^2_n)}$$
$$\times\sum_{\tilde{k}_z\in\tilde{K}^{\pm}_z}\Big[\left(\tilde{U}^{\mathrm{p}}_{1,nl}\right)^{\mu\nu}(k_z=\tilde{k}_z)\Theta\left(q^0-\sqrt{q^2_z+(M_l+M_n)^2}\right)$$
$$+\left(\tilde{U}^{\mathrm{p}}_{2,nl}\right)^{\mu\nu}(k_z=\tilde{k}_z)\Theta\left(-q^0-\sqrt{q^2_z+(M_l+M_n)^2}\right)$$
$$+\left(\tilde{L}^{\mathrm{p}}_{1,nl}\right)^{\mu\nu}(k_z=\tilde{k}_z)\Theta\left(q^0-\min\left(q_z,E'_{\pm}\right)\right)\Theta\left(-q^0+\max\left(q_z,E'_{\pm}\right)\right)$$
$$+\left(\tilde{L}^{\mathrm{p}}_{2,nl}\right)^{\mu\nu}(k_z=\tilde{k}_z)\Theta\left(-q^0-\min\left(q_z,E'_{\pm}\right)\right)\Theta\left(q^0+\max\left(q_z,E'_{\pm}\right)\right)\Big] \tag{4.137}$$

where,

$$\left(\tilde{U}^{\mathrm{p}}_{1,nl}\right)^{\mu\nu}=\left\{1-f^-(\tilde{\Omega}^l_k)-f^+(\tilde{\Omega}^n_p)+2f^-(\tilde{\Omega}^l_k)f^+(\tilde{\Omega}^n_p)\right\}\tilde{N}^{\mu\nu}_{\mathrm{p},nl}(k^0=-\tilde{\Omega}^l_k) \tag{4.138}$$
$$\left(\tilde{U}^{\mathrm{p}}_{1,nl}\right)^{\mu\nu}=\left\{1-f^+(\tilde{\Omega}^l_k)-f^-(\tilde{\Omega}^n_p)+2f^+(\tilde{\Omega}^l_k)f^-(\tilde{\Omega}^n_p)\right\}\tilde{N}^{\mu\nu}_{\mathrm{p},nl}(k^0=\tilde{\Omega}^l_k) \tag{4.139}$$
$$\left(\tilde{L}^{\mathrm{p}}_{1,nl}\right)^{\mu\nu}=\left\{-f^+(\tilde{\Omega}^l_k)-f^+(\tilde{\Omega}^n_p)+2f(\tilde{\Omega}^l_k)f(\tilde{\Omega}^n_p)\right\}\tilde{N}^{\mu\nu}_{\mathrm{p},nl}(k^0=\tilde{\Omega}^l_k) \tag{4.140}$$
$$\left(\tilde{L}^{\mathrm{p}}_{1,nl}\right)^{\mu\nu}=\left\{-f^-(\tilde{\Omega}^l_k)-f^-(\tilde{\Omega}^n_p)+2f(\tilde{\Omega}^l_k)f(\tilde{\Omega}^n_p)\right\}\tilde{N}^{\mu\nu}_{\mathrm{p},nl}(k^0=-\tilde{\Omega}^l_k) \tag{4.141}$$

with, $\tilde{K}^{\pm}_z=\frac{1}{2q^2_\parallel}\left[-Yq_z\pm|q^0|\lambda^{1/2}\left(q^2_\parallel,M^2_l,M^2_n\right)\right]$, $Y=(q^2_\parallel+M^2_l-M^2_n)$, $\tilde{\Omega}^l_k=\sqrt{\tilde{K}^2_z+M^2_l}$, and $E'_{\pm}=\frac{M_l-M_n}{|M_l\pm M_n|}\sqrt{q^2_z+(M_l\pm M_n)^2}$. The first term on the RHS of Eq. (4.137) is the contribution from the neutron-neutron loop (which is not affected by the external magnetic field) whose simplified form is given in Eq. (4.118).

4.7 Numerical Results

We begin this section by presenting the real and imaginary parts of the in-medium self energy functions of ρ^0. As can be seen from Eqs. (4.89)-(4.115), we have only two non-zero form factors for the self energy which are Π_α and Π_β for $q_\perp = 0$. Let us first consider the zero magnetic field case for which the imaginary and real parts of Π_α and Π_β are depicted in Figs. 4.2 and 4.3 respectively. In Fig. 4.2(a), $\mathrm{Im}\Pi_\alpha$ and $\mathrm{Im}\Pi_\beta$ due to $\pi\pi$ loop are plotted as

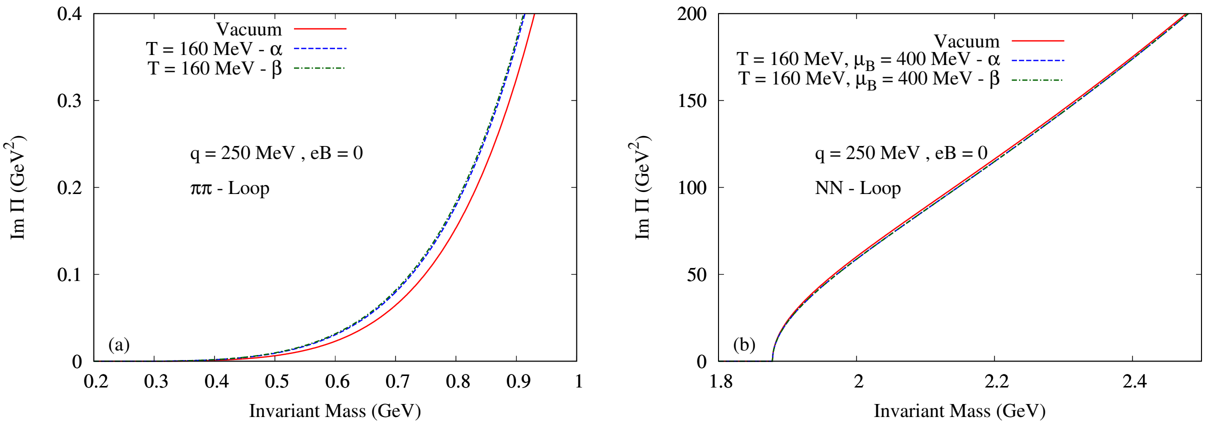

Figure 4.2: Imaginary part of the self energy of ρ^0 as a function of invariant mass at zero magnetic field and at ρ^0 three momentum $|\vec{q}| = 250$ MeV. The vacuum self energy for $T = \mu_B = 0$ is compared with the in-medium one obtained at temperature $T = 160$ MeV and baryon chemical potential $\mu_B = 400$ MeV for the (a) $\pi\pi$ loop and (b) NN Loop.

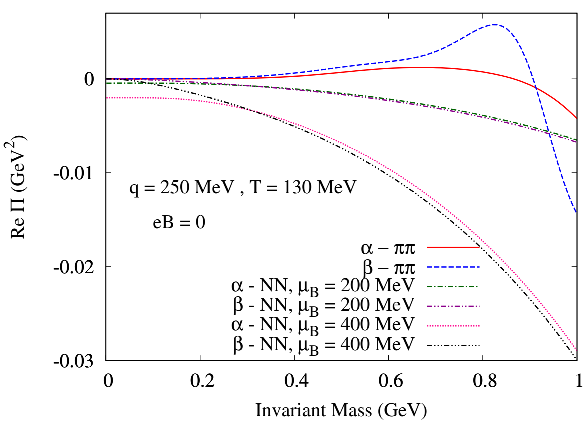

Figure 4.3: Real part of the self energy of ρ^0 as a function of invariant mass at zero magnetic field and at temperature $T = 130$ MeV with ρ^0 three momentum $|\vec{q}| = 250$ MeV. The contributions from NN loop is shown for two different values of baryon chemical potential ($\mu_B = 200$ and 400 MeV respectively).

a function of invariant mass ($\sqrt{q^2}$) of ρ^0 for vacuum as well as for medium ($T = 160$ MeV and $\mu_B = 400$ MeV) with $q_z = 250$ MeV. It is to be understood that in the case of vacuum the two form factors are equal. In this case, the only contribution comes from the Unitary-I cut which starts at $2m_\pi$ in the invariant mass axis. With the increase in temperature , the degeneracy between the form factor get lifted as well as they are enhanced with respect to the vacuum. This is due to the enhancement of the thermal factor in Eq. (4.120) which increases the available phase space with the increase in temperature. The corresponding results for the NN loop is shown in Fig. 4.2(b) for which the threshold of the Unitary-I cut is $2m_N$. In this case, with the increase in temperature and density, the imaginary part decreases slightly with respect to the vacuum which can be understood from Eq. (4.124) where, because of the negative signs in front of the thermal distribution functions of the nucleons, the thermal factor reduces with the increase in temperature thus showing opposite behavior as compared to the $\pi\pi$ loop.

In Fig. 4.3, $\mathrm{Re}\Pi_\alpha$ and $\mathrm{Re}\Pi_\beta$ are shown as a function of ρ^0 invariant mass at zero external magnetic field with ρ^0 longitudinal momentum $q_z = 250$ MeV at temperature $T = 130$ MeV. For the $\pi\pi$ loop, the real part is positive at low invariant mass and becomes negative in the high invariant mass region in contrast to the NN loop for which the contribution to the real part is always negative. The real part due to NN loop is shown for two different values of baryon chemical potential $\mu_B = 200$ and 400 MeV respectively. For low values of μ_B, the contribution of the NN loop is almost of the same order as $\pi\pi$ loop, however at high μ_B, the contribution from NN loop dominates over the $\pi\pi$ loop.

We now turn on the external magnetic field. For the check of consistency of the calculation at non-zero magnetic field, it is essential that $eB \to 0$ limit of non-zero magnetic field results reproduces the $eB = 0$ one. In order to take the $eB \to 0$ limit numerically, we have considered up to 500 Landau levels for a convergent result. We have shown the imaginary part of the self energy as a function of invariant mass of ρ^0 with longitudinal momentum $q_z = 250$ MeV at temperature $T = 130$ MeV and at baryon chemical potential $\mu_B = 300$ MeV for the two cases: $eB = 0$ and $eB \to 0$ in Fig. 4.4 separately for the $\pi\pi$ and NN loops. Fig. 4.4(a) shows $\mathrm{Im}\Pi_\alpha$ for the $\pi\pi$ loop in which the $eB \to 0$ graph has a series of spikes infinitesimally separated from each other all over the whole invariant mass region whereas the $eB = 0$ graph is finite and well behaved. Interestingly, the $eB \to 0$ graph does not miss the $eB = 0$ curve which implies that when average is done, the $eB = 0$ line will be exactly reproduced. The appearance of these spikes are due to the "threshold singularities" [173, 194, 195] at each Landau level as can be understood from Eq. (4.132) where the Källén function goes to zero at each threshold of the Unitary and Landau cuts defined in terms of the unit step functions therein, which is a consequence of the dimensional reduction. In order to extract physical and finite results out of these spikes, we have used

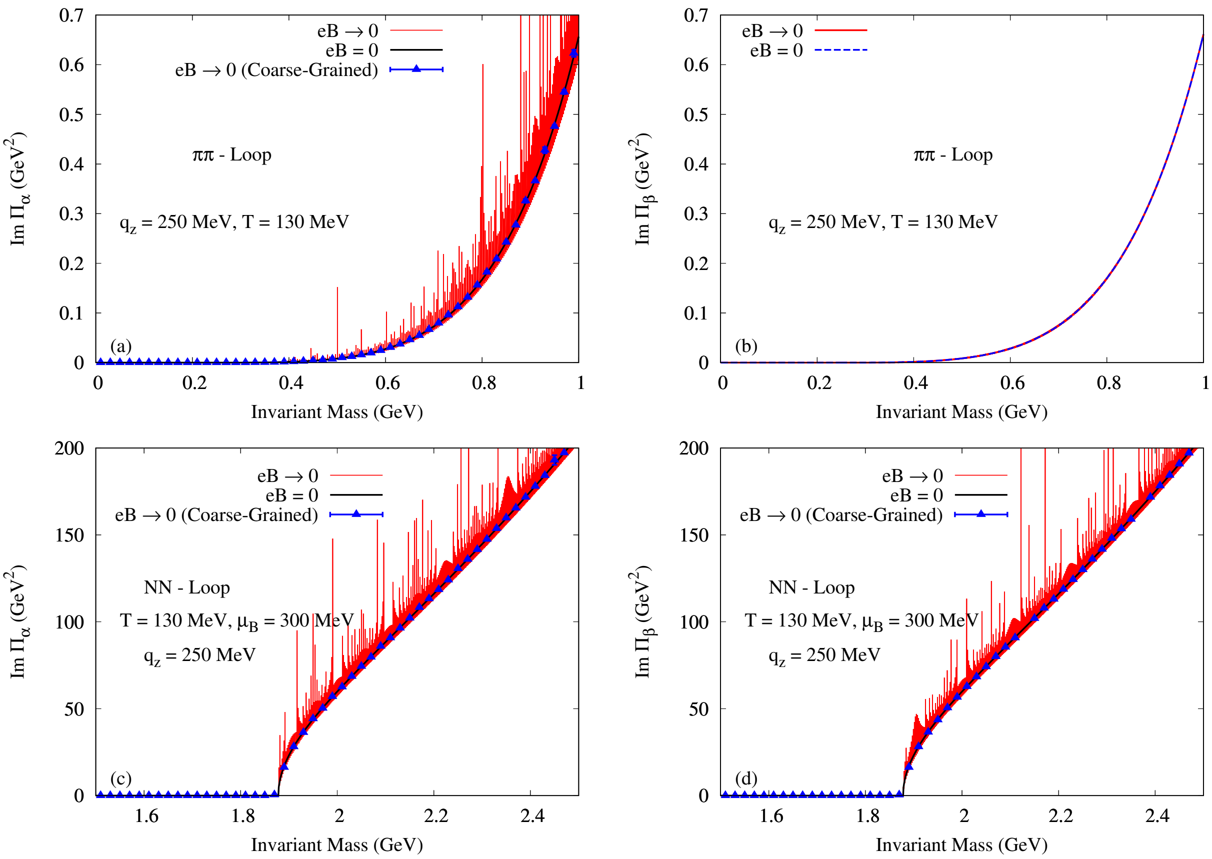

Figure 4.4: The imaginary part of the form factors as a function of the invariant mass at $eB = 0$ have been compared with the imaginary part at non zero magnetic field in the numerical limit $eB \to 0$ at temperature $T = 130$ MeV and at baryon chemical potential $\mu_B = 300$ MeV with ρ^0 longitudinal momentum $q_z = 250$ MeV. The contribution due the $\pi\pi$ loop from the form factors Π_α and Π_β are shown in panels (a) and (b) respectively. The corresponding contributions due the NN loop are shown in panels (c) and (d). The respective coarse-grained (CG) quantities from the $eB \to 0$ results are also shown in (a), (c) and (d).

Ehrenfest's coarse-graining (CG) [194, 196, 197]. In this method, the whole invariant mass region has been discretized in small bins followed by bin averages. In other words, the self energy at a given $\sqrt{q_\parallel^2}$ is approximated by its average over the neighbourhood around that point. This in turn smears out the spike like structures. As can be seen in the figure, after CG, ImΠ_α exactly matches with the analytic $eB = 0$ graph. The corresponding comparison of $eB \to 0$ and $eB = 0$ result for ImΠ_β due to $\pi\pi$ loop is shown in Fig. 4.4(b). In this case, $eB \to 0$ graph is finite and free from the threshold singularities and it matches exactly with the $eB = 0$ graph. The absence of the threshold singularities in this case is due to an overall factor of Källén functions coming from $\tilde{\mathcal{N}}^{00}_{\pi,nl}$ in Eq. (4.133) which cancels the Källén functions in the denominator of Eq. (4.132). Thus the ImΠ_β due to the $\pi\pi$ loop does not require to be coarse grained.

The corresponding results for the NN loop is depicted in Figs. 4.4(c) and 4.4(d). In this

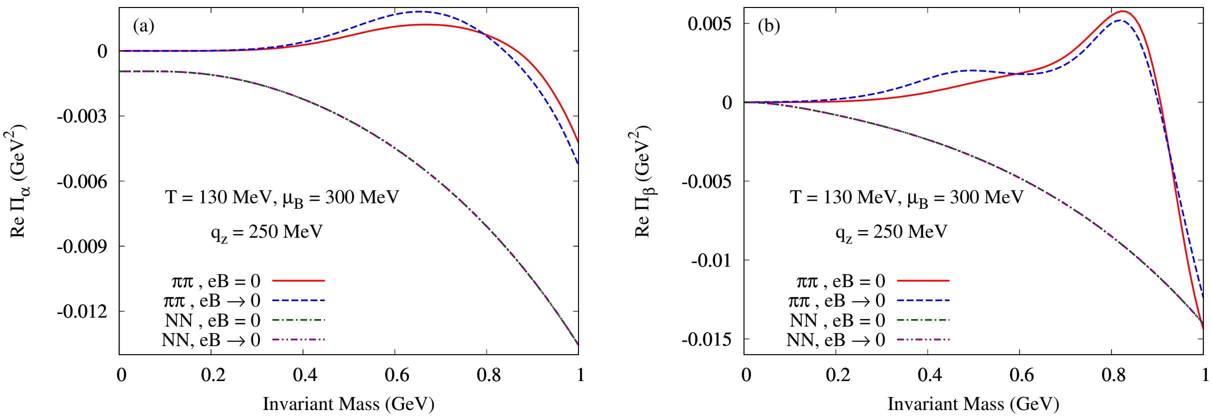

Figure 4.5: The real part of the form factors as a function of the invariant mass at $eB = 0$ have been compared with the real part at non zero magnetic field in the numerical limit $eB \to 0$ at temperature $T = 130$ MeV and at baryon chemical potential $\mu_B = 300$ with ρ^0 longitudinal momentum $q_z = 250$ MeV. The contribution from the form factors (a) Π_α and (b) Π_β are shown separately due to $\pi\pi$ and NN loop.

case, both the ImΠ_α and ImΠ_β suffer threshold singularities as there is no overall Källén functions coming from $\tilde{\mathcal{N}}^{\mu\nu}_{\mathrm{p},nl}$. So both the form factors have to be coarse grained after which they exactly reproduce the $eB = 0$ graphs.

We now turn our attention to the real part of the self energy at non-zero magnetic field and show how a numerical limit of $eB \to 0$ agrees with the $eB = 0$ results. This has been shown in Fig. 4.5 where the real part of the form factors is shown as a function of ρ^0 invariant mass with longitudinal momentum $q_z = 250$ MeV at temperature $T = 130$ MeV and at baryon chemical potential $\mu_B = 300$ MeV for the two cases $eB \to 0$ and $eB = 0$. The contributions from the $\pi\pi$ and NN loops are shown separately. Fig. 4.5(a) depicts ReΠ_α whereas Fig. 4.5(b) shows ReΠ_β. As can be seen from the figure, the $eB \to 0$ graphs exactly reproduce the $eB = 0$ for the case of NN loop. Whereas, for the $\pi\pi$ loop, $eB \to 0$ is slightly deviated from the $eB = 0$ graph but with an excellent qualitative agreement in their behavior with respect to the variation of invariant mass of ρ^0. This small disagreement between the $eB \to 0$ and $eB = 0$ graph is due to the inaccuracy in the numerical principal value integration of Eqs. (4.20) and (4.50) for which the two particle bound state threshold $\sqrt{q_\parallel^2} > 2m_\pi = 280$ MeV is less than the ρ^0 mass pole $m_\rho = 0.770$ (in contrast, for the NN loop, the two particle bound state threshold is at $\sqrt{q_\parallel^2} > 2m_N = 1.878$ GeV much higher than the range of the plot).

Having checked the consistency of the non-zero magnetic field calculations, we now proceed to present the imaginary part of the self energy for nonzero values of the magnetic field. In Fig. 4.6, the variation of ImΠ_α is shown as a function of ρ^0 invariant mass with

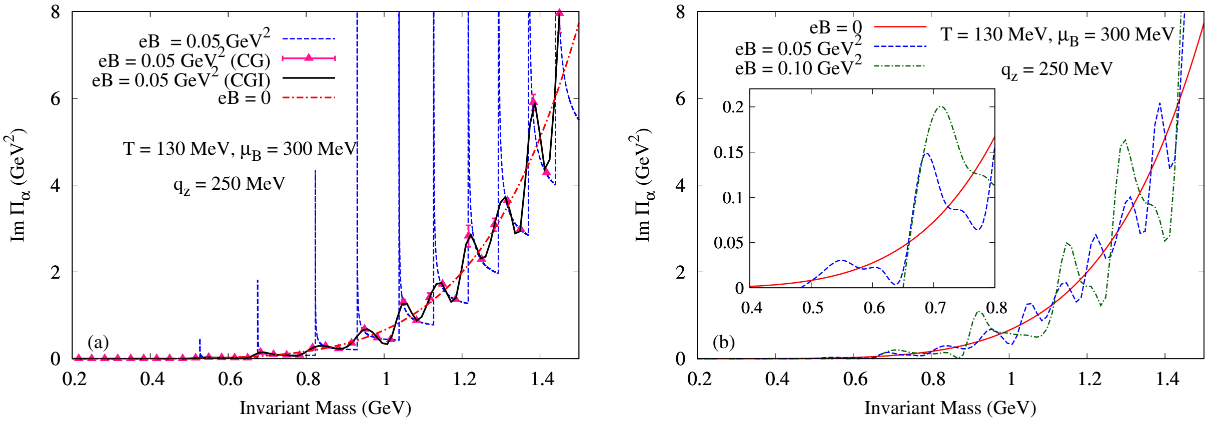

Figure 4.6: The contribution from the form factor ImΠ_α to the imaginary part of the ρ^0 self energy is shown as a function of invariant mass at temperature $T = 130$ MeV and at baryon chemical potential $\mu_B = 300$ with ρ^0 longitudinal momentum $q_z = 250$ MeV for (a) two different values of magnetic field ($eB = 0$ and 0.05 GeV^2 respectively) and (b) three different values of magnetic field ($eB = 0$, 0.05 and 0.10 GeV^2 respectively). The coarse-grained (CG) as well as coarse-grained interpolated (CGI) results are shown in (a) whereas (b) shows only the CGI results. The inset plot in (b) shows the movement of the Unitary cut threshold by focusing in smaller range of invariant mass.

longitudinal momentum $q_z = 250$ MeV at temperature $T = 130$ MeV and at baryon chemical potential $\mu_B = 300$ MeV. We have plotted the self energy up to $\sqrt{q_\parallel^2} = 1.5$ GeV for which the Unitary cut of the NN loop does not contribute. Fig. 4.6(a) depicts ImΠ_α at magnetic field $eB = 0.05$ GeV^2 in which the spikes get separated from each other by a finite value and it oscillates about the $eB = 0$ graph. This is more clearly visible in the CG points which are used to obtain a coarse-grained interpolated (CGI) graph. Fig. 4.6(b) shows the CGI imaginary part at two different values of the magnetic field ($eB = 0.05$ and 0.10 GeV^2 respectively); both of them are found to oscillate about the $eB = 0$ graph. Moreover, with the increase in magnetic field, the oscillation frequency decreases with an increase in the oscillation amplitude. This behavior of the imaginary part with increasing magnetic field is consistent with Fig. 4.4, where for the $eB \to 0$ case, the oscillation frequency becomes infinite and amplitude becomes zero, thus reproducing the $eB = 0$ graph. Also with the increase in magnetic field, the threshold of the unitary cut moves towards the higher invariant mass value as discussed in Sec. 4.6. This has been shown clearly in the inset plot.

The corresponding results for the ImΠ_β due to $\pi\pi$ loop as a function of ρ^0 invariant mass with longitudinal momentum $q_z = 250$ MeV at temperature $T = 130$ MeV and at baryon chemical potential $\mu_B = 300$ MeV are shown in Fig. 4.7 for the two different values of the magnetic field $eB = 0.10$ and 0.20 GeV^2. Analogous to ImΠ_α, ImΠ_β also oscillates about $eB = 0$ curve, but in this case the oscillation frequency is much smaller as compared

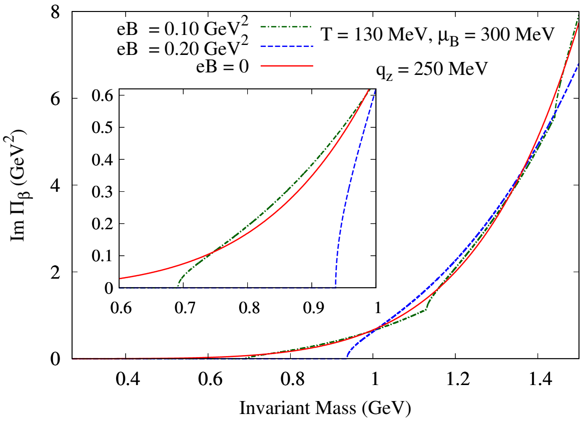

Figure 4.7: The contribution from the form factor $\mathrm{Im}\Pi_\beta$ to the imaginary part of the ρ^0 self energy is shown as a function of invariant mass at temperature $T = 130$ MeV and at baryon chemical potential $\mu_B = 300$ with ρ^0 longitudinal momentum $q_z = 250$ MeV for three different values of magnetic field ($eB = 0$, 0.05 and 0.10 GeV^2 respectively). The inset plot shows the movement of the Unitary cut threshold by focusing in smaller range of invariant mass.

to $\mathrm{Im}\Pi_\alpha$. The threshold of the Unitary cut moves towards higher invariant mass with the increase in magnetic field as clearly depicted in the inset plot.

As discussed in Sec. 4.6, a non trivial Landau cut contribution in presence of external magnetic field may appear even if the loop particles have the same mass. In this case, we have observed Landau cut contribution only in $\mathrm{Im}\Pi_\alpha$, whereas the Landau cut does not appear in $\mathrm{Im}\Pi_\beta$. This can be understood from the expressions of trace and 00 component of $\tilde{\mathcal{N}}^{\mu\nu}_{\pi,nl}$ and $\tilde{\mathcal{N}}^{\mu\nu}_{\mathrm{p},nl}$ as given in Appendix D.6. It can be noticed that, for both the $\pi\pi$ and proton-proton loops, the expression for the trace (i.e $\tilde{\mathcal{N}}^{\mu}_{\mu}$) contains two additional Kronecker delta functions $\delta_l^{n\pm1}$ along with δ_l^n which is absent in the expressions for the 00 component (i.e $\tilde{\mathcal{N}}^{00}$) (see Eqs.(D.49)-(D.52)). This implies that, for $\mathrm{Im}\Pi_\alpha$, the loop particles can be in different Landau levels whereas for $\mathrm{Im}\Pi_\beta$ the loop particles will always stay in the same Landau levels. Thus, as discussed in Se. 4.6, the non-trivial Landau cuts will appear only in $\mathrm{Im}\Pi_\alpha$ and not in $\mathrm{Im}\Pi_\beta$. The contribution of the CGI Landau cuts to $\mathrm{Im}\Pi_\alpha$ as a function of ρ^0 invariant mass with longitudinal momentum $q_z = 250$ MeV is shown in Fig. 4.8. It is to be noted that, the Landau cuts also contain the threshold singularities and thus have to be coarse grained. Fig. 4.8(a) shows the variation of $\mathrm{Im}\Pi_\alpha$ at a temperature $T = 130$ MeV and at baryon chemical potential $\mu_B = 300$ MeV for three different values of the magnetic field ($eB = 0.05$, 0.07 and 0.10 GeV^2 respectively), whereas Fig. 4.8(b) shows the corresponding variation at magnetic field ($eB = 0.10$ GeV^2) for two different values of temperature ($T = 100$ and 130 MeV respectively). The contributions due to $\pi\pi$ loop and proton-proton loops are shown separately and in Fig. 4.8(b); the contribution due to proton-proton loop is shown

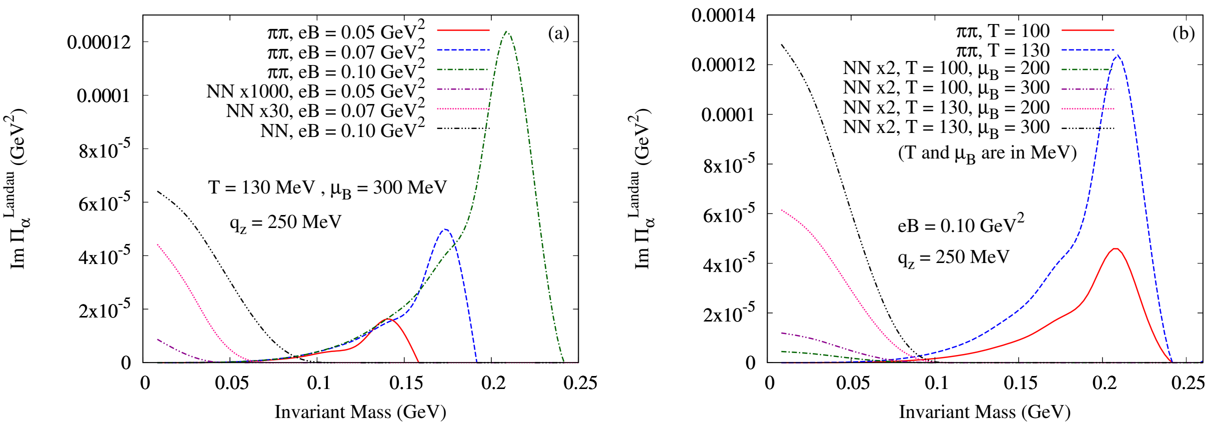

Figure 4.8: The contribution from the form factor Π_α to the Landau cut of the coarse grained (CG) imaginary part of the ρ^0 self energy is shown as a function of invariant mass with ρ^0 longitudinal momentum $q_z = 250$ MeV (a) at temperature $T = 130$ MeV and at baryon chemical potential $\mu_B = 300$ for three different values of magnetic field ($eB = 0.05$, 0.07 and 0.10 GeV^2 respectively) and (b) at magnetic field $eB = 0.10$ GeV^2 for two different values of temperature ($T = 100$ and 130 MeV respectively) and at baryon chemical potential ($\mu_B = 200$ and 300 MeV respectively). The contribution from the $\pi\pi$ and NN loops are shown separately in which the later is scaled with different factors for the sake of presentation.

for two different values of baryon chemical potential ($\mu_B = 200$ and 300 MeV). As can be seen from the figures, the threshold of the Landau cuts due to $\pi\pi$ loop is different (greater) than that of proton-proton loop which can be understood from the discussions of Sec. 4.6. The threshold for $\pi\pi$ loop is $\sqrt{q_\parallel^2} < \left(\sqrt{m_\pi^2 + eB} - \sqrt{m_\pi^2 + 3eB}\right)$, whereas the same for proton-proton loop is $\sqrt{q_\parallel^2} < \left(m_N - \sqrt{m_N^2 + 2eB}\right)$. The shift of the Landau cut threshold towards the higher invariant mass values with the increase in magnetic field can be clearly seen in Fig. 4.8(a). It is observed the the magnitude of the Landau cut contribution due to proton-proton loop is much less than that of $\pi\pi$ loop at lower values of the magnetic field and they become comparable to each other only at $eB \gtrsim 0.10$ GeV^2. In Fig. 4.8(a), we observe that with the increase in temperature and density, the Landau cut contribution increases without changing its threshold in the invariant mass axis.

We now turn our attention to the real part of the self energy at finite temperature under external magnetic field. In Fig. 4.9, we have shown the thermal contribution to the real part of the self energy as a function of invariant mass with ρ^0 longitudinal momentum $q_z = 250$ MeV at temperature $T = 130$ MeV and at baryon chemical potential $\mu_B = 300$ MeV for two different values of the magnetic field ($eB = 0.05$ and 0.10 GeV^2 respectively). The contributions from the $\pi\pi$ and NN loops are summed up in this figure. We notice that, with the increase in magnetic field, the thermal contribution to the real part of the self energy oscillates about the $eB = 0$ curve. The oscillation frequency and the oscillation amplitude

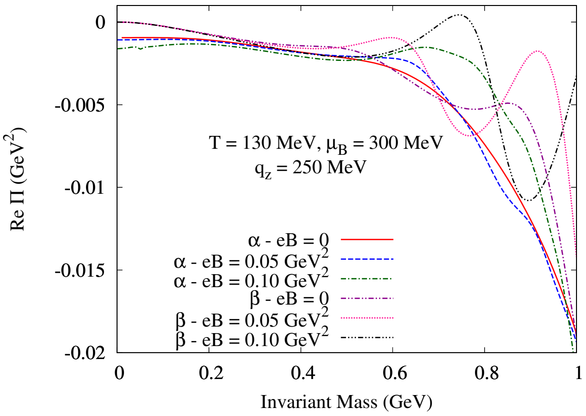

Figure 4.9: The real part of the thermal self energy of ρ^0 as a function of invariant mass at temperature $T = 130$ MeV and at baryon chemical potential $\mu_B = 300$ MeV with ρ^0 longitudinal momentum $q_z = 250$ MeV is shown for three different values of magnetic field (0, 0.05 and 0.10 GeV^2 respectively).

respectively decreases and increases with the magnetic field.

Next in Fig. 4.10, the "eB-dependent vacuum" contribution to the real part of the self energy is shown as a function of ρ^0 invariant mass with longitudinal momentum $q_z = 250$ MeV for two different values of magnetic field ($eB = 0.10$ and 0.20 GeV^2 respectively). Figs. 4.10(a) and 4.10(b) show the contributions from Π_α and Π_β respectively. The contributions due to $\pi\pi$ and proton-proton loops are shown separately. First of all, we note that at $eB = 0$, these term will vanish. With the increase of the magnetic field, the eB-dependent vacuum term also increases and the contribution of Π_β is more than Π_α.

Having obtained the real and imaginary parts of the self energy, we now proceed to evaluate the in-medium spectral functions of ρ^0 under external magnetic field. We have from Eq. (4.106), the complete ρ^0 propagator as

$$\overline{\overline{D}}^{\mu\nu} = A_\alpha P_1^{\mu\nu} + A_\beta P_2^{\mu\nu} + A_\gamma P_3^{\mu\nu} + A_\delta Q^{\mu\nu} + \xi q^\mu q^\nu \tag{4.142}$$

where the coefficients are given in Esq. (4.107)-(4.111) and the basis tensors are provided in Eqs. (4.72)-(4.75). Since we will be considering the special case $q_\perp = 0$ for which $\Pi_\alpha = \Pi_\gamma$ and $\Pi_\delta = 0$ as given in Eq. (4.112), the coefficients in the above equation become

$$A_\alpha = \left(\frac{1}{q_\parallel^2 - m_\rho^2 + \Pi_\alpha}\right) \tag{4.143}$$

$$A_\beta = \left(\frac{1}{q_\parallel^2 - m_\rho^2 + \Pi_\beta}\right) \tag{4.144}$$

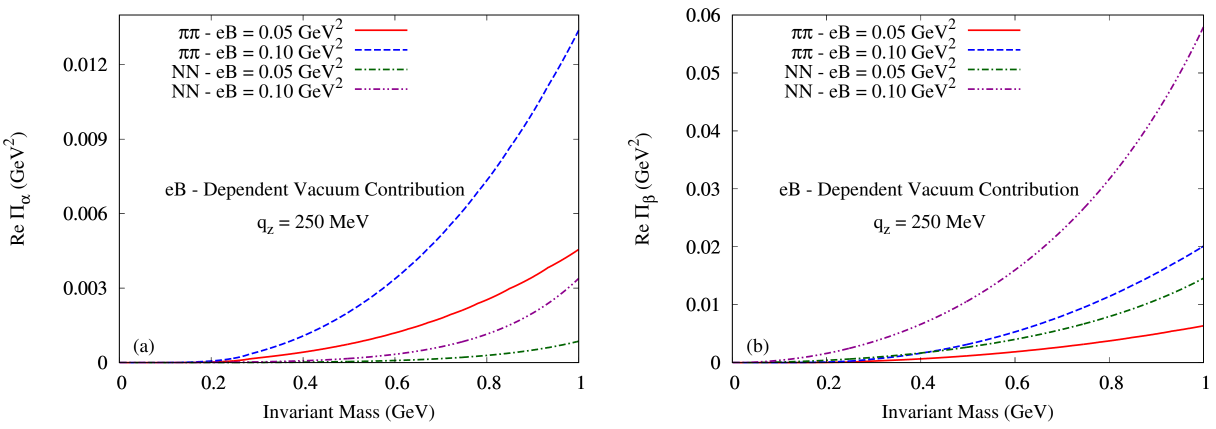

Figure 4.10: The eB-dependent vacuum contribution to the real part of the self energy of ρ^0 as a function of invariant mass with ρ^0 longitudinal momentum $q_z = 250$ MeV is shown at two different values of magnetic field ($eB = 0.05$ and 0.10 Gev^2 respectively) for the form factors (a) Π_α and (b) Π_β. The contribution due to $\pi\pi$ and proton-proton loops are shown separately.

$$A_\gamma = \left(\frac{1}{q_\parallel^2 - m_\rho^2 + \Pi_\gamma}\right) \tag{4.145}$$

$$A_\delta = 0 \tag{4.146}$$

$$\xi = \frac{-1}{q_\parallel^2 m_\rho^2} \tag{4.147}$$

so that the complete in-medium interacting propagator is given by

$$\overline{\overline{D}}^{\mu\nu}(q^0, q_z) = \frac{P_1^{\mu\nu}}{\left(q_\parallel^2 - m_\rho^2 + \Pi_\alpha\right)} + \frac{P_2^{\mu\nu}}{\left(q_\parallel^2 - m_\rho^2 + \Pi_\beta\right)} + \frac{P_3^{\mu\nu}}{\left(q_\parallel^2 - m_\rho^2 + \Pi_\alpha\right)} - \frac{q_\parallel^\mu q_\parallel^\nu}{q_\parallel^2 m_\rho^2} \; . \tag{4.148}$$

It is clear from the above equation, that there will be three modes for the propagation of ρ^0 meson in magnetized medium for vanishing transverse momentum of ρ^0. Of the three modes, two are found to be degenerate (the first and third term in the RHS of above equation) leaving two distinct modes for the propagation of ρ^0 which we denote as Mode-A and Mode-B respectively.

We now define the spectral function S_ρ of ρ^0 for the two distinct modes as the the imaginary part of the complete propagator which is obtained from Eq. (4.148) as

$$S_\rho^{(A)} = \mathrm{Im}\left[\frac{-1}{q_\parallel^2 - m_\rho^2 + \Pi_\alpha}\right] = \frac{\mathrm{Im}\Pi_\alpha}{(q_\parallel^2 - m_\rho^2 + \mathrm{Re}\Pi_\alpha)^2 + (\mathrm{Im}\Pi_\alpha)^2} \tag{4.149}$$

and

$$S_\rho^{(B)} = \mathrm{Im}\left[\frac{-1}{q_\parallel^2 - m_\rho^2 + \Pi_\beta}\right] = \frac{\mathrm{Im}\Pi_\beta}{(q_\parallel^2 - m_\rho^2 + \mathrm{Re}\Pi_\beta)^2 + (\mathrm{Im}\Pi_\beta)^2}. \tag{4.150}$$

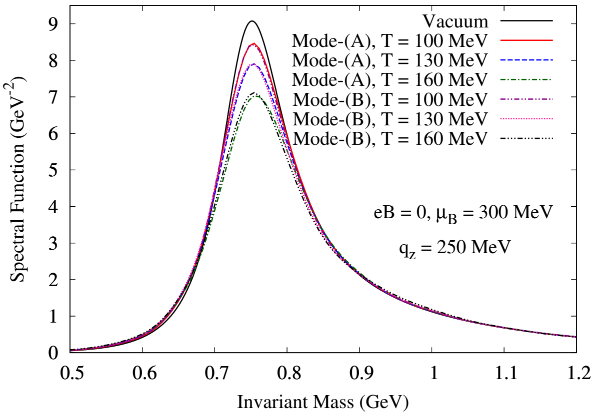

Figure 4.11: The in-medium spectral function of ρ^0 as a function of invariant mass at zero magnetic field and at baryon chemical potential μ_B=300 MeV with ρ^0 longitudinal momentum $q_z = 250$ MeV is shown for three different values of temperature ($T = 100$, 130 and 160 MeV) and for different modes. The vacuum spectral function is also shown for comparison.

In Fig. 4.11, the spectral function for the two modes at zero magnetic field is shown as a function of ρ^0 invariant mass with ρ^0 longitudinal momentum $q_z = 250$ MeV at baryon chemical potential $\mu_B = 300$ MeV for three different values of temperature ($T = 100$, 130 and 160 MeV respectively). The vacuum spectral function (which is same for the two modes) is also shown for comparison. We find that, the spectral functions have a nice Breit-Wigner shape around the ρ^0 mass pole with a width $\mathcal{O}(150$ MeV) corresponding to the decay of $\rho^0 \to \pi^+\pi^-$. With the increase in temperature, the width of the spectral function increases and the peak decreases. Physically, it corresponds to the enhancement of the decay process in the medium implying that the ρ^0 become more unstable at a high temperature. It is important to note that, for the invariant mass region shown in the plot, the imaginary part of the self energy that enters in the calculation of spectral function is completely due to the Unitary-I cut of $\pi\pi$ loop. On the other hand, the real part of the self energy that enters in the spectral function calculation has contributions from both the $\pi\pi$ and NN loops.

It can be noticed that, even at a higher temperature ($T \sim 160$ MeV), the peak of the spectral functions have marginal shifts over the invariant mass axis which correspond to a negligible mass shift of the ρ meson with respect to its vacuum mass. However, the hadron-QGP phase transition of QCD occurs around this particular temperature ($T \sim 160$ MeV) for which a significant mass shift of ρ meson is expected. In some earlier works, small decrease ($< 20\%$) in ρ mass at high temperature ($T \sim 160$ MeV) have been reported, for example: in Ref. [198] using QCD sum rule approach; in Ref. [189] using Walecka model and in Ref. [199] using effective interactions of ρ with π, ω, h_1 and a_1 mesons. The observed negligible mass shift of ρ in the medium is a consequence of non-chiral phenomenological $\rho\pi\pi$ and ρNN

interaction considered in this work. However in case of Walecka model, the shift of the spectral function with temperature can be achieved by considering, in the loop, the effective nucleon mass which will also be a function of temperature and chemical potential. However, in that case, generalisation to the non-zero magnetic fields also requires proper incorporation of the magnetically modified effective nucleon mass which is beyond the scope of the present work. We should also mention that hadronic description is expected to brek down arround the hadron-QGP phase transition region. A more sophisticated and realistic approach to include the effect of chiral phase transition of QCD is to use models like NJL, PNJL, PQM etc. for the study of the in medium spectral properties of ρ meson. Moreover, in presence of the background magnetic field, those approaches can also shed light on the magnetic catalysis or the inverse magnetic catalysis of the critical temperature corresponding to the quark-hadron phase transition [139].

We now turn on the external magnetic field and show the spectral function of ρ^0 as a function of its invariant mass for the two modes in Fig. 4.12. The range of the invariant mass axis is taken as 0.5-1.2 GeV which is dominated by the Unitary cut contributions from the $\pi\pi$ loop. In Fig. 4.12(a), the spectral function with ρ^0 longitudinal momentum $q_z = 250$ MeV at temperature $T = 130$ MeV and at baryon chemical potential $\mu_B = 300$ MeV is shown for three different values of the magnetic field ($eB = 0.10$, 0.15 and 0.20 GeV^2 respectively). It is observed that, with the increase in the magnetic field, the two modes get well separated from each other and the threshold of the spectral function moves towards higher values of invariant mass corresponding to the magnetic field dependent Unitary cut threshold of the imaginary part of the self energy. At sufficiently high values of the magnetic field, the spectral function misses the ρ^0 mass pole (770 MeV) so that it looses its Breit-Wigner shape which may be termed as ρ^0 "melting" in presence of magnetic field. The critical value of the magnetic field for a given temperature and baryon chemical potential for which the ρ^0 will melt is discussed later.

In Fig. 4.12(b), the spectral function with ρ^0 longitudinal momentum $q_z = 250$ MeV at a magnetic field $eB = 0.10$ GeV^2 and at a baryon chemical potential $\mu_B = 300$ MeV is shown for three different values of temperature ($T = 100$, 130 and 160 MeV respectively). In this case, the threshold of the spectral function remains fixed and for both the modes, the spectral function becomes shorter and wider with the increase in temperature with a marginal shift of its peak. The shift of the peak is due to the modification in the real part of the self energy with the change in temperature.

Fig. 4.12(c) depicts the spectral function with ρ^0 longitudinal momentum $q_z = 250$ MeV at a magnetic field $eB = 0.10$ GeV^2 and at a temperature $T = 160$ MeV for three different values of the baryon chemical potential ($\mu_B = 200$, 300 and 400 MeV respectively). Analogous to the previous case, the threshold of the spectral function remains fixed for both the modes. Since the baryon chemical potential only affects the real part of the self energy in the given kinematic region, the peak of the spectral function changes its position (keeping the width almost same) with the change in baryon chemical potential. It can be noticed, that in contrast to Fig. 4.12(b), the peak position of the spectral function is more sensitive to μ_B as compared to the temperature which is due to the dominant contribution coming from NN loop.

In Fig. 4.12(d), the spectral function at a magnetic field $eB = 0.10$ GeV^2 and at a temperature $T = 130$ MeV with baryon chemical potential $\mu_B = 300$ MeV is shown for two different values of ρ^0 longitudinal momentum ($q_z = 0$ and 500 MeV). In this case, the threshold of the spectral function remains same and the height of the spectral function increases with the increase of the longitudinal momentum.

We have already mentioned that, a non-trivial Landau cut in the physical kinematic region would appear in presence of the external magnetic field. In our case, the non-zero contribution to the Landau cut comes only from the form factor $\text{Im}\Pi_\alpha$ which is reflected in the the spectral function of Mode-(A). In Fig. 4.13, the spectral function as a function of ρ^0 invariant mass with ρ^0 longitudinal momentum $q_z = 250$ MeV is shown in the low invariant mass region which is dominated by the Landau cut contribution. It can be observed that the magnitude of the spectral function in this region is much lower as compared to the Unitary cut regions. Fig. 4.13(a) shows the spectral function at temperature $T = 130$ MeV and at baryon chemical potential $\mu_B = 300$ MeV for three different values of magnetic field ($eB = 0.10$, 0.15 and 0.20 GeV^2 respectively). As can be seen in the graph, the threshold of the Landau cut moves towards the higher values of invariant mass with the increase in magnetic field as a consequence of similar behavior of the Landau cut contribution to the imaginary part as shown in Fig. 4.8. Also the height of the spectral function is enhanced with the increase in eB. Fig. 4.13(b) shows the corresponding plots of spectral function at magnetic field $eB = 0.10$ GeV^2 for four different combinations of temperature and baryon chemical potential (($T = 100$ MeV, $\mu_B = 300$ MeV), ($T = 130$ MeV, $\mu_B = 300$ MeV), ($T = 160$ MeV, $\mu_B = 300$ MeV) and ($T = 160$ MeV, $\mu_B = 400$ MeV) respectively). As can be seen in the graph, the height of the spectral function increases with the increase in temperature and density owing to an enhancement of the corresponding scattering processes in presence of external magnetic field.

We now proceed to obtain the effective mass and dispersion relation of the ρ^0 in a magnetized medium. They follow from the pole of the complete ρ^0 propagator given in Eq. (4.148) which are obtained by solving the following transcendental equations

$$\omega^2 - q_z^2 - m_\rho^2 + \text{Re}\Pi_\alpha(q^0 = \omega, q_z, eB, T, \mu_B) = 0 \tag{4.151}$$

$$\omega^2 - q_z^2 - m_\rho^2 + \text{Re}\Pi_\beta(q^0 = \omega, q_z, eB, T, \mu_B) = 0 \tag{4.152}$$

whose numerical solutions $\omega = \omega(q_z, eB, T, \mu_B)$ represent the dispersion relations for the Mode-(A) and (B) corresponding to ρ^0 propagation in the magnetized medium. The effective mass m_ρ^* of ρ^0 is obtained from the dispersion relation by setting $q_z = 0$ i.e. $m_\rho^*(eB, T, \mu_B) = \omega(q_z = 0, eB, T, \mu_B)$.

Fig. 4.14(a) depicts the variation of m_ρ^*/m_ρ as a function of magnetic field at a temperature $T = 130$ MeV and at a baryon chemical potential $\mu_B = 300$ MeV. The effective mass for the two modes starts from the same value arround $eB = 0$ and with the increase in magnetic field, they get separated. For both the modes, the effective ρ^0 mass decreases with the increase in the magnetic field which is due to the strong positive contribution coming from the dominating eB-dependent vacuum part. The effect of magnetic field is found to be more in Mode-(B) as compared to Mode-(A). At a magnetic field value $eB = 0.20$ GeV^2, the effective ρ^0 mass in Mode-(A) decreases by about 2% whereas for the Mode-(B) it decreases by about 10%. Fig. 4.14(b) depicts the corresponding variation of effective mass with temperature at a magnetic field $eB = 0.10$ GeV^2 and at a baryon chemical potential $\mu_B = 300$ MeV. We find that, for both the modes effective mass of ρ^0 get enhanced by a small amount with the increase in temperature. Even at $T = 160$ MeV the change in effective mass is less than 2%. In Fig. 4.14(c), the variation of effective ρ^0 mass is shown as a function of baryon chemical potential at a magnetic field $eB = 0.10$ GeV^2 and at a temperature $T = 130$ MeV. In this case also, we observe an enhancement of the effective mass for both the modes with the increase in baryon density. Though the effect of μ_B on effective mass is more at a higher value of μ_B the change in the effective mass remains less than 2% even at $\mu_B = 500$ MeV.

Next, we present the dispersion curves of ρ^0 propagation in magnetized medium for both the modes in Fig. 4.15. We have plotted the energy ω of the ρ^0 scaled with the inverse of the vacuum rho mass $m_\rho = 770$ MeV as a function of the longitudinal momentum of ρ^0. Fig. 4.15(a) depicts the dispersion curves at temperature $T = 130$ MeV and at baryon chemical potential $\mu_B = 300$ MeV for two different values of magnetic field ($eB = 0.10$ and 0.20 GeV^2 respectively). Fig. 4.15(b) shows the same at a magnetic field $eB = 0.10$ GeV^2

and baryon chemical potential $\mu_B = 300$ MeV for two different temperatures ($T = 100$ and 160 MeV respectively). Finally, Fig. 4.15(c) shows the corresponding graphs at a magnetic field $eB = 0.10$ GeV^2 and at a temperature $T = 130$ MeV for two different values of baryon chemical potential ($\mu_B = 200$ and 400 MeV respectively). In all the cases, the dispersion curves are well separated from each other at lower transverse momentum. With the increase in q_z, the loop correction becomes subleading with respect to the kinetic energy of ρ^0 and thus, it approaches to a light-like dispersion.

Finally we calculate the decay width of ρ^0 for the decay into charged pions which is defined for the two modes as

$$\Gamma^{(A)}(eB,T,\mu_B) = \frac{\mathrm{Im}\Pi_\alpha(q^0 = m_\rho^*, q_z = 0, eB, T, \mu_B)}{m_\rho^*(eB,T,\mu_B)} \tag{4.153}$$

$$\Gamma^{(B)}(eB,T,\mu_B) = \frac{\mathrm{Im}\Pi_\beta(q^0 = m_\rho^*, q_z = 0, eB, T, \mu_B)}{m_\rho^*(eB,T,\mu_B)} . \tag{4.154}$$

In Fig. 4.16, the variation of the decay width Γ of ρ^0 scaled with inverse of its vacuum width ($\Gamma_0 = 156$ MeV) for the two modes is shown as a function of magnetic field. Note that the vacuum decay width is obtained from the imaginary part of the vacuum self energy as

$$\Gamma_0 = \frac{\mathrm{Im}\Pi_{\text{pure-vac}}(q^0 = m_\rho, \vec{q} = \vec{0})}{m_\rho} = 156 \text{ MeV} . \tag{4.155}$$

Results are presented for two different combinations of temperature and baryon chemical potential (($T = 130$ MeV, $\mu_B = 300$ MeV) and ($T = 160$ MeV, $\mu_B = 400$ MeV) respectively). Because of the presence of threshold singularity in $\mathrm{Im}\Pi_\alpha$, $\Gamma^{(A)}$ also suffers from the presence of threshold singularity for which it needs to be coarse grained. However, $\mathrm{Im}\Pi_\beta$ and hence $\Gamma^{(B)}$ is finite and free from the singularities. As can be seen from the figure, the ratio Γ/Γ_0 starts from a value greater than unity near $eB = 0$ which is due to the enhancement of the decay width over its vacuum value due to the effect of finite temperature and density. Also for a particular value of magnetic field, larger decay width is observed at higher temperature and density. Near $eB = 0$, the two modes have almost the same decay widths which begin to differ from each other with the increase in the magnetic field. An oscillatory behavior of the decay width can be clearly seen throughout the magnetic field range. One should also notice that, for both the modes, the oscillation amplitude increases whereas oscillation frequency decreases with eB. Finally at a critical value of the magnetic field, the decay width becomes zero. This is because of fact that, the eB-dependent Unitary cut threshold for the $\pi\pi$ loop has to satisfy

$$m_\rho^*(eB) > 2\sqrt{m_\pi^2 + eB} \tag{4.156}$$

for a kinematically favorable decay of $\rho^0 \to \pi^+\pi^-$. But, with the increase in magnetic field, the RHS of the above equation increases, whereas m_ρ^* in the LHS decreases so that at some critical value of magnetic field, the above inequality is violated and the decay width becomes zero. Physically it means, that ρ^0 becomes stable against the decay into $\pi^+\pi^-$ pair. This critical value of the field may be considered as the critical value of the magnetic field required for the "melting" of the spectral function of ρ^0.

In order to calculate the critical value of the magnetic field eB_c for a given temperature T and baryon chemical potential μ_B, we need to solve the transcendental equation

$$m_\rho^*(eB_c, T, \mu_B) = 2\sqrt{m_\pi^2 + eB_c}\ . \tag{4.157}$$

The green dash-dotted curve in Fig. 4.14(a) corresponds to $m_\rho^*/m_\rho = 2\sqrt{m_\pi^2 + eB}$ so that, the intersection of this curve with the $m_\rho^* = m_\rho^*(eB)$ represents the solution of the above equation. In Fig. 4.17, we show the variation of the critical magnetic field eB_c for the two decay modes. Fig. 4.17(a) depicts eB_c as a function of temperature for two different values of baryon chemical potential ($\mu_B = 50$ and 200 MeV) whereas Fig. 4.17(b) shows the corresponding variation with baryon chemical potential at two different values of temperature ($T = 100$ and 160 MeV). Although, with fixed temperature, the variation with respect to μ_B shows monotonically increasing trend, both the plots suggests non-monotonic variations of the critical magnetic field with respect to the temperature. More specifically, there exists a maximum value of chemical potential (see Fig. 4.17(b)) below which the critical field decreases with the temperature there by requiring relatively weaker magnetic field to completely stop the particular decay channel. However, for even larger values of μ_B, a significant increase with temperature can be observed for both of the decay modes.

Few comments on the magnitude of the external magnetic field are in order. The analytical expressions provided in this paper are valid for any arbitrary value of the external magnetic field which is constant in space-time. In presenting numerical results, we have considered magnetic field values in the range $0 \leq eB \leq 0.20$ GeV^2. It is worth noting that the magnetic field created in the HIC experiments is expected to decay rapidly with time [89]. However, a non-zero electrical conductivity of the strongly interacting fireball could possibly sustain the external magnetic field a bit longer [92, 98, 99] implying a slowly varying function of time during the entire life time of the QGP. The magnitude of the external magnetic field at the time of chemical freezeout (when the hadronic degrees of freedom manifests) is expected to be small because of the very small conductivity of the hadron gas. The experimental estimation of the same is not reported yet. In order to understand the plasma properties from the experimental data one solves relativistic magnetohydrodynamics equation usually with the assumption of ideal QGP fluid in the background electromagnetic field [100**?** , 101]. However, the ideal fluidity assumption can only be validated after knowing the transport coefficients at temperatures of phenomenological interest which are not yet certain. Despite these uncertinities, it should be mentioned here that the complete blocking of the neutral rho decay seems to be quite unlikely in the recent energy regimes of the HIC experiments. Though, one might expect a suppression in the $\rho^0 \to \pi^+\pi^-$ channel. Being the only possible strong decay channel of ρ^0 meson, its suppression is expected to lead to the enhancement of dilepton and photon production from ρ^0 decay. For example $\rho^0 \to \pi^0\gamma$ channel is expected to possess 64% branching ratio at the critical magnetic field of the order 10^{15} T [200]. However, recent measurement [201] showing no suppression in the strong decay channel of ρ^0 suggests that the magnetic effects on the neutral ρ decay, if exists, is negligibly small in the current HIC scenario. On the other hand, such magnetic modifications of mesonic properties can occur in situations present inside the high density compact objects with strong magnetic field such as magnetars. As a consequence, different relevant properties like equation of state, mass radius relationship etc. can be influenced.

4.8 Summary

In this chapter the spectral properties of the neutral rho meson is studied at finite temperature and density in a constant external magnetic field using the real time formalism of finite temperature field theory. The effective $\rho\pi\pi$ and ρNN interactions are considered for the evaluation of the one loop self energy of ρ^0. Accordingly, the magnetically modified in-medium propagators for pions and protons are used which contain infinite sum over the Landau levels implying no constraint on the strength of the external magnetic field. From the self-energy, the eB-dependent vacuum part is extracted by means of dimensional regularization in which the ultraviolet divergence corresponding to the pure vacuum self energy is isolated as the pole of gamma and Hurwitz zeta functions. It is shown that the external magnetic field does not create additional divergences so that the vacuum counter terms required in absence of the background field remain sufficient to renormalize the theory at non zero magnetic field.

The general Lorentz structure for the in-medium massive vector boson self energy in presence of external magnetic field has been constructed with four linearly independent basis tensors out of which three form a mutually orthogonal set. Thus, the the extraction of the form factors from the self energy becomes considerably simple. Moreover, it is shown that with vanishing perpendicular momentum of the external particle, one can arrive at new set of constraint relations among the form factors which essentially leave only two form factors to be determined from the self energy. As a consistency check, the numerical $B \to 0$ limit of the real as well as imaginary parts of the form factors are shown to reproduce the zero field results. Solving the Dyson-Schwinger equation with the one loop self energy, the complete interacting ρ^0 propagator is obtained. Consequently, two distinct modes are observed in the study of the effective mass, dispersion relations and the spectral function of ρ^0 where one of the modes (Mode-A) possesses two fold degeneracy. It is known [173, 194] that non trivial Landau cuts appear in presence of external magnetic field along with finite temperature even if the loop particles are of equal mass which is completely a magnetic field effect. However, in contrast to Mode-A, the non-trivial Landau cut is found to be absent in case of Mode-B. Also, sharper decrease in the effective mass is observed for the later which essentially stems from the dominant eB-dependent vacuum contribution in the real part of the corresponding form factor.

Finally, the decay width for $\rho^0 \to \pi^+\pi^-$ channel is obtained for the two distinct modes and is found to become zero at certain critical values of magnetic field depending upon the temperature and baryon chemical potential. The corresponding variation of the critical field with these external parameters shows increasing trend for large baryonic chemical potential. However, it is observed that, both the distinct modes possess a maximum value of μ_B below which the temperature dependence gets reversed. Especially, at a given temperature (say $T = 160$ MeV) , eB_c attains the lowest values (123 MeV^2 for Mode-A and 116 MeV^2 for Mode-B) in case of zero chemical potential [172].

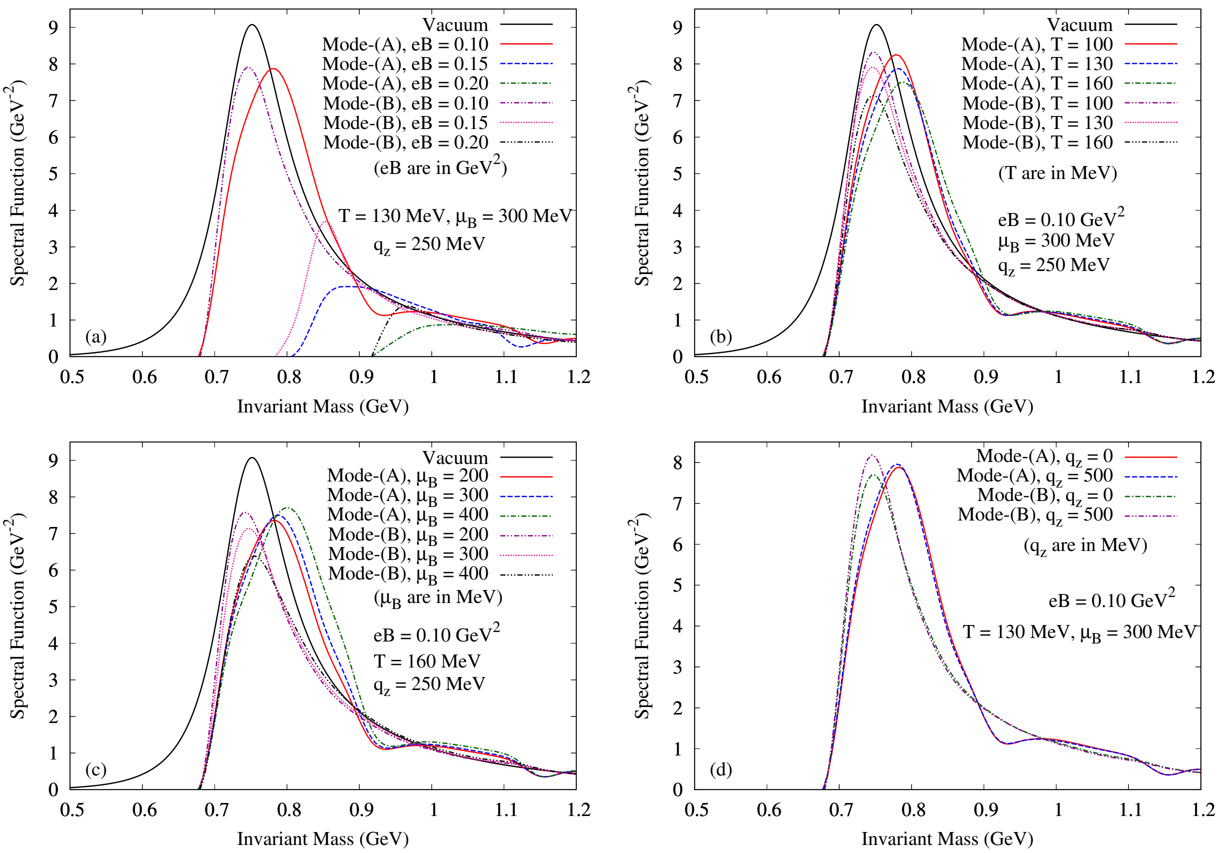

Figure 4.12: The in-medium spectral functions of ρ^0 as a function of invariant mass is shown for different modes (a) at temperature $T = 130$ MeV and at baryon chemical potential $\mu_B = 300$ MeV with ρ^0 longitudinal momentum $q_z = 250$ MeV for three different values of magnetic field ($eB = 0.10$, 0.15 and 0.20 GeV^2 respectively) (b) at magnetic field $eB = 0.10$ GeV^2 and at baryon chemical potential $\mu_B = 300$ MeV with ρ^0 longitudinal momentum $q_z = 250$ MeV for three different values of temperature ($T = 100$, 130 and 160 MeV respectively) (c) at magnetic field $eB = 0.10$ GeV^2 and at temperature $T = 160$ MeV with ρ^0 longitudinal momentum $q_z = 250$ MeV for three different values of baryon chemical potential ($\mu_B = 200$, 300 and 400 MeV respectively) and (d) at magnetic field $eB = 0.10$ GeV^2 and at temperature $T = 130$ MeV with baryon chemical potential $\mu_B = 300$ MeV for two different values of ρ^0 longitudinal momentum ($q_z = 0$ and 500 MeV respectively). The vacuum spectral function is also shown for comparison.

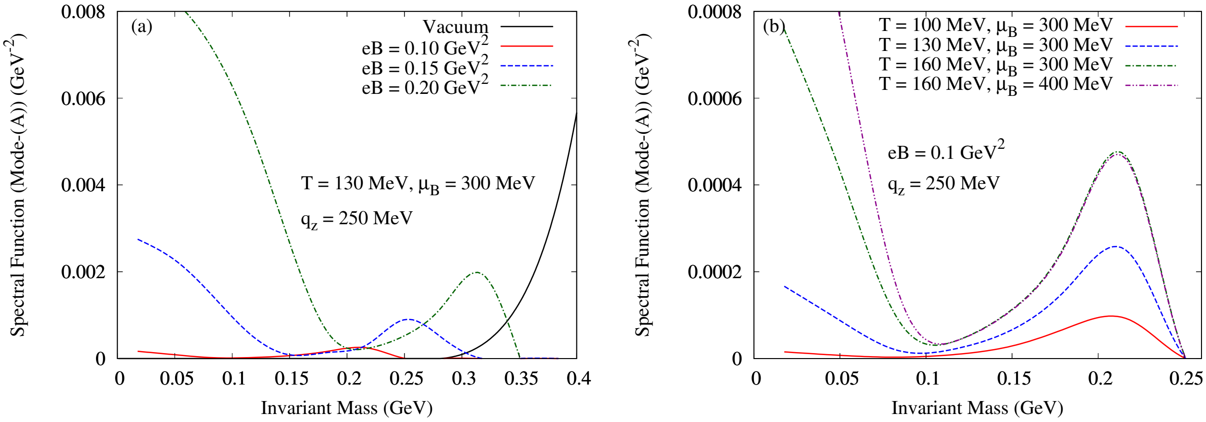

Figure 4.13: The in-medium spectral functions of ρ^0 for Mode-(A) as a function of invariant mass is shown in the low invariant mass region dominated by Landau cut contributions with ρ^0 longitudinal momentum $q_z = 250$ MeV : (a) At temperature $T = 130$ MeV and at baryon chemical potential $\mu_B = 300$ MeV for three different values of magnetic field ($eB = 0.10$, 0.15 and 0.20 GeV^2 respectively) and (b) at magnetic field $eB = 0.10$ GeV^2 for four different combinations of temperature and baryon chemical potential (($T = 100$ MeV, $\mu_B = 300$ MeV), ($T = 130$ MeV, $\mu_B = 300$ MeV), ($T = 160$ MeV, $\mu_B = 300$ MeV) and ($T = 160$ MeV, $\mu_B = 400$ MeV) respectively).

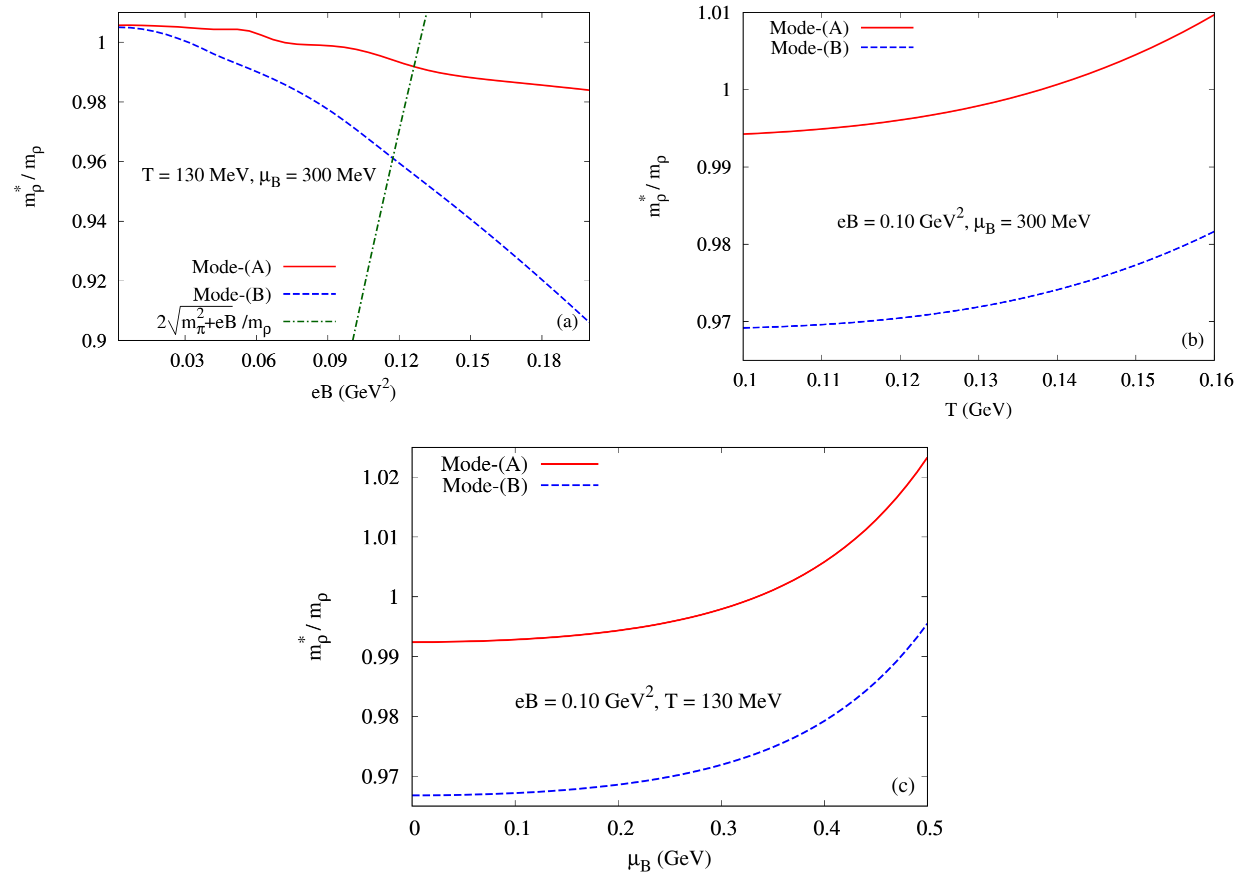

Figure 4.14: The ratio of effective mass of ρ^0 to its vacuum mass for different modes (a) as a function of magnetic field at temperature $T = 130$ MeV and at baryon chemical potential $\mu_B = 300$ MeV (b) as a function of temperature at magnetic field $eB = 0.10$ GeV^2 and at baryon chemical potential $\mu_B = 300$ MeV and (c) as a function of baryon chemical potential at temperature $T = 130$ MeV and at magnetic field $eB = 0.10$ GeV^2. The green dash-dotted curve in (a) corresponds to the Unitary cut threshold for decay of $\rho^0 \to \pi^+\pi^-$. Here $m_\rho = 770$ MeV.

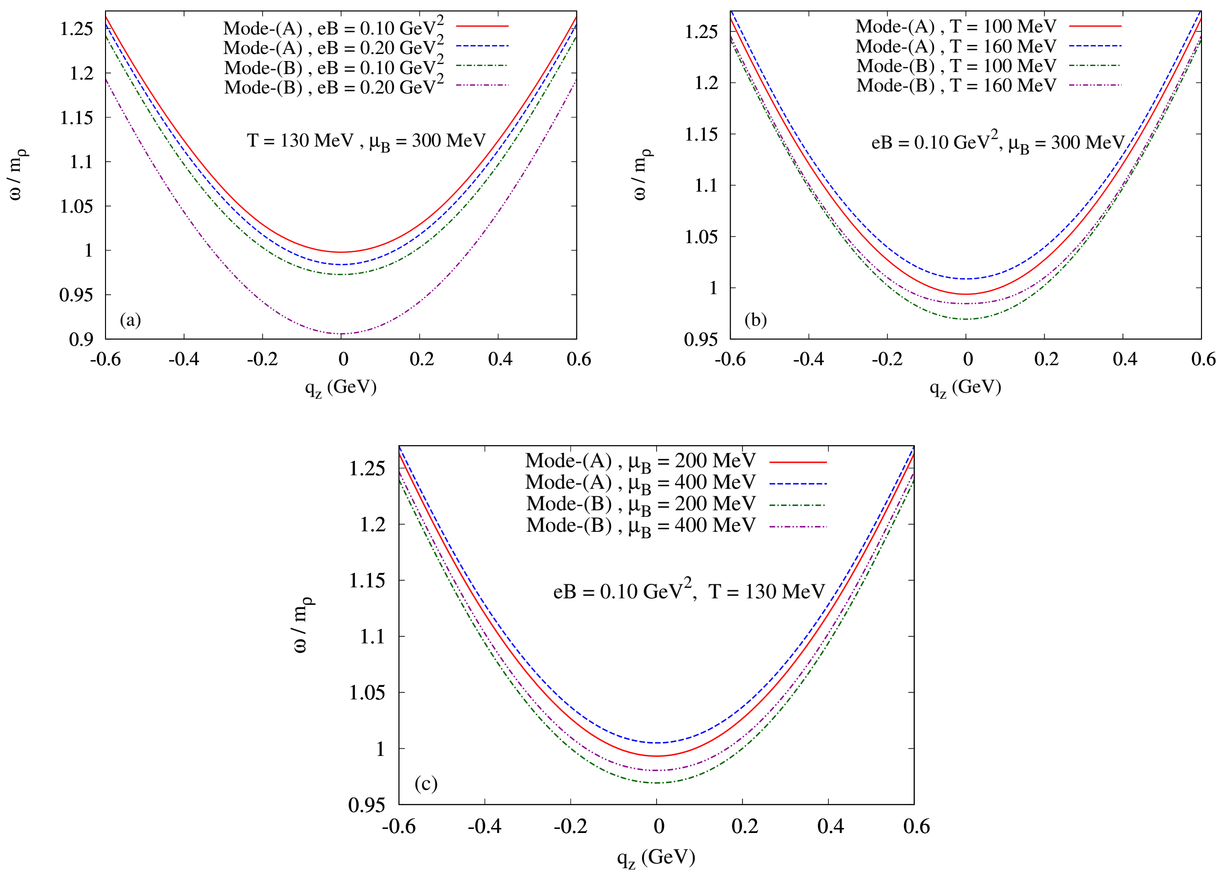

Figure 4.15: The dispersion relations of ρ^0 for different modes: (a) At temperature $T = 130$ MeV and at baryon chemical potential $\mu_B = 300$ MeV for two different values of magnetic field ($eB = 0.10$ and 0.20 GeV^2 respectively), (b) at magnetic field $eB = 0.10$ GeV^2 and at baryon chemical potential $\mu_B = 300$ MeV for two different temperatures ($T = 100$ and 160 MeV respectively) and (c) at magnetic field $eB = 0.10$ GeV^2 and at temperature $T = 130$ MeV for two different values of baryon chemical potential ($\mu_B = 200$ and 400 MeV respectively).

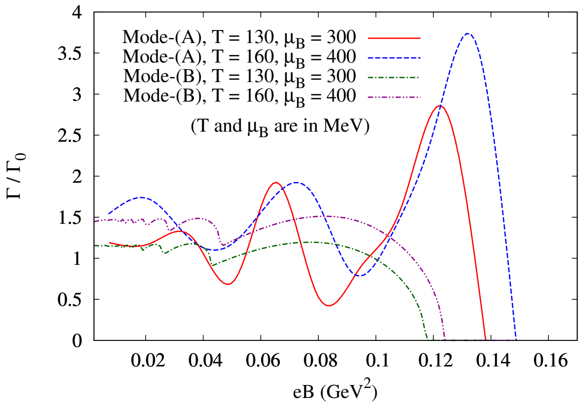

Figure 4.16: The ratio of the decay width of ρ^0 to its vacuum width as a function of magnetic field for different modes with two different combinations of temperature and baryon chemical potential (($T = 130$ MeV, $\mu_B = 300$ MeV) and ($T = 160$ MeV, $\mu_B = 400$ MeV) respectively). Here $\Gamma_0 = 156$ MeV.

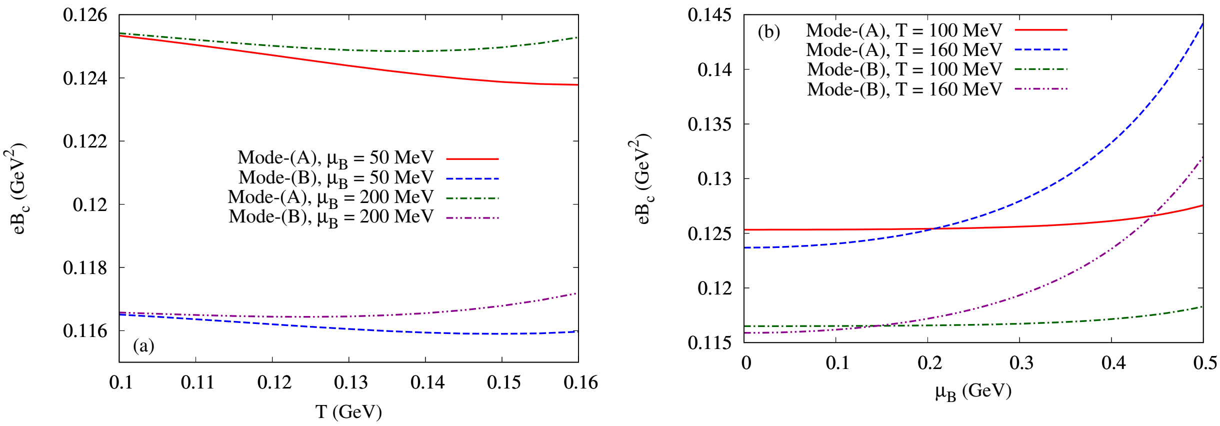

Figure 4.17: The variation of the critical value of magnetic field for stopping the decay of ρ^0 into $\pi^+\pi^-$ pair for different modes as a function of (a) temperature at two different values of baryon chemical potential ($\mu_B = 50$ and 200 MeV respectively) and (b) baryon chemical potential at two different values of temperature ($T = 100$ and 160 MeV respectively).

Chapter 5

Summary and Conclusions

The main focus of the thesis has been the modification of hadronic properties in presence of a uniform background magnetic field having magnitude typically of the order of m_π^2. Among the hadrons, specifically nucleons and neutral ρ mesons have been studied in two different contexts. More explicitly, nucleons are considered in the study of vacuum to nuclear matter phase transitions as discussed in chapter 3 whereas the main motivation for studying the spectral properties of ρ^0 (presented in chapter 4) is to investigate the magnetic field effects on the $\rho^0 \to \pi^+\pi^-$ decay in presence of a hot and dense medium.

The study related to nucleons considers Walecka model with mean field approximation in presence of weak external background magnetic field. The most important feature of the study is the incorporation of the anomalous magnetic moment of nucleons which brings in non-trivial correction terms in the nucleon propagators. As a result, unlike the case with vanishing magnetic moment, it is observed that the critical temperature decreases with the external magnetic field. Thus, it can be inferred that in presence of external magnetic field, the anomalous magnetic moment of the nucleons plays a crucial role in characterizing the nature of vacuum to nuclear matter transition at finite temperature and density. It should be mentioned here that Haber et.al [146] had speculated that the incorporation of AMM could counteract the effect of magnetic catalysis [153]. Our study not only supports the speculation but also concludes that the effect is significant enough to alter the qualitative behavior of the nucleon effective mass even in weak magnetic field regime. However, it should be noted here that the weak field approximation actually restricts the regime of validity of the present study. The maximum value of the external magnetic field used in the present study is taken to be 0.04 GeV^2 and it has been argued to be considered as 'weak' only up to density 1.8 ρ_0 where the assumption of 'weakness' is fixed by the condition that the chosen external field has to remain less than 50% of the effective mass. One should also notice that in case of

Walecka model, MC or IMC can only be seen indirectly. Similar studies in extended linear sigma model might be interesting as in that case the possibility of (approximate) chiral symmetry restoration is incorporated within the model framework. However, we should also mention that in case of zero magnetic moment, only the quantitative difference in the behavior of the effective mass is found to be attributed to the presence of the chiral partners [146] whereas the qualitative behavior, which has been the main interest throughout our work, seems to show model independence. Before applying the present results to obtain the characteristics of compact stars such as mass radius relationship or the equation of state, beta equilibrium and charge neutrality conditions have to be properly incorporated which can be an important extension of the present study.

The main observation in the study of neutral ρ meson is that at certain critical value of magnetic field, the decay width for $\rho^0 \to \pi^+\pi^-$ channel vanishes. The magnitude of the critical magnetic field depends on the temperature (T) and baryon chemical potential (μ_B) and is different for the two decay modes. Though the corresponding variation of the critical field with T and μ_B shows increasing trend for large baryonic chemical potential, there exists a maximum value of μ_B below which the temperature dependence gets reversed.

In Ref. [168], charged rho meson condensation has been studied at finite temperature and density. For charged rho mesons, the critical field for which the vector meson mass vanishes is observed to lie in the range of 0.2-0.6 GeV^2 at zero density with temperature in the range 0.2-0.5 GeV. However, in case of ρ^0, the absence of the trivial Landau shift in the energy eigenvalue results in much slower decrease in the effective mass. As a consequence, unrealistically high magnetic field values are required to observe neutral rho condensation in presence of temperature and medium (see Fig.4.14). In this scenario, the suppression in the $\rho^0 \to \pi^+\pi^-$ channel can serve as an important alternative. However, one has to remember that the magnetic modification of rho meson properties studied in this work deals with effective hadronic interactions. Thus, the observable modification can only occur if the initial burst of magnetic field survives up to hadronization retaining an appreciable field strength. However, the recent report [201] suggests no detectable suppression in the branching ratio of $\rho^0 \to \pi^+\pi^-$ channel implying that the magnetic field effects in the neutral ρ decay is negligible in HIC experiments. On the other hand, the present study can be relevant in situations present inside magnetars.

Appendices

Appendix A

Essential steps used in the derivation of propagator

A.1 Solution of Drac equation in presence of magnetic field

We consider magnetic field is along z direction. So we choose magnetic vector potential as $\vec{A} = (0, Bx^1, 0)$ in Landau gauge. However, we can write this in other gauges also.
Modified Dirac equation in presence of magnetic field can be written as,

$$i\frac{\partial \Psi}{\partial t} = H_B \Psi \tag{A.1}$$

where modified Hamiltonian is given by

$$H_B = \vec{\alpha} \cdot \vec{\Pi} + \beta m \ , \ \vec{\alpha} = \gamma_0 \vec{\gamma} \ , \ \beta = \gamma_0 \tag{A.2}$$

$$\alpha_i \ = \ \gamma_0 \gamma_i = \begin{pmatrix} 0 & \sigma_i \\ \sigma_i & 0 \end{pmatrix} \tag{A.3}$$

$$\beta = \gamma_0 = \begin{pmatrix} 1 & 0 \\ 0 & -1 \end{pmatrix} \tag{A.4}$$

Modified momentum in presence of magnetic field is

$$\vec{\Pi} = -i\vec{\nabla} - q\vec{A} \tag{A.5}$$

Solution of Dirac equation is 4 component vector.

We can write plane wave solution of Eq. (A.1) as

$$\Psi = e^{-iEt}\begin{pmatrix} \phi \\ \chi \end{pmatrix} \tag{A.6}$$

Now Eq. (A.1) implies,

$$E\begin{pmatrix} \phi \\ \chi \end{pmatrix} e^{-iEt} = \begin{pmatrix} m & \vec{\sigma}\cdot\vec{\Pi} \\ \vec{\sigma}\cdot\vec{\Pi} & -m \end{pmatrix}\begin{pmatrix} \phi \\ \chi \end{pmatrix} e^{-iEt} \tag{A.7}$$

$$\begin{pmatrix} E\phi \\ E\chi \end{pmatrix} = \begin{pmatrix} m\,\phi + \vec{\sigma}\cdot\vec{\Pi}\,\chi \\ \vec{\sigma}\cdot\vec{\Pi}\,\phi - m\,\chi \end{pmatrix} \tag{A.8}$$

So we get two coupled equations,

$$(E-m)\phi = \vec{\sigma}\cdot\vec{\Pi}\,\chi \tag{A.9}$$

$$(E+m)\chi = \vec{\sigma}\cdot\vec{\Pi}\,\phi \tag{A.10}$$

From Eq. (A.9) using Eq. (A.10), we get decoupled equation.

$$\begin{aligned} (E-m)\vec{\sigma}\cdot\vec{\Pi}\,\phi &= (\vec{\sigma}\cdot\vec{\Pi})^2\chi \\ (E+m)(E-m)\chi &= (\vec{\sigma}\cdot\vec{\Pi})^2\chi \end{aligned} \tag{A.11}$$

$$\text{Similarly, } (E+m)(E-m)\phi = (\vec{\sigma}\cdot\vec{\Pi})^2\phi \tag{A.12}$$

$$\Pi^i = -i\frac{\partial}{\partial x^i} - qA^i \tag{A.13}$$

$$\Pi^1 = -i\frac{\partial}{\partial x^1}\,,\ \Pi^2 = -i\frac{\partial}{\partial x^2} - qBx^1\,,\ \Pi^3 = -i\frac{\partial}{\partial x^3} \tag{A.14}$$

We use the well known identity

$$(\vec{\sigma}\cdot\vec{a})(\vec{\sigma}\cdot\vec{b}) = \vec{a}\cdot\vec{b} + i(\vec{a}\times\vec{b})\cdot\vec{\sigma} \tag{A.15}$$

$$\begin{aligned}\left(\vec{\sigma}\cdot\vec{\Pi}\right)^2 &= \left(\vec{\sigma}\cdot\vec{\Pi}\right)\left(\vec{\sigma}\cdot\vec{\Pi}\right)\\ &= (\Pi)^2 + i\left(\vec{\Pi}\times\vec{\Pi}\right)\cdot\vec{\sigma}\\ &= (\Pi)^2 + i\epsilon_{ijk}\Pi_j\Pi_k\sigma_i\end{aligned} \tag{A.16}$$

Here we note that, $\vec{\Pi}\times\vec{\Pi}\neq 0$.

$$\begin{aligned}i\epsilon_{ijk}\Pi_i\Pi_j\sigma_i &= i\epsilon_{312}\Pi_1\Pi_2\sigma_3 + i\epsilon_{321}\Pi_2\Pi_1\sigma_3\,,\ \text{(Other terms vanish)}\\ &= i\Pi_1\Pi_2\sigma_3 - i\Pi_2\Pi_1\sigma_3 = i\left[\Pi_1,\Pi_2\right]\sigma_3\end{aligned} \tag{A.17}$$

$$\begin{aligned}\Pi^1\Pi^2\psi &= (-i\frac{\partial}{\partial x^1})(-i\frac{\partial}{\partial x^2} - qBx^1)\psi\\ &= (-i\frac{\partial}{\partial x^1})(-i\frac{\partial\psi}{\partial x^2} - qBx^1\psi)\\ &= -\frac{\partial^2\psi}{\partial x^1\,\partial x^2} + iqB\psi + iqBx^1\frac{\partial\psi}{\partial x^1}\end{aligned} \tag{A.18}$$

$$\begin{aligned}\Pi^2\Pi^1\psi &= (-i\frac{\partial}{\partial x^2} - qBx^1)(-i\frac{\partial}{\partial x^1})\psi\\ &= (-i\frac{\partial}{\partial x^2} - qBx^1)(-i\frac{\partial\psi}{\partial x^1})\\ &= -\frac{\partial^2\psi}{\partial x^2\,\partial x^1} + iqBx^1\frac{\partial\psi}{\partial x^1}\end{aligned} \tag{A.19}$$

So we get[1] $[\Pi_1,\Pi_2] = iqB$. Using this in Eq. (A.16) one can get

$$\left(\vec{\sigma}\cdot\vec{\Pi}\right)^2 = (\Pi)^2 - qB\sigma_3 \tag{A.20}$$

From Eq. (A.12)

$$((\Pi)^2 - qB\sigma_3)\phi = (E^2 - m^2)\phi \tag{A.21}$$

[1] ψ and it's derivatives need to be well behaved to satisfy $\frac{\partial^2\psi}{\partial x^1\,\partial x^2} = \frac{\partial^2\psi}{\partial x^2\,\partial x^1}$.

$$
\begin{aligned}
\text{LHS,} \qquad & \left[-\frac{\partial^2}{\partial x^2} + (i\frac{\partial}{\partial y} + qBx)^2 - \frac{\partial^2}{\partial z^2} - qB\sigma_3\right]\phi \\
= \quad & \left[-\nabla^2 + 2iqBx\frac{\partial}{\partial y} + q^2B^2x^2 - qB\sigma_3\right]\phi
\end{aligned}
$$

Here only x is explicitly present in the expression. y and z are cyclic co-ordinates[2]. So we write trial solution as,

$$\phi = e^{i(p_y y + p_z z)} f(x) \tag{A.22}$$

σ_3 is 2×2 matrix. So $f(x)$ must be 2 component vector. Now we write $f(x)$ in eigen basis of σ_3.

$$f(x) = F_+(x)\begin{pmatrix}1\\0\end{pmatrix} + F_-(x)\begin{pmatrix}0\\1\end{pmatrix} \tag{A.23}$$

So we have

$$
\begin{aligned}
& \left[-\nabla^2 + 2iqBx\frac{\partial}{\partial y} + q^2B^2x^2 - qB\sigma_3\right] e^{i(p_y y + p_z z)} \begin{pmatrix}F_+(x)\\F_-(x)\end{pmatrix} \\
= \quad & \left[\left(-\frac{d^2}{dx^2} + p_y^2 + p_z^2 + 2qBxp_y + q^2B^2x^2\right)\mathbb{I} - qB\sigma_3\right] e^{i(p_y y + p_z z)} \begin{pmatrix}F_+(x)\\F_-(x)\end{pmatrix} \\
= \quad & \left[\hat{A}\mathbb{I} - qB\sigma_3\right]\left[F_+(x)\begin{pmatrix}1\\0\end{pmatrix} + F_-(x)\begin{pmatrix}0\\1\end{pmatrix}\right] \\
= \quad & \hat{A}F_+\begin{pmatrix}1\\0\end{pmatrix} - qB(+1)F_+\begin{pmatrix}1\\0\end{pmatrix} + \hat{A}F_-\begin{pmatrix}0\\1\end{pmatrix} - qB(-1)F_-\begin{pmatrix}0\\1\end{pmatrix}
\end{aligned} \tag{A.24}
$$

$$\begin{pmatrix}\hat{A}F_+ - qBF_+\\ \hat{A}F_- + qBF_-\end{pmatrix} = (E^2 - m^2)\begin{pmatrix}F_+\\F_-\end{pmatrix} \tag{A.25}$$

By writing this in compact notation,

$$
\begin{aligned}
& \hat{A}F_s - sqBF_s = (E^2 - m^2)F_s \ , s = \pm 1 \\
& -\frac{d^2F_s}{dx^2} - (p_y - qBx)^2F_s + (E^2 - m^2 - p_z^2 + sqB)F_s = 0
\end{aligned} \tag{A.26}
$$

[2]We have chosen $A^\mu = (0, Bx, 0)$, so y,z become cyclic. For symmetric gauge, z is cyclic and corresponding momentum is conserved.

(A.27)

Now we change the variable.

$$\xi = \sqrt{|qB|}\left(\frac{p_y}{qB} - x\right) \tag{A.28}$$

where $\xi^2 = \frac{|qB|}{(qB)^2}(p_y - qxB)^2$.

$$\frac{d}{dx} = \frac{d}{d\xi}\frac{d\xi}{dx} = -\sqrt{|qB|}\frac{d}{d\xi} \tag{A.29}$$

$$\frac{d^2}{dx^2} = \frac{d}{dx}(-\sqrt{|qB|}\frac{d}{d\xi}) = |qB|\frac{d^2}{d\xi^2} \tag{A.30}$$

From Eq. (A.26) we get,

$$\begin{aligned} \left[|qB|\frac{d^2}{d\xi^2} - |qB|\xi^2 + (E^2 - m^2 - p_z^2 + sqB)\right] F_s = 0 \\ \left[\frac{d^2}{d\xi^2} - \xi^2 + a_s\right] F_s = 0 \end{aligned} \tag{A.31}$$

where $a_s = \frac{1}{|qB|}(E^2 - m^2 - p_z^2 + sqB)$.
Again we apply a variable transformation,

$$\begin{aligned} F_s &= e^{-\frac{\xi^2}{2}} H(\xi) \\ \frac{dF_s}{d\xi} &= -e^{-\frac{\xi^2}{2}}\xi H(\xi) + e^{-\frac{\xi^2}{2}} H'(\xi) \\ \frac{d^2F_s}{d\xi^2} &= e^{-\frac{\xi^2}{2}}(\xi^2 - 1)H(\xi) - 2e^{-\frac{\xi^2}{2}}\xi H'(\xi) + e^{-\frac{\xi^2}{2}} H''(\xi) \end{aligned}$$

We can now write Eq. (A.31) as,

$$[H'' - 2\xi H' + (a_s - 1)H] = 0 \tag{A.32}$$

Solution of Eq. (A.32) is Hermite polynomial when $a_s - 1 = 2k$,$k \geq 0$.

$$E^2 = m^2 + p_z^2 - sqB + (2k + 1)|qB| \tag{A.33}$$

1. When $s = +1$ and $q = +e$

$$E^2 = m^2 + p_z^2 + 2kB. \tag{A.34}$$

2. When $s = +1$ and $q = -e$

$$\begin{aligned} E^2 &= m^2 + p_z^2 + 2(k+1)B \\ &= E^2 = m^2 + p_z^2 + 2k'B \end{aligned} \tag{A.35}$$

   where $k' = k + 1$.

3. When $s = -1$ and $q = +e$

$$E^2 = m^2 + p_z^2 + 2k'B \tag{A.36}$$

4. When $s = -1$ and $q = -e$

$$E^2 = m^2 + p_z^2 + 2kB. \tag{A.37}$$

Energy of fermion becomes quantised in presence of magnetic field.

$$E^2 = m^2 + p_z^2 + 2nB \tag{A.38}$$

Various values of n in Eq. (A.38) gives various Landau levels. In case of lowest Landau level ($n = 0$) $k = -1$ for case 2 and 3. This is not allowed for Hermite polynomial.

1. $s = +1$, $q = -e$

2. $s = -1$, $q = +e$

These states are not allowed. That means for negative charge particle $s = +1$ state (spin up) is not possible for LLL. And for positive charge particle $s = -1$ state (spin down) is not possible.

A.2 The details of completeness relations and operators

At first we prove the wave function normalizability.

$$
\begin{aligned}
& \int d^2\boldsymbol{r}_\perp \psi_{kp_2}(\boldsymbol{r}_\perp)^* \psi_{k'p'_2}(\boldsymbol{r}_\perp) \\
= & \frac{1}{2\pi\ell}\frac{1}{\sqrt{2^k k!\sqrt{\pi}}}\frac{1}{\sqrt{2^{k'}k'!\sqrt{\pi}}} \\
\times & \int dx^1 H_k\Big(\frac{x^1}{\ell}+p_2\ell\Big)H_{k'}\Big(\frac{x^1}{\ell}+p'_2\ell\Big)e^{-\frac{1}{2\ell^2}(x^1+p_2\ell^2)^2}e^{-\frac{1}{2\ell^2}(x^1+p'_2\ell^2)^2} \\
\times & \int dx^2 e^{is_\perp x^2 p_2}e^{-is_\perp x^2 p'_2} \\
= & \frac{1}{2\pi\ell}\frac{1}{\sqrt{2^k k!\sqrt{\pi}}}\frac{1}{\sqrt{2^{k'}k'!\sqrt{\pi}}} \\
\times & \int dx^1 H_k\Big(\frac{x^1}{\ell}+p_2\ell\Big)H_{k'}\Big(\frac{x^1}{\ell}+p'_2\ell\Big)e^{-\frac{1}{2\ell^2}(x^1+p_2\ell^2)^2}e^{-\frac{1}{2\ell^2}(x^1+p'_2\ell^2)^2} \\
\times & \frac{2\pi}{|s_\perp|}\delta(p_2-p'_2) \\
= & \frac{1}{\ell}\frac{1}{\sqrt{2^k k!\sqrt{\pi}}}\frac{1}{\sqrt{2^{k'}k'!\sqrt{\pi}}} \\
\times & \int dx^1 H_k\Big(\frac{x^1}{\ell}+p_2\ell\Big)H_{k'}\Big(\frac{x^1}{\ell}+p_2\ell\Big)e^{-\frac{1}{2\ell^2}(x^1+p_2\ell^2)^2}e^{-\frac{1}{2\ell^2}(x^1+p_2\ell^2)^2} \\
\times & \delta(p_2-p'_2) \\
= & \frac{1}{\sqrt{2^k k!\sqrt{\pi}}}\frac{1}{\sqrt{2^{k'}k'!\sqrt{\pi}}} \\
\times & \int \frac{dx^1}{\ell} H_k\Big(\frac{x^1}{\ell}+p_2\ell\Big)H_{k'}\Big(\frac{x^1}{\ell}+p_2\ell\Big)e^{-\frac{1}{\ell^2}(x^1+p_2\ell^2)^2}\delta(p_2-p'_2) \\
= & \frac{\delta(p_2-p'_2)}{\sqrt{2^k k!\sqrt{\pi}}\sqrt{2^{k'}k'!\sqrt{\pi}}} \\
\times & \int d\Big(\frac{x^1}{\ell}+p_2\ell\Big)H_k\Big(\frac{x^1}{\ell}+p_2\ell\Big)H_{k'}\Big(\frac{x^1}{\ell}+p_2\ell\Big)e^{-(\frac{x^1}{\ell}+p_2\ell)^2} \\
= & \delta_{kk'}\delta(p_2-p'_2)
\end{aligned}
\tag{A.39}
$$

where we have used

$$
\int dz H_k(z)H_{k'}(z)e^{-z^2} = 2^k k!\sqrt{\pi}\delta_{kk'} \tag{A.40}
$$

$$
|s_\perp| = 1 \tag{A.41}
$$

Another completeness relation we have used is

$$
\begin{aligned}
& \int_{-\infty}^{\infty} dp_2 \sum_{k=0}^{k=\infty} \psi_{kp_2}(\boldsymbol{r}_\perp)\psi^*_{kp_2}(\boldsymbol{r}'_\perp) \\
= & \int_{-\infty}^{\infty} dp_2 \frac{1}{2\pi\ell} \sum_{k=0}^{k=\infty} \Big[\frac{1}{2^k k!\sqrt{\pi}} H_k\Big(\frac{x^1}{\ell}+p_2\ell\Big) H_k\Big(\frac{x^{1'}}{\ell}+p_2\ell\Big)\Big] \\
\times & \; e^{-\frac{1}{2\ell^2}(x^1+p_2\ell^2)^2} e^{-\frac{1}{2\ell^2}(x^{1'}+p_2\ell^2)^2} e^{-is_\perp x^2 p_2} e^{is_\perp x^{2'} p_2} \\
= & \int_{-\infty}^{\infty} dp_2 \frac{1}{2\pi\ell} \sum_{k=0}^{k=\infty} \Big[\frac{1}{2^k k!\sqrt{\pi}} H_k\Big(\frac{x^1}{\ell}+p_2\ell\Big) H_k\Big(\frac{x^{1'}}{\ell}+p_2\ell\Big)\Big] \\
\times & \; e^{-\frac{1}{2}\Big[(\frac{x^1}{\ell}+p_2\ell)^2+(\frac{x^{1'}}{\ell}+p_2\ell)^2\Big]} e^{-is_\perp(x^2-x^{2'})p_2} \\
= & \int_{-\infty}^{\infty} dp_2 \frac{1}{2\pi\ell} \delta\Big(\frac{x^1}{\ell}+p_2\ell-\frac{x^{1'}}{\ell}-p_2\ell\Big) e^{-is_\perp(x^2-x^{2'})p_2} \\
= & \frac{|\ell|}{\ell}\delta(x^1-x^{1'}) \int_{-\infty}^{\infty} \frac{dp_2}{2\pi} e^{-is_\perp(x^2-x^{2'})p_2} \\
= & \; \delta(x^1-x^{1'}) \frac{\delta(x^2-x^{2'})}{|s_\perp|} \\
= & \; \delta^2(\boldsymbol{r}_\perp-\boldsymbol{r}'_\perp)
\end{aligned}
\tag{A.42}
$$

Here we have used

$$
\sum_{k=0}^{k=\infty} \Big[\frac{1}{2^k k!\sqrt{\pi}} H_k(x) H_k(y)\Big] = e^{\frac{x^2+y^2}{2}} \delta(x-y) \tag{A.43}
$$

$$
|\ell| = \ell \tag{A.44}
$$

Now we need to know the result of the operator $\boldsymbol{\Pi}_\perp \cdot \boldsymbol{\gamma}_\perp$ operating on the wavefunction.

$$
(\boldsymbol{\Pi}_\perp \cdot \boldsymbol{\gamma}_\perp)\psi_{kp_2}(\boldsymbol{r}_\perp) = (\Pi^1_\perp \gamma^1 + \Pi^2_\perp \gamma^2)\psi_{kp_2}(\boldsymbol{r}_\perp) \tag{A.45}
$$

$$
\begin{aligned}
(\Pi^1_\perp\gamma^1)\psi_{kp_2}(\boldsymbol{r}_\perp) &= \gamma^1\Big(-i\frac{\partial}{\partial x^1}\Big)\frac{1}{\sqrt{2\pi\ell}}\frac{1}{\sqrt{2^k k!\sqrt{\pi}}} H_k\Big(\frac{x^1}{\ell}+p_2\ell\Big) e^{-\frac{1}{2\ell^2}(x^1+p_2\ell^2)^2} e^{-is_\perp x^2 p_2} \\
&= (-i\gamma^1)\frac{1}{\sqrt{2\pi\ell}}\frac{1}{\sqrt{2^k k!\sqrt{\pi}}}\Big(\frac{\partial}{\partial x^1}\Big)\Big[H_k\Big(\frac{x^1}{\ell}+p_2\ell\Big) e^{-\frac{1}{2}(\frac{x^1}{\ell}+p_2\ell)^2}\Big] e^{-is_\perp x^2 p_2} \\
&= (-i\gamma^1)\frac{1}{\sqrt{2\pi\ell}}\frac{1}{\sqrt{2^k k!\sqrt{\pi}}}\Big[\frac{1}{\ell}H'_k\Big(\frac{x^1}{\ell}+p_2\ell\Big) - \frac{1}{\ell}(\frac{x^1}{\ell}+p_2\ell) H_k\Big(\frac{x^1}{\ell}+p_2\ell\Big)\Big] \\
&\times e^{-\frac{1}{2}(\frac{x^1}{\ell}+p_2\ell)^2} e^{-is_\perp x^2 p_2} \\
&= -\frac{i\gamma^1}{\ell}\frac{1}{\sqrt{2\pi\ell}}\frac{1}{\sqrt{2^k k!\sqrt{\pi}}}\Big[H'_k\Big(\frac{x^1}{\ell}+p_2\ell\Big) - (\frac{x^1}{\ell}+p_2\ell) H_k\Big(\frac{x^1}{\ell}+p_2\ell\Big)\Big]
\end{aligned}
$$

$$\times\, e^{-\frac{1}{2}(\frac{x^1}{\ell}+p_2\ell)^2} e^{-is_\perp x^2 p_2} \tag{A.46}$$

$$\begin{aligned}
&(\Pi_\perp^2\gamma^2)\psi_{kp_2}(\boldsymbol{r}_\perp) \\
&= \gamma^2\Big(-i\frac{\partial}{\partial x^2} - eBx^1\Big)\frac{1}{\sqrt{2\pi\ell}}\frac{1}{\sqrt{2^k k!\sqrt{\pi}}}H_k\Big(\frac{x^1}{\ell}+p_2\ell\Big)e^{-\frac{1}{2\ell^2}(x^1+p_2\ell^2)^2}e^{-is_\perp x^2 p_2} \\
&= \gamma^2\frac{1}{\sqrt{2\pi\ell}}\frac{1}{\sqrt{2^k k!\sqrt{\pi}}}H_k\Big(\frac{x^1}{\ell}+p_2\ell\Big)e^{-\frac{1}{2\ell^2}(x^1+p_2\ell^2)^2}\Big(-s_\perp p_2 - eBx^1\Big)e^{-is_\perp x^2 p_2} \\
&= \gamma^2\frac{1}{\sqrt{2\pi\ell}}\frac{1}{\sqrt{2^k k!\sqrt{\pi}}}H_k\Big(\frac{x^1}{\ell}+p_2\ell\Big)e^{-\frac{1}{2\ell^2}(x^1+p_2\ell^2)^2}\Big(-s_\perp p_2 - s_\perp|eB|x^1\Big)e^{-is_\perp x^2 p_2} \\
&= \gamma^2\frac{1}{\sqrt{2\pi\ell}}\frac{1}{\sqrt{2^k k!\sqrt{\pi}}}H_k\Big(\frac{x^1}{\ell}+p_2\ell\Big)e^{-\frac{1}{2\ell^2}(x^1+p_2\ell^2)^2}\Big(-s_\perp p_2 - s_\perp\frac{x^1}{\ell^2}\Big)e^{-is_\perp x^2 p_2} \\
&= \frac{1}{\sqrt{2\pi\ell}}\frac{1}{\sqrt{2^k k!\sqrt{\pi}}}(-s_\perp)\frac{\gamma^2}{\ell}\Big(\frac{x^1}{\ell}+p_2\ell\Big)H_k\Big(\frac{x^1}{\ell}+p_2\ell\Big)e^{-\frac{1}{2\ell^2}(x^1+p_2\ell^2)^2}e^{-is_\perp x^2 p_2} \\
&= -\frac{i\gamma^1}{\ell}\frac{1}{\sqrt{2\pi\ell}}\frac{1}{\sqrt{2^k k!\sqrt{\pi}}}(is_\perp)\gamma^1\gamma^2\Big(\frac{x^1}{\ell}+p_2\ell\Big)H_k\Big(\frac{x^1}{\ell}+p_2\ell\Big) \\
&\times e^{-\frac{1}{2\ell^2}(x^1+p_2\ell^2)^2}e^{-is_\perp x^2 p_2}
\end{aligned} \tag{A.47}$$

$$\begin{aligned}
(\boldsymbol{\Pi}_\perp\cdot\boldsymbol{\gamma}_\perp)\psi_{kp_2}(\boldsymbol{r}_\perp) &= -\frac{i\gamma^1}{\ell}\frac{1}{\sqrt{2\pi\ell}}\frac{1}{\sqrt{2^k k!\sqrt{\pi}}}\Big[H_k'\Big(\frac{x^1}{\ell}+p_2\ell\Big) - (1-is_\perp\gamma^1\gamma^2)(\frac{x^1}{\ell}+p_2\ell) \\
&\times H_k\Big(\frac{x^1}{\ell}+p_2\ell\Big)\Big]e^{-\frac{1}{2}(\frac{x^1}{\ell}+p_2\ell)^2}e^{-is_\perp x^2 p_2} \\
&= -\frac{i\gamma^1}{\ell}\frac{1}{\sqrt{2\pi\ell}}\frac{1}{\sqrt{2^k k!\sqrt{\pi}}}\Big[H_k'\Big(\frac{x^1}{\ell}+p_2\ell\Big) - 2(\frac{x^1}{\ell}+p_2\ell) \\
&\times H_k\Big(\frac{x^1}{\ell}+p_2\ell\Big)\mathcal{P}_-\Big]e^{-\frac{1}{2}(\frac{x^1}{\ell}+p_2\ell)^2}e^{-is_\perp x^2 p_2}
\end{aligned} \tag{A.48}$$

where $\mathcal{P}_-$ is a projection opeartor defined along with $\mathcal{P}_+$ as

$$\mathcal{P}_\pm \;=\; \frac{1}{2}\big(1\pm s_\perp\gamma^1\gamma^2\big) \tag{A.49}$$

Now we can use two identities of hermite polynomials.

$$H_n'(x) \;=\; 2nH_{n-1}(x) \tag{A.50}$$

$$H_{n+1}(x) \;=\; 2xH_n(x) - 2nH_{n-1} \tag{A.51}$$

$$
\begin{aligned}
(\boldsymbol{\Pi}_\perp\cdot\boldsymbol{\gamma}_\perp)\psi_{kp_2}(\boldsymbol{r}_\perp) &= -\frac{i\gamma^1}{\ell}\frac{1}{\sqrt{2\pi\ell}}\frac{1}{\sqrt{2^k k!\sqrt{\pi}}} \\
&\times\Big[2kH_{k-1}\Big(\frac{x^1}{\ell}+p_2\ell\Big)-\Big\{H_{k+1}\Big(\frac{x^1}{\ell}+p_2\ell\Big)+2kH_{k-1}\Big(\frac{x^1}{\ell}+p_2\ell\Big)\Big\}\mathcal{P}_-\Big] \\
&\times e^{-\frac{1}{2}(\frac{x^1}{\ell}+p_2\ell)^2}e^{-is_\perp x^2p_2} \\
&= -\frac{i\gamma^1}{\ell}\frac{1}{\sqrt{2\pi\ell}}\frac{1}{\sqrt{2^k k!\sqrt{\pi}}}\Big[2kH_{k-1}\Big(\frac{x^1}{\ell}+p_2\ell\Big)\Big(1-\mathcal{P}_-\Big) \\
&- H_{k+1}\Big(\frac{x^1}{\ell}+p_2\ell\Big)\mathcal{P}_-\Big]e^{-\frac{1}{2}(\frac{x^1}{\ell}+p_2\ell)^2}e^{-is_\perp x^2p_2} \\
&= \frac{i\gamma^1}{\ell}\frac{1}{\sqrt{2\pi\ell}}\frac{1}{\sqrt{2^k k!\sqrt{\pi}}}\Big[H_{k+1}\Big(\frac{x^1}{\ell}+p_2\ell\Big)\mathcal{P}_- - 2kH_{k-1}\Big(\frac{x^1}{\ell}+p_2\ell\Big)\mathcal{P}_+\Big] \\
&\times e^{-\frac{1}{2}(\frac{x^1}{\ell}+p_2\ell)^2}e^{-is_\perp x^2p_2} \\
&= \frac{i\gamma^1}{\ell}\Big[\frac{\sqrt{2(k+1)}}{\sqrt{2^{(k+1)}(k+1)!\sqrt{\pi}}}H_{k+1}\Big(\frac{x^1}{\ell}+p_2\ell\Big)\mathcal{P}_- \\
&- \frac{\sqrt{2k}}{\sqrt{2^{(k-1)}(k-1)!\sqrt{\pi}}}H_{k-1}\Big(\frac{x^1}{\ell}+p_2\ell\Big)\mathcal{P}_+\Big]e^{-\frac{1}{2}(\frac{x^1}{\ell}+p_2\ell)^2}e^{-is_\perp x^2p_2} \\
&= \frac{i\gamma^1}{\ell}\Big[\sqrt{2(k+1)}\psi_{(k+1)p_2}(\boldsymbol{r}_\perp)\mathcal{P}_- - \sqrt{2k}\psi_{(k-1)p_2}(\boldsymbol{r}_\perp)\mathcal{P}_+\Big] \qquad \text{(A.52)}
\end{aligned}
$$

Another operator used is

$$
\boldsymbol{\Pi}_\perp^2\psi_{kp_2}(\boldsymbol{r}_\perp) = \frac{2k+1}{\ell^2}\psi_{kp_2}(\boldsymbol{r}_\perp) \qquad \text{(A.53)}
$$

Earlier we have seen $(\boldsymbol{\Pi}_\perp\cdot g_\perp)^2 = -\boldsymbol{\Pi}_\perp^2 + ieB\gamma^1\gamma^2$. Now using this we find

$$
\begin{aligned}
\boldsymbol{\Pi}_\perp^2\psi_{kp_2}(\boldsymbol{r}_\perp) &= \Big[ieB\gamma^1\gamma^2-(\boldsymbol{\Pi}_\perp\cdot g_\perp)^2\Big]\psi_{kp_2} \\
&= \frac{1}{\ell^2}(is_\perp\gamma^1\gamma^2)\psi_{kp_2}-(\boldsymbol{\Pi}_\perp\cdot g_\perp)\Big[(\boldsymbol{\Pi}_\perp\cdot g_\perp)\psi_{kp_2}\Big] \\
&= \frac{1}{\ell^2}\Big[\mathcal{P}_+-\mathcal{P}_-\Big]\psi_{kp_2} \\
&- (\boldsymbol{\Pi}_\perp\cdot g_\perp)\frac{i\gamma^1}{\ell}\Big[\sqrt{2(k+1)}\psi_{(k+1)p_2}(\boldsymbol{r}_\perp)\mathcal{P}_- - \sqrt{2k}\psi_{(k-1)p_2}(\boldsymbol{r}_\perp)\mathcal{P}_+\Big] \\
&= \frac{1}{\ell^2}\Big[\mathcal{P}_+-\mathcal{P}_-\Big]\psi_{kp_2}-\Big[\sqrt{2(k+1)}(\boldsymbol{\Pi}_\perp\cdot g_\perp)\psi_{(k+1)p_2}(\boldsymbol{r}_\perp)\frac{i\gamma^1}{\ell}\mathcal{P}_- \\
&- \sqrt{2k}(\boldsymbol{\Pi}_\perp\cdot g_\perp)\psi_{(k-1)p_2}(\boldsymbol{r}_\perp)\frac{i\gamma^1}{\ell}\mathcal{P}_+\Big] \\
&= \frac{1}{\ell^2}\Big[\mathcal{P}_+-\mathcal{P}_-\Big]\psi_{kp_2}-\Big[\sqrt{2(k+1)}(\boldsymbol{\Pi}_\perp\cdot g_\perp)\psi_{(k+1)p_2}(\boldsymbol{r}_\perp)\mathcal{P}_+\frac{i\gamma^1}{\ell} \\
&- \sqrt{2k}(\boldsymbol{\Pi}_\perp\cdot g_\perp)\psi_{(k-1)p_2}(\boldsymbol{r}_\perp)\mathcal{P}_-\frac{i\gamma^1}{\ell}\Big] \qquad \text{(A.54)}
\end{aligned}
$$

In the last line we have used

$$
\begin{aligned}
\gamma^1\mathcal{P}_\pm &= \gamma^1\frac{1}{2}\Big[1 \pm is_\perp\gamma^1\gamma^2\Big] \\
&= \frac{1}{2}\Big[\gamma^1 \pm is_\perp\gamma^1\gamma^1\gamma^2\Big] \\
&= \frac{1}{2}\Big[\gamma^1 \pm is_\perp\gamma^1(-)\gamma^2\gamma^1\Big] \\
&= \frac{1}{2}\Big[1 \mp is_\perp\gamma^1\gamma^2\Big]\gamma^1 \\
&= \mathcal{P}_\mp\gamma^1
\end{aligned}
\tag{A.55}
$$

Again, as $\mathcal{P}_\pm\mathcal{P}_\mp = 0$ so only coefficient of $\mathcal{P}_{+(-)}$ contributes out of the two terms comming from $(\mathbf{\Pi}_\perp \cdot g_\perp)\psi_{(k+(-)1)p_2}(\boldsymbol{r}_\perp)$ and keeping only those terms we get

$$
\begin{aligned}
\mathbf{\Pi}^2_\perp\psi_{kp_2}(\boldsymbol{r}_\perp) &= \frac{1}{\ell^2}\Big[\mathcal{P}_+ - \mathcal{P}_-\Big]\psi_{kp_2} - \Big[\sqrt{2(k+1)}\Big(-\sqrt{2(k+1)}\psi_{kp_2}(\boldsymbol{r}_\perp)\frac{i\gamma^1}{\ell}\mathcal{P}_+\Big)\mathcal{P}_+\frac{i\gamma^1}{\ell} \\
&- \sqrt{2k}\Big(\sqrt{2k}\psi_{kp_2}(\boldsymbol{r}_\perp)\frac{i\gamma^1}{\ell}\mathcal{P}_-\Big)\mathcal{P}_-\frac{i\gamma^1}{\ell}\Big] \\
&= \frac{1}{\ell^2}\Big[\mathcal{P}_+ - \mathcal{P}_-\Big]\psi_{kp_2} + 2(k+1)\psi_{kp_2}(\boldsymbol{r}_\perp)\frac{i\gamma^1}{\ell}\mathcal{P}_+\frac{i\gamma^1}{\ell} \\
&+ 2k\psi_{kp_2}(\boldsymbol{r}_\perp)\frac{i\gamma^1}{\ell}\mathcal{P}_-\frac{i\gamma^1}{\ell} \quad \text{As} \quad \mathcal{P}^2_\pm = \mathcal{P}_\pm \\
&= \frac{1}{\ell^2}\Big[\mathcal{P}_+ - \mathcal{P}_-\Big]\psi_{kp_2} + 2(k+1)\psi_{kp_2}(\boldsymbol{r}_\perp)\mathcal{P}_-\frac{i\gamma^1}{\ell}\frac{i\gamma^1}{\ell} \\
&+ 2k\psi_{kp_2}(\boldsymbol{r}_\perp)\mathcal{P}_+\frac{i\gamma^1}{\ell}\frac{i\gamma^1}{\ell} \\
&= \frac{1}{\ell^2}\Big[\mathcal{P}_+ - \mathcal{P}_-\Big]\psi_{kp_2} + \frac{2(k+1)}{\ell^2}\psi_{kp_2}(\boldsymbol{r}_\perp)\mathcal{P}_- + \frac{2k}{\ell^2}\psi_{kp_2}(\boldsymbol{r}_\perp)\mathcal{P}_+ \\
&= \frac{2k+1}{\ell^2}\psi_{kp_2}(\boldsymbol{r}_\perp)\Big[\mathcal{P}_+ + \mathcal{P}_-\Big] \\
&= \frac{2k+1}{\ell^2}\psi_{kp_2}(\boldsymbol{r}_\perp)
\end{aligned}
\tag{A.56}
$$

A.3 Simplification

Now using the operator relations we proceed to simplify the r.h.s of Eq.(2.15). Starting with the first term we get

$$
\begin{aligned}
E1(\omega, p^3; \boldsymbol{r}_\perp, \boldsymbol{r}'_\perp) &= i\int_{-\infty}^{\infty} dp_2 \sum_{k=0}^{k=\infty} \frac{\gamma^0\omega - \gamma^3 p^3 + m}{\omega^2 - p^{3^2} - m^2 - (2k+1)|eB| + ieB\gamma^1\gamma^2}\psi_{kp_2}(\boldsymbol{r}_\perp)\psi^*_{kp_2}(\boldsymbol{r}'_\perp) \\
&= i\sum_{k=0}^{k=\infty} \frac{\gamma^0\omega - \gamma^3 p^3 + m}{\omega^2 - p^{3^2} - m^2 - (2k+1)|eB| + ieB\gamma^1\gamma^2}\int_{-\infty}^{\infty} dp_2\psi_{kp_2}(\boldsymbol{r}_\perp)\psi^*_{kp_2}(\boldsymbol{r}'_\perp)
\end{aligned}
$$

$$
\begin{aligned}
&= i\sum_{k=0}^{k=\infty}\frac{\gamma^0\omega-\gamma^3p^3+m}{\omega^2-p^{3^2}-m^2-(2k+1)|eB|+ieB\gamma^1\gamma^2} \\
&\times \int_{-\infty}^{\infty}dp_2\frac{1}{2\pi\ell}\Big[\frac{1}{2^k k!\sqrt{\pi}}H_k\Big(\frac{x^1}{\ell}+p_2\ell\Big)H_k\Big(\frac{x^{1'}}{\ell}+p_2\ell\Big)\Big] \\
&\times\ e^{-\frac{1}{2\ell^2}(x^1+p_2\ell^2)^2}e^{-\frac{1}{2\ell^2}(x^{1'}+p_2\ell^2)^2}e^{-is_\perp x^2p_2}e^{is_\perp x^{2'}p_2}
\end{aligned}
$$

Let us concentrate on the phase part separately.

$$
\begin{aligned}
& e^{-\frac{1}{2\ell^2}(x^1+p_2\ell^2)^2}e^{-\frac{1}{2\ell^2}(x^{1'}+p_2\ell^2)^2}e^{-is_\perp x^2p_2}e^{is_\perp x^{2'}p_2} \\
&= \exp\Big[-\frac{1}{2}\Big\{\Big(\frac{x^1}{\ell}+p_2\ell\Big)^2+\Big(\frac{x^{1'}}{\ell}+p_2\ell\Big)^2\Big\}-is_\perp p_2\ell\frac{x^2-x^{2'}}{\ell}\Big] \\
&= \exp\Big(-\Big[\frac{1}{2}\Big\{\Big(\frac{x^1}{\ell}\Big)^2+\Big(\frac{x^{1'}}{\ell}\Big)^2\Big\}+\big(p_2\ell\big)^2+p_2\ell\frac{x^1+x^{1'}}{\ell}+is_\perp p_2\ell\frac{x^2-x^{2'}}{\ell}\Big]\Big) \\
&= \exp\Big(-\Big[\frac{1}{2}\Big\{\Big(\frac{x^1}{\ell}\Big)^2+\Big(\frac{x^{1'}}{\ell}\Big)^2\Big\}+\big(p_2\ell\big)^2+2p_2\ell\Big\{\frac{x^1+x^{1'}}{2\ell}+is_\perp\frac{x^2-x^{2'}}{2\ell}\Big\}\Big]\Big) \\
&= e^{-\left(p_2\ell+\left\{\frac{x^1+x^{1'}}{2\ell}+is_\perp\frac{x^2-x^{2'}}{2\ell}\right\}\right)^2} \\
&\times \exp\Big(-\Big[\frac{1}{2}\Big\{\Big(\frac{x^1}{\ell}\Big)^2+\Big(\frac{x^{1'}}{\ell}\Big)^2\Big\}-\Big(\frac{x^1+x^{1'}}{2\ell}+is_\perp\frac{x^2-x^{2'}}{2\ell}\Big)^2\Big]\Big) \\
&= e^{-\left(p_2\ell+\left\{\frac{x^1+x^{1'}}{2\ell}+is_\perp\frac{x^2-x^{2'}}{2\ell}\right\}\right)^2}e^{is_\perp\frac{(x^1+x^{1'})(x^2-x^{2'})}{2\ell^2}} \\
&\times \exp\Big(-\Big[\frac{1}{2}\Big\{\Big(\frac{x^1}{\ell}\Big)^2+\Big(\frac{x^{1'}}{\ell}\Big)^2\Big\}-\Big(\frac{x^1+x^{1'}}{2\ell}\Big)^2+s_\perp^2\Big(\frac{x^2-x^{2'}}{2\ell}\Big)^2\Big]\Big) \\
&= e^{-\left(p_2\ell+\left\{\frac{x^1+x^{1'}}{2\ell}+is_\perp\frac{x^2-x^{2'}}{2\ell}\right\}\right)^2}e^{i\Phi(\boldsymbol{r}_\perp,\boldsymbol{r}'_\perp)}e^{-\left(\frac{x^2-x^{2'}}{2\ell}\right)^2} \\
&\times \exp\Big(-\Big[\frac{1}{2}\Big\{\Big(\frac{x^1}{\ell}\Big)^2+\Big(\frac{x^{1'}}{\ell}\Big)^2\Big\}-\Big(\frac{x^1+x^{1'}}{2\ell}\Big)^2\Big]\Big) \text{ as } s_\perp^2=1 \\
&= e^{-\left(p_2\ell+\left\{\frac{x^1+x^{1'}}{2\ell}+is_\perp\frac{x^2-x^{2'}}{2\ell}\right\}\right)^2}e^{i\Phi(\boldsymbol{r}_\perp,\boldsymbol{r}'_\perp)}e^{-\left(\frac{x^2-x^{2'}}{2\ell}\right)^2}e^{-\left(\frac{x^1-x^{1'}}{2\ell}\right)^2} \\
&= e^{-\left(p_2\ell+\left\{\frac{x^1+x^{1'}}{2\ell}+is_\perp\frac{x^2-x^{2'}}{2\ell}\right\}\right)^2}e^{i\Phi(\boldsymbol{r}_\perp,\boldsymbol{r}'_\perp)}e^{-\frac{1}{2}\frac{(x^1-x^{1'})^2+(x^2-x^{2'})^2}{2\ell^2}} \\
&= e^{-\left(p_2\ell+\left\{\frac{x^1+x^{1'}}{2\ell}+is_\perp\frac{x^2-x^{2'}}{2\ell}\right\}\right)^2}e^{i\Phi(\boldsymbol{r}_\perp,\boldsymbol{r}'_\perp)}e^{-\frac{\zeta}{2}} \qquad \text{(A.57)}
\end{aligned}
$$

with

$$
\Phi(\boldsymbol{r}_\perp,\boldsymbol{r}'_\perp) = s_\perp\frac{(x^1+x^{1'})(x^2-x^{2'})}{2\ell^2} \qquad \text{(A.58)}
$$

$$
\zeta = \frac{(x^1-x^{1'})^2+(x^2-x^{2'})^2}{2\ell^2} = \frac{(\boldsymbol{r}_\perp-\boldsymbol{r}'_\perp)^2}{2\ell^2} \qquad \text{(A.59)}
$$

Putting back the phase factor we obtain

$$
E1(\omega,p^3;\boldsymbol{r}_\perp,\boldsymbol{r}'_\perp) = i\sum_{k=0}^{k=\infty}\frac{\gamma^0\omega-\gamma^3p^3+m}{\omega^2-p^{3^2}-m^2-(2k+1)|eB|+ieB\gamma^1\gamma^2}
$$

$$
\begin{aligned}
&\times \int_{-\infty}^{\infty} dp_2 \frac{1}{2\pi\ell}\Big[\frac{1}{2^k k!\sqrt{\pi}} H_k\Big(\frac{x^1}{\ell}+p_2\ell\Big) H_k\Big(\frac{x^{1'}}{\ell}+p_2\ell\Big)\Big] \\
&\times\; e^{-\Big(p_2\ell+\Big\{\frac{x^1+x^{1'}}{2\ell}+is_\perp\frac{x^2-x^{2'}}{2\ell}\Big\}\Big)^2} e^{i\Phi(\boldsymbol{r}_\perp,\boldsymbol{r}'_\perp)} e^{-\frac{\zeta}{2}} \\
&= i\frac{e^{i\Phi(\boldsymbol{r}_\perp,\boldsymbol{r}'_\perp)}}{2\pi\ell^2} e^{-\frac{\zeta}{2}} \sum_{k=0}^{k=\infty} \frac{\gamma^0\omega-\gamma^3 p^3+m}{\omega^2-p^{3^2}-m^2-(2k+1)|eB|+ieB\gamma^1\gamma^2} \\
&\times \int_{-\infty}^{\infty} d\Big(p_2\ell+\Big\{\frac{x^1+x^{1'}}{2\ell}+is_\perp\frac{x^2-x^{2'}}{2\ell}\Big\}\Big) e^{-\Big(p_2\ell+\Big\{\frac{x^1+x^{1'}}{2\ell}+is_\perp\frac{x^2-x^{2'}}{2\ell}\Big\}\Big)^2} \\
&\times \Big[\frac{1}{2^k k!\sqrt{\pi}} H_k\Big(\frac{x^1}{\ell}+p_2\ell\Big) H_k\Big(\frac{x^{1'}}{\ell}+p_2\ell\Big)\Big] \\
&= i\frac{e^{i\Phi(\boldsymbol{r}_\perp,\boldsymbol{r}'_\perp)}}{2\pi\ell^2} e^{-\frac{\zeta}{2}} \sum_{k=0}^{k=\infty} \frac{\gamma^0\omega-\gamma^3 p^3+m}{\omega^2-p^{3^2}-m^2-(2k+1)|eB|+ieB\gamma^1\gamma^2}\frac{1}{2^k k!\sqrt{\pi}} \\
&\times \int_{-\infty}^{\infty} dx e^{-x^2}\Big[H_k\Big(x+\frac{x^1}{\ell}+p_2\ell-\Big\{p_2\ell+\frac{x^1+x^{1'}}{2\ell}+is_\perp\frac{x^2-x^{2'}}{2\ell}\Big\}\Big) \\
&\times\; H_k\Big(x+\frac{x^{1'}}{\ell}+p_2\ell-\Big\{p_2\ell+\frac{x^1+x^{1'}}{2\ell}+is_\perp\frac{x^2-x^{2'}}{2\ell}\Big\}\Big)\Big] \\
&= i\frac{e^{i\Phi(\boldsymbol{r}_\perp,\boldsymbol{r}'_\perp)}}{2\pi\ell^2} e^{-\frac{\zeta}{2}} \sum_{k=0}^{k=\infty} \frac{\gamma^0\omega-\gamma^3 p^3+m}{\omega^2-p^{3^2}-m^2-(2k+1)|eB|+ieB\gamma^1\gamma^2}\frac{1}{2^k k!\sqrt{\pi}} \\
&\times \int_{-\infty}^{\infty} dx e^{-x^2}\Big[H_k(x+y)H_k(x+z)\Big] \qquad \text{(A.60)}
\end{aligned}
$$

where we define

$$
\begin{aligned}
x &= p_2\ell+\frac{x^1+x^{1'}}{2\ell}+is_\perp\frac{x^2-x^{2'}}{2\ell} \\
y &= \frac{x^1-x^{1'}}{2\ell}-is_\perp\frac{x^2-x^{2'}}{2\ell} \\
z &= -\frac{x^1-x^{1'}}{2\ell}-is_\perp\frac{x^2-x^{2'}}{2\ell} \qquad \text{(A.61)}
\end{aligned}
$$

Now we can apply an identity

$$
\int_{-\infty}^{\infty} dx e^{-x^2} H_m(x+y)H_n(x+z) = 2^n\pi^{\frac{1}{2}} m! z^{n-m}\mathrm{L}_m^{n-m}(-2yz) \text{ for } m\le n \qquad \text{(A.62)}
$$

with

$\mathrm{L}_m^0{=}\mathrm{L}_m$

Before using that we see

$$
\begin{aligned}
-2yz &= -2\Big[\frac{x^1-x^{1'}}{2\ell}-is_\perp\frac{x^2-x^{2'}}{2\ell}\Big](-1)\Big[\frac{x^1-x^{1'}}{2\ell}+is_\perp\frac{x^2-x^{2'}}{2\ell}\Big] \\
&= 2\Big[\Big(\frac{x^1-x^{1'}}{2\ell}\Big)^2+\Big(\frac{x^2-x^{2'}}{2\ell}\Big)^2\Big] \\
&= \zeta \qquad \text{(A.63)}
\end{aligned}
$$

Thus we obtain

$$
\begin{aligned}
E1(\omega,p^3;\boldsymbol{r}_\perp,\boldsymbol{r}'_\perp) &= i\frac{e^{i\Phi(\boldsymbol{r}_\perp,\boldsymbol{r}'_\perp)}}{2\pi\ell^2}e^{-\frac{\zeta}{2}}\sum_{k=0}^{k=\infty}\frac{\gamma^0\omega-\gamma^3p^3+m}{\omega^2-p^{3^2}-m^2-(2k+1)|eB|+ieB\gamma^1\gamma^2}\mathrm{L}_k(\zeta)\\
&= i\frac{e^{i\Phi(\boldsymbol{r}_\perp,\boldsymbol{r}'_\perp)}}{2\pi\ell^2}e^{-\frac{\zeta}{2}}\sum_{k=0}^{k=\infty}\frac{\gamma^0\omega-\gamma^3p^3+m}{\omega^2-p^{3^2}-m^2-(2k+1)|eB|+s_\perp s|eB|}\mathrm{L}_k(\zeta)
\end{aligned}
\tag{A.64}
$$

Now we begin the second part of Eq.(2.15).

$$
\begin{aligned}
&E2(\omega,p^3;\boldsymbol{r}_\perp,\boldsymbol{r}'_\perp)\\
&= i\int_{-\infty}^{\infty}dp_2\sum_{k=0}^{k=\infty}\frac{\boldsymbol{\Pi}_\perp\cdot\boldsymbol{\gamma}_\perp}{\omega^2-p^{3^2}-m^2-(2k+1)|eB|+ieB\gamma^1\gamma^2}\psi_{kp_2}(\boldsymbol{r}_\perp)\psi^*_{kp_2}(\boldsymbol{r}'_\perp)\\
&= i\int_{-\infty}^{\infty}dp_2\sum_{k=0}^{k=\infty}\frac{\frac{i\gamma^1}{\ell}\Big[\sqrt{2(k+1)}\psi_{(k+1)p_2}(\boldsymbol{r}_\perp)\mathcal{P}_- - \sqrt{2k}\psi_{(k-1)p_2}(\boldsymbol{r}_\perp)\mathcal{P}_+\Big]}{\omega^2-p^{3^2}-m^2-(2k+1)|eB|+ieB\gamma^1\gamma^2}\psi^*_{kp_2}(\boldsymbol{r}'_\perp)\\
&= i\sum_{k=0}^{k=\infty}\frac{1}{\omega^2-p^{3^2}-m^2-(2k+1)|eB|+ieB\gamma^1\gamma^2}\frac{i\gamma^1}{\ell}\\
&\times\Big[\sqrt{2(k+1)}\int_{-\infty}^{\infty}dp_2\psi_{(k+1)p_2}(\boldsymbol{r}_\perp)\psi^*_{kp_2}(\boldsymbol{r}'_\perp)\mathcal{P}_- - \sqrt{2k}\int_{-\infty}^{\infty}dp_2\psi_{(k-1)p_2}(\boldsymbol{r}_\perp)\psi^*_{kp_2}(\boldsymbol{r}'_\perp)\mathcal{P}_+\Big]
\end{aligned}
\tag{A.65}
$$

We need to know the two integrals now. First one is

$$
\begin{aligned}
\int_{-\infty}^{\infty}dp_2\psi_{(k+1)p_2}(\boldsymbol{r}_\perp)\psi^*_{kp_2}(\boldsymbol{r}'_\perp) &= \frac{1}{2\pi\ell}\Big[\frac{1}{\sqrt{2^{k+1}(k+1)!\sqrt{\pi}}}\frac{1}{\sqrt{2^kk!\sqrt{\pi}}}H_{k+1}\Big(\frac{x^1}{\ell}+p_2\ell\Big)\\
&\times H_k\Big(\frac{x^{1'}}{\ell}+p_2\ell\Big)\Big]e^{-\frac{1}{2\ell^2}(x^1+p_2\ell^2)^2}e^{-\frac{1}{2\ell^2}(x^{1'}+p_2\ell^2)^2}e^{-is_\perp x^2p_2}e^{is_\perp x^{2'}p_2}
\end{aligned}
\tag{A.66}
$$

This is similar to the case of Eq.(A.60) and we can write it as

$$
\begin{aligned}
&\int_{-\infty}^{\infty}dp_2\psi_{(k+1)p_2}(\boldsymbol{r}_\perp)\psi^*_{kp_2}(\boldsymbol{r}'_\perp)\\
&\quad=\frac{1}{\sqrt{2(k+1)}}\frac{1}{2\pi\ell}\frac{1}{2^kk!\sqrt{\pi}}\int_{-\infty}^{\infty}dp_2H_{k+1}\Big(\frac{x^1}{\ell}+p_2\ell\Big)H_k\Big(\frac{x^{1'}}{\ell}+p_2\ell\Big)\Big]\\
&\quad\times e^{-\frac{1}{2\ell^2}(x^1+p_2\ell^2)^2}e^{-\frac{1}{2\ell^2}(x^{1'}+p_2\ell^2)^2}e^{-is_\perp x^2p_2}e^{is_\perp x^{2'}p_2}\\
&\quad=\frac{1}{\sqrt{2(k+1)}}\frac{e^{i\Phi(\boldsymbol{r}_\perp,\boldsymbol{r}'_\perp)}}{2\pi\ell^2}e^{-\frac{\zeta}{2}}\frac{1}{2^kk!\sqrt{\pi}}\int_{-\infty}^{\infty}dxe^{-x^2}\Big[H_{k+1}(x+y)H_k(x+z)\Big]
\end{aligned}
\tag{A.67}
$$

See, in Eq.(A.62) the condition is $m\le n$ which means in the above integral $m=k$ and $n=k+1$ and the factor sitting outside should be y as it is in the argument of higher polynomial order. Thus we have

$$\begin{aligned}\int_{-\infty}^{\infty} dp_2 \psi_{(k+1)p_2}(\boldsymbol{r}_\perp)\psi^*_{kp_2}(\boldsymbol{r}'_\perp) &= \frac{1}{\sqrt{2(k+1)}} \frac{2^{k+1}\sqrt{\pi}k!}{2^k k!\sqrt{\pi}} \frac{e^{i\Phi(\boldsymbol{r}_\perp,\boldsymbol{r}'_\perp)}}{2\pi\ell^2} e^{-\frac{\zeta}{2}} y \mathrm{L}^1_k(\zeta) \\ &= \frac{1}{\sqrt{2(k+1)}} \frac{e^{i\Phi(\boldsymbol{r}_\perp,\boldsymbol{r}'_\perp)}}{2\pi\ell^2} e^{-\frac{\zeta}{2}} 2y \mathrm{L}^1_k(\zeta)\end{aligned} \tag{A.68}$$

Similarly

$$\begin{aligned}&\int_{-\infty}^{\infty} dp_2 \psi_{(k-1)p_2}(\boldsymbol{r}_\perp)\psi^*_{kp_2}(\boldsymbol{r}'_\perp) \\ &= \frac{1}{2\pi\ell}\Big[\frac{1}{\sqrt{2^{k-1}(k-1)!\sqrt{\pi}}} \frac{1}{\sqrt{2^k k!\sqrt{\pi}}} H_{k-1}\Big(\frac{x^1}{\ell} + p_2\ell\Big) H_k\Big(\frac{x^{1'}}{\ell} + p_2\ell\Big)\Big] \\ &\times e^{-\frac{1}{2\ell^2}(x^1+p_2\ell^2)^2} e^{-\frac{1}{2\ell^2}(x^{1'}+p_2\ell^2)^2} e^{-is_\perp x^2 p_2} e^{is_\perp x^{2'} p_2} \\ &= \sqrt{2k}\frac{e^{i\Phi(\boldsymbol{r}_\perp,\boldsymbol{r}'_\perp)}}{2\pi\ell^2} e^{-\frac{\zeta}{2}} \frac{1}{2^k k!\sqrt{\pi}} \int_{-\infty}^{\infty} dx e^{-x^2}\Big[H_{k-1}(x+y)H_k(x+z)\Big]\end{aligned} \tag{A.69}$$

This time we have $m = k-1$ and $n = k$ and we get

$$\begin{aligned}\int_{-\infty}^{\infty} dp_2 \psi_{(k-1)p_2}(\boldsymbol{r}_\perp)\psi^*_{kp_2}(\boldsymbol{r}'_\perp) &= \sqrt{2k}\frac{2^k\sqrt{\pi}(k-1)!}{2^k k!\sqrt{\pi}} \frac{e^{i\Phi(\boldsymbol{r}_\perp,\boldsymbol{r}'_\perp)}}{2\pi\ell^2} e^{-\frac{\zeta}{2}} z \mathrm{L}^1_{k-1}(\zeta) \\ &= \frac{\sqrt{2k}}{k} \frac{e^{i\Phi(\boldsymbol{r}_\perp,\boldsymbol{r}'_\perp)}}{2\pi\ell^2} e^{-\frac{\zeta}{2}} z \mathrm{L}^1_{k-1}(\zeta)\end{aligned} \tag{A.70}$$

Thus putting these integrals we get

$$\begin{aligned}E2(\omega, p^3; \boldsymbol{r}_\perp, \boldsymbol{r}'_\perp) &= i\sum_{k=0}^{k=\infty} \frac{1}{\omega^2 - p^{3^2} - m^2 - (2k+1)|eB| + ieB\gamma^1\gamma^2} \frac{i\gamma^1}{\ell} \\ &\times \Big[\sqrt{2(k+1)}\int_{-\infty}^{\infty} dp_2 \psi_{(k+1)p_2}(\boldsymbol{r}_\perp)\psi^*_{kp_2}(\boldsymbol{r}'_\perp)\mathcal{P}_- - \sqrt{2k}\int_{-\infty}^{\infty} dp_2 \psi_{(k-1)p_2}(\boldsymbol{r}_\perp)\psi^*_{kp_2}(\boldsymbol{r}'_\perp)\mathcal{P}_+\Big] \\ &= i\sum_{k=0}^{k=\infty} \frac{1}{\omega^2 - p^{3^2} - m^2 - (2k+1)|eB| + ieB\gamma^1\gamma^2} \frac{i\gamma^1}{\ell} \\ &\times \Big[\sqrt{2(k+1)}\frac{1}{\sqrt{2(k+1)}} \frac{e^{i\Phi(\boldsymbol{r}_\perp,\boldsymbol{r}'_\perp)}}{2\pi\ell^2} e^{-\frac{\zeta}{2}} 2y\mathrm{L}^1_k(\zeta)\mathcal{P}_- - \sqrt{2k}\frac{\sqrt{2k}}{k}\frac{e^{i\Phi(\boldsymbol{r}_\perp,\boldsymbol{r}'_\perp)}}{2\pi\ell^2} e^{-\frac{\zeta}{2}} z\mathrm{L}^1_{k-1}(\zeta)\mathcal{P}_+\Big] \\ &= i\frac{e^{i\Phi(\boldsymbol{r}_\perp,\boldsymbol{r}'_\perp)}}{2\pi\ell^2} e^{-\frac{\zeta}{2}} \sum_{k=0}^{k=\infty} \frac{1}{\omega^2 - p^{3^2} - m^2 - (2k+1)|eB| + ieB\gamma^1\gamma^2} \frac{i\gamma^1}{\ell} \\ &\times \Big[2y\mathrm{L}^1_k(\zeta)\mathcal{P}_- - 2z\mathrm{L}^1_{k-1}(\zeta)\mathcal{P}_+\Big]\end{aligned} \tag{A.71}$$

A.4 Numerator simplification

- For $s = +1$ case, any coefficient of $\mathcal{P}_-$ does not contribute and that implies the numerator can be simplified as

$$\begin{aligned}
&\frac{i\gamma^1}{\ell}\Big[-2z\mathrm{L}^1_{k-1}(\zeta)\mathcal{P}_+\Big] = \frac{i}{\ell}\Big[-\Big(-\frac{x^1-x^{1'}}{\ell} - i\frac{x^2-x^{2'}}{\ell}\Big)\frac{1}{2}(\gamma^1 - i\gamma^2)\mathrm{L}^1_{k-1}(\zeta)\Big] \\
&= \frac{i}{\ell}\Big[\Big(\frac{x^1-x^{1'}}{2\ell} + i\frac{x^2-x^{2'}}{2\ell}\Big)(\gamma^1 - i\gamma^2)\Big]\mathrm{L}^1_{k-1}(\zeta) \\
&= \frac{i}{\ell}\Big[\Big(\frac{x^1-x^{1'}}{2\ell}\gamma^1 + \frac{x^2-x^{2'}}{2\ell}\gamma^2 + i\frac{x^2-x^{2'}}{2\ell}\gamma^1 - i\frac{x^1-x^{1'}}{2\ell}\gamma^2\Big)\Big]\mathrm{L}^1_{k-1}(\zeta) \\
&= \frac{i}{\ell}\Big[\frac{x^1-x^{1'}}{\ell}\gamma^1 + \frac{x^2-x^{2'}}{\ell}\gamma^2 - \frac{x^1-x^{1'}}{2\ell}\gamma^1 - i\frac{x^1-x^{1'}}{2\ell}\gamma^2 \\
&+ i\frac{x^2-x^{2'}}{2\ell}\gamma^1 - \frac{x^2-x^{2'}}{2\ell}\gamma^2\Big]\mathrm{L}^1_{k-1}(\zeta) \\
&= \frac{i}{\ell}\Big[\frac{x^1-x^{1'}}{\ell}\gamma^1 + \frac{x^2-x^{2'}}{\ell}\gamma^2 - \frac{x^1-x^{1'}}{\ell}\gamma^1\frac{1}{2}\Big(1 - i\gamma^1\gamma^2\Big) \\
&+ i\frac{x^2-x^{2'}}{\ell}\gamma^1\frac{1}{2}\Big(1 - i\gamma^1\gamma^2\Big)\Big]\mathrm{L}^1_{k-1}(\zeta) \\
&= \frac{i}{\ell}\Big[\frac{x^1-x^{1'}}{\ell}\gamma^1 + \frac{x^2-x^{2'}}{\ell}\gamma^2 - \frac{x^1-x^{1'}}{\ell}\gamma^1\mathcal{P}_- + i\frac{x^2-x^{2'}}{\ell}\gamma^1\mathcal{P}_-\Big]\mathrm{L}^1_{k-1}(\zeta) \\
&= \frac{i}{\ell}\Big[\frac{x^1-x^{1'}}{\ell}\gamma^1 + \frac{x^2-x^{2'}}{\ell}\gamma^2\Big]\mathrm{L}^1_{k-1}(\zeta) \\
&= \frac{i}{\ell^2}\boldsymbol{\gamma}_\perp\cdot(\boldsymbol{r}_\perp - \boldsymbol{r}'_\perp)\mathrm{L}^1_{n-1}(\zeta) \text{ as } k = n
\end{aligned} \tag{A.72}$$

- For $s = -1$ case, any coefficient of $\mathcal{P}_+$ does not contribute and we get form the numerator

$$\begin{aligned}
&\frac{i\gamma^1}{\ell}\Big[2y\mathrm{L}^1_{k}(\zeta)\mathcal{P}_-\Big] = \frac{i}{\ell}\Big[\Big(\frac{x^1-x^{1'}}{\ell} - i\frac{x^2-x^{2'}}{\ell}\Big)\frac{1}{2}(\gamma^1 + i\gamma^2)\mathrm{L}^1_{k}(\zeta)\Big] \\
&= \frac{i}{\ell}\Big[\Big(\frac{x^1-x^{1'}}{2\ell} - i\frac{x^2-x^{2'}}{2\ell}\Big)(\gamma^1 + i\gamma^2)\Big]\mathrm{L}^1_{k}(\zeta) \\
&= \frac{i}{\ell}\Big[\Big(\frac{x^1-x^{1'}}{2\ell}\gamma^1 + \frac{x^2-x^{2'}}{2\ell}\gamma^2 - i\frac{x^2-x^{2'}}{2\ell}\gamma^1 + i\frac{x^1-x^{1'}}{2\ell}\gamma^2\Big)\Big]\mathrm{L}^1_{k}(\zeta) \\
&= \frac{i}{\ell}\Big[\frac{x^1-x^{1'}}{\ell}\gamma^1 + \frac{x^2-x^{2'}}{\ell}\gamma^2 - \frac{x^1-x^{1'}}{2\ell}\gamma^1 + i\frac{x^1-x^{1'}}{2\ell}\gamma^2 \\
&- i\frac{x^2-x^{2'}}{2\ell}\gamma^1 - \frac{x^2-x^{2'}}{2\ell}\gamma^2\Big]\mathrm{L}^1_{k}(\zeta) \\
&= \frac{i}{\ell}\Big[\frac{x^1-x^{1'}}{\ell}\gamma^1 + \frac{x^2-x^{2'}}{\ell}\gamma^2 - \frac{x^1-x^{1'}}{\ell}\gamma^1\frac{1}{2}\Big(1 + i\gamma^1\gamma^2\Big) \\
&- i\frac{x^2-x^{2'}}{\ell}\gamma^1\frac{1}{2}\Big(1 + i\gamma^1\gamma^2\Big)\Big]\mathrm{L}^1_{k}(\zeta) \\
&= \frac{i}{\ell}\Big[\frac{x^1-x^{1'}}{\ell}\gamma^1 + \frac{x^2-x^{2'}}{\ell}\gamma^2 - \frac{x^1-x^{1'}}{\ell}\gamma^1\mathcal{P}_+ - i\frac{x^2-x^{2'}}{\ell}\gamma^1\mathcal{P}_+\Big]\mathrm{L}^1_{k}(\zeta) \\
&= \frac{i}{\ell}\Big[\frac{x^1-x^{1'}}{\ell}\gamma^1 + \frac{x^2-x^{2'}}{\ell}\gamma^2\Big]\mathrm{L}^1_{k}(\zeta)
\end{aligned}$$

$$= \frac{i}{\ell^2}\boldsymbol{\gamma}_\perp \cdot (\boldsymbol{r}_\perp - \boldsymbol{r}'_\perp)\mathrm{L}^1_{n-1}(\zeta) \text{ as } k = n-1 \tag{A.73}$$

Thus we obtain

$$\begin{aligned} E2(\omega, p^3; \boldsymbol{r}_\perp, \boldsymbol{r}'_\perp) &= i\frac{e^{i\Phi(\boldsymbol{r}_\perp, \boldsymbol{r}'_\perp)}}{2\pi\ell^2} e^{-\frac{\zeta}{2}} \sum_{k=0}^{k=\infty} \frac{1}{\omega^2 - p^{3^2} - m^2 - (2k+1)|eB| + ieB\gamma^1\gamma^2} \frac{i\gamma^1}{\ell} \\ &\times \left[2y\mathrm{L}^1_k(\zeta)\mathcal{P}_- - 2z\mathrm{L}^1_{k-1}(\zeta)\mathcal{P}_+\right] \\ &= i\frac{e^{i\Phi(\boldsymbol{r}_\perp, \boldsymbol{r}'_\perp)}}{2\pi\ell^2} e^{-\frac{\zeta}{2}} \sum_{n=0}^{n=\infty} \frac{1}{\omega^2 - p^{3^2} - m^2 - 2n|eB|} \\ &\times \left[\frac{i}{\ell^2}\boldsymbol{\gamma}_\perp \cdot (\boldsymbol{r}_\perp - \boldsymbol{r}'_\perp)\mathrm{L}^1_{n-1}(\zeta)\right] \end{aligned} \tag{A.74}$$

Appendix B

Weak field expansion of the propagator

B.1 Power series expansion of Dirac equation

Dirac equation along with magnetic moment is given by

$$\Big[i\partial\!\!\!/ - e_f A\!\!\!/ - m_f - \frac{1}{2}k_f \sigma \cdot F\Big] S(x,x') = \delta^{(4)}(x-x') \; . \tag{B.1}$$

We choose the gauge such that

$$A_\mu = -\frac{1}{2}F_{\mu\nu}x^\nu \; . \tag{B.2}$$

The idea is to write

$$S(x,x') = \phi(x,x')\int \frac{d^4p}{(2\pi)^4}e^{-ip\cdot(x-x')}S_F(p) \tag{B.3}$$

$$\text{with} \quad \phi(x,x') = e^{\frac{i}{2}e_f x^\mu F_{\mu\nu}x'^\nu} \tag{B.4}$$

$$i\partial_\mu\phi = -\frac{e_f}{2}F_{\mu\nu}x'^\nu\phi \; . \tag{B.5}$$

In that case

$$\begin{aligned}
(i\partial_\mu - e_f A_\mu)S(x,x') &= (i\partial_\mu - e_f A_\mu)\phi(x,x')\int \frac{d^4p}{(2\pi)^4}e^{-ip\cdot(x-x')}S_F(p) \\
&= i\partial_\mu\phi\int \frac{d^4p}{(2\pi)^4}e^{-ip\cdot(x-x')}S_F(p) + \phi\int \frac{d^4p}{(2\pi)^4}p_\mu e^{-ip\cdot(x-x')}S_F(p) \\
&- e_f A_\mu\phi(x,x')\int \frac{d^4p}{(2\pi)^4}e^{-ip\cdot(x-x')}S_F(p)
\end{aligned}$$

$$
\begin{aligned}
&= -\frac{e_f}{2}F_{\mu\nu}x'^{\nu}\phi\int\frac{d^4p}{(2\pi)^4}e^{-ip\cdot(x-x')}S_F(p)+\phi\int\frac{d^4p}{(2\pi)^4}p_\mu e^{-ip\cdot(x-x')}S_F(p)\\
&+ \frac{e_f}{2}F_{\mu\nu}x^{\nu}\phi(x,x')\int\frac{d^4p}{(2\pi)^4}e^{-ip\cdot(x-x')}S_F(p)\\
&= \frac{e_f}{2}F_{\mu\nu}(x-x')^{\nu}\phi\int\frac{d^4p}{(2\pi)^4}e^{-ip\cdot(x-x')}S_F(p)\\
&+ \phi(x,x')\int\frac{d^4p}{(2\pi)^4}e^{-ip\cdot(x-x')}p_\mu S_F(p)\\
&= \frac{e_f}{2}F_{\mu\nu}\phi\int\frac{d^4p}{(2\pi)^4}i\frac{\partial}{\partial p_\nu}e^{-ip\cdot(x-x')}S_F(p)\\
&+ \phi(x,x')\int\frac{d^4p}{(2\pi)^4}e^{-ip\cdot(x-x')}p_\mu S_F(p)\\
&= \phi(x,x')\int\frac{d^4p}{(2\pi)^4}e^{-ip\cdot(x-x')}\Big[p_\mu-\frac{i}{2}e_fF_{\mu\nu}\frac{\partial}{\partial p_\nu}\Big]S_F(p)\ .
\end{aligned}
\tag{B.6}
$$

The Dirac equation in the momentum space representation thus becomes

$$
\Big[\not p-\frac{i}{2}e_fF^{\mu\nu}\gamma_\mu\frac{\partial}{\partial p^\nu}-m_f-\frac{1}{2}k_f\sigma\cdot F\Big]S_F(p)=1 \tag{B.7}
$$

The strategy to obtain the power expansion is to write $S_F = S_0 + S_1$. Defining the operator

$$
\hat O \;=\; \Big[\frac{i}{2}e_fF^{\mu\nu}\gamma_\mu\frac{\partial}{\partial p^\nu}+\frac{1}{2}k_f\sigma\cdot F\Big] \tag{B.8}
$$

the Dirac equation can be simplified as

$$
\begin{aligned}
1 &= \Big[\not p-m_f-\hat O\Big](S_0+S_1)\\
&= (\not p-m_f)S_0+(\not p-m_f)S_1-\hat OS_0-\hat OS_1\\
&= 1+S_0^{-1}S_1-\hat OS_0 \quad \text{As}\ \ \hat OS_1 \quad \text{is higher order}\\
S_1 &= S_0\hat OS_0\ .
\end{aligned}
\tag{B.9}
$$

The obtained propagator up to leading order with moment is given by :

$$
\begin{aligned}
S_1 &= S_0\hat OS_0\\
&= S_0\Big[\frac{i}{2}e_fF^{\mu\nu}\gamma_\mu\frac{\partial}{\partial p^\nu}+\frac{1}{2}k_f\sigma\cdot F\Big]S_0\\
&= \frac{\not p+m_f}{p^2-m_f^2+i\epsilon}\Big[\frac{i}{2}e_fF^{\mu\nu}\gamma_\mu\frac{\partial}{\partial p^\nu}+\frac{1}{2}k_f\sigma\cdot F\Big]\frac{\not p+m_f}{p^2-m_f^2+i\epsilon}\ .
\end{aligned}
\tag{B.10}
$$

At $k_f = 0$ we get

$$\begin{aligned}
S_1 &= \frac{\not p + m_f}{p^2 - m_f^2 + i\epsilon}\Big[\frac{i}{2}e_f F^{\mu\nu}\gamma_\mu \frac{\partial}{\partial p^\nu}\Big]\frac{\not p + m_f}{p^2 - m_f^2 + i\epsilon} \\
&= \frac{\not p + m_f}{p^2 - m_f^2 + i\epsilon}\Big[\frac{i}{2}e_f \frac{F^{\mu\nu}\gamma_\mu\gamma_\nu}{p^2 - m_f^2 + i\epsilon} - \frac{i}{2}e_f F^{\mu\nu}\gamma_\mu \frac{(\not p + m_f)2p_\nu}{(p^2 - m_f^2 + i\epsilon)^2}\Big] \\
&= \frac{\not p + m_f}{p^2 - m_f^2 + i\epsilon}\Big[(e_f B)\frac{\gamma_5 \not u \not b}{p^2 - m_f^2 + i\epsilon} - \frac{i}{2}e_f F^{\mu\nu}\gamma_\mu \frac{(\not p + m_f)2p_\nu}{(p^2 - m_f^2 + i\epsilon)^2}\Big] \\
&= \frac{1}{p^2 - m_f^2 + i\epsilon}\Big[(e_f B)\frac{(\not p + m_f)\gamma_5 \not u \not b}{p^2 - m_f^2 + i\epsilon} - \frac{i}{2}e_f F^{\mu\nu} \frac{(\not p + m_f)\gamma_\mu(\not p + m_f)2p_\nu}{(p^2 - m_f^2 + i\epsilon)^2}\Big] \\
&= \frac{1}{p^2 - m_f^2 + i\epsilon}\Big[(e_f B)\frac{(\not p + m_f)\gamma_5 \not u \not b}{p^2 - m_f^2 + i\epsilon} - \frac{i}{2}e_f F^{\mu\nu} \frac{\big[2p_\mu - \gamma_\mu(\not p - m_f)\big](\not p + m_f)2p_\nu}{(p^2 - m_f^2 + i\epsilon)^2}\Big] \\
&= \frac{1}{p^2 - m_f^2 + i\epsilon}\Big[(e_f B)\frac{(\not p + m_f)\gamma_5 \not u \not b}{p^2 - m_f^2 + i\epsilon} - \frac{i}{2}e_f F^{\mu\nu} \frac{\big[-\gamma_\mu(\not p - m_f)\big](\not p + m_f)2p_\nu}{(p^2 - m_f^2 + i\epsilon)^2}\Big] \\
&= \frac{1}{p^2 - m_f^2 + i\epsilon}\Big[(e_f B)\frac{(\not p + m_f)\gamma_5 \not u \not b}{p^2 - m_f^2 + i\epsilon} + ie_f \frac{F^{\mu\nu}\gamma_\mu p_\nu}{(p^2 - m_f^2 + i\epsilon)}\Big] \\
&= \frac{1}{p^2 - m_f^2 + i\epsilon}\Big[(e_f B)\frac{(\not p + m_f)\gamma_5 \not u \not b}{p^2 - m_f^2 + i\epsilon} + ie_f \frac{iB\gamma_5 \not u \not b \not p_\perp}{(p^2 - m_f^2 + i\epsilon)}\Big] \\
&= \frac{1}{p^2 - m_f^2 + i\epsilon}\Big[(e_f B)\frac{(\not p_{||} - \not p_\perp + m_f)\gamma_5 \not u \not b}{p^2 - m_f^2 + i\epsilon} - (e_f B)\frac{\gamma_5 \not u \not b \not p_\perp}{(p^2 - m_f^2 + i\epsilon)}\Big] \\
&= \frac{1}{p^2 - m_f^2 + i\epsilon}\Big[(e_f B)\frac{(\gamma_5 \not u \not b \not p_{||} + \gamma_5 \not u \not b \not p_\perp + \gamma_5 \not u \not b m_f)}{p^2 - m_f^2 + i\epsilon} - (e_f B)\frac{\gamma_5 \not u \not b \not p_\perp}{(p^2 - m_f^2 + i\epsilon)}\Big] \\
&= (e_f B)\frac{\Big[\gamma_5 \not u \not b(\not p_{||} + m_f)\Big]}{(p^2 - m_f^2 + i\epsilon)^2} = -i(e_f B)\frac{\Big[\gamma^1\gamma^2(\not p_{||} + m_f)\Big]}{(p^2 - m_f^2 + i\epsilon)^2} \\
&= (e_f B)\frac{\Big[\gamma_5 \not u \not b(p^0\gamma^0 - p^3\gamma^3 + m_f)\Big]}{(p^2 - m_f^2 + i\epsilon)^2} \\
&= (e_f B)\frac{\Big[\gamma_5(-p^0 \not b - p^3 \not u + m_f \not u \not b)\Big]}{(p^2 - m_f^2 + i\epsilon)^2} \qquad \Big[\text{as } \not b = -\gamma^3\Big] \\
&= (e_f B)\frac{\Big[\gamma_5((p\cdot b)\not u - (p\cdot u)\not b + m_f \not u \not b)\Big]}{(p^2 - m_f^2 + i\epsilon)^2}\,. \qquad \text{(B.11)}
\end{aligned}$$

Following the similar strategy we write

$$S_F = S_0 + S_1 + S_2 \qquad \text{(B.12)}$$

and simplify

$$\begin{aligned}
1 &= \Big[\not p - m_f - \hat{O}\Big](S_0 + S_1 + S_2) \\
&= (\not p - m_f)S_0 + (\not p - m_f)S_1 + (\not p - m_f)S_2 - \hat{O}S_0 - \hat{O}S_1
\end{aligned}$$

$$
\begin{aligned}
&= 1 + S_0^{-1}S_1 + S_0^{-1}S_2 - \hat{O}S_0 - \hat{O}S_1 \\
&= 1 + \hat{O}S_0 + S_0^{-1}S_2 - \hat{O}S_0 - \hat{O}S_1 \\
S_2 &= S_0\hat{O}S_1 \ . \qquad \text{(B.13)}
\end{aligned}
$$

Thus the propagator in second order along with the moment is given by

$$
S_2 = S_0\hat{O}S_1 \ . \qquad \text{(B.14)}
$$

where we already know $S_1 = S_0\hat{O}S_0$.

B.2 Detailed derivation of the second order term in eB

$$
\begin{aligned}
S_2 &= \frac{\not{p} + m_f}{p^2 - m_f^2 + i\epsilon}\Big[\frac{i}{2}e_f F^{\mu\nu}\gamma_\mu\frac{\partial}{\partial p^\nu} + k_f B\gamma_5\not{u}\not{b}\Big]\frac{1}{(p^2 - m_f^2 + i\epsilon)^2} \\
&\times \Big[e_f B\gamma_5\big[(p\cdot b)\not{u} - (p\cdot u)\not{b} + m_f\not{u}\not{b}\big] + k_f B\big[(\not{p} + m_f)\gamma_5\not{u}\not{b}(\not{p} + m_f)\big]\Big] \ . \qquad \text{(B.15)}
\end{aligned}
$$

We can re-write the equation as a sum of two contributions: part involving differentiation and part without it.

$$
S_2 = D + \overline{\overline{D}}
$$

where

$$
\begin{aligned}
D &= \frac{\not{p} + m_f}{p^2 - m_f^2 + i\epsilon}\Big[\frac{i}{2}e_f F^{\mu\nu}\gamma_\mu\frac{\partial}{\partial p^\nu}\Big]\frac{1}{(p^2 - m_f^2 + i\epsilon)^2}\Big[e_f B\gamma_5\big[(p\cdot b)\not{u} - (p\cdot u)\not{b} + m_f\not{u}\not{b}\big] \\
&+ k_f B\big[(\not{p} + m_f)\gamma_5\not{u}\not{b}(\not{p} + m_f)\big]\Big] \qquad \text{(B.16)}
\end{aligned}
$$

and

$$
\begin{aligned}
\overline{\overline{D}} &= \frac{\not{p} + m_f}{p^2 - m_f^2 + i\epsilon}\Big[k_f B\gamma_5\not{u}\not{b}\Big]\frac{1}{(p^2 - m_f^2 + i\epsilon)^2}\Big[e_f B\gamma_5\big[(p\cdot b)\not{u} - (p\cdot u)\not{b} + m_f\not{u}\not{b}\big] \\
&+ k_f B\big[(\not{p} + m_f)\gamma_5\not{u}\not{b}(\not{p} + m_f)\big]\Big] \ . \qquad \text{(B.17)}
\end{aligned}
$$

Simplification of the first part:

$$
D = \frac{\not{p} + m_f}{p^2 - m_f^2 + i\epsilon}\Big[\frac{i}{2}e_f F^{\mu\nu}\gamma_\mu\Big]\frac{-4p_\nu}{(p^2 - m_f^2 + i\epsilon)^3}
$$

$$
\begin{aligned}
&\times \quad \Big[e_f B\gamma_5\big[(p\cdot b)\not{u} - (p\cdot u)\not{b} + m_f\not{u}\not{b}\big] + k_f B\big[(\not{p}+m_f)\gamma_5\not{u}\not{b}(\not{p}+m_f)\big]\Big] \\
&+ \quad \frac{\not{p}+m_f}{p^2-m_f^2+i\epsilon}\Big[\frac{i}{2}e_f F^{\mu\nu}\gamma_\mu\Big]\frac{1}{(p^2-m_f^2+i\epsilon)^2} \\
&\times \quad \Big[e_f B\gamma_5\big[b_\nu\not{u} - u_\nu\not{b}\big] + k_f B\big[\gamma_\nu\gamma_5\not{u}\not{b}(\not{p}+m_f) + (\not{p}+m_f)\gamma_5\not{u}\not{b}\gamma_\nu\big]\Big] \ . \qquad \text{(B.18)}
\end{aligned}
$$

To verify the vanishing magnetic moment case we first put $k_f = 0$ and see that $\overline{\overline{D}}$ does not contribute and the expression for D simplifies to

$$
\begin{aligned}
D &= \frac{\not{p}+m_f}{p^2-m_f^2+i\epsilon}\Big[\frac{i}{2}e_f F^{\mu\nu}\gamma_\mu\Big]\frac{-4p_\nu}{(p^2-m_f^2+i\epsilon)^3}\Big[e_f B\gamma_5\big[(p\cdot b)\not{u} - (p\cdot u)\not{b} + m_f\not{u}\not{b}\big]\Big] \\
&+ \frac{\not{p}+m_f}{p^2-m_f^2+i\epsilon}\Big[\frac{i}{2}e_f F^{\mu\nu}\gamma_\mu\Big]\frac{1}{(p^2-m_f^2+i\epsilon)^2}\Big[e_f B\gamma_5\big[b_\nu\not{u} - u_\nu\not{b}\big]\Big] \\
&= a + b \ . \qquad \text{(B.19)}
\end{aligned}
$$

In case of pure magnetic field

$$
\begin{aligned}
F^{\mu\nu} &= iBP^{\mu\nu} \\
P^{\mu\nu} &= i\epsilon^{\mu\nu\alpha\beta}b_\alpha u_\beta \\
F^{\mu\nu} &= iBi\epsilon^{\mu\nu\alpha\beta}b_\alpha u_\beta \\
&= -B\epsilon^{\mu\nu\alpha\beta}b_\alpha u_\beta \ .
\end{aligned}
$$

At first take a look at the second term:

$$
\begin{aligned}
b_1 &= \frac{\not{p}+m_f}{p^2-m_f^2+i\epsilon}\Big[\frac{i}{2}e_f F^{\mu\nu}\gamma_\mu\Big]\frac{1}{(p^2-m_f^2+i\epsilon)^2}\Big[e_f B\gamma_5\big[b_\nu\not{u}\big]\Big] \\
&= \frac{\not{p}+m_f}{p^2-m_f^2+i\epsilon}\Big[\frac{i}{2}e_f F^{\mu\nu}\gamma_\mu b_\nu\Big]\frac{1}{(p^2-m_f^2+i\epsilon)^2}\Big[e_f B\gamma_5\big[\not{u}\big]\Big] \\
&= 0 \qquad \text{(B.20)}
\end{aligned}
$$

using

$$
\begin{aligned}
F^{\mu\nu}\gamma_\mu b_\nu &= -B\epsilon^{\mu\nu\alpha\beta}b_\alpha b_\nu u_\beta\gamma_\mu = -B\epsilon^{\mu\alpha\nu\beta}b_\nu b_\alpha u_\beta\gamma_\mu \\
&= B\epsilon^{\mu\nu\alpha\beta}b_\alpha b_\nu u_\beta\gamma_\mu = -F^{\mu\nu}\gamma_\mu b_\nu \qquad \text{(B.21)}
\end{aligned}
$$

and similar relation for $F^{\mu\nu}\gamma_\mu u_\nu$. We should mention here that we follow the convention $\epsilon^{0123} = 1$. The consequence of it is

$$
\frac{1}{2}\sigma\cdot F = B\gamma_5\not{u}\not{b} \ . \qquad \text{(B.22)}
$$

To be more explicit, with $\gamma_\mu = (\gamma^0, -\gamma^1, -\gamma^2, -\gamma^3)$ we have

$$
\begin{aligned}
\frac{1}{2}\sigma\cdot F &= \frac{1}{2}\frac{i}{2}\big[\gamma_\mu,\gamma_\nu\big]F^{\mu\nu} \\
&= \frac{i}{2}\gamma_\mu\gamma_\nu F^{\mu\nu} \\
&= -Bi\gamma^1\gamma^2 \ . \qquad \text{(B.23)}
\end{aligned}
$$

where we have used the special case that magnetic field only along $+\hat{z}$ we get in the rest frame

$$
\begin{gathered}
b^\alpha = (0,0,0,1), \quad b_\alpha = (0,0,0,-1), \quad u^\beta = (1,0,0,0), \quad u_\beta = (1,0,0,0) \\
F^{12} = -B\epsilon^{1230}b_3u_0 = Bb_3u_0 = -B \ . \qquad \text{(B.24)}
\end{gathered}
$$

Now the simplification can be performed in a straightforward manner as:

$$
\begin{aligned}
a &= \frac{\not{p}+m_f}{p^2-m_f^2+i\epsilon}\Big[\frac{i}{2}e_fF^{\mu\nu}\gamma_\mu\Big]\frac{-4p_\nu}{(p^2-m_f^2+i\epsilon)^3}\Big[e_fB\gamma_5\big[(p\cdot b)\not{u}-(p\cdot u)\not{b}+m_f\not{u}\not{b}\big]\Big] \\
&= \frac{\not{p}+m_f}{p^2-m_f^2+i\epsilon}ie_f\Big[\frac{-2F^{\mu\nu}\gamma_\mu p_\nu}{(p^2-m_f^2+i\epsilon)^3}\Big]\Big[e_fB\gamma_5\big[(p\cdot b)\not{u}-(p\cdot u)\not{b}+m_f\not{u}\not{b}\big]\Big] \\
&= \frac{-2ie_f}{(p^2-m_f^2+i\epsilon)^4}(\not{p}+m_f)\big[-B(\gamma^1p^2-\gamma^2p^1)\big]\Big[e_fB\gamma_5\big[(p\cdot b)\not{u}-(p\cdot u)\not{b}+m_f\not{u}\not{b}\big]\Big] \\
&= (e_fB)^2\frac{2i}{(p^2-m_f^2+i\epsilon)^4}(\not{p}+m_f)\big[(\gamma^1p^2-\gamma^2p^1)\big]\Big[\gamma_5\big[-p^3\gamma^0+p^0\gamma^3-m_f\gamma^0\gamma^3\big]\Big] \\
&= (e_fB)^2\frac{2i}{(p^2-m_f^2+i\epsilon)^4}(\not{p}+m_f)\big[(\gamma^1p^2-\gamma^2p^1)\big]\Big[ip^3\gamma^1\gamma^2\gamma^3-ip^0\gamma^1\gamma^2\gamma^0-im_f\gamma^1\gamma^2\Big] \\
&= (e_fB)^2\frac{-2}{(p^2-m_f^2+i\epsilon)^4}(\not{p}+m_f) \\
&\times \Big[-p^2p^3\gamma^2\gamma^3+p^2p^0\gamma^2\gamma^0+m_fp^2\gamma^2-p^1p^3\gamma^1\gamma^3+p^1p^0\gamma^1\gamma^0+m_fp^1\gamma^1\Big] \ . \qquad \text{(B.25)}
\end{aligned}
$$

Up to now we have not used any new definitions regarding parallel and perpendicular components. Now we specify them as follows:

$$
(a\cdot b)_{||} = a^0b^0 - a^3b^3, \quad (a\cdot b)_\perp = a^1b^1 + a^2b^2 \ . \qquad \text{(B.26)}
$$

It means :

$$
\begin{gathered}
\not{p} = \gamma^0p^0 - \gamma^3p^3 - \gamma^1p^1 - \gamma^2p^2 = \not{p}_{||} - \not{p}_\perp, \quad p_{||}^2 = (p^0)^2 - (p^3)^2 \\
p_\perp^2 = (p^1)^2 + (p^2)^2, \quad \not{p}_{||}\not{p}_{||} = p_{||}^2, \quad \not{p}_\perp\not{p}_\perp = -p_\perp^2 \ . \qquad \text{(B.27)}
\end{gathered}
$$

Using the relations along with the fact that $\not{p}_\perp \not{p}_{||} = -\not{p}_{||}\not{p}_\perp$ one can further simplify as:

$$\begin{aligned}
a &= (e_f B)^2 \frac{-2}{(p^2-m_f^2+i\epsilon)^4}(\not{p}+m_f)\Big[p^1\gamma^1(\not{p}_{||}+m_f)+p^2\gamma^2(\not{p}_{||}+m_f)\Big] \\
&= (e_f B)^2 \frac{-2}{(p^2-m_f^2+i\epsilon)^4}(\not{p}_{||}-\not{p}_\perp+m_f)\Big[\not{p}_\perp(\not{p}_{||}+m_f)\Big] \\
&= (e_f B)^2 \frac{-2}{(p^2-m_f^2+i\epsilon)^4}\Big[(\not{p}_{||}+m_f)-\not{p}_\perp\Big]\Big[\not{p}_\perp(\not{p}_{||}+m_f)\Big] \\
&= (e_f B)^2 \frac{-2}{(p^2-m_f^2+i\epsilon)^4}\Big[(\not{p}_{||}+m_f)\not{p}_\perp(\not{p}_{||}+m_f)+p_\perp^2(\not{p}_{||}+m_f)\Big] \\
&= (e_f B)^2 \frac{-2}{(p^2-m_f^2+i\epsilon)^4}\Big[(\not{p}_{||}+m_f)(-\not{p}_{||}+m_f)\not{p}_\perp+p_\perp^2(\not{p}_{||}+m_f)\Big] \\
&= (e_f B)^2 \frac{-2}{(p^2-m_f^2+i\epsilon)^4}\Big[(m_f^2-p_{||}^2)\not{p}_\perp+p_\perp^2(\not{p}_{||}+m_f)\Big] \\
&= (e_f B)^2 \frac{-2p_\perp^2}{(p^2-m_f^2+i\epsilon)^4}\Big[(\not{p}_{||}+m_f)+\not{p}_\perp\frac{m_f^2-p_{||}^2}{p_\perp^2}\Big] \,. \qquad \text{(B.28)}
\end{aligned}$$

From Eq.(B.17) consists of two parts: (1) The part with $(k_f B)(e_f B)$ is given by

$$\begin{aligned}
\overline{\overline{D_1}} &= \frac{\not{p}+m_f}{p^2-m_f^2+i\epsilon}\Big[k_f B\gamma_5\not{u}\not{b}\Big]\frac{1}{(p^2-m_f^2+i\epsilon)^2}\Big[e_f B\gamma_5\big[(p\cdot b)\not{u}-(p\cdot u)\not{b}+m_f\not{u}\not{b}\big]\Big] \\
&= \frac{\not{p}+m_f}{(p^2-m_f^2+i\epsilon)^3}\Big[(k_f B)(e_f B)\Big]\Big[\not{u}\not{b}\big[(p\cdot b)\not{u}-(p\cdot u)\not{b}+m_f\not{u}\not{b}\big]\Big] \\
&= \frac{\not{p}+m_f}{(p^2-m_f^2+i\epsilon)^3}\Big[(k_f B)(e_f B)\Big]\Big[-(p\cdot b)\not{u}\not{u}\not{b}-(p\cdot u)\not{u}\not{b}\not{b}-m_f\not{u}\not{u}\not{b}\not{b}\Big] \\
&= \frac{\not{p}+m_f}{(p^2-m_f^2+i\epsilon)^3}\Big[(k_f B)(e_f B)\Big]\Big[-(p\cdot b)\not{b}+(p\cdot u)\not{u}+m_f\Big] \\
&= \Big[(k_f B)(e_f B)\Big]\frac{\not{p}+m_f}{(p^2-m_f^2+i\epsilon)^3}\Big[-p^3\gamma^3+p^0\gamma^0+m_f\Big] \\
&= \Big[(k_f B)(e_f B)\Big]\frac{\not{p}+m_f}{(p^2-m_f^2+i\epsilon)^3}\Big[\not{p}_{||}+m_f\Big] \\
&= \Big[(k_f B)(e_f B)\Big]\frac{(\not{p}_{||}-\not{p}_\perp+m_f)(\not{p}_{||}+m_f)}{(p^2-m_f^2+i\epsilon)^3} \\
&= \Big[(k_f B)(e_f B)\Big]\frac{p_{||}^2-\not{p}_\perp\not{p}_{||}+m_f(2\not{p}_{||}-\not{p}_\perp)+m_f^2}{(p^2-m_f^2+i\epsilon)^3} \,. \qquad \text{(B.29)}
\end{aligned}$$

Other terms in this order comes from D :

$$\begin{aligned}
D_2+D_4 &= \frac{\not{p}+m_f}{p^2-m_f^2+i\epsilon}\Big[\frac{i}{2}e_f F^{\mu\nu}\gamma_\mu\Big]\frac{-4p_\nu}{(p^2-m_f^2+i\epsilon)^3}\Big[k_f B\big[(\not{p}+m_f)\gamma_5\not{u}\not{b}(\not{p}+m_f)\big]\Big] \\
&+\frac{\not{p}+m_f}{p^2-m_f^2+i\epsilon}\Big[\frac{i}{2}e_f F^{\mu\nu}\gamma_\mu\Big]\frac{1}{(p^2-m_f^2+i\epsilon)^2}\Big[k_f B\big[\gamma_\nu\gamma_5\not{u}\not{b}(\not{p}+m_f)+(\not{p}+m_f)\gamma_5\not{u}\not{b}\gamma_\nu\big]\Big] \,. \qquad \text{(B.30)}
\end{aligned}$$

Let us calculate each part one by one:

$$
\begin{aligned}
D_2 &= \frac{\not{p}+m_f}{p^2-m_f^2+i\epsilon}\Big[\frac{i}{2}e_fF^{\mu\nu}\gamma_\mu\Big]\frac{-4p_\nu}{(p^2-m_f^2+i\epsilon)^3}\Big[k_fB\big[(\not{p}+m_f)\gamma_5\not{u}\not{b}(\not{p}+m_f)\big]\Big] \\
&= \Big[\frac{i}{2}e_f(k_fB)F^{\mu\nu}(-4p_\nu)\Big]\frac{1}{(p^2-m_f^2+i\epsilon)^4}\Big[(\not{p}+m_f)\gamma_\mu(\not{p}+m_f)\gamma_5\not{u}\not{b}(\not{p}+m_f)\Big] \\
&= \Big[\frac{i}{2}e_f(k_fB)F^{\mu\nu}(-4p_\nu)\Big]\frac{1}{(p^2-m_f^2+i\epsilon)^4}\Big[(\not{p}\gamma_\mu+\gamma_\mu m_f)(\not{p}+m_f)\gamma_5\not{u}\not{b}(\not{p}+m_f)\Big] \\
&= \Big[\frac{i}{2}e_f(k_fB)F^{\mu\nu}(-4p_\nu)\Big]\frac{1}{(p^2-m_f^2+i\epsilon)^4}\Big[(p^\rho\gamma_\rho\gamma_\mu+\gamma_\mu m_f)(\not{p}+m_f)\gamma_5\not{u}\not{b}(\not{p}+m_f)\Big] \\
&= \Big[\frac{i}{2}e_f(k_fB)F^{\mu\nu}(-4p_\nu)\Big]\frac{1}{(p^2-m_f^2+i\epsilon)^4}\Big[(2p_\mu-\gamma_\mu\gamma_\rho p^\rho+\gamma_\mu m_f)(\not{p}+m_f)\gamma_5\not{u}\not{b}(\not{p}+m_f)\Big] \\
&= \Big[\frac{i}{2}e_f(k_fB)F^{\mu\nu}(-4p_\nu)\Big]\frac{1}{(p^2-m_f^2+i\epsilon)^4}\Big[-\gamma_\mu(\not{p}-m_f)(\not{p}+m_f)\gamma_5\not{u}\not{b}(\not{p}+m_f)\Big] \\
&= \Big[\frac{i}{2}e_f(k_fB)F^{\mu\nu}(4\gamma_\mu p_\nu)\Big]\frac{1}{(p^2-m_f^2+i\epsilon)^3}\Big[\gamma_5\not{u}\not{b}(\not{p}+m_f)\Big] \\
&= \Big[2i(e_fB)(k_fB)(\gamma^2p^1-\gamma^1p^2)\Big]\frac{1}{(p^2-m_f^2+i\epsilon)^3}\Big[-i\gamma^1\gamma^2(\not{p}+m_f)\Big] \\
&= \Big[2(e_fB)(k_fB)(\gamma^2p^1-\gamma^1p^2)\gamma^1\gamma^2\Big]\frac{1}{(p^2-m_f^2+i\epsilon)^3}\Big[(\not{p}+m_f)\Big] \\
&= \Big[2(e_fB)(k_fB)(\gamma^1p^1+\gamma^2p^2)\Big]\frac{1}{(p^2-m_f^2+i\epsilon)^3}\Big[(\not{p}+m_f)\Big] \\
&= \Big[(e_fB)(k_fB)\Big]\frac{2\not{p}_\perp}{(p^2-m_f^2+i\epsilon)^3}\Big[(\not{p}+m_f)\Big]\ .
\end{aligned}
\tag{B.31}
$$

Next we decompose the D_4 into two parts and consider one at a time:

$$
\begin{aligned}
D_4^1 &= \frac{\not{p}+m_f}{p^2-m_f^2+i\epsilon}\Big[\frac{i}{2}e_fF^{\mu\nu}\gamma_\mu\Big]\frac{1}{(p^2-m_f^2+i\epsilon)^2}\Big[k_fB\big[\gamma_\nu\gamma_5\not{u}\not{b}(\not{p}+m_f)\big]\Big] \\
&= e_f(k_fB)\frac{\not{p}+m_f}{(p^2-m_f^2+i\epsilon)^3}\Big[\frac{i}{2}F^{\mu\nu}\gamma_\mu\gamma_\nu\gamma_5\not{u}\not{b}(\not{p}+m_f)\big]\Big] \\
&= e_f(k_fB)\frac{\not{p}+m_f}{(p^2-m_f^2+i\epsilon)^3}\Big[B\gamma_5\not{u}\not{b}\gamma_5\not{u}\not{b}(\not{p}+m_f)\big]\Big] \\
&= \Big[(e_fB)(k_fB)\Big]\frac{(\not{p}+m_f)(\not{p}+m_f)}{(p^2-m_f^2+i\epsilon)^3} \\
&= \Big[(e_fB)(k_fB)\Big]\frac{p^2+m_f^2+2m_f\not{p}}{(p^2-m_f^2+i\epsilon)^3} \\
&= \Big[(e_fB)(k_fB)\Big]\frac{p^2-m_f^2+2m_f\not{p}+2m_f^2}{(p^2-m_f^2+i\epsilon)^3} \\
&= \Big[(e_fB)(k_fB)\Big]\Big[\frac{1}{(p^2-m_f^2+i\epsilon)^2}+2m_f\frac{\not{p}+m_f}{(p^2-m_f^2+i\epsilon)^3}\Big]\ .
\end{aligned}
\tag{B.32}
$$

$$
\begin{aligned}
D_4^2 &= \frac{\not p + m_f}{p^2 - m_f^2 + i\epsilon}\Big[\frac{i}{2}e_f F^{\mu\nu}\gamma_\mu\Big]\frac{1}{(p^2 - m_f^2 + i\epsilon)^2}\Big[k_f B\big[(\not p + m_f)\gamma_5 \not u \not b \gamma_\nu\big]\Big] \\
&= \frac{1}{(p^2 - m_f^2 + i\epsilon)^3}\Big[\frac{i}{2}e_f (k_f B) F^{\mu\nu}\Big]\Big[(\not p + m_f)\gamma_\mu(\not p + m_f)\gamma_5 \not u \not b \gamma_\nu\Big] \\
&= \frac{1}{(p^2 - m_f^2 + i\epsilon)^3}\Big[\frac{i}{2}e_f (k_f B) F^{\mu\nu}\Big]\Big[\big[2p_\mu - \gamma_\mu(\not p - m_f)\big](\not p + m_f)\gamma_5 \not u \not b \gamma_\nu\Big] \\
&= \Big[\frac{i}{2}e_f (k_f B)\Big]\frac{1}{(p^2 - m_f^2 + i\epsilon)^3}\Big[F^{\mu\nu}\big[2p_\mu(\not p + m_f)\gamma_5 \not u \not b \gamma_\nu - \gamma_\mu(\not p - m_f)(\not p + m_f)\gamma_5 \not u \not b \gamma_\nu\big]\Big] \\
&= \Big[\frac{i}{2}e_f (k_f B)\Big]\Big[\frac{2(\not p + m_f)\gamma_5 \not u \not b F^{\mu\nu} p_\mu \gamma_\nu}{(p^2 - m_f^2 + i\epsilon)^3} - \frac{F^{\mu\nu}\gamma_\mu \gamma_5 \not u \not b \gamma_\nu}{(p^2 - m_f^2 + i\epsilon)^2}\Big] \\
&= \Big[\frac{i}{2}(e_f B)(k_f B)\Big]\Big[\frac{2(\not p + m_f)(-i\gamma^1\gamma^2)(p^2\gamma^1 - p^1\gamma^2)}{(p^2 - m_f^2 + i\epsilon)^3} - \frac{\gamma^2(-i\gamma^1\gamma^2)\gamma^1 - \gamma^1(-i\gamma^1\gamma^2)\gamma^2}{(p^2 - m_f^2 + i\epsilon)^2}\Big] \\
&= \Big[\frac{i}{2}(e_f B)(k_f B)\Big]\Big[\frac{2(\not p + m_f)(-i)(p^2\gamma^2 + p^1\gamma^1)}{(p^2 - m_f^2 + i\epsilon)^3} - \frac{(+i) - (-i)}{(p^2 - m_f^2 + i\epsilon)^2}\Big] \\
&= \Big[(e_f B)(k_f B)\Big]\Big[\frac{(\not p + m_f)\not p_\perp}{(p^2 - m_f^2 + i\epsilon)^3} + \frac{1}{(p^2 - m_f^2 + i\epsilon)^2}\Big]\,. \qquad \text{(B.33)}
\end{aligned}
$$

The term having $(k_f B)^2$ as proportional factor comes from 2nd term of $\overline{\overline{D}}$ in Eq.(B.17):

$$
\begin{aligned}
\overline{\overline{D}} &= \frac{\not p + m_f}{p^2 - m_f^2 + i\epsilon}\Big[k_f B \gamma_5 \not u \not b\Big]\frac{1}{(p^2 - m_f^2 + i\epsilon)^2}\Big[k_f B\big[(\not p + m_f)\gamma_5 \not u \not b(\not p + m_f)\big]\Big] \\
&= \frac{(k_f B)^2}{(p^2 - m_f^2 + i\epsilon)^3}\Big[(\not p + m_f)\big[\gamma_5 \not u \not b(\not p + m_f)\gamma_5 \not u \not b\big](\not p + m_f)\Big] \\
&= \frac{(k_f B)^2}{(p^2 - m_f^2 + i\epsilon)^3}\Big[(\not p + m_f)\big[(-i\gamma^1\gamma^2)\not p_{||}(-i\gamma^1\gamma^2) - (-i\gamma^1\gamma^2)\not p_\perp(-i\gamma^1\gamma^2) \\
&+ (-i\gamma^1\gamma^2)m_f(-i\gamma^1\gamma^2)\big](\not p + m_f)\Big] \\
&= -\frac{(k_f B)^2}{(p^2 - m_f^2 + i\epsilon)^3}\Big[(\not p + m_f)\big[(\gamma^1\gamma^2)(\gamma^1\gamma^2)\not p_{||} - (\gamma^1\gamma^2)\not p_\perp(\gamma^1\gamma^2) \\
&+ (\gamma^1\gamma^2)(\gamma^1\gamma^2)m_f\big](\not p + m_f)\Big] \\
&= -\frac{(k_f B)^2}{(p^2 - m_f^2 + i\epsilon)^3}\Big[(\not p + m_f)\big[-\not p_{||} - (\gamma^1\gamma^2)(\gamma^1 p^1 + \gamma^2 p^2)(\gamma^1\gamma^2) - m_f\big](\not p + m_f)\Big] \\
&= -\frac{(k_f B)^2}{(p^2 - m_f^2 + i\epsilon)^3}\Big[(\not p + m_f)\big[-\not p_{||} - \not p_\perp - m_f\big](\not p + m_f)\Big] \\
&= \frac{(k_f B)^2}{(p^2 - m_f^2 + i\epsilon)^3}\Big[(\not p + m_f)\big[\not p_{||} + \not p_\perp + m_f\big](\not p + m_f)\Big]\,. \qquad \text{(B.34)}
\end{aligned}
$$

Thus the second order term can be written as :

$$
\begin{aligned}
S_2 &= (e_f B)^2 \frac{-2p_\perp^2}{(p^2 - m_f^2 + i\epsilon)^4}\Big[(\not p_{||} + m_f) + \not p_\perp \frac{m_f^2 - p_{||}^2}{p_\perp^2}\Big] \\
&+ \Big[(e_f B)(k_f B)\Big]\frac{\not p + m_f}{(p^2 - m_f^2 + i\epsilon)^3}\Big[\not p_{||} + m_f\Big]
\end{aligned}
$$

$$
\begin{aligned}
&+ \Big[(e_fB)(k_fB)\Big]\frac{2\not{p}_\perp}{(p^2-m_f^2+i\epsilon)^3}\Big[(\not{p}+m_f)\Big] \\
&+ \Big[(e_fB)(k_fB)\Big]\Big[\frac{1}{(p^2-m_f^2+i\epsilon)^2}+2m_f\frac{\not{p}+m_f}{(p^2-m_f^2+i\epsilon)^3}\Big] \\
&+ \Big[(e_fB)(k_fB)\Big]\Big[\frac{(\not{p}+m_f)\not{p}_\perp}{(p^2-m_f^2+i\epsilon)^3}+\frac{1}{(p^2-m_f^2+i\epsilon)^2}\Big] \\
&+ \frac{(k_fB)^2}{(p^2-m_f^2+i\epsilon)^3}\Big[(\not{p}+m_f)\big[\not{p}_{||}+\not{p}_\perp+m_f\big](\not{p}+m_f)\Big] \\
&= (e_fB)^2\frac{-2p_\perp^2}{(p^2-m_f^2+i\epsilon)^4}\Big[(\not{p}_{||}+m_f)+\not{p}_\perp\frac{m_f^2-p_{||}^2}{p_\perp^2}\Big] \\
&+ (e_fB)(k_fB)\Big[\frac{\not{p}+m_f}{(p^2-m_f^2+i\epsilon)^3}(\not{p}_{||}+3m_f) \\
&+ \frac{2\not{p}_\perp}{(p^2-m_f^2+i\epsilon)^3}(\not{p}+m_f)+\frac{(\not{p}+m_f)\not{p}_\perp}{(p^2-m_f^2+i\epsilon)^3}+\frac{2}{(p^2-m_f^2+i\epsilon)^2}\Big] \\
&+ \frac{(k_fB)^2}{(p^2-m_f^2+i\epsilon)^3}\Big[(\not{p}+m_f)\big[\not{p}_{||}+\not{p}_\perp+m_f\big](\not{p}+m_f)\Big]\ . \qquad \text{(B.35)}
\end{aligned}
$$

Further we can reduce the second term as :

$$
\begin{aligned}
S_2^{e_fk_f} &= (e_fB)(k_fB)\Big[\frac{\not{p}+m_f}{(p^2-m_f^2+i\epsilon)^3}(\not{p}_{||}+3m_f)+\frac{2\not{p}_\perp}{(p^2-m_f^2+i\epsilon)^3}(\not{p}+m_f) \\
&+ \frac{(\not{p}+m_f)\not{p}_\perp}{(p^2-m_f^2+i\epsilon)^3}+\frac{2}{(p^2-m_f^2+i\epsilon)^2}\Big] \\
&= (e_fB)(k_fB)\Big[\frac{p_{||}^2+4m_f\not{p}_{||}+3p_\perp^2+3m_f^2}{(p^2-m_f^2+i\epsilon)^3}+\frac{2}{(p^2-m_f^2+i\epsilon)^2}\Big] \\
&= (e_fB)(k_fB)\Big[\frac{4(p_{||}^2+m_f\not{p}_{||})-3(p^2-m_f^2)}{(p^2-m_f^2+i\epsilon)^3}+\frac{2}{(p^2-m_f^2+i\epsilon)^2}\Big] \\
&= (e_fB)(k_fB)\Big[\frac{4\not{p}_{||}(\not{p}_{||}+m_f)}{(p^2-m_f^2+i\epsilon)^3}-\frac{1}{(p^2-m_f^2+i\epsilon)^2}\Big]\ . \qquad \text{(B.36)}
\end{aligned}
$$

Thus, the weak field propagator along with anomalous magnetic moment is given by:

$$
\begin{aligned}
S_2 &= (e_fB)^2\frac{-2p_\perp^2}{(p^2-m_f^2+i\epsilon)^4}\Big[(\not{p}_{||}+m_f)+\not{p}_\perp\frac{m_f^2-p_{||}^2}{p_\perp^2}\Big] \\
&+ (e_fB)(k_fB)\Big[\frac{4\not{p}_{||}(\not{p}_{||}+m_f)}{(p^2-m_f^2+i\epsilon)^3}-\frac{1}{(p^2-m_f^2+i\epsilon)^2}\Big] \\
&+ \frac{(k_fB)^2}{(p^2-m_f^2+i\epsilon)^3}\Big[(\not{p}+m_f)\big[\not{p}_{||}+\not{p}_\perp+m_f\big](\not{p}+m_f)\Big]\ . \qquad \text{(B.37)}
\end{aligned}
$$

Appendix C

Walecka model

C.1 Calculation of $\Sigma_s^{\text{(vacuum)}}$

We have from Eq. (3.38),

$$\Sigma_s^{\text{(vacuum)}} = \left(\frac{g_{\sigma NN}^2}{m_\sigma^2}\right) \text{Re}\ i \int \frac{d^dp}{(2\pi)^d} \hat{T}\left(p, m_N^*, m_1\right) \frac{1}{p^2 - m_1^2 + i\epsilon}\Bigg|_{m_1 = m_N^*, d\to 4} \tag{C.1}$$

In order to perform the d^4p integration, we use the following identities [202]

$$\int \frac{d^dp}{(2\pi)^d}\left(\frac{1}{p^2-\Delta}\right) = \frac{-i}{(4\pi)^{d/2}}\Gamma\left(1-\frac{d}{2}\right)\left(\frac{1}{\Delta}\right)^{1-d/2} \tag{C.2}$$

$$\int \frac{d^dp}{(2\pi)^d}\left(\frac{p_\perp^2}{p^2-\Delta}\right) = \frac{i}{(4\pi)^{d/2}}\left(\frac{d}{4}\right)\Gamma\left(-\frac{d}{2}\right)\left(\frac{1}{\Delta}\right)^{-d/2} \tag{C.3}$$

$$\int \frac{d^dp}{(2\pi)^d}\left(\frac{p_\parallel^2}{p^2-\Delta}\right) = \frac{i}{(4\pi)^{d/2}}\left(\frac{d}{4}\right)\Gamma\left(-\frac{d}{2}\right)\left(\frac{1}{\Delta}\right)^{-d/2} \tag{C.4}$$

$$\int \frac{d^dp}{(2\pi)^d}\left(\frac{p^2}{p^2-\Delta}\right) = \frac{i}{(4\pi)^{d/2}}\left(\frac{d}{2}\right)\Gamma\left(-\frac{d}{2}\right)\left(\frac{1}{\Delta}\right)^{-d/2} \tag{C.5}$$

so that, Eq. (C.1) will become

$$\Sigma_s^{\text{(vacuum)}} = \text{Re}\Sigma_s^{\text{(pure vacuum)}} + \Sigma_s^{\text{(divergent)}} + \Sigma_s^{\text{(regular)}} \tag{C.6}$$

where $\text{Re}\Sigma_s^{\text{(pure vacuum)}}$ is the ultra-violate divergent pure vacuum contribution given in Eq. 3.34 and

$$\Sigma_s^{\text{(divergent)}} = -\left(\frac{g_{\sigma NN}^2}{4\pi^2 m_\sigma^2}\right)\left\{\left(\kappa_{\text{p}}B\right)^2 m_N^* + \left(\kappa_{\text{n}}B\right)^2 m_N^* \ + \ \left(|e|\, B\right)\left(\kappa_{\text{p}}B\right)\right\}$$

$$\times \Gamma\left(2-\frac{d}{2}\right)\left(\frac{1}{m_N^{*2}}\right)^{2-d/2}\Bigg|_{d\to 4} \tag{C.7}$$

$$\Sigma_s^{(\text{regular})} = \left(\frac{g_{\sigma NN}^2}{4\pi^2 m_\sigma^2}\right)\left[\frac{(eB)^2}{3m_N^*} + \frac{1}{2}\left\{(\kappa_{\rm p}B)^2\, m_N^* + (\kappa_{\rm n}B)^2\, m_N^* \;+\; (|e|\,B)\,(\kappa_{\rm p}B)\right\}\right]\ . \tag{C.8}$$

In this case also, we will neglect the pure vacuum contribution $\mathrm{Re}\Sigma_s^{(\text{pure vacuum})}$ which is equivalent to use the MFT. We now extract the divergence of $\Sigma_s^{(\text{divergent})}$ from the pole of the Gamma function and use $\overline{\rm MS}$ scheme to obtain,

$$\Sigma_s^{(\text{divergent})} = \left(\frac{g_{\sigma NN}^2}{4\pi^2 m_\sigma^2}\right)\left\{(\kappa_{\rm p}B)^2\, m_N^* + (\kappa_{\rm n}B)^2\, m_N^* \;+\; (|e|\,B)\,(\kappa_{\rm p}B)\right\}\ln\left(\frac{m_N^{*2}}{\Lambda}\right) \tag{C.9}$$

where Λ is a scale of dimension GeV^2. Its value is fixed from the condition

$$\Sigma_s^{(\text{divergent})}\left(m_N^* = m_N\right) = 0 \tag{C.10}$$

which gives $\Lambda = m_N^2$. So the final expression of $\Sigma_s^{(\text{vacuum})}$ becomes

$$\begin{aligned}\Sigma_s^{(\text{vacuum})} = \left(\frac{g_{\sigma NN}^2}{4\pi^2 m_\sigma^2}\right)&\left[\frac{(eB)^2}{3m_N^*} + \left\{(\kappa_{\rm p}B)^2\, m_N^* + (\kappa_{\rm n}B)^2\, m_N^* + (|e|\,B)\,(\kappa_{\rm p}B)\right\}\right. \\ &\left.\times\left\{\frac{1}{2} + 2\ln\left(\frac{m_N^*}{m_N}\right)\right\}\right]\ .\end{aligned} \tag{C.11}$$

C.2 Calculation of $\Sigma_s^{(\text{medium})}$

We have from Eq. (3.39)

$$\Sigma_s^{(\text{medium})} = -\left(\frac{g_{\sigma NN}^2}{m_\sigma^2}\right)\int\frac{d^4p}{(2\pi)^4}\hat{T}\left(p, m_N^*, m_1\right)\ 2\pi\eta\left(p\cdot u\right)\delta\left(p^2 - m_1^2\right)\Big|_{m_1 = m_N^*} \tag{C.12}$$

where $\hat{T}\left(p, m_N^*, m_1\right)$ is given in Eq. (3.40). Using Eqs. (3.15) and (3.16), we can write the above equation as,

$$\begin{aligned}\Sigma_s^{(\text{medium})} = -\left(\frac{g_{\sigma NN}^2}{m_\sigma^2}\right)&\int\frac{d^3p}{(2\pi)^3}\int_{-\infty}^{+\infty}dp^0\hat{T}\left(p^0, \vec{p}, m_N^*, m_1\right)\left(\frac{1}{2\omega_1}\right)\times \\ &\left[f_+\left(\omega_1\right)\delta\left(p^0-\omega_1\right) + f_-\left(\omega_1\right)\delta\left(p^0+\omega_1\right)\right]_{m_1 = m_N^*}\end{aligned}$$

where $\omega_1 = \sqrt{\vec{p}^2 + m_1^2}$. Performing the dp^0 integration using the Dirac delta functions and noting that $\hat{T}\left(p^0, \vec{p}, m_N^*, m_1\right)$ is an even function of p^0, we get

$$\Sigma_s^{(\text{medium})} = -\left(\frac{g_{\sigma NN}^2}{2m_\sigma^2}\right)\int \frac{d^3p}{(2\pi)^3}\hat{T}\left(p^0 = \Omega_p, \vec{p}, m_N^*, m_1\right)\left(\frac{1}{\omega_1}\right)\Big[f_+\left(\omega_1\right) + f_-\left(\omega_1\right)\Big]_{m_1 = m_N^*} \quad \text{(C.13)}$$

Substituting Eq. (3.40) into (C.13) and performing the angular integration we get,

$$\Sigma_s^{(\text{medium})} = -\left(\frac{g_{\sigma NN}^2}{8\pi^2 m_\sigma^2}\right)\int_0^\infty |\vec{p}|^2 \, d|\vec{p}| \, \hat{B}\left(\vec{p}, m_N^*, m_1\right)\left(\frac{1}{\omega_1}\right)\Big[f_+\left(\omega_1\right) + f_-\left(\omega_1\right)\Big]_{m_1 = m_N^*} \quad \text{(C.14)}$$

where,

$$\begin{aligned}\hat{B}\left(\vec{p}, m_N^*, m_1\right) = 16m_N^* + \frac{32}{3}(eB)^2 m_N^* |\vec{p}|^2 \hat{A}_3 + 16\left(2m_N^{*2} + \frac{4}{3}|\vec{p}|^2\right) \\ \times\left\{m_N^*\left(\kappa_{\mathrm{p}}B\right)^2 + m_N^*\left(\kappa_{\mathrm{n}}B\right)^2 + \left(|e|\,B\right)\left(\kappa_{\mathrm{p}}B\right)\right\}\hat{A}_2 \,.\end{aligned} \quad \text{(C.15)}$$

C.2.1 Zero Temperature Case

From Eq. (3.16) we have at $T = 0$,

$$\lim_{T\to 0} f_\pm\left(\omega_1\right) = \Theta\left(\pm\mu_{\mathrm{B}} - \omega_1\right) \quad \text{(C.16)}$$

where μ_{B} is the baryon chemical potential of the medium. Substituting Eq. (C.16) into (C.14) we get,

$$\Sigma_s^{(\text{medium})} = -\left(\frac{g_{\sigma NN}^2}{8\pi^2 m_\sigma^2}\right)\int_0^\infty |\vec{p}|^2 \, d|\vec{p}| \; \hat{B}\left(\vec{p}, m_N^*, m_1\right)\frac{1}{\omega_1}\Theta\left(\mu_{\mathrm{B}} - \omega_1\right)\Big|_{m_1 = m_N^*} . \quad \text{(C.17)}$$

The the $d|\vec{p}|$ integration of the above equation can be evaluated analytically using the following identities

$$I_2(\mu, m) = \int_0^{\sqrt{\mu^2 - m^2}} \frac{|\vec{p}|^2 \, d|\vec{p}|}{\sqrt{|\vec{p}|^2 + m^2}} = \frac{1}{2}\left[\mu\sqrt{\mu^2 - m^2} + m^2 \ln\left\{\frac{m}{\mu + \sqrt{\mu^2 - m^2}}\right\}\right] \quad \text{(C.18)}$$

$$\begin{aligned} I_4(\mu, m) &= \int_0^{\sqrt{\mu^2 - m^2}} \frac{|\vec{p}|^4 \, d|\vec{p}|}{\sqrt{|\vec{p}|^2 + m^2}} \\ &= \frac{1}{8}\left[\mu\left(2\mu^2 - 5m^2\right)\sqrt{\mu^2 - m^2} - 3m^4 \ln\left\{\frac{m}{\mu + \sqrt{\mu^2 - m^2}}\right\}\right] \end{aligned} \quad \text{(C.19)}$$

and we get,

$$\Sigma_s^{(\text{medium})} = -\left(\frac{2g_{\sigma NN}^2}{\pi^2 m_\sigma^2}\right)\left[m_N^* I_2\left(\mu_{\rm B}, m_1\right) + \frac{2}{3}\left(eB\right)^2 m_N^* \hat{A}_3 I_4\left(\mu_{\rm B}, m_1\right)\right.$$
$$+2\left\{m_N^*\left(\kappa_{\rm p}B\right)^2 + m_N^*\left(\kappa_{\rm n}B\right)^2 + \left(|e|\,B\right)\left(\kappa_{\rm p}B\right)\right\}$$
$$\left.\times\left\{m_N^{*2}\hat{A}_2 I_2\left(\mu_{\rm B}, m_1\right) + \frac{1}{3}\hat{A}_2 I_4\left(\mu_{\rm B}, m_1\right)\right\}\right]_{m_1 = m_N^*}. \tag{C.20}$$

It is now trivial to check that

$$\hat{A}_2 I_2\left(\mu, m_1\right)\Big|_{m_1=m_N^*} = 2\hat{A}_3 I_4\left(\mu, m_1\right)\Big|_{m_1=m_N^*} = \frac{\mu}{8m_N^{*2}\sqrt{\mu^2 - m_N^{*2}}} = C_1\left(\mu, m_N^*\right) \tag{C.21}$$

$$\hat{A}_2 I_4\left(\mu, m_1\right)\Big|_{m_1=m_N^*} = -\left(\frac{3}{8}\right)\ln\left\{\frac{m_N^*}{\mu + \sqrt{\mu^2 - m_N^{*2}}}\right\} = C_2\left(\mu, m_N^*\right) \quad (\text{say})\,. \tag{C.22}$$

So finally $\Sigma_s^{(\text{medium})}$ becomes,

$$\Sigma_s^{(\text{medium})} = -\left(\frac{2g_{\sigma NN}^2}{\pi^2 m_\sigma^2}\right)\left[m_N^* I_2\left(\mu_{\rm B}, m_N^*\right) + \frac{1}{3}\left(eB\right)^2 m_N^* C_1\left(\mu_{\rm B}, m_N^*\right) + 2\left\{m_N^*\left(\kappa_{\rm p}B\right)^2\right.\right.$$
$$\left.\left.+m_N^*\left(\kappa_{\rm n}B\right)^2 + \left(|e|\,B\right)\left(\kappa_{\rm p}B\right)\right\}\left\{m_N^{*2}C_1\left(\mu_{\rm B}, m_N^*\right) + \frac{1}{3}C_2\left(\mu_{\rm B}, m_N^*\right)\right\}\right]\,. \tag{C.23}$$

C.2.2 Finite Temperature Case

At finite temperature, the $d\,|\vec{p}|$ integration in Eq. (C.14) can not be performed analytically. We simplify the expression by evaluating the derivatives with respect to m_1^2 explicitly. For this we use the following results

$$\left[\frac{f_\pm\left(\omega_1\right)}{\omega_1}\right]_{m_1=m_N^*} = \frac{N_\pm^p}{\Omega_p} = \tilde{C}_1^{\pm p} \tag{C.24}$$

$$\hat{A}_2\left[\frac{f_\pm\left(\omega_1\right)}{\omega_1}\right]_{m_1=m_N^*} = \frac{N_\pm^p}{8\Omega_p^5}\left[3 + 3\left(1 - N_\pm^p\right)\beta\Omega_p + \left\{1 - 3N_\pm^p + 2\left(N_\pm^p\right)^2\right\}\beta^2\Omega_p^2\right] = \tilde{C}_2^{\pm p} \tag{C.25}$$

$$\hat{A}_3\left[\frac{f_\pm\left(\omega_1\right)}{\omega_1}\right]_{m_1=m_N^*} = \frac{N_\pm^p}{48\Omega_p^7}\left[15 + 15\left(1 - N_\pm^p\right)\beta\Omega_p + 6\left\{1 - 3N_\pm^p + 2\left(N_\pm^p\right)^2\right\}\beta^2\Omega_p^2\right.$$
$$\left.+\left\{1 - 7N_\pm^p + 12\left(N_\pm^p\right)^2 - 6\left(N_\pm^p\right)^3\right\}\beta^3\Omega_p^3\right] = \tilde{C}_3^{\pm p} \quad (\text{say}) \tag{C.26}$$

and obtain from Eq. (C.14)

$$\Sigma_s^{(\text{medium})} = -\left(\frac{2g_{\sigma NN}^2}{\pi^2 m_\sigma^2}\right)\int_0^\infty |\vec{p}|^2\, d\,|\vec{p}|\left[m_N^*\left(\tilde{C}_1^{+p} + \tilde{C}_1^{-p}\right) + \frac{2}{3}m_N^*\left(eB\right)^2|\vec{p}|^2\left(\tilde{C}_3^{+p} + \tilde{C}_3^{-p}\right)\right.$$

$$+2\left(m_N^{*2}+\frac{2}{3}\left|\vec{p}\right|^2\right)\left\{m_N^*\left(\kappa_{\mathrm{p}}B\right)^2+m_N^*\left(\kappa_{\mathrm{n}}B\right)^2+\left(\left|e\right|B\right)\left(\kappa_{\mathrm{p}}B\right)\right\}\left(\tilde{C}_2^{+p}+\tilde{C}_2^{-p}\right)\Bigg] \tag{C.27}$$

Appendix D

Calculation of the self-energy of ρ meson

D.1 Useful Identities

We have the following list of d-dimensional integrals in Minkowski space [202]:

$$\int \frac{d^d k}{(2\pi)^d} \frac{1}{(k^2 - \Delta)^n} = \frac{i\,(-1)^n}{(4\pi)^{d/2}} \frac{\Gamma\,(n - d/2)}{\Gamma\,(n)} \left(\frac{1}{\Delta}\right)^{n-d/2} \tag{D.1}$$

$$\int \frac{d^d k}{(2\pi)^d} \frac{k^2}{(k^2 - \Delta)^n} = \frac{i\,(-1)^{n-1}}{(4\pi)^{d/2}} \left(\frac{d}{2}\right) \frac{\Gamma\,(n - 1 - d/2)}{\Gamma\,(n)} \left(\frac{1}{\Delta}\right)^{n-1-d/2} \tag{D.2}$$

$$\int \frac{d^d k}{(2\pi)^d} \frac{k^\mu k^\nu}{(k^2 - \Delta)^n} = \frac{i\,(-1)^{n-1}}{(4\pi)^{d/2}} \left(\frac{g^{\mu\nu}}{2}\right) \frac{\Gamma\,(n - 1 - d/2)}{\Gamma\,(n)} \left(\frac{1}{\Delta}\right)^{n-1-d/2}. \tag{D.3}$$

Using the orthogonality properties of the generalized Laguerre polynomials, one can derive the identity

$$\int \frac{d^2 k_\perp}{(2\pi)^2} e^{-2\alpha_k} L_l(2\alpha_k) L_n(2\alpha_k) k_\perp^\mu k_\perp^\nu = -g_\perp^{\mu\nu} \frac{(eB)^2}{32\pi} \left[(2n+1)\delta_l^n - (n+1)\delta_l^{n+1} - n\delta_l^{n-1}\right] \tag{D.4}$$

where, $\alpha_k = -k_\perp^2/eB$. Other relevant identities used in the calculations are

$$\int \frac{d^2 k_\perp}{(2\pi)^2} e^{-2\alpha_k} L_l(2\alpha_k) L_n(2\alpha_k) = \frac{eB}{8\pi} \delta_l^n \tag{D.5}$$

$$\int \frac{d^2 k_\perp}{(2\pi)^2} e^{-2\alpha_k} L_{l-1}^1(2\alpha_k) L_{n-1}^1(2\alpha_k) k_\perp^\mu k_\perp^\nu = -g_\perp^{\mu\nu} \frac{(eB)^2}{32\pi} n\delta_{l-1}^{n-1} \tag{D.6}$$

$$\int \frac{d^2 k_\perp}{(2\pi)^2} e^{-2\alpha_k} L_{l-1}^1(2\alpha_k) L_{n-1}^1(2\alpha_k) k_\perp^2 = -\frac{(eB)^2}{16\pi} n\delta_{l-1}^{n-1}. \tag{D.7}$$

D.2 Calculation of Vacuum Self Energy

In order to evaluate the momentum integrals in Eqs. (4.3) and (4.4), they are rewritten as

$$\left(\Pi_\pi^{\mu\nu}\right)_{\text{pure-vac}}(q) = i\int\frac{d^4k}{(2\pi)^4}\frac{\mathcal{N}_\pi^{\mu\nu}(q,k)}{(k^2-m_\pi^2+i\epsilon)((q+k)^2-m_\pi^2+i\epsilon)} \tag{D.8}$$

$$\left(\Pi_{\rm N}^{\mu\nu}\right)_{\text{pure-vac}}(q) = i\int\frac{d^4k}{(2\pi)^4}\frac{\mathcal{N}_{\rm N}^{\mu\nu}(q,k)}{(k^2-m_N^2+i\epsilon)((q+k)^2-m_N^2+i\epsilon)} \tag{D.9}$$

where, $\mathcal{N}_{\rm N}^{\mu\nu}(q,k)$ contains the trace over Dirac matrices:

$$\begin{aligned}\mathcal{N}_{\rm N}^{\mu\nu}(q,k) &= -2g_{\rho NN}^2\,\mathsf{Tr}\left[\Gamma^\nu(q)(\not{q}+\not{k}+m_N)\Gamma^\mu(-q)(\not{k}+m_N)\right]\\ &= -8g_{\rho NN}^2\Big[(m_N^2-k^2-k\cdot q)g^{\mu\nu}+2k^\mu k^\nu+(q^\mu k^\nu+q^\nu k^\mu)+\kappa_\rho\left(q^2g^{\mu\nu}-q^\mu q^\nu\right)\\ &\quad+\frac{\kappa_\rho^2}{4m_N^2}\Big\{(m_N^2+k^2-k\cdot q)(q^2g^{\mu\nu}-q^\mu q^\nu)\\ &\quad-2q^2k^\mu k^\nu-2(k\cdot q)^2g^{\mu\nu}+2(k\cdot q)(q^\mu k^\nu+q^\nu k^\mu)\Big\}\Big].\end{aligned} \tag{D.10}$$

Applying standard Feynman paramerization, the denominators of Eqs. (D.8) and (D.9) are combined to get,

$$\left(\Pi_\pi^{\mu\nu}\right)_{\text{pure-vac}}(q) = i\int_0^1 dx\int\frac{d^dk}{(2\pi)^d}\Lambda_\pi^{2-d/2}\frac{\mathcal{N}_\pi^{\mu\nu}(q,k)}{\left[(k+xq)^2-\Delta_\pi\right]^2}\Bigg|_{d\to4} \tag{D.11}$$

$$\left(\Pi_{\rm N}^{\mu\nu}\right)_{\text{pure-vac}}(q) = i\int_0^1 dx\int\frac{d^dk}{(2\pi)^d}\Lambda_{\rm N}^{2-d/2}\frac{\mathcal{N}_{\rm N}^{\mu\nu}(q,k)}{\left[(k+xq)^2-\Delta_{\rm N}\right]^2}\Bigg|_{d\to4} \tag{D.12}$$

where,

$$\Delta_\pi = m_\pi^2 - x(1-x)q^2 - i\epsilon \tag{D.13}$$

$$\Delta_{\rm N} = m_N^2 - x(1-x)q^2 - i\epsilon \tag{D.14}$$

and the space-time dimension has been changed from 4 to d in order to work with the dimensional regularization so that the additional scale parameters Λ_π and $\Lambda_{\rm N}$ of dimension GeV^2 have been introduced to keep the overall dimension of the self energy same. It is now straight forward to perform the momentum integrals of the above equations after a momentum shift $k\to(k-xq)$ using the identities provided in Appendix D.1, so that, the vacuum self energies becomes

$$\left(\Pi_\pi^{\mu\nu}\right)_{\text{pure-vac}}(q) = (q^2g^{\mu\nu}-q^\mu q^\nu)\left(\frac{g_{\rho\pi\pi}^2q^2}{32\pi^2}\right)\int_0^1 dx\,\Gamma(\varepsilon-1)\left(\frac{\Delta_\pi}{4\pi\Lambda_\pi}\right)^{-\varepsilon}\Bigg|_{\varepsilon\to0} \tag{D.15}$$

$$\left(\Pi^{\mu\nu}_{\rm N}\right)_{\text{pure-vac}}(q) = (q^2g^{\mu\nu} - q^\mu q^\nu)\left(\frac{g^2_{\rho NN}}{2\pi^2}\right)\int_0^1 dx\left[\left\{2x(1-x)+\kappa_\rho+\frac{\kappa_\rho^2}{2}\right\}\Gamma(\varepsilon) + \frac{\kappa_\rho^2}{4m_N^2}\Delta_{\rm N}\Gamma(\varepsilon-1)\right]\left(\frac{\Delta_{\rm N}}{4\pi\Lambda_{\rm N}}\right)^{-\varepsilon}\Bigg|_{\varepsilon\to 0} \tag{D.16}$$

where $\varepsilon = (2 - d/2)$. Expanding the above equations about $\varepsilon = 0$, we get

$$\left(\Pi^{\mu\nu}_{\pi}\right)_{\text{pure-vac}}(q) = (q^2g^{\mu\nu} - q^\mu q^\nu)\left(\frac{-g^2_{\rho\pi\pi}q^2}{32\pi^2}\right) \times \int_0^1 dx\Delta_\pi\left[\frac{1}{\varepsilon} - \gamma_{\rm E} + 1 - \ln\left(\frac{\Delta_\pi}{4\pi\Lambda_\pi}\right)\right]\Bigg|_{\varepsilon\to 0} \tag{D.17}$$

$$\left(\Pi^{\mu\nu}_{\rm N}\right)_{\text{pure-vac}}(q) = (q^2g^{\mu\nu} - q^\mu q^\nu)\left(\frac{g^2_{\rho NN}}{2\pi^2}\right)\int_0^1 dx\left[\left\{2x(1-x)+\kappa_\rho+\frac{\kappa_\rho^2}{2} - \frac{\kappa_\rho^2}{4m_N^2}\Delta_{\rm N}\right\} \times \left\{\frac{1}{\varepsilon} - \gamma_{\rm E} - \ln\left(\frac{\Delta_{\rm N}}{4\pi\Lambda_{\rm N}}\right)\right\} - \frac{\kappa_\rho^2}{4m_N^2}\Delta_{\rm N}\right]\Bigg|_{\varepsilon\to 0} \tag{D.18}$$

where, $\gamma_{\rm E}$ is the Euler-Mascheroni constant.

D.3 Calculation of eB-dependent Vacuum Contribution for $\pi\pi$ Loop

In this appendix, we sketch how to obtain Eqs. (4.46) and (4.48). We rewrite Eq. (4.44) as

$$\left(\Pi^{\mu\nu}_{\pi}\right)_{\rm vac}(q, eB) = i\sum_{l=0}^{\infty}\sum_{n=0}^{\infty}\int\frac{d^2k_\parallel}{(2\pi)^2}\int\frac{d^2k_\perp}{(2\pi)^2}\frac{\mathcal{N}^{\mu\nu}_{\pi,nl}(q,k)}{(k_\parallel^2 - m_l^2 + i\epsilon)((q_\parallel + k_\parallel)^2 - m_n^2 + i\epsilon)} \tag{D.19}$$

For the simplicity in analytic calculations, we take the transverse momentum of the ρ^0 to be zero i.e. $q_\perp = 0$. This implies that the $d^2k_\perp$ integration can be performed analytically using the orthogonality of the Laguerre polynomial details of which can be obtained from Appendix D.5, so that the self energy becomes

$$\left(\Pi^{\mu\nu}_{\pi}\right)_{\rm vac}(q_\parallel, eB) = i\sum_{l=0}^{\infty}\sum_{n=0}^{\infty}\int\frac{d^2k_\parallel}{(2\pi)^2}\frac{\tilde{\mathcal{N}}^{\mu\nu}_{\pi,nl}(q_\parallel,k_\parallel)}{(k_\parallel^2 - m_l^2 + i\epsilon)((q_\parallel + k_\parallel)^2 - m_n^2 + i\epsilon)} \tag{D.20}$$

where, $\tilde{\mathcal{N}}^{\mu\nu}_{\pi,nl}(q_\parallel,k_\parallel)$ is given in Eq. (D.41). Next, we use the standard Feynman parametrization technique to combine the denominators of Eq. (D.20) and change the reduced space-time dimension from 2 to d in order to apply the dimensional regularization for which a scale parameter Λ_π of dimension GeV^2 has to be introduced in order to keep the overall dimension of the self energy same. This leads to

$$\left(\Pi^{\mu\nu}_{\pi}\right)_{\rm vac}(q_\parallel, eB) = i\sum_{l=0}^{\infty}\sum_{n=0}^{\infty}\int_0^1 dx \int \frac{d^dk_\parallel}{(2\pi)^d}\Lambda_\pi^{1-d/2}\frac{\tilde{\mathcal{N}}^{\mu\nu}_{\pi,nl}(q_\parallel,k_\parallel)}{\left[(k_\parallel + xq_\parallel)^2 - \Delta^\pi_{nl}\right]^2}\Bigg|_{d\to 2} \tag{D.21}$$

where,

$$\Delta^\pi_{nl} = \Delta_\pi(q_\perp = 0) + 2eB\left\{l + 1 - x(l-n)\right\} \tag{D.22}$$

with Δ_π is defined in Eq. (D.13). It is now trivial to perform the $d^dk_\parallel$ integration after a shift of momentum $k_\parallel \to (k_\parallel - xq_\parallel)$ using the identities provided in Appendix D.1, so that the self energy becomes

$$\begin{aligned}\left(\Pi^{\mu\nu}_{\pi}\right)_{\rm vac}(q_\parallel, eB) = \frac{-g^2_{\rho\pi\pi}q^2_\parallel}{16\pi^2}eB\int_0^1 dx\sum_{n=0}^{\infty}\sum_{l=(n-1)}^{(n+1)}(-1)^{n+l}\left(4\pi\Lambda_\pi\right)^\varepsilon \\ \times\Bigg[-(q^2_\parallel g^{\mu\nu}_\parallel - q^\mu_\parallel q^\nu_\parallel)\delta^n_l\Gamma(\varepsilon)\left(\Delta^\pi_{nl}\right)^{-\varepsilon} - q^2_\parallel g^{\mu\nu}_\perp\frac{eB}{2}\left\{(2n+1)\delta^n_l\right. \\ \left. -(n+1)\delta^{n+1}_l - n\delta^{n-1}_l\right\}\Gamma(\varepsilon+1)\left(\Delta^\pi_{nl}\right)^{-\varepsilon-1}\Bigg]\Bigg|_{\varepsilon\to 0}\end{aligned} \tag{D.23}$$

where $\varepsilon = (1 - d/2)$ and the presence of Kronecker delta functions in Eq. (D.41) has made the double sum into a single one or in other words the sum over index l runs only from $(n-1)$ to $(n+1)$. The infinite sum in the above equations can be expressed in terms of Hurwitz zeta function so that we get after some simplifications

$$\begin{aligned}\left(\Pi^{\mu\nu}_{\pi}\right)_{\rm vac}(q_\parallel, eB) = \frac{-g^2_{\rho\pi\pi}q^2_\parallel}{16\pi^2}eB\int_0^1 dx\left(\frac{4\pi\Lambda_\pi}{2eB}\right)^\varepsilon\Bigg[-(q^2_\parallel g^{\mu\nu}_\parallel - q^\mu_\parallel q^\nu_\parallel)\Gamma(\varepsilon)\zeta\left(\varepsilon, z_\pi + \frac{1}{2}\right) \\ -\frac{q^2_\parallel}{2}g^{\mu\nu}_\perp\Gamma(\varepsilon+1)\left\{\zeta\left(\varepsilon, z_\pi + \frac{1}{2}\right) + \zeta\left(\varepsilon, z_\pi + x + \frac{1}{2}\right)\right. \\ \left. -z_\pi\zeta\left(\varepsilon+1, z_\pi + \frac{1}{2}\right) - z_\pi\zeta\left(\varepsilon+1, z_\pi + x + \frac{1}{2}\right)\right\}\Bigg]\Bigg|_{\varepsilon\to 0}.\end{aligned} \tag{D.24}$$

where, $z_\pi = \frac{\Delta_\pi(q_\perp=0)}{2eB}$. Expanding the above equation about $\varepsilon = 0$, we get,

$$\begin{aligned}\left(\Pi^{\mu\nu}_{\pi}\right)_{\rm vac}(q_\parallel, eB) &= \frac{-g^2_{\rho\pi\pi}q^2_\parallel}{32\pi^2}\int_0^1 dx\Bigg[\left\{\frac{1}{\varepsilon} - \gamma_{\rm E} + \ln\left(\frac{4\pi\Lambda_\pi}{2eB}\right)\right\}\Delta_\pi(q_\perp = 0)(q^2_\parallel g^{\mu\nu} - q^\mu_\parallel q^\nu_\parallel) \\ &\quad -(q^2_\parallel g^{\mu\nu}_\parallel - q^\mu_\parallel q^\nu_\parallel)2eB\left\{\ln\Gamma\left(z_\pi + \frac{1}{2}\right) - \ln\sqrt{2\pi}\right\} \\ &\quad +q^2_\parallel g^{\mu\nu}_\perp\left\{\Delta_\pi(q_\perp = 0) + \frac{eB}{2} - \frac{1}{2}\Delta_\pi(q_\perp = 0)\right.\end{aligned}$$

$$\times\left\{\psi\left(z_\pi+\frac{1}{2}\right)+\psi\left(z_\pi+x+\frac{1}{2}\right)\right\}\Bigg\}\Bigg]\Bigg|_{\varepsilon\to 0} \tag{D.25}$$

where, $\psi(z)$ is the digamma function. It is now trivial to check that, in the limit $eB \to 0$, the above equation exactly boils down to the pure vacuum contribution given in Eq. (4.9). Thus extracting the pure vacuum contribution from the above equation we get,

$$\left(\Pi^{\mu\nu}_{\pi}\right)_{\text{vac}}(q_\parallel, eB) = \left(\Pi^{\mu\nu}_{\pi}\right)_{\text{pure-vac}}(q_\parallel) + \left(\Pi^{\mu\nu}_{\pi}\right)_{\text{eB-vac}}(q_\parallel, eB) \tag{D.26}$$

where,

$$\begin{aligned}\left(\Pi^{\mu\nu}_{\pi}\right)_{\text{eB-vac}}(q_\parallel, eB) = \frac{-g^2_{\rho\pi\pi}q^2_\parallel}{32\pi^2}\int_0^1 dx\, \Bigg[\left\{\ln\left(\frac{\Delta_\pi(q_\perp=0)}{2eB}\right)-1\right\}\Delta_\pi(q_\perp=0)(q^2_\parallel g^{\mu\nu}_\parallel - q^\mu_\parallel q^\nu_\parallel)\\ -(q^2_\parallel g^{\mu\nu}_\parallel - q^\mu_\parallel q^\nu_\parallel)2eB\left\{\ln\Gamma\left(z_\pi+\frac{1}{2}\right)-\ln\sqrt{2\pi}\right\}+q^2_\parallel g^{\mu\nu}_\perp\Bigg\{\Delta_\pi(q_\perp=0)\\ +\frac{eB}{2}-\frac{1}{2}\Delta_\pi(q_\perp=0)\left\{\psi\left(z_\pi+\frac{1}{2}\right)+\psi\left(z_\pi+x+\frac{1}{2}\right)\right\}\Bigg\}\Bigg]\end{aligned} \tag{D.27}$$

which is finite and independent of scale.

D.4 Calculation of eB-dependent Vacuum Contribution for proton-proton Loop

In this appendix, we sketch how to obtain Eqs. (4.47) and (4.49) We rewrite Eq. (4.45) as

$$\left(\Pi^{\mu\nu}_{\text{p}}\right)_{\text{vac}}(q, eB) = i\sum_{l=0}^{\infty}\sum_{n=0}^{\infty}\int\frac{d^2k_\parallel}{(2\pi)^2}\int\frac{d^2k_\perp}{(2\pi)^2}\frac{\mathcal{N}^{\mu\nu}_{\text{p},nl}(q,k)}{(k^2_\parallel - M^2_l + i\epsilon)((q_\parallel+k_\parallel)^2 - M^2_n + i\epsilon)} \tag{D.28}$$

where, $\mathcal{N}^{\mu\nu}_{\text{p},nl}(q,k)$ is given in Eq. (4.42). For the simplicity in analytic calculations, we take the transverse momentum of the ρ^0 to be zero i.e. $q_\perp = 0$. This implies that the $d^2k_\perp$ integration can be performed analytically using the orthogonality of the Laguerre polynomial details of which can be obtained from Appendix D.5, so that the self energy becomes

$$\left(\Pi^{\mu\nu}_{\text{p}}\right)_{\text{vac}}(q_\parallel, eB) = i\sum_{l=0}^{\infty}\sum_{n=0}^{\infty}\int\frac{d^2k_\parallel}{(2\pi)^2}\frac{\tilde{\mathcal{N}}^{\mu\nu}_{\text{p},nl}(q_\parallel,k_\parallel)}{(k^2_\parallel - M^2_l + i\epsilon)((q_\parallel+k_\parallel)^2 - M^2_n + i\epsilon)} \tag{D.29}$$

where, $\tilde{\mathcal{N}}^{\mu\nu}_{\text{p},nl}(q_\parallel,k_\parallel)$ can be read off from Eq. (D.44). Next, we use the standard Feynman parametrization technique to combine the denominators of Eq. (D.29) and change the reduced space-time dimension from 2 to d in order to apply the dimensional regularization for which a scale parameter Λ_N of dimension GeV^2 has to be introduced in order to keep the overall dimension of the self energy same. This leads to

$$\left(\Pi^{\mu\nu}_{\rm p}\right)_{\rm vac}(q_\parallel, eB) = i\sum_{l=0}^{\infty}\sum_{n=0}^{\infty}\int_0^1 dx\int\frac{d^dk_\parallel}{(2\pi)^d}\Lambda_N^{1-d/2}\left.\frac{\tilde{\mathcal{N}}^{\mu\nu}_{{\rm p},nl}(q_\parallel, k_\parallel)}{\left[(k_\parallel + xq_\parallel)^2 - \Delta^{\rm p}_{nl}\right]^2}\right|_{d\to 2} \tag{D.30}$$

where,

$$\Delta^{\rm p}_{nl} = \Delta_N(q_\perp = 0) + 2eB\left\{l - x(l-n)\right\} \tag{D.31}$$

with Δ_N is defined in Eq. (D.14). Performing the $d^dk_\parallel$ integration after a shift of momentum $k_\parallel \to (k_\parallel - xq_\parallel)$ the self energy becomes

$$\begin{aligned}\left(\Pi^{\mu\nu}_{\rm p}\right)_{\rm vac}(q_\parallel, eB) &= \frac{g^2_{\rho NN}}{4\pi^2}eB\int_0^1 dx\sum_{n=0}^{\infty}\sum_{l=(n-1)}^{(n+1)}(-1)^{n+l}\left(4\pi\Lambda_\pi\right)^\varepsilon\Bigg[\Big[4eBg^{\mu\nu}_\parallel n\delta^{n-1}_{l-1}\\
&+\left\{(m_N^2 + x(1-x)q_\parallel^2)g^{\mu\nu}_\parallel - 2x(1-x)q^\mu_\parallel q^\nu_\parallel\right\}\left(\delta^{n-1}_{l-1} + \delta^n_l\right)\\
&- g^{\mu\nu}_\perp(m_N^2 + x(1-x)q_\parallel^2)\left(\delta^n_{l-1} + \delta^{n-1}_l\right)\Big]\Gamma(\varepsilon+1)\left(\Delta^{\rm p}_{nl}\right)^{-\varepsilon-1}\\
&- \left\{g^{\mu\nu}_\parallel\left(\delta^{n-1}_{l-1} + \delta^n_l\right)\varepsilon + g^{\mu\nu}_\perp\left(\delta^n_{l-1} + \delta^{n-1}_l\right)(-\varepsilon+1)\right\}\Gamma(\varepsilon)\left(\Delta^{\rm p}_{nl}\right)^{-\varepsilon}\\
&+ \kappa_\rho\left\{(q_\parallel^2 g^{\mu\nu}_\parallel - q^\mu_\parallel q^\nu_\parallel)\left(\delta^{n-1}_{l-1} + \delta^n_l\right) - q_\parallel^2 g^{\mu\nu}_\perp\left(\delta^n_{l-1} + \delta^{n-1}_l\right)\right\}\Gamma(\varepsilon+1)\left(\Delta^{\rm p}_{nl}\right)^{-\varepsilon-1}\\
&+ \frac{\kappa_\rho^2}{4m_N^2}\Big[\left\{-4eBn\delta^{n-1}_{l-1} + (m_N^2 + x(1-x)q_\parallel^2)\left(\delta^{n-1}_{l-1} + \delta^n_l\right)\right\}(q_\parallel^2 g^{\mu\nu}_\parallel - q^\mu_\parallel q^\nu_\parallel)\\
&- q_\parallel^2(m_N^2 + x(1+x)q_\parallel^2)g^{\mu\nu}_\perp\left(\delta^n_{l-1} + \delta^{n-1}_l\right)\Big]\Gamma(\varepsilon+1)\left(\Delta^{\rm p}_{nl}\right)^{-\varepsilon-1}\\
&- \frac{\kappa_\rho^2}{4m_N^2}\left\{(q_\parallel^2 g^{\mu\nu}_\parallel - q^\mu_\parallel q^\nu_\parallel)(-\varepsilon-1)\left(\delta^{n-1}_{l-1} + \delta^n_l\right) + q_\parallel^2 g^{\mu\nu}_\perp\left(\delta^n_{l-1} + \delta^{n-1}_l\right)\varepsilon\right\}\Gamma(\varepsilon)\left(\Delta^{\rm p}_{nl}\right)^{-\varepsilon}\Bigg]\Bigg|_{\varepsilon\to 0}\end{aligned} \tag{D.32}$$

where $\varepsilon = (1 - d/2)$ and the presence of Kronecker delta functions in Eq. (D.44) has made the double sum into a single one or in other words the sum over index l runs only from $(n-1)$ to $(n+1)$. The infinite sum in the above equations can be expressed in terms of Hurwitz zeta function so that we get after some simplifications

$$\begin{aligned}\left(\Pi^{\mu\nu}_{\rm p}\right)_{\rm vac}(q_\parallel, eB) &= \frac{g^2_{\rho\pi\pi}}{4\pi^2}\int_0^1 dx\left(\frac{4\pi\Lambda_N}{2eB}\right)^\varepsilon\Bigg[\Big[2eBg^{\mu\nu}_\parallel\left\{\zeta(\varepsilon, z_N) - z_N\zeta(\varepsilon+1, z_N)\right\}\\
&+\left\{(m_N^2 + x(1-x)q_\parallel^2)g^{\mu\nu}_\parallel - 2x(1-x)q^\mu_\parallel q^\nu_\parallel\right\}\left\{\zeta(\varepsilon+1, z_N) - \frac{1}{2}z_N^{-\varepsilon-1}\right\}\\
&+(m_N^2 + x(1-x)q_\parallel^2)g^{\mu\nu}_\perp\zeta(\varepsilon+1, z_N + x)\Big]\Gamma(\varepsilon+1) - 2eB\left\{g^{\mu\nu}_\parallel\varepsilon\left(\zeta(\varepsilon, z_N) - \frac{1}{2}z_N^{-\varepsilon}\right)\right.\end{aligned}$$

$$+g_\perp^{\mu\nu}(\varepsilon-1)\zeta(\varepsilon,z_N+x)\Big\}\Gamma(\varepsilon)+\kappa_\rho\Big\{(q_\parallel^2 g_\parallel^{\mu\nu}-q_\parallel^\mu q_\parallel^\nu)\Big(\zeta(1+\varepsilon,z_N)-\frac{1}{2}z_N^{-\varepsilon-1}\Big)$$
$$+q_\parallel^2 g_\perp^{\mu\nu}\zeta(\varepsilon+1,z_N+x)\Big\}\Gamma(\varepsilon+1)+\frac{\kappa_\rho^2}{4m_N^2}\Big[\Big\{-2eB\Big(\zeta(\varepsilon,z_N)-z_N\zeta(\varepsilon+1,z_N)\Big)$$
$$+(m_N^2+x(1-x)q_\parallel^2)\Big(\zeta(\varepsilon+1,z_N)-\frac{1}{2}z_N^{-\varepsilon-1}\Big)\Big\}(q_\parallel^2 g_\parallel^{\mu\nu}-q_\parallel^\mu q_\parallel^\nu)$$
$$+q_\parallel^2 g_\perp^{\mu\nu}(m_N^2+x(1-x)q_\parallel^2)\zeta(\varepsilon+1,z_N+x)\Big]\Gamma(\varepsilon+1)+\frac{\kappa_\rho^2}{4m_N^2}2eB\Big\{(q_\parallel^2 g_\parallel^{\mu\nu}-q_\parallel^\mu q_\parallel^\nu)(\varepsilon+1)$$
$$\times\Big(\zeta(\varepsilon,z_N)-\frac{1}{2}z_N^{-\varepsilon}\Big)+q_\parallel^2 g_\perp^{\mu\nu}\varepsilon\zeta(\varepsilon,z_N+x)\Big\}\Gamma(\varepsilon)\Big]\Big]\Bigg|_{\varepsilon\to 0}, \tag{D.33}$$

where, $z_N = \frac{\Delta_N(q_\perp=0)}{2eB}$. Expanding the above equation about $\varepsilon = 0$, we get,

$$\left(\Pi_{\rm p}^{\mu\nu}\right)_{\rm vac}(q_\parallel,eB)=\frac{g_{\rho NN}^2}{4\pi^2}\int_0^1 dx\Big[\Big\{\frac{1}{\varepsilon}-\gamma_{\rm E}+\ln\Big(\frac{4\pi\Lambda_N}{2eB}\Big)\Big\}$$
$$\times\Big\{2x(1-x)+\kappa_\rho+\frac{\kappa_\rho^2}{2}-\frac{\kappa_\rho^2}{4m_N^2}\Delta_N(q_\perp=0)\Big\}(q_\parallel^2 g^{\mu\nu}-q_\parallel^\mu q_\parallel^\nu)$$
$$-2x(1-x)\Big(\psi(z_N)+\frac{1}{2z_N}\Big)(q_\parallel^2 g_\parallel^{\mu\nu}-q_\parallel^\mu q_\parallel^\nu)+2eBg_\perp^{\mu\nu}\Big\{\Big(z_N-\frac{m_N^2}{eB}\Big)\psi(z_N+x)+z_N$$
$$+\ln\Gamma(z+x)-\ln\sqrt{2\pi}\Big\}-\kappa_\rho\Big\{(q_\parallel^2 g_\parallel^{\mu\nu}-q_\parallel^\mu q_\parallel^\nu)\Big(\psi(z_N)+\frac{1}{2z_N}\Big)+q_\parallel^2 g_\perp^{\mu\nu}\psi(z+x)\Big\}$$
$$+\frac{\kappa_\rho^2}{4m_N^2}2eB\Big[(q_\parallel^2 g_\parallel^{\mu\nu}-q_\parallel^\mu q_\parallel^\nu)\Big\{-\frac{m_N^2}{eB}\Big(\psi(z_N)+\frac{1}{2z_N}\Big)+\frac{1}{2}\ln(z_N)+\ln\Gamma(z_N)-\ln\sqrt{2\pi}\Big\}$$
$$-q_\parallel^2 g_\perp^{\mu\nu}\Big\{\Big(\frac{m_N^2}{eB}-z_N\Big)\psi(z_N+x)+\Delta_N(q_\perp=0)\Big\}\Big]\Big]\Bigg|_{\varepsilon\to 0}. \tag{D.34}$$

It is now trivial to check that, in the limit $eB\to 0$, the above equation exactly boils down to the $\frac{1}{2}$ times pure vacuum contribution given in Eq. (4.10). Thus extracting the pure vacuum contribution from the above equation we get,

$$\left(\Pi_{\rm p}^{\mu\nu}\right)_{\rm vac}(q_\parallel,eB)=\frac{1}{2}\left(\Pi_{\rm N}^{\mu\nu}\right)_{\text{pure-vac}}(q_\parallel)+\left(\Pi_{\rm p}^{\mu\nu}\right)_{\text{eB-vac}}(q_\parallel,eB) \tag{D.35}$$

where,

$$\left(\Pi_{\rm p}^{\mu\nu}\right)_{\text{eB-vac}}(q_\parallel,eB)=\frac{g_{\rho NN}^2}{4\pi^2}\int_0^1 dx\Big[\ln\Big(\frac{\Delta_N(q_\perp=0)}{2eB}\Big)$$
$$\times(q_\parallel^2 g^{\mu\nu}-q_\parallel^\mu q_\parallel^\nu)\Big\{2x(1-x)+\kappa_\rho+\frac{\kappa_\rho^2}{2}-\frac{\kappa_\rho^2}{4m_N^2}\Delta_N(q_\perp=0)\Big\}$$
$$-2x(1-x)\Big(\psi(z_N)+\frac{1}{2z_N}\Big)(q_\parallel^2 g_\parallel^{\mu\nu}-q_\parallel^\mu q_\parallel^\nu)+2eBg_\perp^{\mu\nu}\Big\{\Big(z_N-\frac{m_N^2}{eB}\Big)\psi(z_N+x)+z_N$$
$$+\ln\Gamma(z+x)-\ln\sqrt{2\pi}\Big\}-\kappa_\rho\Big\{(q_\parallel^2 g_\parallel^{\mu\nu}-q_\parallel^\mu q_\parallel^\nu)\Big(\psi(z_N)+\frac{1}{2z_N}\Big)+q_\parallel^2 g_\perp^{\mu\nu}\psi(z+x)\Big\}$$

$$+\frac{\kappa_\rho^2}{4m_N^2}2eB\left[(q_\parallel^2 g_\parallel^{\mu\nu}-q_\parallel^\mu q_\parallel^\nu)\left\{-\frac{m_N^2}{eB}\left(\psi(z_N)+\frac{1}{2z_N}\right)+\frac{1}{2}\ln(z_N)+\ln\Gamma(z_N)-\ln\sqrt{2\pi}\right\}\right.$$
$$\left.-q_\parallel^2 g_\perp^{\mu\nu}\left\{\left(\frac{m_N^2}{eB}-z_N\right)\psi(z_N+x)+\Delta_N(q_\perp=0)\right\}+\frac{\kappa_\rho^2}{4m_N^2}(q_\parallel^2 g^{\mu\nu}-q_\parallel^\mu q_\parallel^\nu)\Delta_N(q_\perp=0)\right] \tag{D.36}$$

which is finite and independent of scale.

D.5 Analytic Evaluation of $d^2k_\perp$ Integral for $q_\perp = 0$

In this appendix we will calculate the quantities

$$\tilde{\mathcal{N}}_{\pi,nl}^{\mu\nu}(q_\parallel,k_\parallel) = \int\frac{d^2k_\perp}{(2\pi)^2}\mathcal{N}_{\pi,nl}^{\mu\nu}(q_\parallel,q_\perp=0,k) \tag{D.37}$$
$$\tilde{\mathcal{N}}_{\mathrm{p},nl}^{\mu\nu}(q_\parallel,k_\parallel) = \int\frac{d^2k_\perp}{(2\pi)^2}\mathcal{N}_{\mathrm{p},nl}^{\mu\nu}(q_\parallel,q_\perp=0,k)\ . \tag{D.38}$$

We have the expression for $\mathcal{N}_{\pi,nl}^{\mu\nu}(q,k)$ from Eqs. (4.40) and (4.7) as

$$\mathcal{N}_{\pi,nl}^{\mu\nu}(q,k) = 4g_{\rho\pi\pi}^2(-1)^{n+l}e^{-\alpha_k-\alpha_p}L_l(2\alpha_k)L_n(2\alpha_p)$$
$$\times\left[q^4k^\mu k^\nu+(q\cdot k)^2q^\mu q^\nu-q^2(q\cdot k)(q^\mu k^\nu+q^\nu k^\mu)\right] \tag{D.39}$$

which for $q_\perp = 0$ becomes

$$\mathcal{N}_{\pi,nl}^{\mu\nu}(q_\parallel,k) = 4g_{\rho\pi\pi}^2(-1)^{n+l}e^{-2\alpha_k}L_l(2\alpha_k)L_n(2\alpha_k)$$
$$\times\left[q_\parallel^4k^\mu k^\nu+(q_\parallel\cdot k_\parallel)^2q_\parallel^\mu q_\parallel^\nu-q_\parallel^2(q_\parallel\cdot k_\parallel)(q_\parallel^\mu k^\nu+q_\parallel^\nu k^\mu)\right]. \tag{D.40}$$

We now perform the $d^2k_\perp$ integration using the orthogonality of the Laguerre polynomial (identities provided in Appendix D.1) to obtain

$$\tilde{\mathcal{N}}_{\pi,nl}^{\mu\nu}(q_\parallel,k_\parallel) = 4g_{\rho\pi\pi}^2(-1)^{n+l}\frac{eB}{8\pi}$$
$$\times\left[\left\{q_\parallel^4k_\parallel^\mu k_\parallel^\nu+(q_\parallel\cdot k_\parallel)^2q_\parallel^\mu q_\parallel^\nu-q_\parallel^2(q_\parallel\cdot k_\parallel)(q_\parallel^\mu k_\parallel^\nu+q_\parallel^\nu k_\parallel^\mu)\right\}\delta_l^n\right.$$
$$\left.-q_\parallel^4g_\perp^{\mu\nu}\frac{eB}{4}\left\{(2n+1)\delta_l^n-(n+1)\delta_l^{n+1}-n\delta_l^{n-1}\right\}\right]. \tag{D.41}$$

Similarly, $\mathcal{N}_{\mathrm{p},nl}^{\mu\nu}(q,k)$ is obtained from Eq. (4.42) as

$$\mathcal{N}_{\mathrm{p},nl}^{\mu\nu}(q,k) = -g_{\rho NN}^2(-1)^{n+l}e^{-\alpha_k-\alpha_p}\mathsf{Tr}\left[\Gamma^\nu(q)\mathcal{D}_n(q+k)\Gamma^\mu(q-)\mathcal{D}_l(k)\right]. \tag{D.42}$$

Evaluating the trace over the Dirac matrices in the above equation, we get for $q_\perp = 0$ (considering the Lorentz symmetric part since the self energy should be symmetric in the two Lorentz indices)

$$\begin{aligned}
&\mathcal{N}^{\mu\nu}_{\mathrm{p},nl}(q_\parallel, k) = -8g^2_{\rho NN}(-1)^{n+l}e^{-2\alpha_k}\Bigg[8(2k^\mu_\perp k^\nu_\perp - k^2_\perp g^{\mu\nu})L^1_{l-1}(2\alpha_k)L^1_{n-1}(2\alpha_k) \\
&+\Big\{(m_N^2 - k_\parallel^2 - k_\parallel\cdot q_\parallel)g^{\mu\nu}_\parallel + 2k^\mu_\parallel k^\nu_\parallel + (q^\mu_\parallel k^\nu_\parallel + q^\nu_\parallel k^\mu_\parallel)\Big\} \\
&\times\Big\{L_{l-1}(2\alpha_k)L_{n-1}(2\alpha_k) + L_l(2\alpha_k)L_n(2\alpha_k)\Big\} \\
&-(m_N^2 - k_\parallel^2 - k_\parallel\cdot q_\parallel)g^{\mu\nu}_\perp\Big\{L_l(2\alpha_k)L_{n-1}(2\alpha_k) + L_{l-1}(2\alpha_k)L_n(2\alpha_k)\Big\} \\
&+\kappa_\rho\Big[(q^2_\parallel g^{\mu\nu}_\parallel - q^\mu_\parallel q^\nu_\parallel)\Big\{L_{l-1}(2\alpha_k)L_{n-1}(2\alpha_k) + L_l(2\alpha_k)L_n(2\alpha_k)\Big\} \\
&-q^2_\parallel g^{\mu\nu}_\perp\Big\{L_l(2\alpha_k)L_{n-1}(2\alpha_k) + L_{l-1}(2\alpha_k)L_n(2\alpha_k)\Big\}\Big] \\
&+\frac{\kappa_\rho^2}{4m_N^2}\Big[8\Big\{k^2_\perp(q^2_\parallel g^{\mu\nu} - q^\mu_\parallel q^\nu_\parallel) - q^2_\parallel g^{\mu\nu}_\perp\Big\{L_l(2\alpha_k)L_{n-1}(2\alpha_k) + L_{l-1}(2\alpha_k)L_n(2\alpha_k)\Big\}\Big\} \\
&-\Big\{2(k_\parallel\cdot q_\parallel)^2 g^{\mu\nu}_\parallel + 2q^2_\parallel k^\mu_\parallel k^\nu_\parallel - 2(k_\parallel\cdot q_\parallel)(q^\mu_\parallel k^\nu_\parallel + q^\nu_\parallel k^\mu_\parallel) - (m_N^2 + k_\parallel^2 - k_\parallel\cdot q_\parallel)(q^2_\parallel g^{\mu\nu}_\parallel - q^\mu_\parallel q^\nu_\parallel)\Big\} \\
&\times\Big\{L_{l-1}(2\alpha_k)L_{n-1}(2\alpha_k) + L_l(2\alpha_k)L_n(2\alpha_k)\Big\} - g^{\mu\nu}_\perp\left\{q^2_\parallel(m_N^2 + k_\parallel^2 - k_\parallel\cdot q_\parallel) - 2(k_\parallel\cdot q_\parallel)^2\right\} \\
&\times\Big\{L_l(2\alpha_k)L_{n-1}(2\alpha_k) + L_{l-1}(2\alpha_k)L_n(2\alpha_k)\Big\}\Big]\Bigg].
\end{aligned} \tag{D.43}$$

We now perform the $d^2k_\perp$ integration using the orthogonality of the Laguerre polynomial (identities provided in Appendix D.1) to obtain,

$$\begin{aligned}
&\tilde{\mathcal{N}}^{\mu\nu}_{\mathrm{p},nl}(q_\parallel, k_\parallel) = -g^2_{\rho NN}(-1)^{n+l}\frac{eB}{\pi}\Bigg[4eBg^{\mu\nu}_\parallel n\delta^{n-1}_{l-1} + \left(\delta^{n-1}_{l-1} + \delta^n_l\right) \\
&\times\Big\{(m_N^2 - k_\parallel^2 - k_\parallel\cdot q_\parallel)g^{\mu\nu}_\parallel + 2k^\mu_\parallel k^\nu_\parallel + (q^\mu_\parallel k^\nu_\parallel + q^\nu_\parallel k^\mu_\parallel)\Big\} - (m_N^2 - k_\parallel^2 - k_\parallel\cdot q_\parallel)g^{\mu\nu}_\perp\left(\delta^n_{l-1} + \delta^{n-1}_l\right) \\
&+\kappa_\rho\Big[(q^2_\parallel g^{\mu\nu}_\parallel - q^\mu_\parallel q^\nu_\parallel)\left(\delta^{n-1}_{l-1} + \delta^n_l\right) - q^2_\parallel g^{\mu\nu}_\perp\left(\delta^n_{l-1} + \delta^{n-1}_l\right)\Big] \\
&+\frac{\kappa_\rho^2}{4m_N^2}\Big[-4eB(q^2_\parallel g^{\mu\nu}_\parallel - q^\mu_\parallel q^\nu_\parallel)n\delta^{n-1}_{l-1} - \Big\{2(k_\parallel\cdot q_\parallel)^2 g^{\mu\nu}_\parallel + 2q^2_\parallel k^\mu_\parallel k^\nu_\parallel - 2(k_\parallel\cdot q_\parallel)(q^\mu_\parallel k^\nu_\parallel + q^\nu_\parallel k^\mu_\parallel) \\
&-(m_N^2 + k_\parallel^2 - k_\parallel\cdot q_\parallel)(q^2_\parallel g^{\mu\nu}_\parallel - q^\mu_\parallel q^\nu_\parallel)\Big\}\left(\delta^{n-1}_{l-1} + \delta^n_l\right) \\
&-\left\{q^2_\parallel(m_N^2 + k_\parallel^2 - k_\parallel\cdot q_\parallel) - 2(k_\parallel\cdot q_\parallel)^2\right\}g^{\mu\nu}_\perp\left(\delta^n_{l-1} + \delta^{n-1}_l\right)\Big]\Bigg]
\end{aligned} \tag{D.44}$$

It is to be noted that, a Kronecker delta with -ve index is zero which comes from our constraint on the Laguerre polynomials $L^a_{-1} = 0$.

D.6 Details of $\mathcal{N}^{\mu}_{\ \mu}$ and $\mathcal{N}^{00}$ for different loop

In this appendix, we list the explicit forms of $\mathcal{N}^{\mu}_{\ \mu}$ and $\mathcal{N}^{00}$ for all the different loops. For the zero magnetic field case, we have for the $\pi\pi$ Loop

$$g_{\mu\nu}\mathcal{N}^{\mu\nu}_{\pi}(q,k) = g^2_{\rho\pi\pi}\left[q^4k^\mu k^\nu + (q\cdot k)^2q^2 - q^2(q\cdot k)2q\cdot k\right] \tag{D.45}$$

$$\mathcal{N}^{00}_{\pi}(q,k) = g^2_{\rho\pi\pi}\left[q^4k_0^2 + (q\cdot k)^2q_0^2 - q^2(q\cdot k)2q^0k^0\right] \tag{D.46}$$

and for the NN-Loop,

$$\begin{aligned} g_{\mu\nu}\mathcal{N}^{\mu\nu}_{\rm N}(q,k) = -8g^2_{\rho NN}\Big[&(m_N^2 - k^2 - k\cdot q)4 + 2k^2 + q\cdot k + \kappa_\rho 3q^2 \\ &+\frac{\kappa_\rho^2}{4m_N^2}\Big\{(m_N^2 + k^2 - k\cdot q)3q^2 - 2q^2k^2 - 2(k\cdot q)^2 4 + 4(k\cdot q)^2\Big\}\Big] \end{aligned} \tag{D.47}$$

$$\begin{aligned} \mathcal{N}^{00}_{\rm N}(q,k) = -8g^2_{\rho NN}\Big[&(m_N^2 - k^2 - k\cdot q) + 2k_0^2 + 2q^0k^0 - \kappa_\rho\vec{q}^2 \\ &+\frac{\kappa_\rho^2}{4m_N^2}\Big\{-(m_N^2 + k^2 - k\cdot q)\vec{q}^2 - 2q^2k_0^2 - 2(k\cdot q)^2 + 4(k\cdot q)q^0k^0\Big\}\Big]. \end{aligned} \tag{D.48}$$

The corresponding expressions for $\pi\pi$ loop for finite magnetic field case are given by

$$\begin{aligned} g_{\mu\nu}\tilde{\mathcal{N}}^{\mu\nu}_{\pi,nl}(q_\parallel,k_\parallel) = {}& 4g^2_{\rho\pi\pi}(-1)^{n+l}\frac{eB}{8\pi}\Big[\Big\{q_\parallel^4k_\parallel^2 + (q_\parallel\cdot k_\parallel)^2q_\parallel^2 - q_\parallel^2(q_\parallel\cdot k_\parallel)2q_\parallel\cdot k_\parallel\Big\}\delta_l^n \\ &-q_\parallel^4\frac{eB}{2}\Big\{(2n+1)\delta_l^n - (n+1)\delta_l^{n+1} - n\delta_l^{n-1}\Big\}\Big] \end{aligned} \tag{D.49}$$

$$\tilde{\mathcal{N}}^{00}_{\pi,nl}(q_\parallel,k_\parallel) = 4g^2_{\rho\pi\pi}(-1)^{n+l}\frac{eB}{8\pi}\left[q_\parallel^4k_0^2 + (q_\parallel\cdot k_\parallel)^2q_0^2 - q_\parallel^2(q_\parallel\cdot k_\parallel)2q^0k^0\right]\delta_l^n \tag{D.50}$$

whereas the same for proton-proton loop are

$$\begin{aligned} g_{\mu\nu}\tilde{\mathcal{N}}^{\mu\nu}_{{\rm p},nl}(q_\parallel,k_\parallel) = {}& -g^2_{\rho NN}(-1)^{n+l}\frac{eB}{\pi}\Big[8eBn\delta_{l-1}^{n-1} + \Big\{2(m_N^2 - k_\parallel^2 - k_\parallel\cdot q_\parallel) + 2k_\parallel^2 + 2q_\parallel\cdot k_\parallel\Big\} \\ &\times\left(\delta_{l-1}^{n-1} + \delta_l^n\right) - 2(m_N^2 - k_\parallel^2 - k_\parallel\cdot q_\parallel)\left(\delta_{l-1}^n + \delta_l^{n-1}\right) + \kappa_\rho\Big[q_\parallel^2\left(\delta_{l-1}^{n-1} + \delta_l^n\right) \\ &-2q_\parallel^2\left(\delta_{l-1}^n + \delta_l^{n-1}\right)\Big] + \frac{\kappa_\rho^2}{4m_N^2}\Big[-4eBq_\parallel^2n\delta_{l-1}^{n-1} - \Big\{2q_\parallel^2k_\parallel^2 - q_\parallel^2(m_N^2 + k_\parallel^2 - k_\parallel\cdot q_\parallel)\Big\} \\ &\times\left(\delta_{l-1}^{n-1} + \delta_l^n\right) - 2\Big\{q_\parallel^2(m_N^2 + k_\parallel^2 - k_\parallel\cdot q_\parallel) - 2(k_\parallel\cdot q_\parallel)^2\Big\}\left(\delta_{l-1}^n + \delta_l^{n-1}\right)\Big]\Big] \end{aligned} \tag{D.51}$$

$$\begin{aligned} \tilde{\mathcal{N}}^{00}_{{\rm p},nl}(q_\parallel,k_\parallel) = {}& -g^2_{\rho NN}(-1)^{n+l}\frac{eB}{\pi}\Big[4eBn\delta_{l-1}^{n-1} + \Big\{(m_N^2 - k_\parallel^2 - k_\parallel\cdot q_\parallel) + 2k_0^2 + 2q^0k^0\Big\} \\ &\times\left(\delta_{l-1}^{n-1} + \delta_l^n\right) + \kappa_\rho\Big[-q_z^2\left(\delta_{l-1}^{n-1} + \delta_l^n\right)\Big] + \frac{\kappa_\rho^2}{4m_N^2}\Big[4eBq_z^2n\delta_{l-1}^{n-1} - \Big\{2(k_\parallel\cdot q_\parallel)^2 + 2q_\parallel^2k_0^2 \end{aligned}$$

$$-2(k_{\parallel}\cdot q_{\parallel})2q^0k^0+(m_N^2+k_{\parallel}^2-k_{\parallel}\cdot q_{\parallel})q_z^2\Big\}\left(\delta_{l-1}^{n-1}+\delta_l^n\right)\Big]\Bigg]. \tag{D.52}$$

Bibliography

[1] J. C. Collins and M. J. Perry, *Superdense Matter: Neutrons Or Asymptotically Free Quarks?*, *Phys. Rev. Lett.* **34** (1975) 1353.

[2] N. Cabibbo and G. Parisi, *Exponential Hadronic Spectrum and Quark Liberation*, *Phys. Lett.* **59B** (1975) 67–69.

[3] D. J. Gross and F. Wilczek, *Ultraviolet Behavior of Nonabelian Gauge Theories*, *Phys. Rev. Lett.* **30** (1973) 1343–1346.

[4] H. D. Politzer, *Reliable Perturbative Results for Strong Interactions?*, *Phys. Rev. Lett.* **30** (1973) 1346–1349.

[5] K. Yagi, T. Hatsuda and Y. Miake, *Quark-gluon plasma: From big bang to little bang*, *Camb. Monogr. Part. Phys. Nucl. Phys. Cosmol.* **23** (2005) 1–446.

[6] M. G. Alford and K. Schwenzer, *What the Timing of Millisecond Pulsars Can Teach us about Their Interior*, *Phys. Rev. Lett.* **113** (2014) 251102, [1310.3524].

[7] D. Boyanovsky, H. J. de Vega and D. J. Schwarz, *Phase transitions in the early and the present universe*, *Ann. Rev. Nucl. Part. Sci.* **56** (2006) 441–500, [hep-ph/0602002].

[8] H. R. Schmidt and J. Schukraft, *The Physics of ultrarelativistic heavy ion collisions*, *J. Phys.* **G19** (1993) 1705–1796.

[9] J. Schukraft and R. Stock, *Toward the Limits of Matter: Ultra-relativistic nuclear collisions at CERN*, *Adv. Ser. Direct. High Energy Phys.* **23** (2015) 61–87, [1505.06853].

[10] U. W. Heinz and M. Jacob, *Evidence for a new state of matter: An Assessment of the results from the CERN lead beam program*, nucl-th/0002042.

[11] BRAHMS collaboration, I. Arsene et al., *Quark gluon plasma and color glass condensate at RHIC? The Perspective from the BRAHMS experiment*, *Nucl. Phys.* **A757** (2005) 1–27, [nucl-ex/0410020].

[12] B. B. Back et al., *The PHOBOS perspective on discoveries at RHIC*, *Nucl. Phys.* **A757** (2005) 28–101, [nucl-ex/0410022].

[13] STAR collaboration, J. Adams et al., *Experimental and theoretical challenges in the search for the quark gluon plasma: The STAR Collaboration's critical assessment of the evidence from RHIC collisions*, *Nucl. Phys.* **A757** (2005) 102–183, [nucl-ex/0501009].

[14] PHENIX collaboration, K. Adcox et al., *Formation of dense partonic matter in relativistic nucleus-nucleus collisions at RHIC: Experimental evaluation by the PHENIX collaboration*, *Nucl. Phys.* **A757** (2005) 184–283, [nucl-ex/0410003].

[15] L. P. Csernai, *Introduction to relativistic heavy ion collisions*. 1994.

[16] R. Vogt, *Ultrarelativistic heavy-ion collisions*. Elsevier, Amsterdam, 2007.

[17] E. Shuryak, *Strongly coupled quark-gluon plasma in heavy ion collisions*, *Rev. Mod. Phys.* **89** (2017) 035001, [1412.8393].

[18] U. Heinz et al., *Exploring the properties of the phases of QCD matter - research opportunities and priorities for the next decade*, 1501.06477.

[19] W. Florkowski, *Basic phenomenology for relativistic heavy-ion collisions*, *Acta Phys. Polon.* **B45** (2014) 2329–2354, [1410.7904].

[20] A. Jaiswal and V. Roy, *Relativistic hydrodynamics in heavy-ion collisions: general aspects and recent developments*, *Adv. High Energy Phys.* **2016** (2016) 9623034, [1605.08694].

[21] P. Foka and M. A. Janik, *An overview of experimental results from ultra-relativistic heavy-ion collisions at the CERN LHC: Hard probes*, *Rev. Phys.* **1** (2016) 172–194, [1702.07231].

[22] P. Foka and M. A. Janik, *An overview of experimental results from ultra-relativistic heavy-ion collisions at the CERN LHC: Bulk properties and dynamical evolution*, *Rev. Phys.* **1** (2016) 154–171, [1702.07233].

[23] Z. Citron et al., *Report from Working Group 5*, *CERN Yellow Rep. Monogr.* **7** (2019) 1159–1410, [1812.06772].

[24] N. Brambilla et al., *QCD and Strongly Coupled Gauge Theories: Challenges and Perspectives*, *Eur. Phys. J.* **C74** (2014) 2981, [1404.3723].

[25] C. D. Roberts, *Strong QCD and Dyson-Schwinger Equations*, *IRMA Lect. Math. Theor. Phys.* **21** (2015) 355–458, [1203.5341].

[26] C. S. Fischer, *QCD at finite temperature and chemical potential from Dyson–Schwinger equations*, *Prog. Part. Nucl. Phys.* **105** (2019) 1–60, [1810.12938].

[27] Z. Fodor, *Selected results in lattice quantum chromodynamics*, *PTEP* **2012** (2012) 01A108.

[28] P. Petreczky, *Lattice QCD at non-zero temperature*, *J. Phys.* **G39** (2012) 093002, [1203.5320].

[29] C. Hoelbling, *Light hadron spectroscopy and pseudoscalar decay constants*, *PoS* **LATTICE2010** (2010) 011, [1102.0410].

[30] S. Sharma, *QCD Thermodynamics on the Lattice*, *Adv. High Energy Phys.* **2013** (2013) 452978, [1403.2102].

[31] F. Karsch, K. Redlich and A. Tawfik, *Thermodynamics at nonzero baryon number density: A Comparison of lattice and hadron resonance gas model calculations*, *Phys. Lett.* **B571** (2003) 67–74, [hep-ph/0306208].

[32] A. Tawfik, *QCD phase diagram: A Comparison of lattice and hadron resonance gas model calculations*, *Phys. Rev.* **D71** (2005) 054502, [hep-ph/0412336].

[33] P. Huovinen and P. Petreczky, *QCD Equation of State and Hadron Resonance Gas*, *Nucl. Phys.* **A837** (2010) 26–53, [0912.2541].

[34] A. Bazavov et al., *The QCD Equation of State to $\mathcal{O}(\mu_B^6)$ from Lattice QCD*, *Phys. Rev.* **D95** (2017) 054504, [1701.04325].

[35] A. Bazavov et al., *Additional Strange Hadrons from QCD Thermodynamics and Strangeness Freezeout in Heavy Ion Collisions*, *Phys. Rev. Lett.* **113** (2014) 072001, [1404.6511].

[36] P. Huovinen and P. Petreczky, *Hadron Resonance Gas with Repulsive Interactions and Fluctuations of Conserved Charges*, *Phys. Lett.* **B777** (2018) 125–130, [1708.00879].

[37] V. Vovchenko, M. I. Gorenstein and H. Stoecker, *van der Waals Interactions in Hadron Resonance Gas: From Nuclear Matter to Lattice QCD*, *Phys. Rev. Lett.* **118** (2017) 182301, [1609.03975].

[38] C. Ratti, M. A. Thaler and W. Weise, *Phases of QCD: Lattice thermodynamics and a field theoretical model*, *Phys. Rev.* **D73** (2006) 014019, [hep-ph/0506234].

[39] K. Fukushima, *Phase diagrams in the three-flavor Nambu-Jona-Lasinio model with the Polyakov loop*, *Phys. Rev.* **D77** (2008) 114028, [0803.3318].

[40] A. G. Grunfeld and G. Lugones, *Finite size effects in strongly interacting matter at zero chemical potential from Polyakov loop Nambu-Jona-Lasinio model in the light of lattice data*, *Eur. Phys. J.* **C78** (2018) 640, [1711.07559].

[41] O. Ivanytskyi, M. A. Pérez-García, V. Sagun and C. Albertus, *Second look to the polyakov loop nambu–jona-lasinio model at finite baryonic density*, *Phys. Rev. D* **100** (Nov, 2019) 103020.

[42] B.-J. Schaefer, J. M. Pawlowski and J. Wambach, *The Phase Structure of the Polyakov–Quark-Meson Model*, *Phys. Rev.* **D76** (2007) 074023, [0704.3234].

[43] V. Skokov, B. Stokic, B. Friman and K. Redlich, *Meson fluctuations and thermodynamics of the Polyakov loop extended quark-meson model*, *Phys. Rev.* **C82** (2010) 015206, [1004.2665].

[44] T. K. Herbst, J. M. Pawlowski and B.-J. Schaefer, *The phase structure of the Polyakov–quark–meson model beyond mean field*, *Phys. Lett.* **B696** (2011) 58–67, [1008.0081].

[45] S. Borsanyi, G. Endrodi, Z. Fodor, A. Jakovac, S. D. Katz, S. Krieg et al., *The QCD equation of state with dynamical quarks*, *JHEP* **11** (2010) 077, [1007.2580].

[46] S. Borsanyi, Z. Fodor, C. Hoelbling, S. D. Katz, S. Krieg and K. K. Szabo, *Full result for the QCD equation of state with 2+1 flavors*, *Phys. Lett.* **B730** (2014) 99–104, [1309.5258].

[47] HotQCD collaboration, A. Bazavov et al., *Equation of state in (2+1)-flavor QCD*, *Phys. Rev.* **D90** (2014) 094503, [1407.6387].

[48] Y. Aoki, S. Borsanyi, S. Durr, Z. Fodor, S. D. Katz, S. Krieg et al., *The QCD transition temperature: results with physical masses in the continuum limit II.*, *JHEP* **06** (2009) 088, [0903.4155].

[49] S. Borsányi, Z. Fodor, C. Hoelbling, S. D. Katz, S. Krieg, C. Ratti et al., *Is there still any tcmystery in lattice qcd?: Results with physical masses in the continuum limit iii*, *Journal of High Energy Physics* **2010** (2010) 73.

[50] S. Borsanyi, *Thermodynamics of the QCD transition from lattice*, *Nucl. Phys.* **A904-905** (2013) 270c–277c, [1210.6901].

[51] K. Rajagopal and F. Wilczek, *The Condensed matter physics of QCD*, in *At the frontier of particle physics. Handbook of QCD. Vol. 1-3* (M. Shifman and B. Ioffe, eds.), pp. 2061–2151. 2000. hep-ph/0011333. DOI.

[52] M. G. Alford, *Color superconducting quark matter*, *Ann. Rev. Nucl. Part. Sci.* **51** (2001) 131–160, [hep-ph/0102047].

[53] M. G. Alford, A. Schmitt, K. Rajagopal and T. Schäfer, *Color superconductivity in dense quark matter*, *Rev. Mod. Phys.* **80** (2008) 1455–1515, [0709.4635].

[54] STAR collaboration, L. Kumar, *STAR Results from the RHIC Beam Energy Scan-I*, *Nucl. Phys.* **A904-905** (2013) 256c–263c, [1211.1350].

[55] A. Taranenko, *Results from the RHIC Beam Energy Scan*, *EPJ Web Conf.* **164** (2017) 06005.

[56] K. Fukushima and T. Hatsuda, *The phase diagram of dense QCD*, *Rept. Prog. Phys.* **74** (2011) 014001, [1005.4814].

[57] Y. Akiba et al., *The Hot QCD White Paper: Exploring the Phases of QCD at RHIC and the LHC*, 1502.02730.

[58] T. Vachaspati, *Magnetic fields from cosmological phase transitions*, *Physics Letters B* **265** (1991) 258 – 261.

[59] L. M. Widrow, *Origin of galactic and extragalactic magnetic fields*, *Rev. Mod. Phys.* **74** (2002) 775–823, [astro-ph/0207240].

[60] L. Campanelli, *Origin of Cosmic Magnetic Fields*, *Phys. Rev. Lett.* **111** (2013) 061301, [1304.6534].

[61] K. Subramanian, *The origin, evolution and signatures of primordial magnetic fields*, *Rept. Prog. Phys.* **79** (2016) 076901, [1504.02311].

[62] A. K. Pandey and J. Bhatt, *Origin and dynamics of the Primordial Magnetic field in a parity violating plasma*. PhD thesis, Ahmedabad, Phys. Res. Lab, 2017. 1712.06291.

[63] M. Giovannini, *Probing large-scale magnetism with the Cosmic Microwave Background*, *Class. Quant. Grav.* **35** (2018) 084003, [1712.07598].

[64] K. E. Kunze, *Cmb anisotropies in the presence of a stochastic magnetic field*, *Phys. Rev. D* **83** (Jan, 2011) 023006.

[65] T. Minoda, H. Tashiro and T. Takahashi, *Insight into primordial magnetic fields from 21-cm line observation with EDGES experiment*, *Mon. Not. Roy. Astron. Soc.* **488** (2019) 2001–2005, [1812.00730].

[66] J. R. Shaw and A. Lewis, *Constraining Primordial Magnetism*, *Phys. Rev.* **D86** (2012) 043510, [1006.4242].

[67] D. Grasso and H. R. Rubinstein, *Magnetic fields in the early universe*, *Phys. Rept.* **348** (2001) 163–266, [astro-ph/0009061].

[68] E. J. Ferrer, V. de la Incera and C. Manuel, *Magnetic color flavor locking phase in high density QCD*, *Phys. Rev. Lett.* **95** (2005) 152002, [hep-ph/0503162].

[69] E. J. Ferrer, V. de la Incera and C. Manuel, *Color-superconducting gap in the presence of a magnetic field*, *Nucl. Phys.* **B747** (2006) 88–112, [hep-ph/0603233].

[70] E. J. Ferrer and V. de la Incera, *Magnetic Phases in Three-Flavor Color Superconductivity*, *Phys. Rev.* **D76** (2007) 045011, [nucl-th/0703034].

[71] K. Fukushima and H. J. Warringa, *Color superconducting matter in a magnetic field*, *Phys. Rev. Lett.* **100** (2008) 032007, [0707.3785].

[72] J. L. Noronha and I. A. Shovkovy, *Color-flavor locked superconductor in a magnetic field*, *Phys. Rev.* **D76** (2007) 105030, [0708.0307].

[73] B. Feng, D. Hou, H.-c. Ren and P.-p. Wu, *The Single Flavor Color Superconductivity in a Magnetic Field*, *Phys. Rev. Lett.* **105** (2010) 042001, [0911.4997].

[74] S. Fayazbakhsh and N. Sadooghi, *Color neutral 2SC phase of cold and dense quark matter in the presence of constant magnetic fields*, *Phys. Rev.* **D82** (2010) 045010, [1005.5022].

[75] D. C. Duarte, P. G. Allen, R. L. S. Farias, P. H. A. Manso, R. O. Ramos and N. N. Scoccola, *BEC-BCS crossover in a cold and magnetized two color NJL model*, *Phys. Rev.* **D93** (2016) 025017, [1510.02756].

[76] W. Chen, P.-Q. Zhang and L.-G. Liu, *The Influence of the magnetic field on the properties of neutron star matter*, *Mod. Phys. Lett.* **A22** (2007) 623–630, [astro-ph/0505113].

[77] V. Dexheimer, R. Negreiros and S. Schramm, *Hybrid Stars in a Strong Magnetic Field*, *Eur. Phys. J.* **A48** (2012) 189, [1108.4479].

[78] L. Paulucci, E. J. Ferrer, V. de la Incera and J. E. Horvath, *Equation of state for the MCFL phase and its implications for compact star models*, *Phys. Rev.* **D83** (2011) 043009, [1010.3041].

[79] E. J. Ferrer and A. Hackebill, *Thermodynamics of Neutrons in a Magnetic Field and its Implications for Neutron Stars*, *Phys. Rev.* **C99** (2019) 065803, [1903.08224].

[80] C. Y. Ng and V. M. Kaspi, *High Magnetic Field Rotation-powered Pulsars*, *AIP Conf. Proc.* **1379** (2011) 60–69, [1010.4592].

[81] V. M. Kaspi and A. Beloborodov, *Magnetars*, *Ann. Rev. Astron. Astrophys.* **55** (2017) 261–301, [1703.00068].

[82] A. Tiengo et al., *A variable absorption feature in the X-ray spectrum of a magnetar*, *Nature* **500** (2013) 312, [1308.4987].

[83] H. An et al., *NuSTAR observations of X-ray bursts from the magnetar 1E 1048.1-5937*, *Astrophys. J.* **790** (2014) 60, [1406.3377].

[84] E. J. Ferrer, V. de la Incera, J. P. Keith, I. Portillo and P. L. Springsteen, *Equation of State of a Dense and Magnetized Fermion System*, *Phys. Rev.* **C82** (2010) 065802, [1009.3521].

[85] J. M. Lattimer and M. Prakash, *The Equation of State of Hot, Dense Matter and Neutron Stars*, *Phys. Rept.* **621** (2016) 127–164, [1512.07820].

[86] G. Baym, T. Hatsuda, T. Kojo, P. D. Powell, Y. Song and T. Takatsuka, *From hadrons to quarks in neutron stars: a review*, *Rept. Prog. Phys.* **81** (2018) 056902, [1707.04966].

[87] D. E. Kharzeev, L. D. McLerran and H. J. Warringa, *The Effects of topological charge change in heavy ion collisions: 'Event by event P and CP violation'*, *Nucl. Phys.* **A803** (2008) 227–253, [0711.0950].

[88] V. Skokov, A. Yu. Illarionov and V. Toneev, *Estimate of the magnetic field strength in heavy-ion collisions*, *Int. J. Mod. Phys.* **A24** (2009) 5925–5932, [0907.1396].

[89] V. Voronyuk, V. D. Toneev, W. Cassing, E. L. Bratkovskaya, V. P. Konchakovski and S. A. Voloshin, *Electromagnetic field evolution in relativistic heavy-ion collisions*, *Phys. Rev. C* **83** (May, 2011) 054911.

[90] W.-T. Deng and X.-G. Huang, *Event-by-event generation of electromagnetic fields in heavy-ion collisions*, *Phys. Rev. C* **85** (Apr, 2012) 044907.

[91] A. Bzdak and V. Skokov, *Event-by-event fluctuations of magnetic and electric fields in heavy ion collisions*, *Phys. Lett.* **B710** (2012) 171–174, [1111.1949].

[92] K. Tuchin, *Initial value problem for magnetic fields in heavy ion collisions*, *Phys. Rev. C* **93** (Jan, 2016) 014905.

[93] Y. Zhong, C.-B. Yang, X. Cai and S.-Q. Feng, *A systematic study of magnetic field in Relativistic Heavy-ion Collisions in the RHIC and LHC energy regions*, *Adv. High Energy Phys.* **2014** (2014) 193039, [1408.5694].

[94] L. McLerran and V. Skokov, *Comments about the electromagnetic field in heavy-ion collisions*, *Nuclear Physics A* **929** (2014) 184 – 190.

[95] K. Tuchin, *Magnetic contribution to dilepton production in heavy-ion collisions*, *Phys. Rev. C* **88** (Aug, 2013) 024910.

[96] K. Tuchin, *Electromagnetic radiation by quark-gluon plasma in a magnetic field*, *Phys. Rev. C* **87** (Feb, 2013) 024912.

[97] K. Tuchin, *Particle production in strong electromagnetic fields in relativistic heavy-ion collisions*, *Advances in High Energy Physics* **2013** (2013) 490495.

[98] K. Tuchin, *Photon decay in a strong magnetic field in heavy-ion collisions*, *Phys. Rev. C* **83** (Jan, 2011) 017901.

[99] K. Tuchin, *Synchrotron radiation by fast fermions in heavy-ion collisions*, *Phys. Rev. C* **82** (Sep, 2010) 034904.

[100] V. Roy, S. Pu, L. Rezzolla and D. H. Rischke, *Effect of intense magnetic fields on reduced-magnetohydrodynamics evolution in $\sqrt{s_{NN}} = 200$ gev au + au collisions*, *Phys. Rev. C* **96** (Nov, 2017) 054909.

[101] A. Das, S. S. Dave, P. S. Saumia and A. M. Srivastava, *Effects of magnetic field on plasma evolution in relativistic heavy-ion collisions*, *Phys. Rev. C* **96** (Sep, 2017) 034902.

[102] G. Inghirami, L. Del Zanna, A. Beraudo, M. H. Moghaddam, F. Becattini and M. Bleicher, *Numerical magneto-hydrodynamics for relativistic nuclear collisions*, *Eur. Phys. J.* **C76** (2016) 659, [1609.03042].

[103] Y. Hirono, M. Hongo and T. Hirano, *Estimation of electric conductivity of the quark gluon plasma via asymmetric heavy-ion collisions*, *Phys. Rev.* **C90** (2014) 021903, [1211.1114].

[104] W.-T. Deng and X.-G. Huang, *Electric fields and chiral magnetic effect in Cu+Au collisions*, *Phys. Lett.* **B742** (2015) 296–302, [1411.2733].

[105] V. Voronyuk, V. D. Toneev, S. A. Voloshin and W. Cassing, *Charge-dependent directed flow in asymmetric nuclear collisions*, *Phys. Rev.* **C90** (2014) 064903, [1410.1402].

[106] K. Fukushima, D. E. Kharzeev and H. J. Warringa, *The Chiral Magnetic Effect*, *Phys. Rev.* **D78** (2008) 074033, [0808.3382].

[107] D. T. Son and A. R. Zhitnitsky, *Quantum anomalies in dense matter*, *Phys. Rev.* **D70** (2004) 074018, [hep-ph/0405216].

[108] M. A. Metlitski and A. R. Zhitnitsky, *Anomalous axion interactions and topological currents in dense matter*, *Phys. Rev.* **D72** (2005) 045011, [hep-ph/0505072].

[109] X.-G. Huang and J. Liao, *Axial Current Generation from Electric Field: Chiral Electric Separation Effect*, Phys. Rev. Lett. **110** (2013) 232302, [1303.7192].

[110] Y. Jiang, X.-G. Huang and J. Liao, *Chiral electric separation effect in the quark-gluon plasma*, Phys. Rev. **D91** (2015) 045001, [1409.6395].

[111] D. E. Kharzeev and H.-U. Yee, *Chiral Magnetic Wave*, Phys. Rev. **D83** (2011) 085007, [1012.6026].

[112] D. T. Son and P. Surowka, *Hydrodynamics with Triangle Anomalies*, Phys. Rev. Lett. **103** (2009) 191601, [0906.5044].

[113] D. E. Kharzeev, K. Landsteiner, A. Schmitt and H.-U. Yee, *'Strongly interacting matter in magnetic fields': an overview*, Lect. Notes Phys. **871** (2013) 1–11, [1211.6245].

[114] X.-G. Huang, *Electromagnetic fields and anomalous transports in heavy-ion collisions — A pedagogical review*, Rept. Prog. Phys. **79** (2016) 076302, [1509.04073].

[115] D. E. Kharzeev, *The Chiral Magnetic Effect and Anomaly-Induced Transport*, Prog. Part. Nucl. Phys. **75** (2014) 133–151, [1312.3348].

[116] D. E. Kharzeev, *Topology, magnetic field, and strongly interacting matter*, Ann. Rev. Nucl. Part. Sci. **65** (2015) 193–214, [1501.01336].

[117] D. E. Kharzeev, J. Liao, S. A. Voloshin and G. Wang, *Chiral magnetic and vortical effects in high-energy nuclear collisions—A status report*, Prog. Part. Nucl. Phys. **88** (2016) 1–28, [1511.04050].

[118] M. D'Elia, S. Mukherjee and F. Sanfilippo, *QCD Phase Transition in a Strong Magnetic Background*, Phys. Rev. **D82** (2010) 051501, [1005.5365].

[119] M. D'Elia and F. Negro, *Chiral Properties of Strong Interactions in a Magnetic Background*, Phys. Rev. **D83** (2011) 114028, [1103.2080].

[120] J. K. Boomsma and D. Boer, *The Influence of strong magnetic fields and instantons on the phase structure of the two-flavor NJL model*, Phys. Rev. **D81** (2010) 074005, [0911.2164].

[121] B. Chatterjee, H. Mishra and A. Mishra, *Vacuum structure and chiral symmetry breaking in strong magnetic fields for hot and dense quark matter*, *Phys. Rev.* **D84** (2011) 014016, [1101.0498].

[122] S. S. Avancini, D. P. Menezes and C. Providencia, *Finite temperature quark matter under strong magnetic fields*, *Phys. Rev.* **C83** (2011) 065805.

[123] M. Frasca and M. Ruggieri, *Magnetic Susceptibility of the Quark Condensate and Polarization from Chiral Models*, *Phys. Rev.* **D83** (2011) 094024, [1103.1194].

[124] A. Rabhi and C. Providencia, *Quark matter under strong magnetic field in chiral models*, *Phys. Rev.* **C83** (2011) 055801, [1104.1512].

[125] R. Gatto and M. Ruggieri, *Dressed Polyakov loop and phase diagram of hot quark matter under magnetic field*, *Phys. Rev.* **D82** (2010) 054027, [1007.0790].

[126] R. Gatto and M. Ruggieri, *Deconfinement and Chiral Symmetry Restoration in a Strong Magnetic Background*, *Phys. Rev.* **D83** (2011) 034016, [1012.1291].

[127] K. Kashiwa, *Entanglement between chiral and deconfinement transitions under strong uniform magnetic background field*, *Phys. Rev.* **D83** (2011) 117901, [1104.5167].

[128] J. O. Andersen and R. Khan, *Chiral transition in a magnetic field and at finite baryon density*, *Phys. Rev.* **D85** (2012) 065026, [1105.1290].

[129] J. O. Andersen and A. Tranberg, *The Chiral transition in a magnetic background: Finite density effects and the functional renormalization group*, *JHEP* **08** (2012) 002, [1204.3360].

[130] A. J. Mizher, M. N. Chernodub and E. S. Fraga, *Phase diagram of hot QCD in an external magnetic field: possible splitting of deconfinement and chiral transitions*, *Phys. Rev.* **D82** (2010) 105016, [1004.2712].

[131] V. Skokov, *Phase diagram in an external magnetic field beyond a mean-field approximation*, *Phys. Rev.* **D85** (2012) 034026, [1112.5137].

[132] D. C. Duarte, R. L. S. Farias and R. O. Ramos, *Optimized perturbation theory for charged scalar fields at finite temperature and in an external magnetic field*, *Phys. Rev.* **D84** (2011) 083525, [1108.4428].

[133] E. S. Fraga and L. F. Palhares, *Deconfinement in the presence of a strong magnetic background: an exercise within the MIT bag model*, Phys. Rev. **D86** (2012) 016008, [1201.5881].

[134] G. S. Bali, F. Bruckmann, G. Endrodi, Z. Fodor, S. D. Katz, S. Krieg et al., *The QCD phase diagram for external magnetic fields*, JHEP **02** (2012) 044, [1111.4956].

[135] G. S. Bali, F. Bruckmann, G. Endrodi, Z. Fodor, S. D. Katz and A. Schafer, *QCD quark condensate in external magnetic fields*, Phys. Rev. **D86** (2012) 071502, [1206.4205].

[136] G. S. Bali, F. Bruckmann, G. Endrodi, F. Gruber and A. Schaefer, *Magnetic field-induced gluonic (inverse) catalysis and pressure (an)isotropy in QCD*, JHEP **04** (2013) 130, [1303.1328].

[137] V. G. Bornyakov, P. V. Buividovich, N. Cundy, O. A. Kochetkov and A. Schäfer, *Deconfinement transition in two-flavor lattice QCD with dynamical overlap fermions in an external magnetic field*, Phys. Rev. **D90** (2014) 034501, [1312.5628].

[138] F. Bruckmann, G. Endrodi and T. G. Kovacs, *Inverse magnetic catalysis and the Polyakov loop*, JHEP **04** (2013) 112, [1303.3972].

[139] J. O. Andersen, W. R. Naylor and A. Tranberg, *Phase diagram of qcd in a magnetic field*, Rev. Mod. Phys. **88** (Apr, 2016) 025001.

[140] M. L. Bellac, *Thermal Field Theory*. Cambridge Monographs on Mathematical Physics. Cambridge University Press, 2011, 10.1017/CBO9780511721700.

[141] S. Mallik and S. Sarkar, *Hadrons at Finite Temperature*. Cambridge University Press, Cambridge, 2016, 10.1017/9781316535585.

[142] A. K. Das, *Finite Temperature Field Theory*. World Scientific, New York, 1997.

[143] M. Laine and A. Vuorinen, *Basics of Thermal Field Theory*, Lect. Notes Phys. **925** (2016) pp.1–281, [1701.01554].

[144] J. I. Kapusta and C. Gale, *Finite-temperature field theory: Principles and applications*. Cambridge Monographs on Mathematical Physics. Cambridge University Press, 2011, 10.1017/CBO9780511535130.

[145] J. S. Schwinger, *On gauge invariance and vacuum polarization*, *Phys. Rev.* **82** (1951) 664–679.

[146] A. Haber, F. Preis and A. Schmitt, *Magnetic catalysis in nuclear matter*, *Phys. Rev. D* **90** (Dec, 2014) 125036.

[147] J. Walecka, *A theory of highly condensed matter*, *Annals of Physics* **83** (1974) 491 – 529.

[148] A. Broderick, M. Prakash and J. M. Lattimer, *The equation of state of neutron star matter in strong magnetic fields*, *The Astrophysical Journal* **537** (jul, 2000) 351–367.

[149] A. Broderick, M. Prakash and J. Lattimer, *Effects of strong magnetic fields in strange baryonic matter*, *Physics Letters B* **531** (2002) 167 – 174.

[150] M. Sinha, B. Mukhopadhyay and A. Sedrakian, *Hypernuclear matter in strong magnetic field*, *Nuclear Physics A* **898** (2013) 43 – 58.

[151] A. Rabhi, P. K. Panda and C. Providência, *Warm and dense stellar matter under strong magnetic fields*, *Phys. Rev. C* **84** (Sep, 2011) 035803.

[152] Dexheimer, V., Negreiros, R. and Schramm, S., *Hybrid stars in a strong magnetic field*, *Eur. Phys. J. A* **48** (2012) 189.

[153] F. Preis, A. Rebhan and A. Schmitt, *Holographic baryonic matter in a background magnetic field*, *Journal of Physics G: Nuclear and Particle Physics* **39** (apr, 2012) 054006.

[154] J. Dong, W. Zuo and J. Gu, *Magnetization of neutron star matter*, *Phys. Rev. D* **87** (May, 2013) 103010.

[155] R. C. R. de Lima, S. S. Avancini and C. Providência, *Effect of strong magnetic fields on the nuclear "pasta" phase structure*, *Phys. Rev. C* **88** (Sep, 2013) 035804.

[156] R. H. Casali, L. B. Castro and D. P. Menezes, *Hadronic and hybrid stars subject to density-dependent magnetic fields*, *Phys. Rev. C* **89** (Jan, 2014) 015805.

[157] F. Preis, A. Rebhan and A. Schmitt, *Inverse magnetic catalysis in dense holographic matter*, *Journal of High Energy Physics* **2011** (2011) 33.

[158] E. J. Ferrer, V. de la Incera, D. M. Paret, A. P. Martínez and A. Sanchez, *Insignificance of the anomalous magnetic moment of charged fermions for the equation of state of a magnetized and dense medium*, *Phys. Rev. D* **91** (Apr, 2015) 085041.

[159] A. Mukherjee, S. Ghosh, M. Mandal, S. Sarkar and P. Roy, *Effect of external magnetic fields on nucleon mass in a hot and dense medium: Inverse magnetic catalysis in the Walecka model*, *Phys. Rev.* **D98** (2018) 056024, [1809.07028].

[160] M. N. Chernodub, *Superconductivity of QCD vacuum in strong magnetic field*, *Phys. Rev.* **D82** (2010) 085011, [1008.1055].

[161] M. N. Chernodub, *Electromagnetic superconductivity of vacuum induced by strong magnetic field*, *Lect. Notes Phys.* **871** (2013) 143–180, [1208.5025].

[162] C. Vafa and E. Witten, *Restrictions on symmetry breaking in vector-like gauge theories*, *Nuclear Physics B* **234** (1984) 173 – 188.

[163] M. N. Chernodub, *Vafa-witten theorem, vector meson condensates, and magnetic-field-induced electromagnetic superconductivity of vacuum*, *Phys. Rev. D* **86** (Nov, 2012) 107703.

[164] C. Li and Q. Wang, *Amending the vafa–witten theorem*, *Physics Letters B* **721** (2013) 141 – 145.

[165] Y. Hidaka and A. Yamamoto, *Charged vector mesons in a strong magnetic field*, *Phys. Rev. D* **87** (May, 2013) 094502.

[166] H. Liu, L. Yu and M. Huang, *Charged and neutral vector ρ mesons in a magnetic field*, *Phys. Rev. D* **91** (Jan, 2015) 014017.

[167] M. Kawaguchi and S. Matsuzaki, *Vector meson masses from a hidden local symmetry in a constant magnetic field*, *Phys. Rev. D* **93** (Jun, 2016) 125027.

[168] H. Liu, L. Yu and M. Huang, *Survival of charged ρ condensation at high temperature and density*, *Chinese Physics C* **40** (2016) 023102.

[169] S. Ghosh, A. Mukherjee, M. Mandal, S. Sarkar and P. Roy, *Spectral properties of ρ meson in a magnetic field*, *Phys. Rev.* **D94** (2016) 094043, [1612.02966].

[170] Bandyopadhyay, Aritra and Mallik, S., *Rho meson decay in the presence of a magnetic field*, Eur. Phys. J. C **77** (2017) 771.

[171] Kawaguchi, Mamiya and Matsuzaki, Shinya, *Lifetime of rho meson in correlation with magnetic-dimensional reduction*, Eur. Phys. J. A **53** (2017) 68.

[172] S. Ghosh, A. Mukherjee, P. Roy and S. Sarkar, *General structure of the neutral ρ meson self-energy and its spectral properties in a hot and dense magnetized medium*, Phys. Rev. D **99** (May, 2019) 096004.

[173] S. Ghosh, A. Mukherjee, M. Mandal, S. Sarkar and P. Roy, *Thermal effects on ρ meson properties in an external magnetic field*, Phys. Rev. **D96** (2017) 116020, [1704.05319].

[174] E. Elizalde, S. D. Odintsov, A. Romeo, A. A. Bytsenko and S. Zerbini, *Zeta Regularization Techniques with Applications*. WORLD SCIENTIFIC, 1994, 10.1142/2065.

[175] T.-K. Chyi, C.-W. Hwang, W. Kao, G.-L. Lin, K.-W. Ng and J.-J. Tseng, *The weak field expansion for processes in a homogeneous background magnetic field*, Phys. Rev. D **62** (2000) 105014, [hep-th/9912134].

[176] V. Ritus, *METHOD OF EIGENFUNCTIONS AND MASS OPERATOR IN QUANTUM ELECTRODYNAMICS OF A CONSTANT FIELD*, Sov. Phys. JETP **48** (1978) 788.

[177] V. Ritus, *Radiative corrections in quantum electrodynamics with intense field and their analytical properties*, Annals Phys. **69** (1972) 555–582.

[178] E. J. Ferrer and V. de la Incera, *Dynamically Generated Anomalous Magnetic Moment in Massless QED*, Nucl. Phys. B **824** (2010) 217–238, [0905.1733].

[179] E. Ferrer, V. de la Incera, D. Manreza Paret, A. Pérez Martínez and A. Sanchez, *Insignificance of the anomalous magnetic moment of charged fermions for the equation of state of a magnetized and dense medium*, Phys. Rev. D **91** (2015) 085041, [1501.06616].

[180] D. Lee, C. N. Leung and Y. Ng, *Chiral symmetry breaking in a uniform external magnetic field*, Phys. Rev. D **55** (1997) 6504–6513, [hep-th/9701172].

[181] N. Sadooghi and F. Taghinavaz, *Local electric current correlation function in an exponentially decaying magnetic field*, *Phys. Rev. D* **85** (2012) 125035, [1203.5634].

[182] I. A. Shovkovy, *Magnetic Catalysis: A Review*, vol. 871, pp. 13–49. 2013. 1207.5081. 10.1007/978-3-642-37305-3_2.

[183] I. Gradshteyn and I. Ryzhik, *Table of Integrals, Series, and Products (Academic, New York, 2007).*

[184] J. F. Nieves, *Nucleon contribution to the induced charge of neutrinos in a matter background and a magnetic field*, *Phys. Rev. D* **70** (Oct, 2004) 073001.

[185] J. F. Nieves and P. B. Pal, *Perturbative versus schwinger-propagator method for the calculation of amplitudes in a magnetic field*, *Phys. Rev. D* **73** (May, 2006) 105003.

[186] A. Bandyopadhyay and S. Mallik, *Effect of magnetic field on dilepton production in a hot plasma*, *Phys. Rev.* **D95** (2017) 074019, [1704.01364].

[187] J. C. D'Olivo, J. F. Nieves and S. Sahu, *Field theory of the photon selfenergy in a medium with a magnetic field and the Faraday effect*, *Phys. Rev.* **D67** (2003) 025018, [hep-ph/0208146].

[188] B. D. Serot, J. D. W. edited by J. Negele and E. Vogt, *Advances in Nuclear Physics*. Plenum Press, New York, 1986.

[189] J. Alam, S. Sarkar, P. Roy, T. Hatsuda and B. Sinha, *Thermal photons and lepton pairs from quark gluon plasma and hot hadronic matter*, *Annals Phys.* **286** (2001) 159–248, [hep-ph/9909267].

[190] Aguirre, R. M. and De Paoli, A. L., *In-medium covariant propagator of baryons under a strong magnetic field: Effect of the intrinsic magnetic moments*, *Eur. Phys. J. A* **52** (2016) 343.

[191] R. M. Aguirre, *Hadronic matter under an external magnetic field: In-medium modification of the pion mass*, *Phys. Rev. D* **95** (Apr, 2017) 074029.

[192] O. Krehl, C. Hanhart, S. Krewald and J. Speth, *What is the structure of the Roper resonance?*, *Phys. Rev.* **C62** (2000) 025207, [nucl-th/9911080].

[193] A. Ayala, A. Sanchez, G. Piccinelli and S. Sahu, *Effective potential at finite temperature in a constant magnetic field. I. Ring diagrams in a scalar theory*, *Phys. Rev.* **D71** (2005) 023004, [hep-ph/0412135].

[194] S. Ghosh and V. Chandra, *Electromagnetic spectral function and dilepton rate in a hot magnetized QCD medium*, *Phys. Rev.* **D98** (2018) 076006, [1808.05176].

[195] P. Chakraborty, *Meson spectral function and screening masses in magnetized quark gluon plasma*, 1711.04404.

[196] A. N. Gorban, *Basic Types of Coarse-Graining*, *Model Reduction and Coarse–Graining Approaches for Multiscale Phenomena, Springer* (2006) 117–176, [cond-mat/0602024].

[197] T. E.-A. P. Ehrenfest, *The Conceptual Foundations of the Statistical Approach in Mechanics*. Dover Phoneix, 2002.

[198] P. M. Hohler and R. Rapp, *Is ρ-meson melting compatible with chiral restoration?*, *Physics Letters B* **731** (2014) 103 – 109.

[199] Ghosh, Sabyasachi, Mallik, S. and Sarkar, Sourav, *Analytic structure of on propagator at finite temperature*, *Eur. Phys. J. C* **70** (2010) .

[200] P. Filip, *Decay of Resonaces in Strong Magnetic Field* , *Journal of Physics: Conference Series 636 012013* (2015) , [1504.07008].

[201] D. Albuquerque, *Hadronic resonances, strange and multi-strange particle production in xe-xe and pb-pb collisions with alice at the lhc*, *Nuclear Physics A* **982** (2019) 823 – 826.

[202] M. E. Peskin and D. V. Schroeder, *An Introduction to quantum field theory*. Addison-Wesley, Reading, USA, 1995.